REPORT NO.
UCB/EERC-90/10
JULY 1990

EARTHQUAKE ENGINEERING RESEARCH CENTER

EXPERIMENTAL TESTING OF THE RESILIENT-FRICTION BASE ISOLATION SYSTEM

by

PETER W. CLARK

JAMES M. KELLY

Report to the National Science Foundation

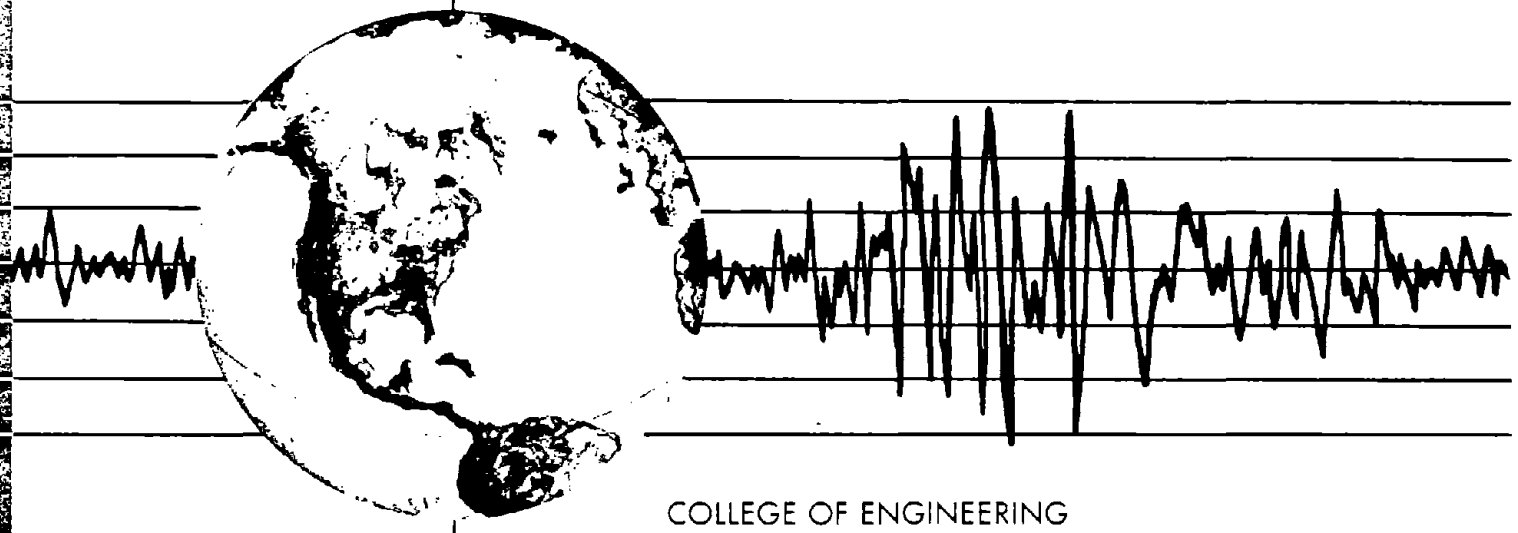

COLLEGE OF ENGINEERING

UNIVERSITY OF CALIFORNIA AT BERKELEY

For sale by the National Technical Information Service, U.S. Department of Commerce, Springfield, Virginia 22161

See back of report for up to date listing of EERC reports.

50272-101

REPORT DOCUMENTATION PAGE	1. REPORT NO. NSF/ENG-90002	2.	3. PB92-143072

4. Title and Subtitle
Experimental Testing of the Resilient-Friction Base Isolation System

5. Report Date
July 1990

6.

7. Author(s)
P.W. Clark and James M. Kelly

8. Performing Organization Rept. No.
UCB/EERC-90/10

9. Performing Organization Name and Address
Earthquake Engineering Research Center
University of California/RFS
1301 So. 46th Street
Richmond, CA 94804-4698

10. Project/Task/Work Unit No.

11. Contract(C) or Grant(G) No.
(C)
(G) CES-8702724

12. Sponsoring Organization Name and Address
National Science Foundation
1800 G. Street, N.W.
Washington, D.C. 21150

13. Type of Report & Period Covered

14.

15. Supplementary Notes

16. Abstract (Limit: 200 words)

This report describes a series of earthquake simulator tests of a five-story steel frame founded on Resilient-Friction Base Isolation (R-FBI) bearings. These bearings use alternating plates of teflon and stainless steel encircling a hard rubber core to absorb damaging horizontal ground motions. System identification tests were performed on the test structure to characterize its fixed base and isolated response, then the frame was subjected to a variety of earthquake motions. To a varying degree for each signal, the isolation system limited the accelerations transmitted to the frame and reduced the amplification of accelerations toward the top of the frame that is typical in conventional fixed-base structures. Measured interstory drifts were below levels likely to cause serious damage to structural or nonstructural components. The sliding displacements in the bearings were smaller than predicted by previous analyses because the measured coefficient of friction during the shake table tests was larger than that predicted by the material properties. The frequency response of the test frame depended greatly on the characteristics of the input signal. In general, the bearings tended to spread the input energy over several modes and a wide range of frequencies for each mode. Attempts were made to develop an equivalent linearized model for the isolated structural system.

17. Document Analysis a. Descriptors

b. Identifiers/Open-Ended Terms

c. COSATI Field/Group

18. Availability Statement	19. Security Class (This Report)	21. No. of Pages
Release Unlimited	unclassified	158
	20. Security Class (This Page) unclassified	22. Price A08

EXPERIMENTAL TESTING OF THE RESILIENT-FRICTION BASE ISOLATION SYSTEM

by

Peter W. Clark

James M. Kelly

Report to the National Science Foundation

Report No. UCB/EERC-90/10

Earthquake Engineering Research Center

College of Engineering

University of California, Berkeley

July 1990

ABSTRACT

This report describes a series of earthquake simulator tests of a five-story steel frame founded on Resilient-Friction Base Isolation (R-FBI) bearings. These bearings use alternating plates of teflon and stainless steel encircling a hard rubber core to absorb damaging horizontal ground motions. System identification tests were performed on the test structure to characterize its fixed base and isolated response, and then the frame was subjected to simulated ground motions from a variety of earthquakes. To a varying degree for each signal, the isolation system limited the accelerations transmitted to the frame and reduced the amplification of accelerations toward the top of the frame that is typical in conventional fixed-base structures. Measured interstory drifts were below levels likely to cause serious damage to structural or nonstructural components. The sliding displacements in the bearings were smaller than predicted by previous analyses because the measured coefficient of friction during the shake table tests was larger than that predicted by the material properties. The frequency response of the test frame was highly dependent on the characteristics of the input signal. In general, the bearings tended to spread the input energy over several modes and a wide range of frequencies for each mode. Attempts to develop an equivalent linearized model for the isolated structural system were unsuccessful because of the highly nonlinear transition between the fixed and sliding phases of the R-FBI bearings. Comparisons were made with results from previous earthquake simulator tests of the same steel test frame founded on various rubber bearing isolation systems.

ACKNOWLEDGEMENTS

This research was conducted at the Earthquake Engineering Research Center of the University of California at Berkeley supported by grant number CES-8702724 from the National Science Foundation under a subcontract from the University of Utah. This support is greatly appreciated.

The authors also extend their gratitude to colleagues and staff at the Earthquake Engineering Research Center for their invaluable assistance, in particular Ian Aiken, Andrew Whittaker, Doug Nims, Eduardo Miranda, Kent Sasaki, and Don Clyde.

TABLE OF CONTENTS

ABSTRACT i

ACKNOWLEDGMENTS ii

TABLE OF CONTENTS iii

LIST OF TABLES v

LIST OF FIGURES vi

1. INTRODUCTION 1
   - 1.1 Background 1
   - 1.2 Frictional Isolation Systems 2
   - 1.3 Resilient-Friction Base Isolator 4

2. EXPERIMENTAL MODEL AND TEST FACILITIES 6
   - 2.1 Test Facilities 6
   - 2.2 Five Story Frame Model 7
   - 2.3 Instrumentation of the Model 7
   - 2.4 Data Acquisition 8

3. EXPERIMENTAL PROGRAM 9
   - 3.1 General 9
   - 3.2 Free Vibration Pull-Back Tests 9
   - 3.3 White Noise Tests 10
   - 3.4 Harmonic Motion Tests 10
   - 3.5 Earthquake Simulator Tests 11

4. DISCUSSION OF EARTHQUAKE SIMULATOR RESULTS 12
   - 4.1 Response to Horizontal Ground Motions 12
     - 4.1.1 Acceleration Response 12
     - 4.1.2 Displacement Response 13
     - 4.1.3 Base Shear Response 16
     - 4.1.4 Interstory Drift 17
     - 4.1.5 Frequency Response 17
   - 4.2 Response to Combined Horizontal and Vertical Ground Motions 19

4.3 Response with and without Steel Rods in Central Rubber Core 19
4.4 Individual Bearing Response 20
4.5 Stability of R-FBI Bearings 22
4.6 Equivalent Linearization 22

5. COMPARISON WITH PREVIOUS ELASTOMERIC BEARING TESTS 24
5.1 Background 24
5.2 Acceleration Response 25
5.3 Hysteretic Response 27
5.4 Interstory Drift 27
5.5 Frequency Response 28
5.6 Discussion 30

6. SUMMARY AND CONCLUSIONS 32

REFERENCES 35

TABLES 37

FIGURES 48

APPENDIX 139

LIST OF TABLES

Table		Page
1	R-FBI Test Log	38
2	History of Absolute and Relative Bearing Offsets	41
3	Maximum Shear in Bearings with and without Center Steel Rod	42
4	Maximum Base Accelerations with and without Center Steel Rod	42
5	Maximum Bearing Displacements with and without Center Steel Rod	43
6	Comparison between R-FBI Earthquake Simulator Tests and Rubber Bearing Earthquake Simulator Tests	44

LIST OF FIGURES

Figure		Page
1	The Resilient-Friction Base Isolator	50
2	Section Through the Isolator	51
3	Dimensions of Rubber Core and Steel Rod	52
4	Dimensions of Sliding Plates and Teflon Rings	53
5	Dimensions of Base Plates and Shear Keys	54
6	Dimensions of Cover Plates	54
7	One-Third Scale Structural Model Showing Main Dimensions and Isolation Mounting	56
8	Test Frame Mounted on R-FBI Bearings	57
9	Fourier Spectra for First Snapback Test	58
10	Fourier Spectra for Second Snapback Test	59
11	Displacement and Acceleration Time Histories and Fourier Acceleration Spectra for Random Noise, span = 600	60
12	Fourier Spectra for Random Noise, span = 600	61
13	Displacement and Acceleration Time Histories and Fourier Acceleration Spectra for Chile, span = 800	62
14	Displacement and Acceleration Time Histories and Fourier Acceleration Spectra for El Centro, span = 600	63
15	Displacement and Acceleration Time Histories and Fourier Acceleration Spectra for Mexico City, span = 900	64
16	Displacement and Acceleration Time Histories and Fourier Acceleration Spectra for Olympia, span = 1000	65
17	Displacement and Acceleration Time Histories and Fourier Acceleration Spectra for Pacoima Dam, span = 800	66
18	Displacement and Acceleration Time Histories and Fourier Acceleration Spectra for Parkfield, span = 600	67
19	Displacement and Acceleration Time Histories and Fourier Acceleration Spectra for San Francisco, span = 600	68
20	Displacement and Acceleration Time Histories and Fourier Acceleration Spectra for Taft, span = 800	69
21	Vertical Displacement and Acceleration Time Histories and Fourier Acceleration Spectra for Chile, sph = 500, spv = 1000	70
22	Vertical Displacement and Acceleration Time Histories and Fourier Acceleration Spectra for San Francisco, sph = 500, spv = 1000	71

23	Normalized Accelerations Throughout Test Frame for Chile	72
24	Normalized Accelerations Throughout Test Frame for El Centro.	73
25	Normalized Accelerations Throughout Test Frame for Mexico City	74
26	Normalized Accelerations Throughout Test Frame for Olympia	75
27	Normalized Accelerations Throughout Test Frame for Pacoima Dam	76
28	Normalized Accelerations Throughout Test Frame for Parkfield	77
29	Normalized Accelerations Throughout Test Frame for San Francisco	78
30	Normalized Accelerations Throughout Test Frame for Taft	79
31	Relative Bearing Displacement Time Histories for Chile	80
32	Relative Bearing Displacement Time Histories for El Centro	81
33	Relative Bearing Displacement Time Histories for Mexico City	83
34	Relative Bearing Displacement Time Histories for Olympia	85
35	Relative Bearing Displacement Time Histories for Pacoima Dam	87
36	Relative Bearing Displacement Time Histories for Parkfield	88
37	Relative Bearing Displacement Time Histories for San Francisco	89
38	Relative Bearing Displacement Time Histories for Taft	90
39	Superposed Frame Accelerations for Mexico City, span = 900	92
40	Superposed Frame Accelerations for Pacoima Dam, span = 800	93
41	Plot of Maximum Bearing Displacement vs. Earthquake Simulator Span Setting	94
42	Plot of Normalized Maximum Bearing Displacement vs. Earthquake Simulator Span Setting	95
43	History of Relative and Absolute Offsets After Each Test	96
44	Hysteretic Behavior for Chile, span = 900	97
45	Hysteretic Behavior for El Centro, span = 600	98
46	Hysteretic Behavior for Mexico City, span = 900	99
47	Hysteretic Behavior for Olympia, span = 1000	100
48	Hysteretic Behavior for Pacoima Dam, span = 800	101
49	Hysteretic Behavior for Parkfield, span = 600	102
50	Hysteretic Behavior for San Francisco, span = 600	103
51	Hysteretic Behavior for Taft, span = 800	104
52	Interstory Drift Index Envelopes for the Maximum Span Test of each Earthquake Signal	105
53	Fourier Spectra of Frame Accelerations for Chile, span = 900	106
54	Fourier Spectra of Frame Accelerations for El Centro, span = 600	107
55	Fourier Spectra of Frame Accelerations for Mexico City, span = 900	108
56	Fourier Spectra of Frame Accelerations for Olympia, span = 1000	109
57	Fourier Spectra of Frame Accelerations for Pacoima Dam, span = 800	110
58	Fourier Spectra of Frame Accelerations for Parkfield, span = 600	111
59	Fourier Spectra of Frame Accelerations for San Francisco, span = 600	112
60	Fourier Spectra of Frame Accelerations for Taft, span = 800	113

61	Normalized Accelerations Throughout Test Frame for Chile	114
62	Normalized Accelerations Throughout Test Frame for San Francisco	115
63	Relative Bearing Displacement Time Histories for Chile	116
64	Total Base Shear Time Histories for Chile	117
65	Relative Bearing Displacement Time Histories for San Francisco	118
66	Total Base Shear Time Histories for San Francisco	119
67	Sliding Deformations Concentrated on One Sliding Plane	120
68	Sliding Deformations Distributed Evenly Across Bearing	120
69	Hysteresis Loops of Individual Bearings for Chile, span = 900	121
70	Hysteresis Loops of Individual Bearings for El Centro, span = 600	122
71	Hysteresis Loops of Individual Bearings for Mexico City, span = 900	123
72	Hysteresis Loops of Individual Bearings for Olympia, span = 1000	124
73	Hysteresis Loops of Individual Bearings for Pacoima Dam, span = 800	125
74	Hysteresis Loops of Individual Bearings for Parkfield, span = 600	126
75	Hysteresis Loops of Individual Bearings for San Francisco, span = 600	127
76	Hysteresis Loops of Individual Bearings for Taft, span = 800	128
77	Response Network for El Centro, span = 600	129
78	Comparison Between Calculated and Recorded Base Acceleration and Displacement Time Histories	130
79	Displacement and Acceleration Time Histories and Fourier Acceleration Spectra of Taft Signal During Rubber Bearing Test Series, span = 350	131
80	Displacement and Acceleration Time Histories and Fourier Acceleration Spectra of Taft Signal During R-FBI Test Series, span = 350	131
81	Normalized Accelerations Throughout Test Frame with Different Base Conditions for Taft, span = 350 and 800	132
82	Hysteretic Behavior with Different Base Conditions for Taft, span = 350	133
83	Interstory Drift Index Throughout Test Frame with Different Base Conditions for Taft, span = 350	134
84	Fourier Spectra of Frame Accelerations Supported on Rubber Bearings with Veriprene Inserts, Taft span = 350	135
85	Fourier Spectra of Frame Accelerations Supported on Rubber Bearings with Adiprene Inserts, Taft span = 350	136
86	Fourier Spectra of Frame Accelerations Supported on Rubber Bearings with Lead Plugs, Taft span = 350	137
87	Fourier Spectra of Frame Accelerations Supported on R-FBI Bearings, Taft span = 350	138

1. INTRODUCTION

1.1 Background

Base isolation is an earthquake-resistant design strategy which separates a structure from the damaging horizontal ground motions of large earthquakes. The main feature of an isolation system is a horizontally flexible foundation which prevents the transmission of lateral earthquake energy upward into the superstructure. In addition, some form of energy dissipation or damping is usually provided to limit lateral deflections at the isolation interface. Although this technique was first proposed in the early 1900s it has only recently been applied to full-scale building construction as new materials that can provide sufficient horizontal flexibility while maintaining vertical stiffness have become available. For example, base isolation bearings made up of alternating layers of steel and natural rubber are now in use in several structures in the United States and more than thirty structures in Japan. In these isolators the rubber layers can provide lateral flexibility to accommodate large shear strains while the embedded steel plates prevent the rubber from distorting horizontally and ensure vertical stiffness.

The most elementary application of base isolation is to detach a structure completely from its foundation, allowing it to slide freely during horizontal ground motion. In this configuration energy can only be transferred to the superstructure through the friction force developed between the moving structure and its base. Several test structures using this principle have been built in China in the wake of the 1976 Tangshan earthquake, and frictional components have been incorporated in several other isolation systems. An isolation bearing based on this concept is the Resilient-Friction Base Isolator (R-FBI) which was developed by Naser Mostaghel of the University of Toledo, while at the University of Utah. In the R-FBI system alternating layers of stainless steel and teflon provide slip planes between the base and the superstructure while maintaining a large vertical stiffness. A hard rubber core in the center of the bearing provides a lateral restoring force to ensure that adjacent plates do not slide off each other. An illustration of a typical isolator is provided in Figure 1.

This report summarizes tests of the R-FBI system performed on the shaking table at the Earthquake Simulator Laboratory of the Earthquake Engineering Research Center (EERC), University of California at Berkeley. An experimental program was developed to test the effectiveness of the R-FBI system under moderate-to-severe earthquake ground motions and to assess the reliability of analytical procedures used to predict the dynamic characteristics of structures founded on the R-FBI system. Earthquake signals similar to those used in previous shake table tests of the same test frame founded on rubber bearings, were also included so that comparisons could be made between the performances of the different isolation systems.

1.2 Frictional Isolation Systems

A significant amount of the recent research in base isolation has focussed on the use of frictional components to concentrate flexibility in the foundations of structural systems and to add damping to isolated structures. Frictional isolation systems have two desirable characteristics which are not found in conventional rubber bearing systems. First, because the friction force developed at any bearing is proportional to the mass supported by that bearing, there is no eccentricity between the center of mass of the superstructure and the center of stiffness of the isolation system. This means that even if the mass distribution in the structure is different from that which is assumed in the original design, the effects of torsion at the foundation level are diminished. The second advantage of frictional systems is their performance over a wide range of input frequencies. Although a structure supported on rubber isolators will have a fundamental frequency much lower than if it were fixed-base, a low frequency ground motion may still drive such an system into resonance. This makes rubber isolators inappropriate for regions where the major part of the earthquake energy is concentrated in the low frequency range. However, frictional isolators have no characteristic frequency and can effectively dissipate energy over a wide range of input frequencies with no risk of resonance with the ground motion. This makes frictional systems practical for use in soft soil regions such as Mexico City.

Several different frictional isolation systems are used today in a variety of structures around the world, and many more have been proposed. One of the first to be implemented was in the Chinese

project noted above in which four full-scale brick buildings, one a four story dormitory building at the Seismological Observatory in Beijing, were constructed with a thin layer of sand separating them from their foundations. These isolated structures are designed to remain fixed relative to an external reference frame by sliding on the sand layer as the ground moves underneath during strong ground motion. Although the structures were intentionally constructed poorly to represent typical construction quality in the region, simulated earthquake tests on one of these buildings using explosively generated ground motions showed that the building avoided collapse by sliding on the sand base [1].

An isolation system already implemented in a nuclear power plant in Kroeberg, South Africa contains a sliding plane made of lead bronze and stainless steel plates on top of conventional laminated neoprene isolation bearings. This two-component design protects against small earthquakes by concentrating deformations in the neoprene bearings. During larger earthquakes, which may cause forces and deformations too large for the neoprene bearings to withstand, the bronze and steel plates are intended to slide and dissipate energy. A coefficient of friction of 0.20 was used in the design of these plates so that the maximum lateral force transferred to the superstructure during a severe earthquake will ideally be only 20 percent of the total weight of the structure [2].

Studies several years ago at the Earthquake Simulator Laboratory of the EERC examined the use of steel beams in parallel with a laminated rubber and steel isolation system as a combination friction damper and fail-safe device. Because the natural rubber and steel bearings undergo vertical displacement as they are strained horizontally, a structure supported on these bearings will drop slightly during peak displacement cycles. By placing a steel beam several millimeters underneath the support beam of the superstructure in its undeformed configuration, frictional restoring forces can be applied to the superstructure as horizontal displacement increases. Furthermore, the underlying steel beam serves as a fail-safe system to catch the superstructure if the bearings become unstable under excessive displacements. Tests showed that this system performed as expected in both reducing peak displacements and protecting against collapse of the frame. However, because the friction forces at the base of the frame change direction instantaneously with change in the direction of the movement, high frequency vibrations which could be undesirable in buildings containing sensitive equipment or piping are transferred

to the structure [3].

Much of the recent research into the application of frictional components in base isolation systems has concentrated on the use of teflon because of its low coefficient of friction which increases with increasing sliding velocity. Experimental studies within the last several years have comprehensively established the dynamic properties of teflon sliding in contact with stainless steel and have investigated how the coefficient of friction of such interfaces varies with contact pressure, sliding velocity and acceleration, frequency of excitation, and surface finish of steel and teflon. Mathematical models have also been developed which can predict the coefficient of friction for a wide range of conditions [4]. Of particular interest for earthquake engineering applications is the dependence on sliding velocity. It has been shown that for the range of velocities and bearing pressures anticipated in isolation systems incorporating pure teflon and polished stainless steel interfaces, the coefficient of friction is less than 0.20 [4,5].

One isolation system which incorporates a teflon and stainless steel interface in a pendulum-shaped slider is the Friction Pendulum System (FPS). Tests on the Earthquake Simulator at the EERC using four different structures with varying aspect ratios and eccentricities demonstrated the effectiveness of this system for resisting strong ground motion and dissipating energy. Long term cyclic tests using the FPS connection also showed that the teflon surface has the durability to withstand the equivalent of 144 El Centro earthquakes without deterioration of its dynamic characteristics [6].

1.3 Resilient-Friction Base Isolator

The Resilient-Friction Base Isolator has been designed to take advantage of the favorable properties of teflon sliding in contact with stainless steel. R-FBI bearings use alternating plates of stainless steel and teflon surrounding a cylindrical core of hard rubber to carry the vertical and horizontal components of the foundation force separately. While the steel and teflon plates take all of the vertical force, the central rubber core contributes only a horizontal restoring force as it shears during strong earthquake motion. This uncoupling of the force response contrasts with isolation systems using

rubber bearings which must simultaneously provide horizontal flexibility and vertical stiffness in a single laminated steel and rubber bearing. The teflon and stainless steel interface in the R-FBI system also acts as a structural fuse to resist small levels of horizontal load (e.g. wind loading or small earthquakes). During moderate-to-severe earthquake loads adjacent teflon and steel layers dissipate energy by sliding while the core limits the relative displacements.

Analysis of structures on the R-FBI system is given in References 7 and 8, and preliminary tests have been performed on individual isolators to quantify their dynamic properties. The isolators used in the present series of experiments were designed using the procedure outlined in Reference 9 in which the following assumptions were made:

seismic intensity, ZNS=0.4

friction coefficient between teflon and steel, μ=0.06, and

isolator seismic coefficient, C=0.1.

This last parameter, chosen by the designer, should limit the lateral force transmitted to the superstructure to 10 percent of the weight of the structure.

Shop drawings showing the final dimensions of the bearings used in these tests are given in Figures 2 through 6. Each of the four bearings supports 20,000 pounds, and each teflon ring has a surface area of 28.89 square inches. The resultant normal stress on the teflon is 707 psi. The friction coefficient predicted by the material properties is 0.06 as required by the design assumptions, for the given expected sliding velocity between any teflon-steel interface of 0.44 inches/second.

2. EXPERIMENTAL MODEL AND TEST FACILITIES

2.1 Test Facilities

The shaking table of the Earthquake Engineering Research Center of the University of California at Berkeley measures 20 ft × 20 ft (6.1 m x 6.1 m) in plan and can support test structures weighing up to 100 kips (444.8 kN). Simulated earthquake motions can be applied vertically and in one horizontal direction with maximum accelerations of 1.0g vertically and 1.5g horizontally.

The shaking table is a heavily reinforced post-tensioned concrete slab 1 ft thick driven by three 50 kip (22.4 kN) actuators in the horizontal direction and four 25 kip (11.2 kN) actuators vertically. During testing a chamber beneath the table is filled with compressed air to carry both the 100 kip (44.8 kN) dead weight of the table and the weight of the model so that the vertical actuators apply only the seismic accelerations and do not carry gravity load. The table is controlled in two translational degrees of freedom (one horizontal and one vertical) as well as three rotational degrees of freedom (pitch, roll, yaw). Displacement in the transverse direction is restricted by a sliding mechanism.

The table is displacement controlled with a horizontal displacement limit of ± 5 in. (± 127 mm) and a vertical displacement limit of ± 2 in. (± 50.8 mm). The extreme displacement for a particular record is prescribed by the span setting where a span of 1000 corresponds to a horizontal displacement of 5 inches or a vertical displacement of 2 inches. Smaller spans produce proportionally smaller peak displacements.

To reproduce earthquake time histories a given acceleration record must first be integrated to produce a digitized displacement time history. This signal is then passed through a *Preston* D/A converter which converts the digitized signal to an analog signal. An *MTS* controller uses this analog signal to generate the table displacement command signal for the translational degrees of freedom while the rotational degrees of freedom are held fixed. A more detailed discussion of the operating characteristics of the shake table is given by Rea and Penzien [10].

2.2 Five Story Frame Model

The test structure used in this study is a five story steel frame previously tested using natural rubber and neoprene isolation bearings [3,11]. The frame has three bays in the direction of shaking with cross bracing only in the center bay of the first floor. The single bay in the transverse direction is heavily stiffened with double angles to minimize out-of-plane motion. This design is intended to represent at one-third scale a section of a steel frame in the weak direction. The entire structure is mounted on a heavy base made of two 16WF girders connected by 8WF cross beams and rests on four R-FBI bearings with load cells underneath. The load cells are in turn connected to the shaking table by high-tension stress rods. Figure 7 shows the details of the frame.

The scaling used for shake table tests is based on constant stress so that accelerations in the model are the same as in the prototype. The five story frame is assumed to be a one-third scale model so that the time scale factor is $\sqrt{3}$ for both the excitation and the response. The applied dead load must produce stress levels equal to those in a full-scale frame. This dead load is supplied by concrete blocks bolted to the frame at different floor levels. The total weight of the blocks is 72 kips (320.26 kN) so that the total weight of the structure is approximately 80 kips (355.84 kN). Figure 8 shows the complete frame with dead load on the shaking table.

2.3 Instrumentation of the Model

Fifty-five channels of data were recorded during each test to measure the response of the combined shake table-structure system. A complete list of the instrumentation used is given in the Appendix. The goal was to measure the following four components of response:

- Earthquake Simulator Response: Ten channels of data recorded shake table displacement and acceleration time histories both horizontally and vertically as well as accelerations in the pitch (x-z plane) and roll (y-z plane) directions. Table acceleration in the twist (x-y plane) direction was not recorded because of a malfunction in the signal conditioner for Channel 7.
- R-FBI Bearing Response: Displacement transducers on top of the southeast and southwest bearings measured the relative top-to-bottom bearing displacements in the direction of shaking while

displacement transducers on the southwest and northwest bearings measured the relative transverse bearing displacements. Load cells under all four bearings measured shear and moment in the direction of shaking.

- Frame Response: Displacement transducers mounted on a reference frame adjacent to the south end of the shake table measured absolute displacements of the base and all five floors of the frame. Displacements relative to the table could then be calculated by subtracting the table displacement from these measurements. Accelerometers were mounted on the southeast and southwest corner columns of the frame at the base and at each floor level to measure accelerations in the direction of shaking. Additional accelerometers were also placed at the southwest and northwest corners of the fifth floor to measure accelerations in the transverse direction and on top of each of the corner columns to measure vertical accelerations.
- Oscillator Response: Three single-mass oscillators were mounted on the frame and instrumented with accelerometers to capture any high frequency vibrations transmitted to the frame through the isolators. These oscillators were tuned to the first three natural frequencies of the fixed-base frame. Oscillators 1 and 2 were mounted on the roof and Oscillator 3 was mounted on the second floor.

2.4 Data Acquisition

The data acquisition system at the Earthquake Simulator Laboratory is centered around a VAX 11-750 mainframe computer. First, *Pacific* signal conditioners power the instrumentation and filter out frequencies above 100 Hz in the analog signal. A *Preston* multiplexer is then used to sample up to 128 channels of data simultaneously with a frequency of up to 400 samples per second. Analog signals from the multiplexer are fed to a *Preston* A/D (analog-to-digital) converter to produce digitized data. Finally, this data is temporarily stored on magnetic disc before being transferred to tape. Maximum and minimum values from each of the instruments are available immediately after each run to check that all channels are operating correctly.

3. EXPERIMENTAL PROGRAM

3.1 General

The base isolated test structure was subjected to four groups of tests: free vibration pull-back tests, white noise input tests, harmonic motion tests, and simulated earthquake ground motion tests. A log of the entire testing program is given in Table 1.

3.2 Free Vibration Pull-Back Tests

The first tests on the base isolated structure were pull-back tests in which a chain attached to the second floor of the frame was tensioned to introduce an initial deformation in the bearings and then quickly cut to set the frame into free vibrations. The purpose of this type of test is to identify the natural frequencies and corresponding mode shapes and damping ratios of the isolated system by examining the peaks in the Fourier spectra calculated using the Fast Fourier Transform (FFT) algorithm and shown in Figures 9 and 10. During the pull-back tests the table is locked and, thus, interaction between the table and the model is avoided. However, in the R-FBI tests only the properties of the fixed-base frame could be determined because without the steel rods in the rubber core the bearings remained in their deformed configuration during free vibration, and the lateral shear forces were carried by static friction. During the tensioning process the bearings had deformed across only one or two plates, resulting in local strain concentrations in the central rubber cores, yet the rubber did not provide sufficient restoring force to eliminate the deformations when the chain was cut. If the steel reinforcing rods were included in the rubber cores during this series of tests it is possible that they may have contributed enough stiffness to recenter the bearings after the initial deformations. This possibility was not explored so that these tests gave data only for the fixed base structure which was used for comparisons with later tests in which the bearings deformed under ground motion.

3.3 White Noise Tests

The second portion of the testing program used a random earthquake signal with a broad-band Fourier spectrum to identify the response of the structure and the isolation system further. The table displacement and acceleration time histories as well as the Fourier spectrum of the table acceleration for the highest intensity signal in the series (span 600) are shown in Figure 11. For the low intensity motions (span 200 and 300) the maximum deformation across the bearings was insignificant (0.0087 inch), and the frame response was predominately fixed base. The results from these tests were combined with the results from the snapback tests described above to identify the first three fixed base frequencies at approximately 3.6, 10.7, and 15.9 Hz.

During the span 600 test the isolation system was fully activated and the maximum deformation across the bearings was larger (0.083 inch) although still relatively small compared with the design displacement. While isolation systems with rubber bearings distinctly shift the fixed base frequencies of the supported structure toward the higher end of the frequency spectrum, specific identification of the isolated frequencies of the test frame on the R-FBI system is difficult. The Fourier spectra of the accelerations throughout the frame in Figure 12 show that the majority of the energy transmitted to the structure is at the same frequency as the peak in the input signal — approximately 3.1 Hz. Significant energy is also contained in the first fixed base mode at a frequency of 3.6 Hz, but distinct frequency peaks above this are not evident. This tendency for the R-FBI system to spread energy evenly across a wide range of frequencies is seen repeatedly in the shake table tests.

3.4 Harmonic Motion Tests

The frame was next subjected to sinusoidal ground motions at frequencies of 2.4 Hz, 2.6 Hz, and 2.8 Hz with various span settings to examine the response of the model to harmonic ground motions. Although a sweep of sinusoidal tests across a wide range of frequencies would be ideal, it was decided to use only this small range of frequencies to save time and try to identify a local trend in the displacement response as the frequency was increased. For a constant span, the peak relative bearing displacement increased with increasing frequency. This is not surprising since an increase in

the frequency of the signal at a constant table displacement implies an increase in the peak table acceleration. However, as larger span signals were used the increase in bearing displacement was not linear with the increase in table displacement. This implies that while the isolation system isolates accelerations more effectively for higher frequency inputs, it does so without a proportional increase in displacement.

3.5 Earthquake Simulator Tests

Finally, the base isolated structure was subjected to ground motions time-scaled by $\sqrt{3}$ from the following eight earthquakes:

- May 18, 1940 El Centro Earthquake, S00E Component
- April 13, 1949 Olympia Earthquake, N86E Component
- July 21, 1952 Taft Earthquake, S69E Component
- March 22, 1957 San Francisco Earthquake (Golden Gate Park), S80E Component
- June 27, 1966 Parkfield Earthquake, N65E Component
- February 9, 1971 Pacoima Dam Earthquake, S16E Component
- March 3, 1985 Llolleo (Chile) Earthquake, N10E Component
- September 19, 1985 Mexico City Earthquake (SCT), Calculated N60E Component

This test program was designed to subject the isolated structure to a variety of earthquakes ranging from relatively high frequency (El Centro) to low frequency (Mexico City) motions. The recorded table displacements and acceleration time histories as well as the Fourier acceleration response spectra for the maximum amplitude tests of each ground motion are shown in Figures 13 through 20.

Tests combining vertical and horizontal ground motions recorded during the San Francisco and Llolleo earthquakes were also conducted to study the influence of vertical ground motion on the isolation system. Plots of the vertical component of the table displacement and acceleration time history and the Fourier spectrum of the vertical acceleration for each of these tests are shown in Figures 21 and 22.

4. DISCUSSION OF EARTHQUAKE SIMULATOR RESULTS

4.1 Response to Horizontal Ground Motions

In general the R-FBI system performed well in isolating the test structure from the simulated earthquake ground motions. For the majority of the earthquake inputs the maximum acceleration recorded in the frame was less than 1.5 times the peak table acceleration, and at no time did the fifth floor acceleration exceed 1.32 g. The interstory drifts measured during the most severe tests remained below 0.5 percent, although during lower intensity tests the isolation system was not fully activated and these drifts were larger. The relative bearing displacements and base shear forces were limited to maximums of 4.5 inches and 18 kips, respectively. For the 80 kip test structure this implies a peak base shear coefficient of approximately 0.23. In most of the tests the measured coefficient of static friction was no greater than about 0.15. However, since the coefficient assumed in the design and preliminary analysis of the bearings was 0.06, the measured bearing displacements were generally lower and the base accelerations higher than those predicted by analysis. The overall effect of the larger friction coefficient was to reduce the effectiveness of the isolation system during low intensity tests while enhancing its performance during the severe tests by keeping the bearing displacements at manageable levels.

4.1.1 Acceleration Response

Figures 23 through 30 show for each earthquake record and for a wide range of span settings the distribution of maximum accelerations throughout the test frame, normalized to the peak table acceleration. Although an increase in span implies an increase in peak table acceleration, for each series of earthquake signals the relative accelerations in the frame tend to decrease with increasing span. For example, the response to the series of El Centro signals with spans 100 through 600 summarized in Figure 24 shows that the highest relative accelerations occurred during the test with the span equal to 100 and the lowest during the 600 span test. Higher intensity tests using other long duration signals such as Mexico City, Taft, and Olympia produced comparable reductions in relative

accelerations. However, the reduction was not as great in the records with short high-energy pulses such as San Francisco and Pacoima Dam because the table accelerations associated with their sharp pulses were sufficient to overcome the static friction of the bearings even at low spans. This allowed the isolation system to absorb the earthquake energy at the lower span settings for these signals as effectively as in the higher intensity tests.

4.1.2 Displacement Response

Because the transition between the fixed and sliding phases of the R-FBI system is inherently nonlinear, the relative bearing displacement response to a random earthquake acceleration time history is highly dependent on the characteristics of the record. The shake table tests showed a tendency for the displacement response of the combined frame and isolation system to alternately drift and then oscillate about a fixed displaced location. The onset of the sliding and the magnitude of the bearing displacement during any particular deformation cycle were very unpredictable because of variations in the intensity, duration, and frequency content of the earthquake signal.. In some cases the same earthquake at different magnitudes resulted in significantly different bearing displacement time histories because in each test the frame was in a different displaced condition when a high-energy pulse hit. Other signals produced very similar time histories from one intensity test to the next because the higher energy acceleration pulses were sufficiently separated from each other for the frame to finish responding to one pulse before the next hit. While the displacement response was generally nonlinear, for many of the signals the maximum relative displacement of the bearings was found to be approximately proportional to the maximum table displacement.

Figures 31 through 38 illustrate the variation in the relative bearing displacement time histories for each of the earthquake signals over a range of span settings. The Pacoima Dam, Parkfield, and San Francisco records are essentially single-pulse ground motions, and the displacement time histories from the high intensity tests using these signals are very similar to the same time histories from the low intensity test runs. Also, the maximum and minimum displacements occur at the same instant regardless of span. This is because the bearings undergo significant deformation only during and

immediately after the strongest pulse in each earthquake as the base shear builds up almost instantaneously and then dissipates just as suddenly as the bearings slide. The table motion after the time of the maximum acceleration is typically not strong enough to produce a base shear greater than the static friction in the bearings, and the energy input into the structure is subsequently dissipated only through conventional viscous damping.

The displacement responses to the longer duration, broad-banded Chile, El Centro, Olympia, and Taft earthquakes are much more dependent on span (or intensity). For each different test of these signals the times of the maximum and minimum displacements are different, and the relationship between any two response peaks is not predictable. For example, the displacements during the Olympia signal at 200 and 400 span reach their minima at approximately 11 seconds and their maxima at about 13 seconds while the same signal run at a span of 1000 yields a maximum and minimum at about 4.2 and 6.5 seconds, respectively. Furthermore, the alternately drifting and sticking deformations lead to very different displacement time histories because a signal run at one intensity may produce no bearing deformation at a certain instant, while a slightly stronger signal causes a slip at the same instant that affects the subsequent displacement time history. This is illustrated by comparing the displacement responses at about 4 seconds into the El Centro signal for the 400 and 500 span runs. The negative displacement at this instant in the 400 span test is smaller than that in the 500 span test and leads to a final offset of about 1 inch. The offset at the end of the 500 span test is negligible.

The displacement response of the structure to the Mexico City signal is unique because the table motion is essentially harmonic with a period of 1.16 seconds. As the intensity of the signal is increased the magnitude of the relative bearing displacement increases in the same fashion as for the single-pulse earthquake signals. Also, the displacement maxima and minima occur at the same time in each of the tests. However, the unique feature of the frame's response to the Mexico City signal is that it is almost entirely in the first isolated mode as shown by the in-phase acceleration time histories throughout the frame, illustrated in Figure 39. This contrasts with similar acceleration time histories from the Pacoima Dam record shown in Figure 40 which result from the contribution of many different vibrational modes.

Figure 41 illustrates the tendency for the maximum relative bearing displacement to increase as the span setting (or alternatively the maximum table displacement) of the earthquake simulator increases while Figure 42 shows a similar relationship using the peak bearing displacement normalized by the peak table displacement. The earthquake records with significant low frequency content such as Mexico City, Taft, and Pacoima Dam show an essentially linear increase in both normalized and absolute relative bearing displacement, whereas the responses to the predominantly high frequency signals are more unpredictable. For example, the response to the El Centro record has peaks and valleys in the normalized displacement response plot, and the Olympia record seems to result in a maximum displacement of about 1.5 inches for all tests with the peak table displacement above ± 2.5 inches. This implies that the response of the R-FBI system to low frequency ground motions could be assumed to be linear as a first approximation, probably because there is time for the sliding deformations of the bearings to stop during a low frequency acceleration pulse before the next pulse hits. Response to higher frequency ground motions, on the other hand, is highly nonlinear because the bearings do not stop sliding before the next acceleration pulse hits, and the displacement at the end of each pulse is not predictable. However, for all of the signals the peak normalized bearing displacement remains below 1.0. This implies that the peak ground displacement could be used in design as a conservative upper limit on the peak bearing displacement.

The offset of the bearings at the end of each test is an important parameter of the bearing response because there is concern that an earthquake with its energy concentrated in one direction could cause a friction isolation system to drift beyond its stability limit. In general, the offset after each of the earthquake signals used in the R-FBI shake table tests is random and does not depend on earthquake intensity. Figure 34 illustrates this randomness for the Olympia record over a range of intensities in which the strongest table motion occurs late in the record and causes the final offset to depend mainly on the deformation in the bearing at this time. The largest offset occurs at the end of the moderate intensity signal (span = 500) and decreases for the lower and higher intensity records. Similar results can be seen in the displacement time histories from the other earthquake records.

Figure 43 shows the residual offset in the bearings over a series of nineteen tests. Numerical values of the offsets are given in Table 2. The relative offset is based on the difference between the displacement at the end of each test and the displacement at the beginning of each test while the absolute offset is the displacement at the end of each test measured from the centerline of the undeformed bearings. The random nature of the offsets and the tendency of the system to recenter itself throughout a series of ground motions are evident. The implication is that the R-FBI system should be able to survive several consecutive shocks without loss of stability.

4.1.3 Base Shear Response

Figures 44 through 51 give time histories of total base shear and relative base displacement as well as the base shear-displacement hysteresis loops from the maximum intensity test of each earthquake signal. The time history plots clearly show that the times of the largest relative base motion coincide with the times at which the base shear reaches its local peaks. Furthermore, the base shear stays approximately constant until the bearing movement stops. On the other hand, as the base shear changes the bearing displacement remains fixed. This slip-stop movement is characteristic of a friction system.

The rectangular hysteresis plots with rounded corners are also typical for a friction system and illustrate the ability of the R-FBI system to absorb large amounts of energy during a single displacement cycle. The static friction coefficient of the bearings is between 0.10 and 0.20 for all of the tests and is usually less than or equal to 0.15 for deformation cycles within ±1 inch. After the onset of sliding the bearing stiffness changes to approximately 0.9 kip/inch and seems to remain constant regardless of the magnitude of the relative displacement during each loop. This stiffness comes partly from the stiffness of the central rubber core and partly from the sliding friction in the isolators, which theoretically varies with sliding velocity. Since the duration of each loop is approximately the same but the relative displacements vary, the relative bearing velocity during some loops should be larger than in others. Although this implies that the sliding stiffnesses should also be larger, in each of the tests the sliding stiffness is approximately constant. The conclusion is that the relative bearing

velocity does not affect the coefficient of friction in the R-FBI bearings as much as predicted by previous studies.

4.1.4 Interstory Drift

The relative displacement between consecutive floors of a building is generally regarded as one indication of the degree to which a structure and its nonstructural components will be damaged during an earthquake. The interstory drift index is the ratio of the relative floor displacement to the story height. Drifts of 1.5-2.0 percent are considered likely to cause damage in typical structural systems. Figure 52 shows the maximum interstory drift index at each level of the test frame for the maximum intensity earthquake inputs. It should be noted that for these severe ground motions the maximum interstory drift at any point in the frame is never greater than 0.5 percent. This implies that the frame is within its elastic range during all of the tests, and in an actual building nonstructural components would suffer minor damage, if any. Normally the interstory drift in a moment-resisting frame would be maximum at the first floor and decrease toward the roof, but in this case the lowest drift is at the first floor because the frame is braced in its first floor center bay. However, the drift is almost constant above the first floor for many of the tests (Chile, Mexico City, Olympia, Parkfield), while it is irregularly distributed in others (Pacoima, San Francisco, Taft). A constant distribution is desirable because it implies that the elastic strain energy is distributed evenly throughout the height of the frame. For the signals with such a distribution the maximum drift remains less than 0.4 percent. The irregular distributions are probably due to the influence of higher modes in the response, especially for the impulsive Pacoima Dam and San Francisco records and to a lesser extent for the Taft record. However, this effect is not necessarily bad because even for these records the interstory drift is always less than 0.5 percent which should not cause significant damage.

4.1.5 Frequency Response

Although the stick-slip nature of the R-FBI bearings makes exact calculation of the frequencies and mode shapes of the isolated structural system impossible because of their dependence on the

characteristics of the input ground motion, bounds for the frequency response of the isolated structure during its sliding phases can be found. Figures 53 through 60 show Fourier spectra of the story accelerations throughout the frame for the maximum span test of each ground motion. In the frequency range where the fundamental mode of the isolated system is expected — between 0 and 2 Hz — each of the Fourier spectra has the same general shape as the spectrum of the corresponding ground motion. This illustrates the adaptive nature of the first mode response of the system, and points out the difficulties in finding the fundamental frequency of the isolated structure because the energy contained in the first mode is transferred to higher modes. The second and third frequencies of the isolated structure appear more readily at approximately 6.5 and 14 Hz, respectively, depending on the earthquake. For example, the Fourier spectra from the Mexico City signal give easily interpreted results because of the lack of high frequency energy in the Mexico City record and show distinct peaks at approximately 6.5 and 14.2 Hz. The results from the other signals are more difficult to pinpoint but give comparable frequency values for the second and third modes of the isolated structure with values ranging between 5 and 7.5 Hz and 13 and 15 Hz, respectively. There is no significant amplification of the Fourier spectra at the frequencies of the fixed-base structure — 3.6, 10.7, and 15.9 Hz. Therefore, although the mode shapes of the isolated structure cannot be determined precisely, they are known to be different from those of the fixed-base frame.

The approximate measured frequency of the second mode can be compared with the theoretical value for a perfectly-isolated system given by the formula

$$\omega_s^* = \frac{\omega_s}{(1-\gamma)^{1/2}}$$

in which ω_s^* = frequency of the second mode of the isolated structure, ω_s = fundamental frequency of the structure if it were fixed-base, and

$$\gamma = \frac{L_1^2 M_1}{M+M_b}$$

where L_1 = participation factor for the fundamental mode in the fixed base structure, M_1 = first modal mass of the fixed base structure, and $M+M_b$ = total mass of the structure [12]. Given that the fundamental fixed-base frequency is 3.61 Hz, and calculating L_1, M_1, and $M+M_b$, the theoretical frequency

for the second mode of the structure is $\omega_s^* = 6.42$ Hz, very near that found from the acceleration spectra. This means that for some earthquake records — especially the Mexico City signal — the frequency response of the R-FBI system is very similar to that of a perfectly-isolated system.

4.2 Response to Combined Horizontal and Vertical Ground Motions

Because the R-FBI system is designed to distribute the horizontal and vertical loads to the central rubber core and the steel and teflon plates, respectively, the response of the combined frame and isolation system to simultaneous horizontal and vertical ground motions should be similar to the response to pure horizontal excitation. The shake table tests confirm this, and the accelerations in the frame, the relative bearing displacements, and the total base shears on the bearings during combined horizontal and vertical shaking are nearly equal to those measured under horizontal shaking alone.

Figures 61 and 62 show the distribution of accelerations throughout the frame for both pure horizontal table excitation and horizontal plus vertical excitation over a range of intensities for the Chile and San Francisco signals. The added vertical ground motion has no significant effect on the maximum horizontal accelerations in the frame, nor does it alter the individual floor acceleration time histories. Base shear and displacement time histories from the maximum horizontal intensity tests and the same tests including vertical motion, illustrated in Figures 63 through 66, also show no change in the bearing response when vertical ground motion is included. This uncoupling of the horizontal and vertical responses implies that time history analyses can be done separately for input in each direction, greatly simplifying the amount of analysis necessary.

4.3 Response with and without Steel Rods in Central Rubber Core

Tests up to and including 880816.15 studied the response of the R-FBI bearings without the steel rod in the central rubber core. In general, the bearing deformations during these tests were concentrated on one sliding surface at a time as shown in Figure 67, although many different sliding surfaces were activated during the course of each earthquake signal. While the mechanics of the core deformation is not known exactly, it is likely that these local deformations lead to strain

concentrations in the rubber which would accelerate the deterioration of the rubber cores over many displacement cycles. However, Figure 68 shows that after the steel rods were inserted the bearings spread the deformations evenly throughout their height. Because the movement in the first test series was not distributed across the height of the bearings the instantaneous sliding velocity at the point of deformation must have been larger than in the later tests. Furthermore, since the coefficient of kinetic friction for teflon in contact with stainless steel increases with increasing sliding velocity, the friction force developed in the bearings should have been greater than in the tests with rods in the bearing cores. Table 3 shows, however, that the maximum shear force does not vary a great deal between the tests with the central steel rod and those without it. Tables 4 and 5 show similar results for the peak base accelerations and base displacements and imply that the quantitative differences between the bearing response with and without the steel rods are negligible. Nevertheless, the steel rods should probably be included in any practical application of the R-FBI bearings because they enhance the stability of the system and inhibit localized deformations in both the rubber core and the sliders.

4.4 Individual Bearing Response

Although the shake table tests of the R-FBI system prove that the bearings effectively limit the transmission of lateral forces into the test frame, the bearings did not behave as anticipated on the basis of the previous analytical studies. The most significant difference was that the coefficient of friction measured during the tests ranged from 0.10 to 0.15, much higher than the assumed value of 0.06. A possible explanation for this large deviation is that the teflon became contaminated during the manufacturing process or that the stainless steel plates had a larger surface roughness than expected. When the bearings were disassembled to install the steel rods after the series of tests up to 880816.15 it was noticed that the sliding surfaces were covered with black residue from the rubber core which also may have increased the friction. However, after the surfaces were cleaned with freon the coefficient was not markedly lower in the following series of tests.

A further explanation for the increased coefficient of friction may lie in the dynamics of the isolator. Although the bearing is designed to deform uniformly throughout its height during its sliding

phases, it is possible that the sliding was concentrated on one plate at a time, even in the tests with the steel rod in the central rubber core. If this was true, the instantaneous velocity along each sliding surface would be much higher and would lead to a much higher friction coefficient. The force imbalance would be absorbed by local stress concentrations in the rubber core. Unfortunately this explanation cannot be checked with the data collected during these tests because measurements of the relative displacement time history across individual sliding surfaces were not taken.

Another unexpected result was that the response of the individual bearings varied greatly since two of the bearings showed a lower friction coefficient than the others. Figures 69 through 76 illustrate this problem for each of the signals run at maximum intensity, and although it is difficult to explain this behavior precisely there are several possible explanations. First, even though the bearings and test frame were carefully leveled during their erection, it is possible that an imbalance caused the bearings at the southwest and northeast corners to take more of the gravity load, leading to a lower coefficient of friction in those bearings. Another possibility is that the coefficient of friction is highly sensitive to dust particles and two of the bearings were inexplicably contaminated while the others remained clean. This is very unlikely because all of the surfaces were cleaned before the first test series and again at the time that the steel rods were inserted in the bearings. It is interesting to note, however, that the variation in the friction coefficients of the bearings did not affect the overall base shear response nor did it cause severe torsional motions in the frame. Either these effects were self-cancelling or were insignificant in the overall response. It can be concluded that the coefficient of friction between the teflon and stainless steel is difficult to determine exactly for individual bearings in a large building system because their bearing pressures cannot be determined exactly. Also, further study is needed to understand and to predict more accurately the variation of the coefficient of friction as well as the mechanics of the interaction between the rubber core and the sliding plates in the R-FBI bearings.

4.5 Stability of R-FBI Bearings

Previous studies have examined the stability of R-FBI bearings and provided a design displacement limit of approximately 4 inches for the bearings used in the R-FBI shake table tests [9,13]. However, the peak relative bearing displacement measured during the test series was 4.5 inches, and the hysteresis loop for this test shows no deterioration in stiffness near the peak displacement (Figure 46). Although a fail-safe mechanism was installed under the test frame to support the frame in the event the bearings overturned, repeated attempts to topple the bearings failed, and the fail-safe mechanism was never activated. This implies that the procedures for stability analysis and design are appropriate and provide a conservative stability limit, below which there is no adverse effect on the bearing response.

4.6 Equivalent Linearization

To simplify the design and analysis of structures founded on the R-FBI system it would be useful to develop equivalent linearization techniques so that standard linear response spectrum analyses could be performed on an equivalent system. Previous research at EERC on a base isolated bridge deck on rubber bearings used the conventional Kelvin model with a spring and a dashpot in parallel to calculate equivalent frequencies and damping values. This research showed good correlation between experimental and analytical displacement and acceleration time histories [14]. The linearization procedure involves calculating a network of spectral acceleration and displacement responses to a recorded table motion for a range of frequencies and damping ratios, and then identifying an equivalent frequency and a damping ratio which correspond to the measured peak base acceleration and displacement. A typical response network for the Maxwell model described below is shown in Figure 77.

Similar analyses were performed using the results of the R-FBI shake table tests with both the Kelvin and the Maxwell models. Note that the Maxwell model has an inherent advantage over the Kelvin model because it contains a spring and a dashpot in series which allow permanent deformations in the dashpot analogous to those found in the R-FBI system. Because of this configuration the

damping ratio in the Maxwell model is necessarily defined differently than in the standard Kelvin model [15]. Although the peak base acceleration and base displacement responses in the Maxwell model analyses are equal to those measured in the shake table tests (because of the way the model is defined), the calculated acceleration and displacement time histories are very different as shown in Figure 78. Unfortunately the Maxwell model fails to model the displacement response of the system because the drift in the model does not occur as rapidly as in the test structure. These analyses imply that for the inherently nonlinear R-FBI system standard equivalent linearization procedures do not suffice, and more thorough nonlinear analyses must be performed to predict the response of the system fully.

5. COMPARISON WITH PREVIOUS ELASTOMERIC BEARING TESTS

5.1 Background

A series of earthquake simulator tests were performed at EERC in 1981 to evaluate the performance of several rubber isolation systems using the same test frame that was used in the R-FBI study. Four natural rubber bearings with a variety of inserts supported the 80 kip frame as it was subjected to the El Centro, Pacoima Dam, Parkfield, and Taft earthquake signals. Each 8 inch × 8 inch bearing had a cylindrical hole in its center into which cores of three different materials were placed to add damping to the isolation system. In the first half of the tests the cores of all four bearings were either left empty or were filled with inserts of Veriprene or Adiprene. The remainder of the tests used two empty bearings in parallel with two bearings containing lead inserts. The combination of the empty bearings with the lead-rubber bearings was necessary because using lead plugs in all four of the rubber bearings would have substantially increased the lateral stiffness of the isolation system and reduced its effectiveness. The results of the rubber bearing tests and tests using the same frame with a fixed base are given in Reference 11. To varying degrees, each isolation system substantially reduced the response of the frame compared with the fixed-base tests.

Recently the shake table has undergone modifications which have altered its frequency response. In tandem with these modifications most of the earthquake signals have been altered to take advantage of the enhanced capabilities of the table with the result that not all of the previous signals may be reproduced exactly. A listing of the maximum table and frame responses (above the isolators) from the El Centro, Pacoima Dam, Parkfield, and Taft records for both the R-FBI and the rubber bearing tests is given in Table 6. For each test the equivalent peak acceleration (EPA) and equivalent peak velocity (EPV) of the shake table for 5 and 10 percent critical damping based on the ATC-3 recommendations [16] is also provided. The different base conditions for the rubber bearing tests are denoted by 50D, 50V, 50A, and 50/2L corresponding to the empty, Veriprene, Adiprene, and lead-filled cases, respectively.

For the El Centro, Pacoima Dam, and Parkfield records, the differences in the table inputs preclude direct comparisons between the response of the R-FBI system and the response of the various rubber bearing configurations. In general, the old versions of these signals were much richer in high frequency content than those used currently so that for a constant span the peak table accelerations in the rubber bearing tests are much higher than in the R-FBI tests. For example, the old El Centro signal run at a span of 200 (peak table displacement ≈ 1 inch) produces a peak table acceleration of about 0.53 g while the current El Centro signal at the same span leads to a maximum acceleration of only 0.383 g.

The only signal which has not been significantly modified is the Taft record. Run at a span of 350 (peak table displacement ≈ 1.75 inches) both the old and the new versions of this signal produce peak table accelerations of approximately 0.56 to 0.58 g. Likewise, the calculated values of EPA and EPV are reasonably close. Figures 79 and 80 show the complete table displacement and acceleration time histories as well as the Fourier spectrum of the table acceleration from a representative rubber bearing test (120281.15) and one of the R-FBI tests (880810.09). Although there is a time offset between the two time histories and the newer signal has a longer duration, the acceleration records are nearly equal during the intervals of strongest shaking. The Fourier amplitudes are different because a different number of points was used to calculate each spectrum, but the shapes of the two spectra are very similar, especially in the range from 0 to 6 Hz where the majority of the input energy is concentrated. Hence, direct comparisons between the responses of the R-FBI system and the response of the various rubber bearing systems tested with the Taft signal at span 350 can be made.

5.2 Acceleration Response

Figure 81 shows the maximum normalized accelerations throughout the test frame recorded during the Taft signal for each of the rubber bearing tests at span 350 as well as for R-FBI tests at spans of 350 and 800. The performance of both the 50V and 50A rubber systems is excellent. Each reduces the frame accelerations to less than 0.3 times the maximum table acceleration with no amplification throughout the height of the frame. The constant distribution of the accelerations

indicates that the frame is essentially rigid as it moves above the bearings in the fundamental mode of the isolated structure.

The lead-rubber system also shows a fairly constant reduction in the frame accelerations to approximately 0.5 to 0.6 times the peak table acceleration. There is some amplification apparent at the top story of the frame. The relative accelerations for the lead-rubber system are larger than those for the bearings with Veriprene and Adiprene inserts because the lead plugs are much stiffer and hence require a larger base shear and thus larger frame accelerations before they deform. The yielding of the lead plugs also leads to a nonlinear force-displacement response in the lead-rubber bearings. The transition between the elastic and yielding states of the lead excites higher modes in the isolated structure which lead to increased accelerations toward the top of the frame.

When compared with the performance of the rubber systems the acceleration response of the frame supported on the R-FBI system appears poor. The minimum frame acceleration is 0.6 times the peak table acceleration, while the amplification towards the top of the frame leads to a peak roof acceleration of 0.706 g — over 1.2 times the peak table acceleration. However, the span 350 Taft signal is a relatively moderate test of the R-FBI system in comparison with a much more severe earthquake such as the 800 span test also plotted in Figure 81. In this test the peak table acceleration reaches 1.319 g, but the accelerations in the middle floors of the frame stay well below half of this value and the relative bearing displacement is 3.705 inches. The peak acceleration at the roof is limited to 0.950 g. This is because the higher intensity test generates larger base shears which lead to more sliding in the frictional isolation system. The increased sliding provides a more effective way of instantaneously dissipating energy and hence reduces frame accelerations more than is possible during the lower intensity tests. The resulting reduction in accelerations is comparable to that attained by the lead-rubber system. Extrapolating from the earlier test results to a span of 800 for this signal would indicate a relative displacement at the lead-rubber bearings of approximately 4 inches which would not be possible for the six-inch diameter bearings.

5.3 Hysteretic Response

Figure 82 shows hysteresis plots of the total base shear versus the relative bearing displacement from the span 350 Taft tests of the rubber bearing systems and the R-FBI system. The bearings with the Veriprene (50V) and Adiprene (50A) inserts reach a peak displacement of almost 3 inches, corresponding to a displacement of 9 inches in a full-scale structure. However, the displacements in the lead-rubber system (50/2L) and the R-FBI system remain under 1.5 and 1.0 inch, respectively. The response is reduced in these two systems because they inherently provide more damping as bearing displacements increase. While the force-displacement relationship for the 50V and 50A bearings is close to linear even for relatively large displacements, the response of the 50/2L and R-FBI bearings is highly nonlinear. In the 50/2L bearings this nonlinearity comes from yielding in the lead plugs while in the R-FBI bearings it comes from sliding between the teflon and stainless steel plates. Thus, each isolation system absorbs much more energy in its hysteresis loops than do the 50V and 50A bearings, especially for large displacement cycles. The ability to absorb so much energy in each cycle increases the effective damping and limits the peak displacements.

The tradeoff for this reduced displacement response is an increase in the maximum base shear — from between 8 and 10 kips for the Veriprene and Adiprene systems to between 12 and 14 kips for the lead-rubber and R-FBI systems. The increased base shears are also reflected in the increased frame accelerations described in the previous section. However, these effects are not necessarily undesirable. In many applications it may be possible to allow slightly higher base shears and accelerations in the superstructure to reduce excessive displacement demands on the isolation system.

5.4 Interstory Drift

The maximum interstory drift measured at each level of the test frame is shown in Figure 83 for each of the rubber bearing tests as well as for the R-FBI test. The drift response of the structure founded on the 50V bearings is excellent. Its maximum drift of less than 0.3 percent is far below that which would cause significant damage, and the uniform distribution of drift with height implies that the strain energy in the superstructure is distributed evenly. This is in contrast to the response of the

frame supported on the 50A bearings in which the drift is constant and very small ($\delta_{interstory} < 0.15\%$) throughout the first four floors of the frame and then jumps to 0.6 percent at the top floor. Although this peak could be caused by higher mode response, such an explanation is not consistent with other measurements of both the 50V and 50A systems. The acceleration profiles discussed above and the frequency response discussed below indicate that when supported on the Veriprene and Adiprene bearings the superstructure remains essentially rigid with negligible participation from the higher modes. It is most likely that the drift peak at the roof during the 50A test is the result of an instrument malfunction.

The profile of the interstory drifts in the frame supported on lead-rubber bearings is interesting because it has a uniform distribution in the lower floors and a peak at the roof. The uneven distribution of the normalized frame accelerations for the 50/2L bearings discussed above indicates that the contribution of higher modes to the overall response of the frame supported on these bearings is significant, and this explains why the drift peaks at the roof. Also, the highest acceleration in the frame was measured at the roof. However, the maximum drift of 0.7 percent is still below the point at which significant structural damage would occur.

The 1.0 percent drift measured at the roof of the frame during the span 350 R-FBI test approaches the threshold of serious damage. However, it is interesting to compare this plot with the interstory drift profile shown in Figure 52 for the frame supported on the R-FBI bearings and subjected to the span 800 signal. Here the maximum drift is only 0.4 percent and occurs at the third floor, even though the peak table acceleration is almost three times greater than in the span 350 test. Because the larger intensity earthquake excites the frictional isolators more than the lower intensity signal, the drift response of the frame is greatly reduced. This demonstrates again how the performance of the R-FBI system improves as the severity of the ground motion increases.

5.5 Frequency Response

The Fourier acceleration spectra at the base and at all five floors of the test frame are shown in Figures 84 through 87 for each of the four different isolation systems. While the 50V and 50A

systems respond primarily at the fundamental frequency of the isolated structure, the 50/2L and R-FBI systems spread energy among several modes and across a wide range of frequencies for each mode. The profiles of the Veriprene and Adiprene systems are very similar both in shape and in Fourier amplitude, but the slightly stiffer Adiprene inserts lead to a higher fundamental frequency — 0.8 hz as compared with 0.6 Hz for the Veriprene system. The amplitude corresponding to these frequencies is approximately 0.025 in the top three floors of the frame and only slightly lower at the base and the bottom two floors. This implies that the fundamental mode shape is essentially a rigid translation of the frame above the bearing level. A relatively small second mode contribution can be seen in both spectra at approximately 6 Hz (slightly higher for the 50A bearings) with a Fourier amplitude approaching 0.003. The third mode of the isolated structure is evident at about 14.5 Hz but with a very small amplitude. The lack of energy in these higher modes reinforces the conclusion that the frame supported on the 50V and 50A systems responds primarily in the fundamental mode. Higher modes are not easily excited because the force-displacement response of the rubber bearings with these inserts is nearly linear.

The Fourier spectra for the lead-rubber and R-FBI systems show a much broader range of frequency response. The lead-rubber system has distinct peaks at 1.0 and 1.6 Hz but also has a significant amount of first-mode energy distributed over the range between 0.75 to 2.5 Hz. For comparison with the 50V and 50A systems, its peak Fourier amplitude is approximately 0.02 and decreases only slightly toward the bottom of the frame. Thus, the fundamental mode shape approximates a rigid translation of the frame atop the bearings with only a slight interstory drift as in the 50V and 50A tests. The second mode appears within the range of 5.5 to 8 Hz and attains a peak amplitude of 0.017 at both the base and the roof corresponding to frequencies of 6.9 and 6.04 Hz respectively. The total energy contained in the second mode appears to be approximately equal to that contained in the first mode. A relatively smaller (but still significant) third mode response is apparent in the range of 14.5 to 16 Hz. The higher mode participation and wide range of modal frequencies is caused by the nonlinear behavior of the lead-rubber system. As the lead core of the bearing yields, the bearing stiffness decreases leading to a decrease in the fundamental frequency of the isolated

structure. The transition between the elastic and yielding phases distributes the frame energy across a wide range of frequencies as well as exciting higher modes in the structure.

The R-FBI system also distributes energy across a wide band of the Fourier spectrum and into the higher modes of the superstructure. However, locating the exact modal frequencies of the structure on the R-FBI bearings is even harder than for the lead-rubber system. The amplitudes of peaks in the spectrum between 0.5 and 1.75 Hz remain approximately constant throughout the height of the frame while above 2.0 Hz the amplitudes of the response peaks increase substantially toward the roof. (Note that because the spectrum from the R-FBI test was not calculated using the same number of points as was used for the other spectra, direct amplitude comparisons are not possible.) It appears that the first mode of the isolated structure is in the range of 2.0 to 3.5 Hz, but it is not a rigid body mode as in the rubber bearing tests. The second mode is even harder to locate since there is a significant amount of energy in the lower and upper floors at frequencies between 5.0 and 9.0 Hz. The third mode frequency is greater than 13 Hz. The frequency response during this test seems to be dominated by a broad-banded first mode which amplifies the lower frequency accelerations toward the roof. Again the wide range of frequencies and participating modes is caused by the nonlinearity of the bearing. In this case the transition between the rigid and sliding phases leads to an approximately bilinear force-displacement relationship for the R-FBI bearing.

5.6 Discussion

Although the comparisons detailed above are based on only one earthquake record, several observations can be made regrading the merits of the R-FBI bearings relative to the various rubber isolation systems. While the response measurements of all four systems were of the same order of magnitude for the moderate intensity Taft earthquake, the bearings filled with Veriprene and Adiprene provided superior reductions in frame accelerations and interstory drifts as compared with the lead-rubber and R-FBI bearings. However, the relative isolator displacements in the lead-rubber and R-FBI systems were limited to manageable levels, equivalent to approximately 4.5 inches in a full-scale structure. The tradeoff for these reduced displacements was an increase in the peak base shears.

The frequency responses of the Veriprene and Adiprene systems were concentrated in the fundamental mode of the isolated structure. When the frame was supported on the lead-rubber and R-FBI systems higher mode response was induced and the input energy spread across a wide range of frequencies because of the nonlinearities in these bearings. The fundamental mode shape of the structure on the lead-rubber bearings was still fairly well defined, approximating a rigid translation of the frame atop the bearings. However, the first mode of the frame supported on the R-FBI bearings was not as evident. One advantage of frictional systems is their lack of a distinct frequency at which resonance can develop, and the results from the R-FBI test series show that it is able to withstand a range of inputs including such low frequency records as the Mexico City earthquake. While the rubber bearing systems each performed well when subjected to the higher frequency Taft signal, a soft soil ground motion like that of Mexico City would certainly drive the Veriprene and Adiprene systems into resonance and might also threaten the lead-rubber bearings. In contrast, the adaptive nature of the R-FBI system makes their use practical in a wider variety of applications.

Finally, the response of the R-FBI system to the 800 span Taft signal should be mentioned in these comparisons because during this test the bearing deformations were much larger and the increased sliding dissipated more of the input energy. While such a severe ground motion probably would have led to roll-out in the rubber bearing systems, the performance of the R-FBI bearings was greatly improved compared with the span 350 test — peak interstory drifts were lowered to less than 0.4 percent, and the normalized frame accelerations were reduced significantly. The peak bearing displacement increased from less than 1.5 inches to approximately 3 inches, but the frequency response of the frame remained similar to that recorded during the span 350 test. While these results show an improvement in the performance of the R-FBI system with increasing earthquake intensity, it should be kept in mind that the coefficient of friction measured throughout the R-FBI test series was much higher than assumed in the design of the bearings. Therefore the displacements were much lower than expected, and the frame accelerations were higher. If the coefficient of friction had been closer to the assumed value of 0.06, it is likely that the bearings would have performed much better during the lower intensity tests but would have been jeopardized by the stronger ground motions.

6. SUMMARY AND CONCLUSIONS

This report has reviewed a series of shake table tests of the Resilient-Friction Base Isolation system using a five story, 1/3 scale steel test structure supported on four R-FBI bearings. The fully instrumented isolated system was subjected to a series of system identification tests and simulated ground motions from a variety of earthquakes. Pull-back tests and low level random noise inputs produced the first isolated response, resulting in structural frequencies spread across a wide range of the spectrum and shifted above those of the fixed-base structure. Finally, earthquake inputs with varying intensities and table accelerations up to 1.98 g tested the displacement response and energy-absorbing capabilities of the system.

During the moderate-to-severe earthquake motions the isolation system performed extremely well, reducing the accelerations transmitted to the frame and the amplification of accelerations toward the top of the frame while undergoing displacements well within the stability limits of the bearings. The base shear on the 80 kip test structure attained a maximum of 18 kips during the most severe test but remained below 15 kips for the majority of the signals. Although a coefficient of friction of 0.06 was predicted by the material properties and was used in the preliminary analysis and design of the test structure, the experimentally determined coefficient calculated from the base shears at the initiation of sliding was much larger, typically in the range of 0.12 to 0.15. This value was unexpected and could not be readily explained by either the experimental setup or the condition of the bearings after repeated shaking. The teflon layers were examined after all of the tests had been completed and showed little deterioration. Based on the inspection of the bearings at the halfway point of the tests at which time each of the sliding layers was thoroughly cleaned, the contribution of residue from the hard rubber core to the coefficient of friction was minimal and also could not explain the difference between the predicted and measured values.

Comparisons of the performance of the R-FBI bearings with previous tests of three different elastomeric bearing systems showed that for a moderate earthquake such as the Taft record the R-FBI

system provides a level of protection similar to the elastomeric systems. While the response of the test frame on the bearings with Veriprene and Adiprene inserts was dominated by the first mode of the isolated structure (a rigid translation on top of the bearings), the lead-rubber and R-FBI bearings distributed energy across a wide range of frequencies and several modes. Consequently, the peak bearing displacements during the lead-rubber and R-FBI tests were kept at more manageable levels than during the Veriprene and Adiprene tests. Although the interstory drifts in the structure when supported on the R-FBI system were larger than for the elastomeric systems during the span 350 tests, the frictional energy dissipation of the R-FBI system was not fully activated during this moderate test. The more severe 800 span Taft signal increased the sliding deformations of the bearings while simultaneously reducing the interstory drifts throughout the height of the frame, demonstrating how the performance of the R-FBI system improves with increasing ground motion intensity.

In conclusion, the following can be said about the behavior of the R-FBI system during this series of shake table tests:

- Damaging horizontal accelerations were reduced and the amplification of accelerations toward the top of the structure was minimal.
- Relative bearing displacements were lower than predicted by analysis (due in large part to the higher coefficient of friction), and at no time did the bearings approach their stability limit or exhibit deterioration of their stiffness properties.
- The frequency response of the structure was spread across a wide range of the spectrum. Specifically, the shape of the low frequency portion of the Fourier acceleration spectra at each story in the frame was similar to that of the ground motion while much of the energy normally associated with the first mode of the isolated structure was shifted to higher modes.
- The response with and without the steel rods in the central rubber cores of the bearings was not quantitatively different. However, the steel rods should be included in practical applications because they prevent concentrated deformations developing at individual sliding surfaces within the bearings.

- Response to combined vertical and horizontal ground motion is similar to the response to purely horizontal motion, and the two effects can be uncoupled to simplify analytical procedures.
- Equivalent linearization procedures for predicting the response of the isolated system are difficult if not impossible because of the highly nonlinear transition between the fixed and sliding phases of the bearings.
- The response of the R-FBI bearings is inherently different from that of the rubber isolators, but the R-FBI system provides a similar degree of protection for the superstructure. The performance improves as the intensity of the ground motion is increased. R-FBI bearings are also applicable to a wider range of structures including those built in soft soil regions.
- Further research is needed to predict the effective coefficient of friction of the isolation bearings more accurately and to understand the interaction between the sliding plates, the hard rubber cylinder, and the steel rod at the core of a bearing.

REFERENCES

[1] L. Li, "Base Isolation Measure for Aseismic Buildings in China," *Proceedings of the 8th World Conference on Earthquake Engineering*, 6: 791-798, San Francisco, CA, 1984.

[2] C. Plichon and F. Jolivet, "Aseismic Foundation Systems for Nuclear Power Plants," *Proceedings of the Fourth International Conference on Structural Mechanics in Reactor Technology SMiRT-4*, K9(2), 1977.

[3] J. M. Kelly, K. E. Beucke, and M. S. Skinner, "Experimental Testing of a Friction Damped Aseismic Base Isolation System With Fail-Safe Characteristics," *Report No. UCB/EERC-80/18*, Earthquake Engineering Research Center, University of California, Berkeley, CA, July 1980.

[4] A. Mokha, M. C. Constantinou, and A. M. Reinhorn, "Teflon Bearings in Aseismic Base Isolation: Experimental Studies and Mathematical Modeling," *Report No. NCEER-88-0038*, National Center for Earthquake Engineering Research, SUNY Buffalo, December 1988.

[5] *Teflon-Flourocarbon Resin — Mechanical Design Data*, E.I. duPont de Nemours & Co. (Inc.), Polymer Products Department, Wilmington, DE, 1981.

[6] V. A. Zayas, S. S. Low, and S. A. Mahin, "The FPS Earthquake Resisting System: Experimental Report," *Report No. UCB/EERC-87/01*, Earthquake Engineering Research Center, University of California, Berkeley, CA, June 1987.

[7] N. Mostaghel and M. Khodaverdian, "Dynamics of Resilient-Friction Base Isolator (R-FBI)," *Earthquake Engineering and Structural Dynamics*, 15(3): 379-390, Salt Lake City, UT, United States, April 1987.

[8] N. Mostaghel and M. Khodaverdian, "Seismic Response of Structures Supported on R-FBI System," *Earthquake Engineering and Structural Dynamics*, 16(6): 839-854, 1988.

[9] N. Mostaghel and J. M. Kelly, "Design Procedure for R-FBI Bearings," *Report No. UCB/EERC-87/18*, Earthquake Engineering Research Center, University of California, Berkeley, CA, November 1987.

[10] D. Rea and J. Penzien, "Dynamic Response of a 20 ft × 20 ft Shaking Table," *Proceedings of the Fifth World Conference on Earthquake Engineering*, Rome, Italy, 1974.

[11] J. M. Kelly and S. B. Hodder, "Experimental Study of Lead and Elastomeric Dampers for Base Isolation Systems," *Report No. UCB/EERC-81/16*, Earthquake Engineering Research Center, University of California, Berkeley, CA, October 1981.

[12] J. M. Kelly, "Base Isolation: Linear Theory and Design," *Earthquake Spectra*, 6(2): 223-244, Earthquake Engineering Research Institute, El Cerrito, California, May 1990.

[13] N. Mostaghel, "Stability Analysis of R-FBI Systems," *Proceedings of the International Symposium on Seismic IsolationHistoric Preservation*, Salt Lake City, UT, May 11-14, 1988.

[14] J. M. Kelly, I. G. Buckle, and H. C. Tsai, "Earthquake Simulator Testing of a Base-Isolated Bridge Deck," *Report No. UCB/EERC-85/09*, Earthquake Engineering Research Center, University of California, Berkeley, CA, January 1986.

[15] Y. Bozorgnia, *Ph.D. Thesis*, Department of Civil Engineering, University of California, Berkeley, CA, 1981.

[16] *ATC 3-06: Tentative Provisions for the Development of Seismic Regulations for Buildings*, Applied Technology Council, 1984.

TABLES

FILENAME	SIGNAL	SPAN	REMARKS
880808.01	Free Vibration[1]	-	System
880808.02	Free Vibration	-	identification
880810.01	Random Noise[2]	200	testing
880810.02	Random Noise	300	
880810.03	El Centro[3]	100	Tests without
880810.04	El Centro	200	steel rods in the
880810.05	El Centro	300	bearing cores
880810.06	Taft[4]	100	
880810.07	Taft	200	
880810.08	Taft	300	
880810.09	Taft	350	
880810.10	Olympia[5]	100	
880810.11	Olympia	200	
880810.12	Olympia	300	
880812.01	Random Noise	600	
880812.02	Harmonic[6] 2.8 hz	200	
880812.03	Harmonic 2.6 hz	200	
880812.04	Harmonic 2.4 hz	200	
880812.05	Harmonic 2.4 hz	300	
880812.06	Harmonic 2.6 hz	300	
880812.07	Harmonic 2.8 hz	300	
880812.08	El Centro	400	
880812.09	Olympia	400	
880812.10	Taft	400	
880812.11	Pacoima[7]	400	
880812.12	Parkfield[8]	400	
880812.13	Mexico City[9]	400	
880812.14	San Francisco[10]	400	
880812.15	Chile[11]	400	
880815.01	Random Noise	300	
880815.02	Random Noise	600	
880815.03	Random Noise	600	
880815.04	El Centro	400	
880815.05	Olympia	400	
880815.06	Taft	400	
880815.07	Pacoima	400	
880815.08	Parkfield	400	
880815.09	Mexico City	400	
880815.10	Chile	400	
880815.11	San Francisco	400	

Table 1 R-FBI Test Log

FILENAME	SIGNAL	SPAN	REMARKS
880815.12	El Centro	500	
880815.13	Olympia	500	
880815.14	Taft	500	
880815.15	Pacoima	500	
880815.16	Parkfield	500	
880815.17	Mexico City	500	
880815.18	San Francisco	500	
880815.19	Chile	500	
880816.01	Chile	100V[12]	
880816.02	Chile	500V	
880816.03	Chile	1000V	
880816.04	Chile	500	
880816.05	Chile	500H 500V	
880816.06	Chile	500H 1000V	
880816.07	Chile	600	
880816.08	El Centro	600	
880816.09	Olympia	600	
880816.10	El Centro	600	
880816.11	Taft	600	
880816.12	Pacoima	600	
880816.13	Parkfield	600	
880816.14	Mexico City	600	
880816.15	San Francisco	600	
880818.01	Chile	400	Tests including steel rods in the bearing cores
880818.02	El Centro	400	
880818.03	Olympia	400	
880818.04	Taft	400	
880818.05	Pacoima	400	
880818.06	Parkfield	400	
880818.07	Mexico City	400	
880818.08	San Francisco	400	
880818.09	San Francisco	600	
880818.10	Mexico City	600	
880818.11	Mexico City	700	
880818.12	Mexico City	800	
880818.13	Parkfield	600	
880818.14	Pacoima	600	
880818.15	Taft	600	
880818.16	Olympia	600	
880818.17	El Centro	600	
880818.18	Chile	600	

Table 1 R-FBI Test Log (Continued)

FILENAME	SIGNAL	SPAN	REMARKS
880818.19	San Francisco	200H 200V	
880818.21	San Francisco	400H 400V	
880818.22	San Francisco	400H 800V	
880818.23	Taft	800	
880818.24	Pacoima	800	
880818.25	Olympia	1000	
880831.01	Mexico City	800	
880831.02	Mexico City	900	
880831.03	Mexico City	950	Table response limits exceeded
880831.04	San Francisco	500H 500V	
880831.05	San Francisco	500H 1000V	
880831.06	Chile	800	
880831.07	Chile	900	

*1 Free Vibration Pullback Test

*2 White Noise Test

*3 1940 El Centro Earthquake S00E

*4 1952 Taft Earthquake S69E

*5 1949 Olympia Earthquake N86E

*6 Harmonic Signal at Indicated Frequency

*7 1971 Pacoima Dam Earthquake S16E

*8 1966 Parkfield Earthquake N65E

*9 1985 Mexico City Earthquake N60E, calculated

*10 1955 San Francisco Earthquake S80E

*11 1985 Llolleo Earthquake N10E

*12 All span values refer to horizontal spans unless followed by a V

Table 1 R-FBI Test Log (Continued)

Data File	Initial Absolute Offset (inches)	Final Absolute Offset (inches)	Final Relative Offset (inches)
880818.01	0.0	-0.1222	-0.1222
880818.02	-0.1212	0.3365	0.4577
880818.03	0.3373	0.7243	0.3870
880818.04	0.7225	0.2336	-0.4889
880818.05	0.2336	0.0121	-0.2215
880818.06	0.0121	0.5503	0.5382
880818.07	0.5503	0.3001	-0.2502
880818.08	0.2993	0.3458	0.0465
880818.09	0.3456	0.2097	-0.1360
880818.10	0.2115	0.3934	0.1819
880818.11	0.3944	0.1350	-0.2594
880818.12	0.1358	-0.1037	-0.2395
880818.13	-0.1021	0.4699	0.5720
880818.14	0.4709	0.1301	-0.3408
880818.15	0.1309	0.4566	0.3257
880818.16	0.4565	1.3392	0.8827
880818.17	0.0582	0.2722	0.2140
880818.18	0.2996	0.3064	0.0068
880818.19	0.3076	0.1034	-0.2042

Table 2 History of Absolute and Relative Bearing Offsets

Earthquake	SW		SE		NW		NE	
	w/o rod	w/ rod	w/o rod	w/ rod	w/o rod	w/ rod	w/o rod	w/ rod
El Centro	4.181	4.613	7.480	6.083	6.107	5.426	3.786	3.402
Taft	4.706	4.515	7.415	6.526	6.086	5.674	3.937	3.399
Olympia	3.785	3.471	6.712	6.359	5.557	5.016	3.177	3.021
Parkfield	3.949	3.742	6.202	5.638	4.893	4.747	3.362	3.078
Pacoima	3.754	3.725	6.190	5.200	5.812	5.175	4.228	3.459
Mexico City	3.148	3.183	5.086	5.396	4.790	5.035	2.915	2.937
Chile	4.366	4.104	7.241	6.943	6.627	6.092	4.284	4.035
San Francisco	4.885	4.883	7.216	7.198	6.902	6.650	5.455	4.872

Shear, kips

Table 3 Maximum Shear in Bearings with and without Center Steel Rod

Earthquake	span = 400		span = 600	
	w/o rod	w/ rod	w/o rod	w/ rod
El Centro	0.471	0.459	0.494	0.512
Taft	0.585	0.578	0.615	0.592
Olympia	0.364	0.363	0.458	0.458
Parkfield	0.436	0.410	0.468	0.438
Pacoima	0.387	0.380	0.496	0.481
Mexico City	0.163	0.166	0.204	0.208
Chile	0.655	0.612	0.759	0.735
San Francisco	0.891	0.925	0.974	0.982

Acceleration, g's

Table 4 Maximum Base Accelerations with and without Center Steel Rod

w/o rod = tests without steel rod in rubber core
w/ rod = tests with steel rod in rubber core

Earthquake	span = 400		span = 600	
	w/o rod	w/ rod	w/o rod	w/ rod
El Centro	1.919	1.642	3.428	3.085
Taft	1.417	1.288	2.481	2.723
Olympia	0.600	0.624	1.451	1.209
Parkfield	1.534	1.532	2.563	2.699
Pacoima	0.839	0.929	1.941	2.067
Mexico City	0.203	0.317	1.585	1.577
Chile	1.862	1.526	2.620	2.609
San Francisco	1.656	1.668	2.138	2.189

Relative Bearing Displacement, inches

w/o rod = tests without steel rod in rubber core
w/ rod = tests with steel rod in rubber core

Table 5 Maximum Bearing Displacements with and without Center Steel Rod

R-FBI TEST FILES

El Centro

file	span	PGA (g's)	EPA (g's)	EPV (in/sec)	$x_{base_{max}}$ (in)	$a_{base_{max}}$ (g's)
880810.03	100	.222	.149 (ξ=5%) .120 (ξ=10%)	2.73 (ξ=5%) 1.99 (ξ=10%)	.291	.272
880810.04	200	.383	.289 .230	5.43 3.94	.604	.318
880810.05	300	.462	.390 .306	8.04 5.82	1.10	.376
880812.08	400	.595	.471 .382	10.73 7.80	1.86	.478
880815.04	400	.569	.470 .376	10.63 7.71	1.92	.471
880815.12	500	.734	.555 .463	13.10 9.57	1.82	.565
880816.08	600	.934	.645 .555	15.30 11.33	2.77	.535
880816.10	600	.986	.650 .559	15.36 11.34	3.43	.494
880818.02	400	.572	.468 .374	10.60 7.68	1.64	.459
880818.17	600	.942	.639 .549	15.40 11.37	3.09	.512

Pacoima Dam

file	span	PGA	EPA	EPV	$x_{base_{max}}$	$a_{base_{max}}$
880812.11	400	.481	.397 (ξ=5%) .305 (ξ=10%)	6.86 (ξ=5%) 5.64 (ξ=10%)	.839	.384
880815.07	400	.493	.396 .301	6.82 5.61	.839	.387
880815.15	500	.609	.494 .378	8.41 6.92	1.36	.471
880816.12	600	.703	.573 .439	9.82 8.07	1.94	.496
880818.05	400	.466	.395 .301	6.79 5.57	.929	.380
880818.14	600	.700	.575 .440	9.79 8.05	2.07	.481
880818.24	800	1.025	.724 .559	11.81 9.65	3.18	.588

Table 6 Comparison between R-FBI Earthquake Simulator Tests and Rubber Bearing Earthquake Simulator Tests

R-FBI TEST FILES (continued)

Parkfield

file	span	PGA	EPA	EPV	$x_{base_{max}}$	$a_{base_{max}}$
880812.12	400	.366	.265 (ξ=5%) .228 (ξ=10%)	3.79 (ξ=5%) 3.31 (ξ=10%)	1.56	.407
880815.08	400	.383	.264 .229	3.78 3.32	1.53	.436
880815.16	500	.488	.341 .296	4.74 4.17	1.82	.483
880816.13	600	.633	.428 .369	5.67 5.02	2.56	.468
880818.06	400	.378	.263 .228	3.78 3.30	1.53	.410
880818.13	600	.627	.421 .363	5.64 4.99	2.70	.438

Taft

file	span	PGA	EPA	EPV	$x_{base_{max}}$	$a_{base_{max}}$
880810.06	100	.145	.122 (ξ=5%) .090 (ξ=10%)	1.78 (ξ=5%) 1.4 (ξ=10%)	.116	.144
880810.07	200	.304	.243 .183	3.53 2.77	.502	.313
880810.08	300	.473	.363 .280	5.23 4.11	.886	.462
880810.09	350	.563	.417 .325	6.07 4.77	.984	.498
880812.10	400	.650	.483 .375	6.94 5.44	1.32	.593
880815.06	400	.666	.481 .375	6.90 5.41	1.42	.585
880815.14	500	.802	.590 .462	8.53 6.71	1.97	.649
880816.11	600	.995	.700 .554	10.07 7.91	2.48	.615
880818.04	400	.653	.483 .375	6.87 5.40	1.29	.578
880818.15	600	.978	.702 .551	10.08 7.93	2.72	.592
880818.23	800	1.319	.892 .720	12.68 9.89	3.71	.686

Table 6 Comparison between R-FBI Earthquake Simulator Tests and Rubber Bearing Earthquake Simulator Tests (Continued)

RUBBER BEARING TEST FILES

El Centro

file	span	PGA (g's)	EPA (g's)	EPV (in/sec)	$x_{base_{max}}$ (in)	$a_{base_{max}}$ (g's)	base
110281.03	200	.533	.441 (ξ=5%) .369 (ξ=10%)	5.85 (ξ=5%) 4.25 (ξ=10%)	2.53	.102	50D
120281.13	200	.536	.438 .367	5.86 4.25	2.28	.107	50V
130281.04	200	.530	.448 .374	5.85 4.25	1.53	.121	50A
180281.09	200	.527	.438 .367	5.83 4.23	.893	.221	50/2L
180281.10	100	.255	.209 .171	2.94 2.14	.493	.157	50/2L
180281.12	300	.853	.665 .556	8.80 6.39	1.44	.276	50/2L
180281.13	400	1.145	.880 .740	11.74 8.52	1.96	.409	50/2L
180281.14	500	1.464	1.071 .909	14.64 10.60	2.46	.654	50/2L

Pacoima Dam

file	span	PGA	EPA	EPV	$x_{base_{max}}$	$a_{base_{max}}$	base
120281.17	300	1.290	1.223 (ξ=5%) .975 (ξ=10%)	11.68 (ξ=5%) 9.26 (ξ=10%)	2.10	.122	50V
130281.09	300	1.284	1.235 .983	11.63 9.23	2.72	.139	50A
180281.02	300	1.331	1.221 .969	11.44 9.09	2.60	.474	50/2L

Parkfield

file	span	PGA	EPA	EPV	$x_{base_{max}}$	$a_{base_{max}}$	base
110281.09	300	.378	.304 (ξ=5%) .262 (ξ=10%)	4.64 (ξ=5%) 3.99 (ξ=10%)	2.56	.097	50D
120281.18	300	.368	.302 .260	4.67 4.03	2.67	.117	50V
130281.10	300	.374	.303 .260	4.64 3.98	3.46	.208	50A
180281.04	300	.381	.300 .257	4.60 3.97	1.97	.322	50/2L

Table 6 Comparison between R-FBI Earthquake Simulator Tests and Rubber Bearing Earthquake Simulator Tests (Continued)

RUBBER BEARING TEST FILES (continued)

Taft

file	span	PGA	EPA	EPV	$x_{base_{max}}$	$a_{base_{max}}$	base
120281.15	350	.564	.464 (ξ=5%) .353 (ξ=10%)	7.34 (ξ=5%) 5.77 (ξ=10%)	3.01	.132	50V
130281.06	350	.578	.476 .362	7.27 5.72	2.91	.152	50A
180281.03	350	.582	.462 .348	7.20 5.66	1.56	.281	50/2L

Base conditions for the rubber bearing tests are as follows:

50D = Rubber Bearing only

50V = Rubber Bearing with Variprene insert

50A = Rubber Bearing with Adiprene insert

50/2L = Rubber Bearing with Lead Plug inserts

Table 6 Comparison between R-FBI Earthquake Simulator Tests and Rubber Bearing Earthquake Simulator Tests (Continued)

FIGURES

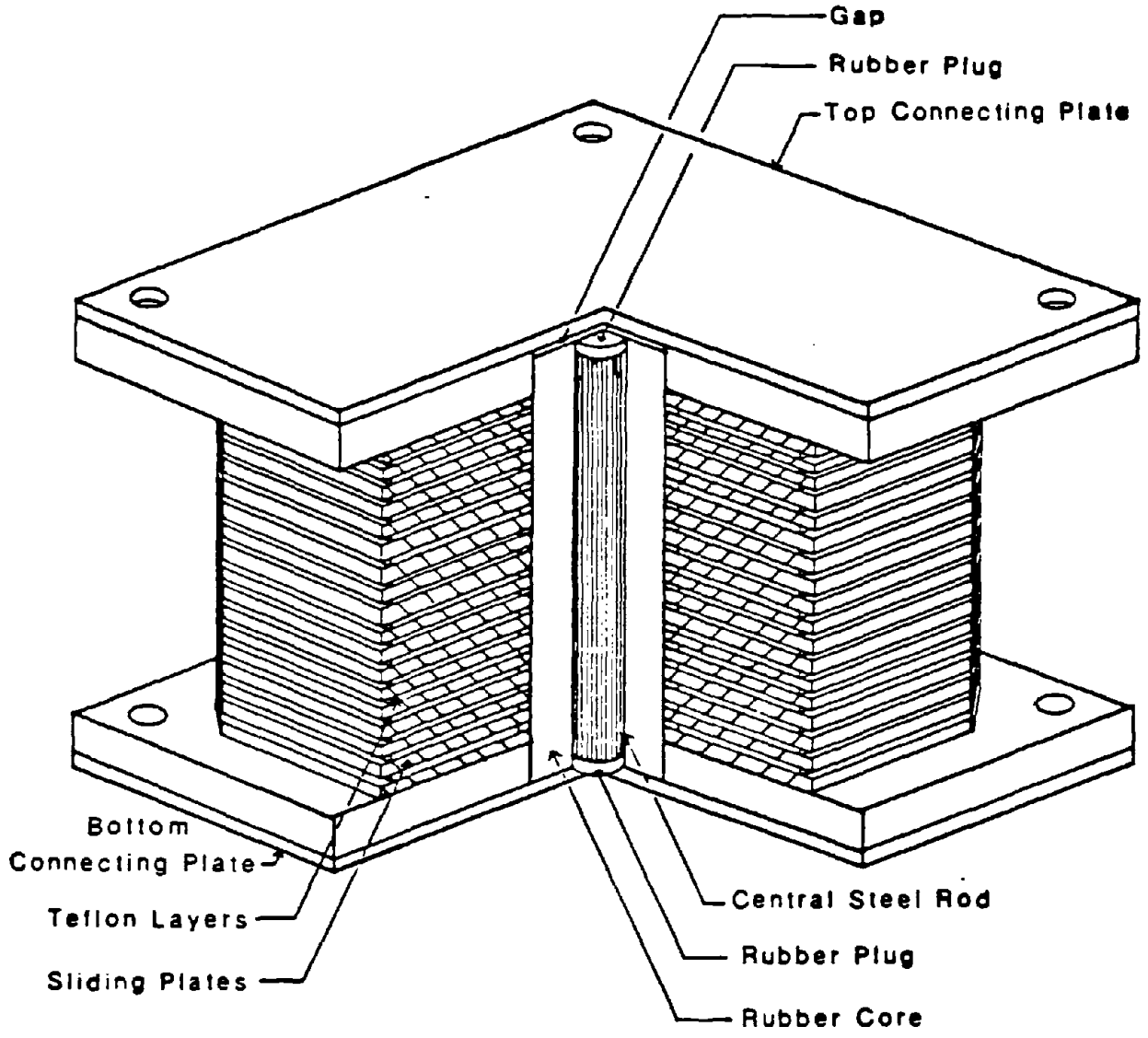

Figure 1 The Resilient-Friction Base Isolator

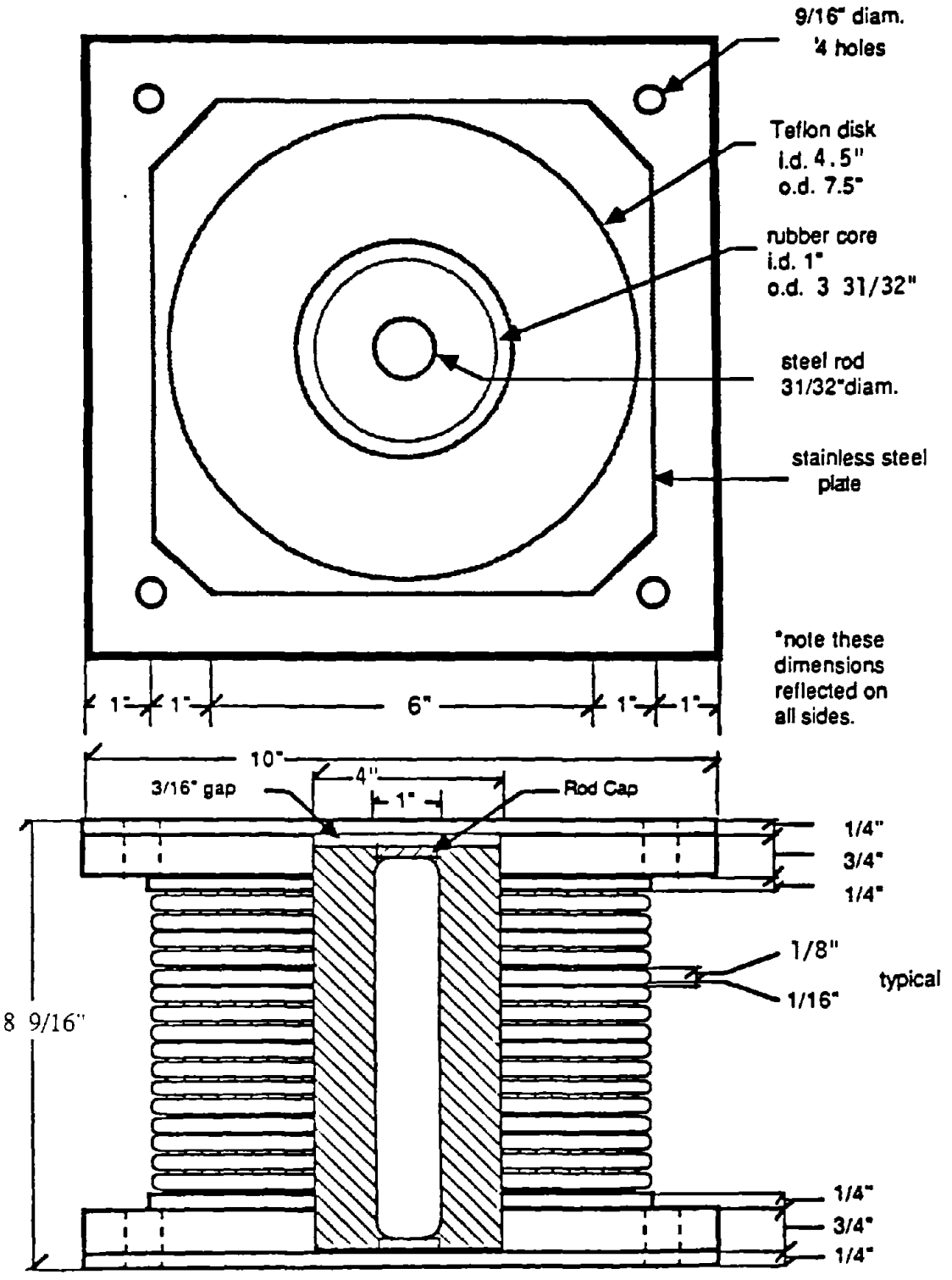

(32 x 2/16" + 33 x 1/16" = 6 1/16")

Figure 2 Section Through the Isolator

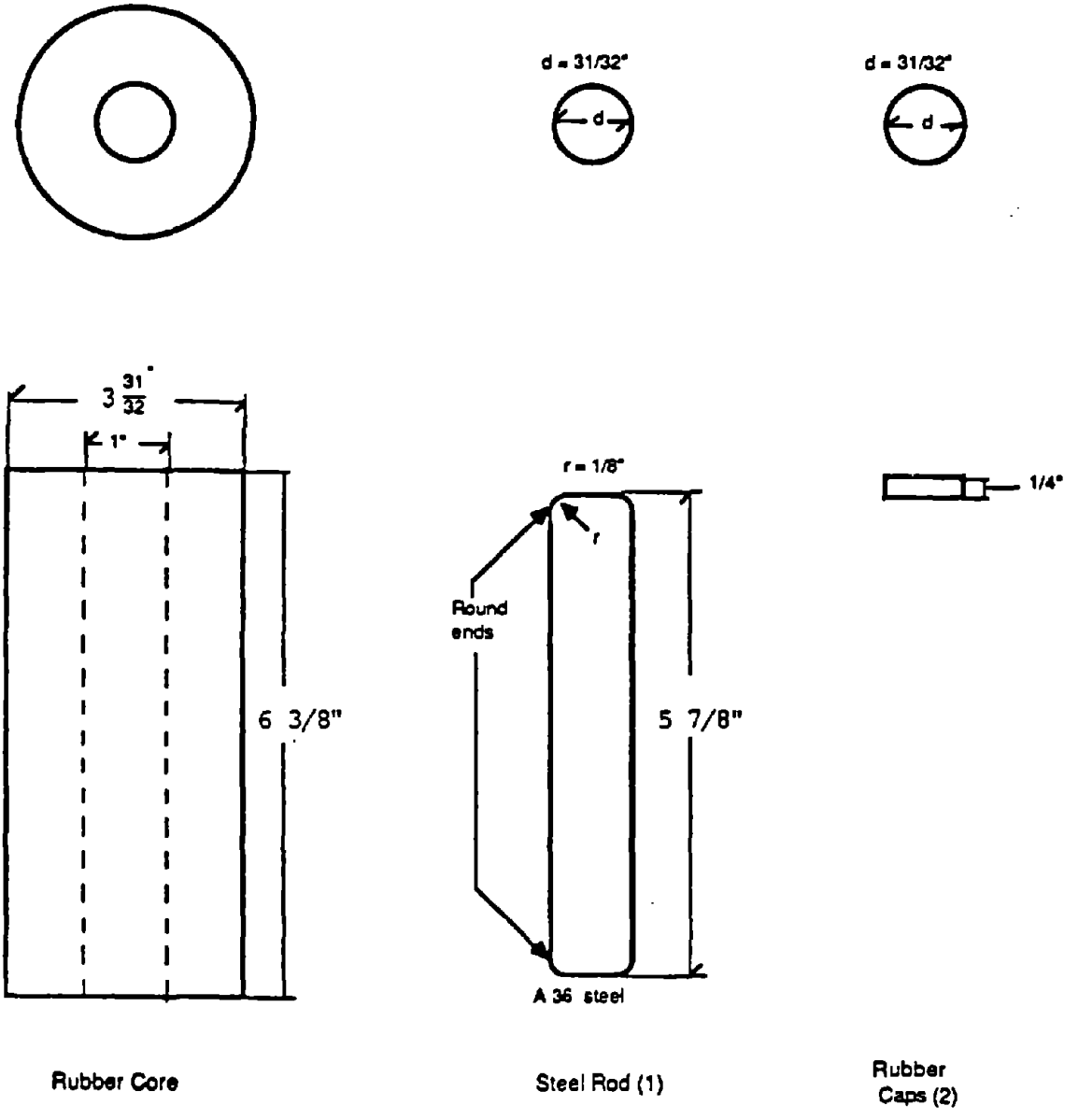

Figure 3 Dimensions of Rubber Core and Steel Rod

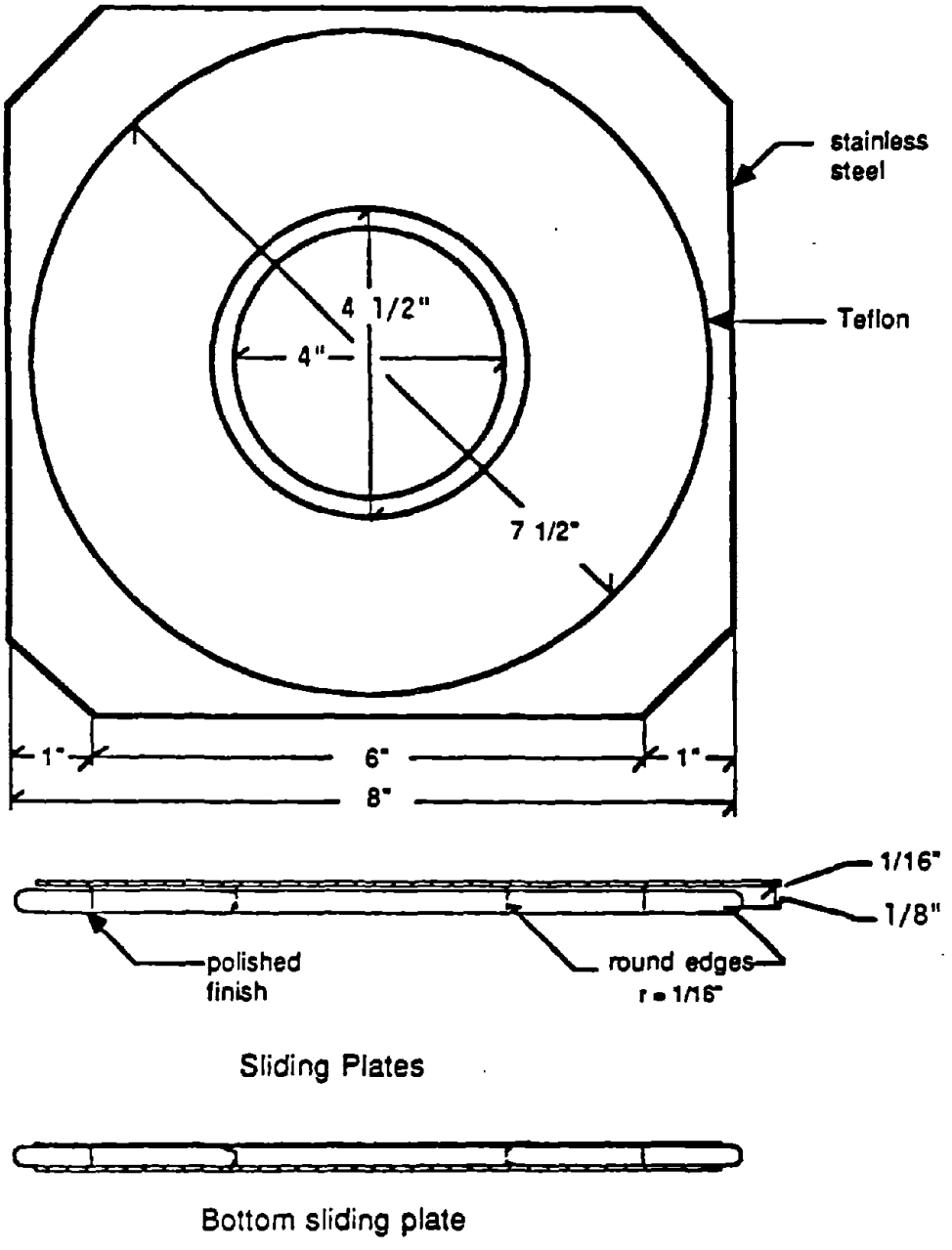

Figure 4 Dimensions of Sliding Plates and Teflon Rings

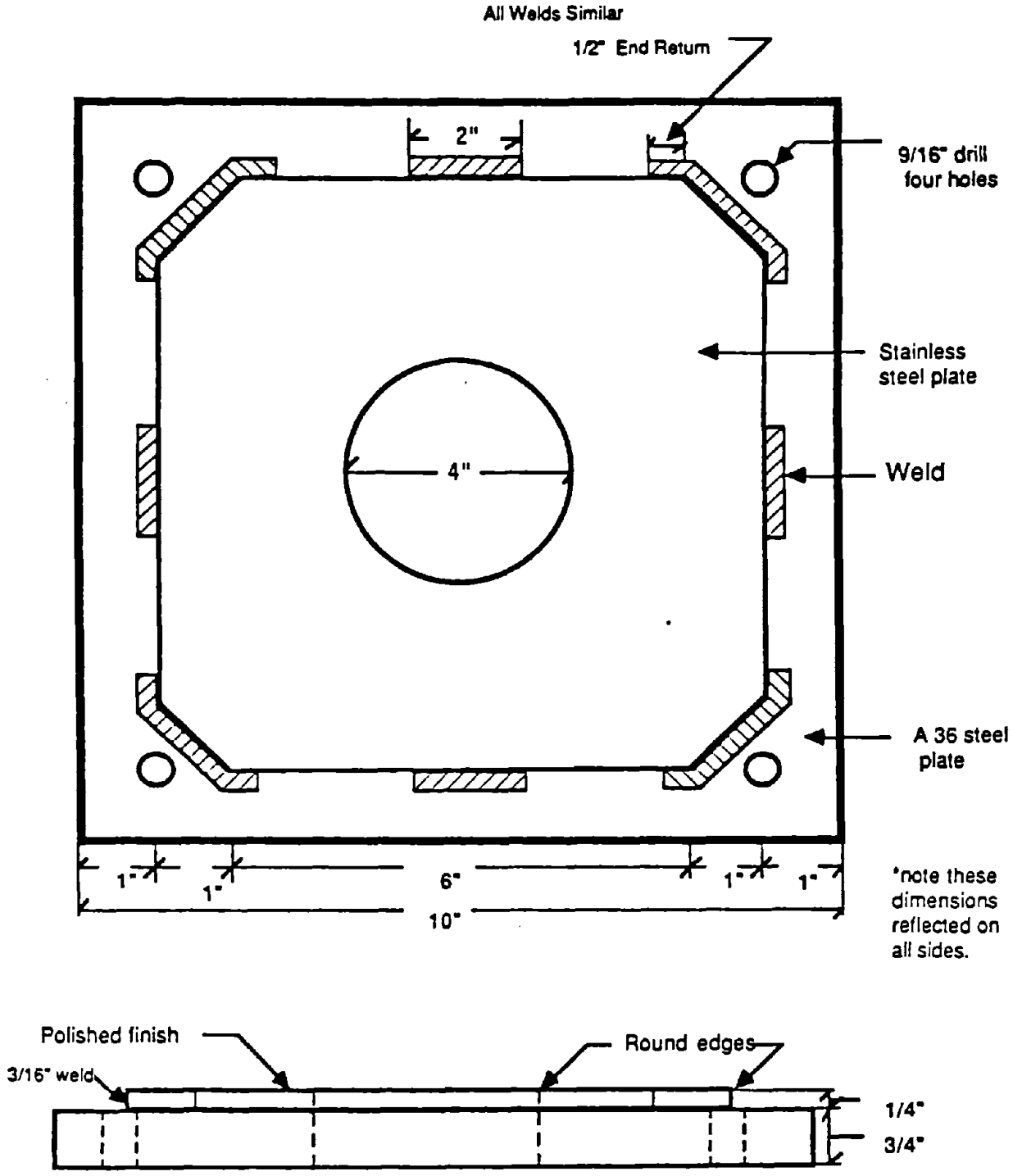

Shear Key

Figure 5 Dimensions of Base Plates and Shear Keys

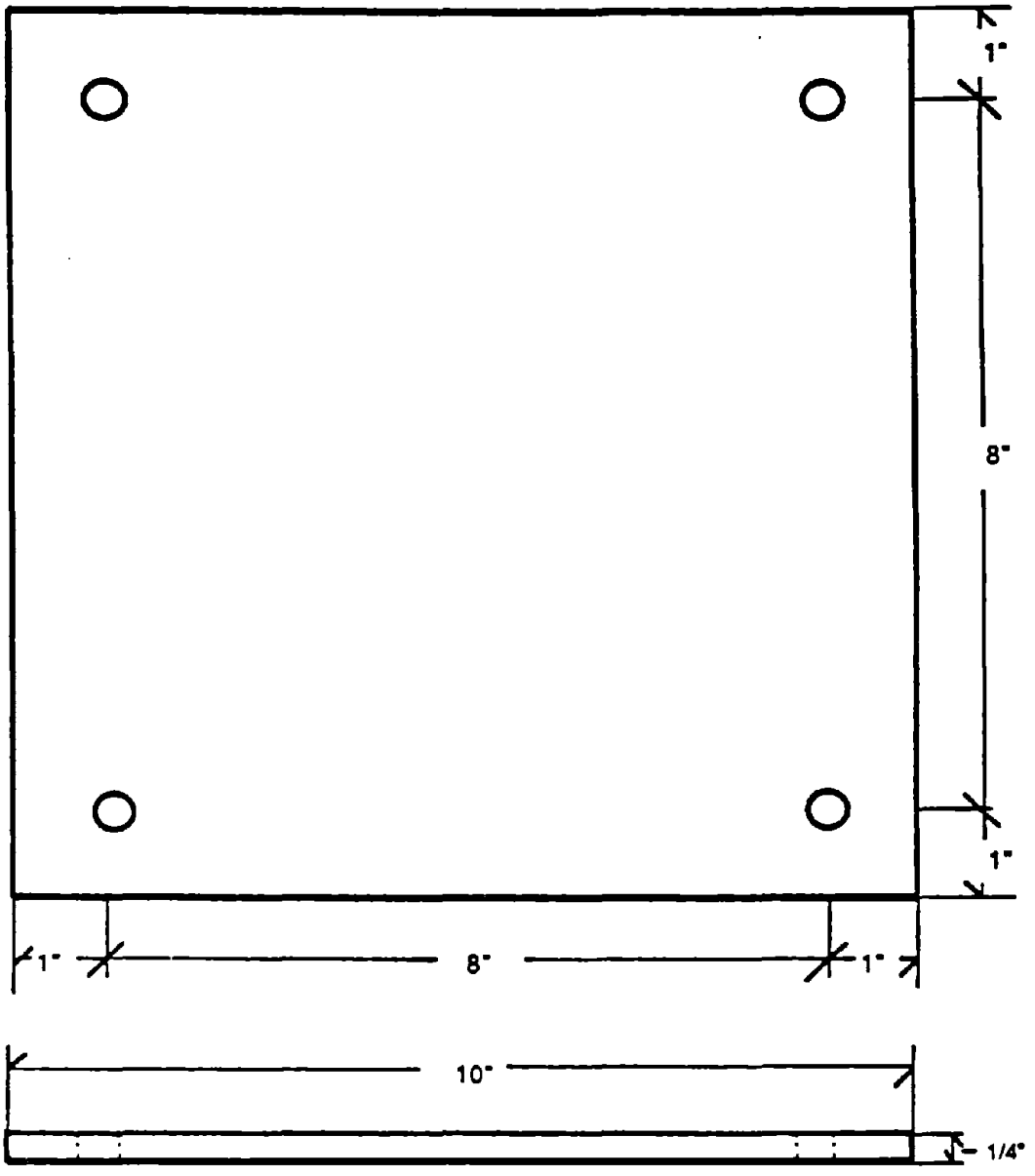

Figure 6 Dimensions of Cover Plates

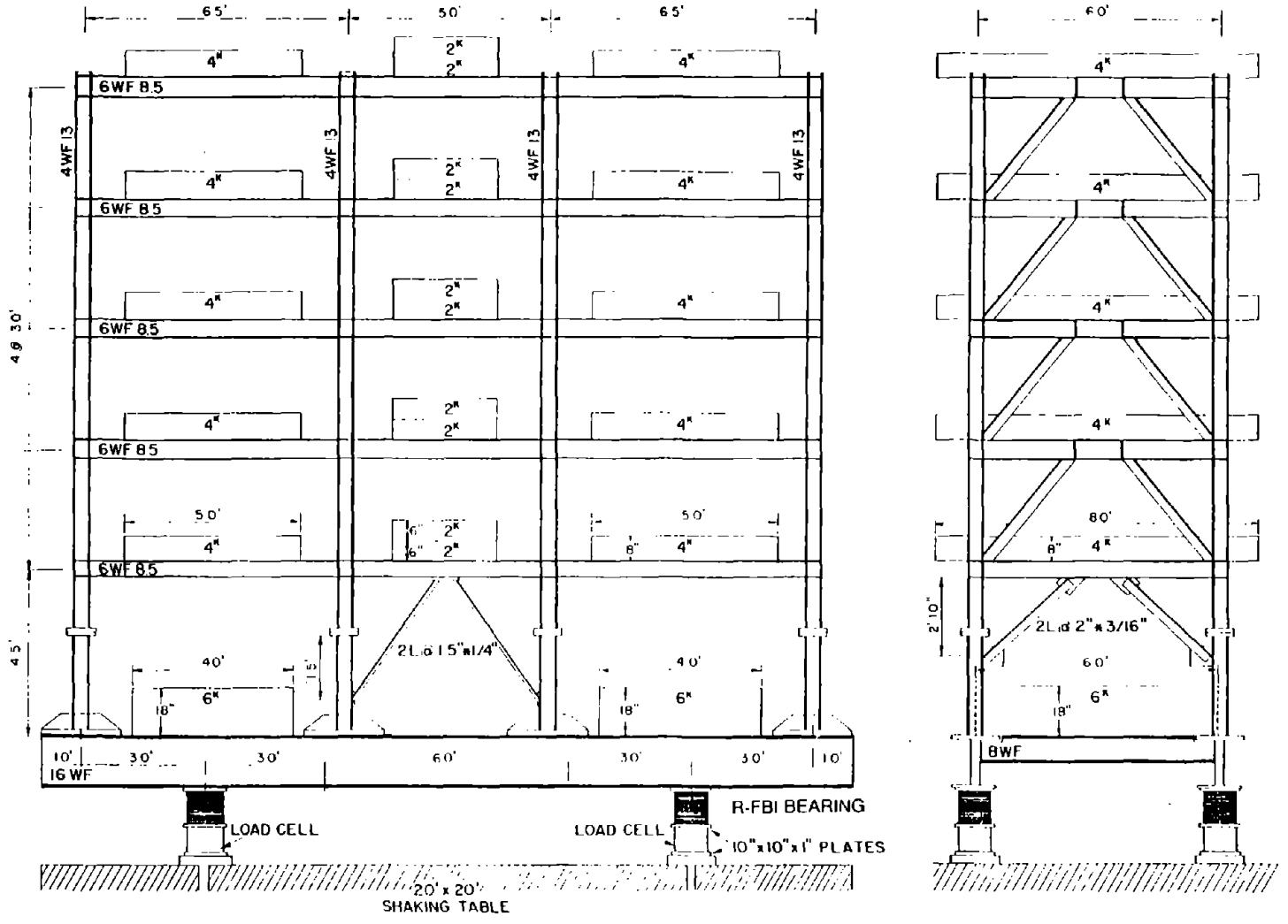

Figure 7 One-Third Scale Structural Model Showing Main Dimensions and Isolation Mounting

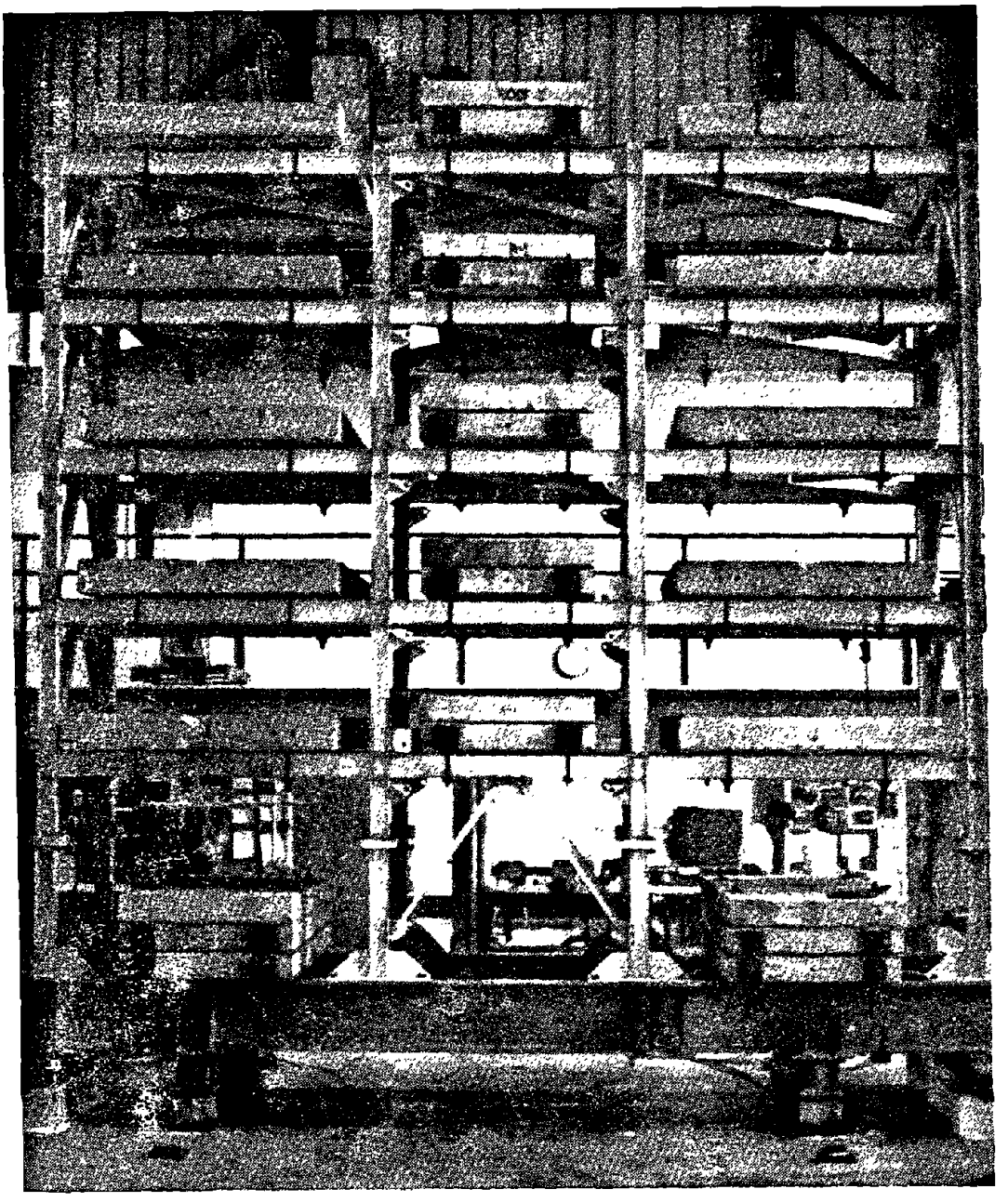

Figure 8 Test Frame Mounted on R-FBI Bearings

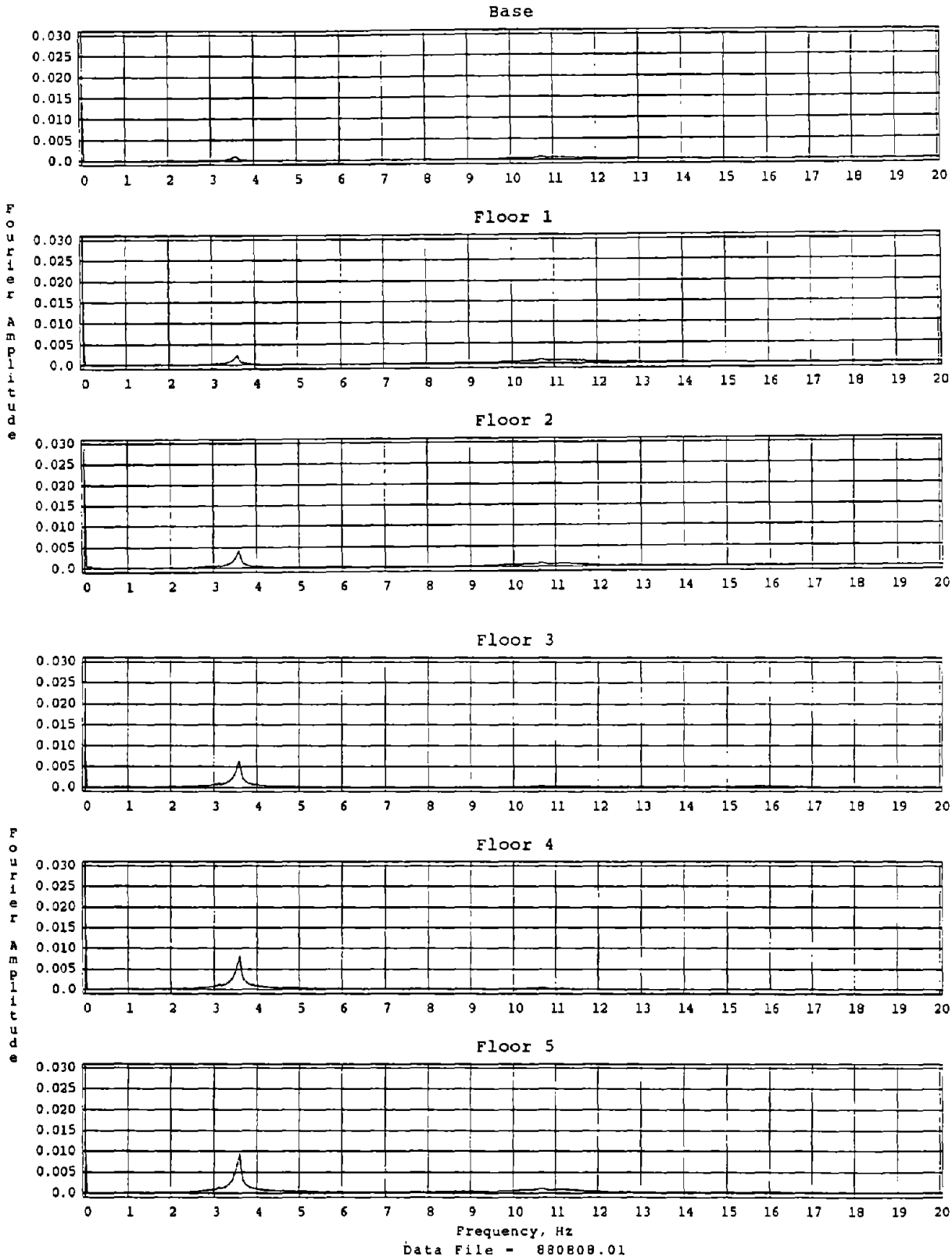

Figure 9 Fourier Spectra for First Snapback Test

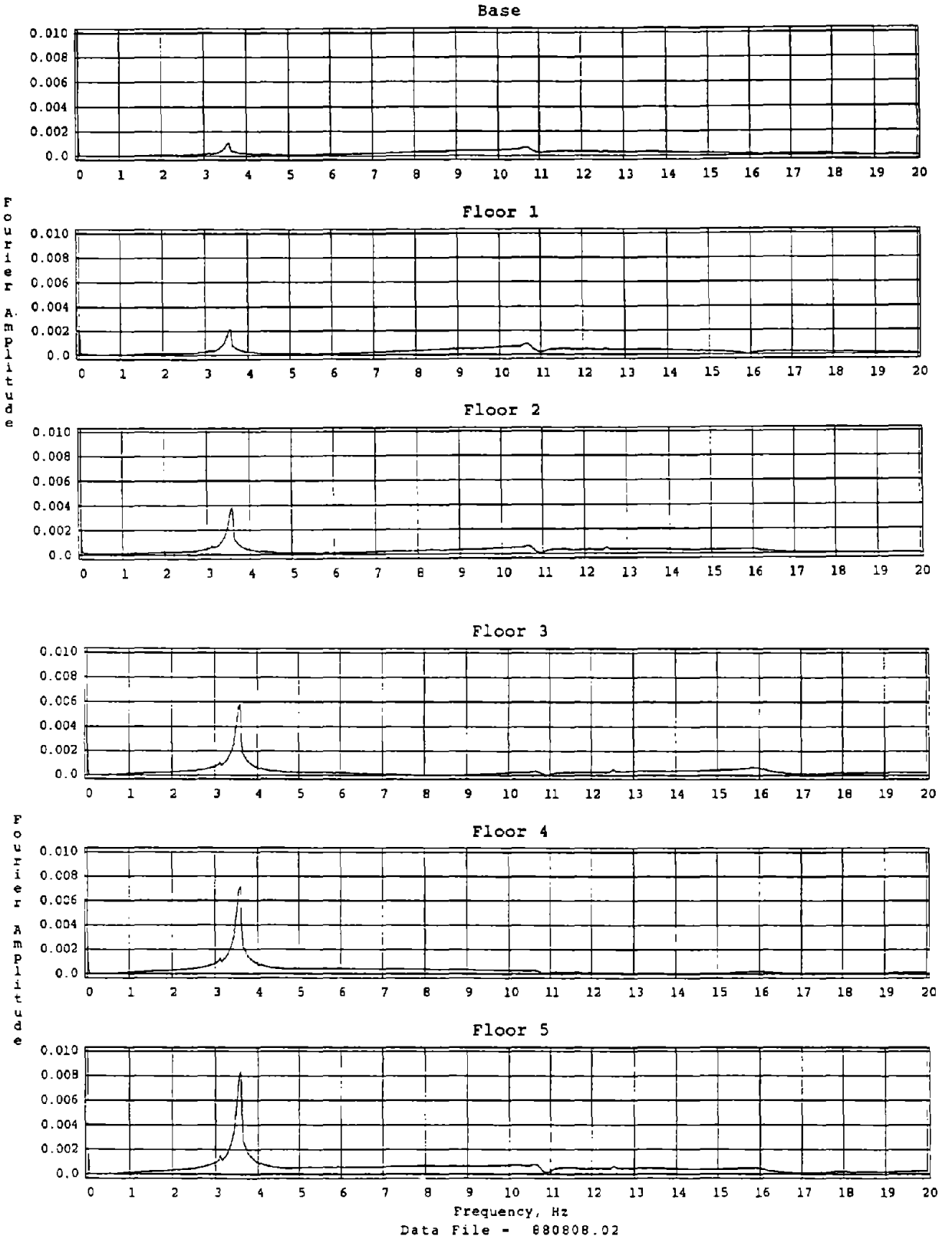

Figure 10 Fourier Spectra for Second Snapback Test

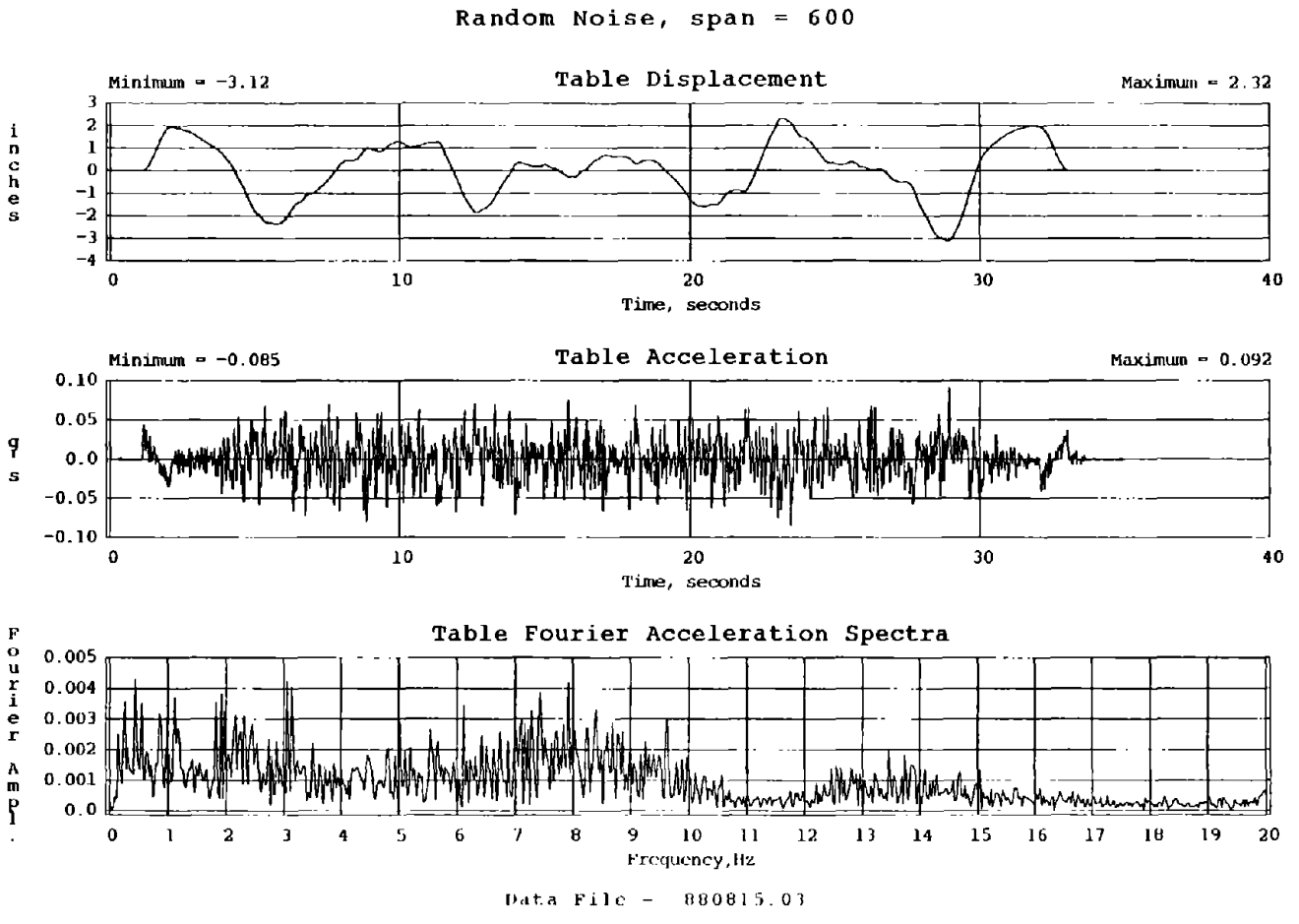

Figure 11 Displacement and Acceleration Time Histories and Fourier Acceleration Spectra for Random Noise, span = 600

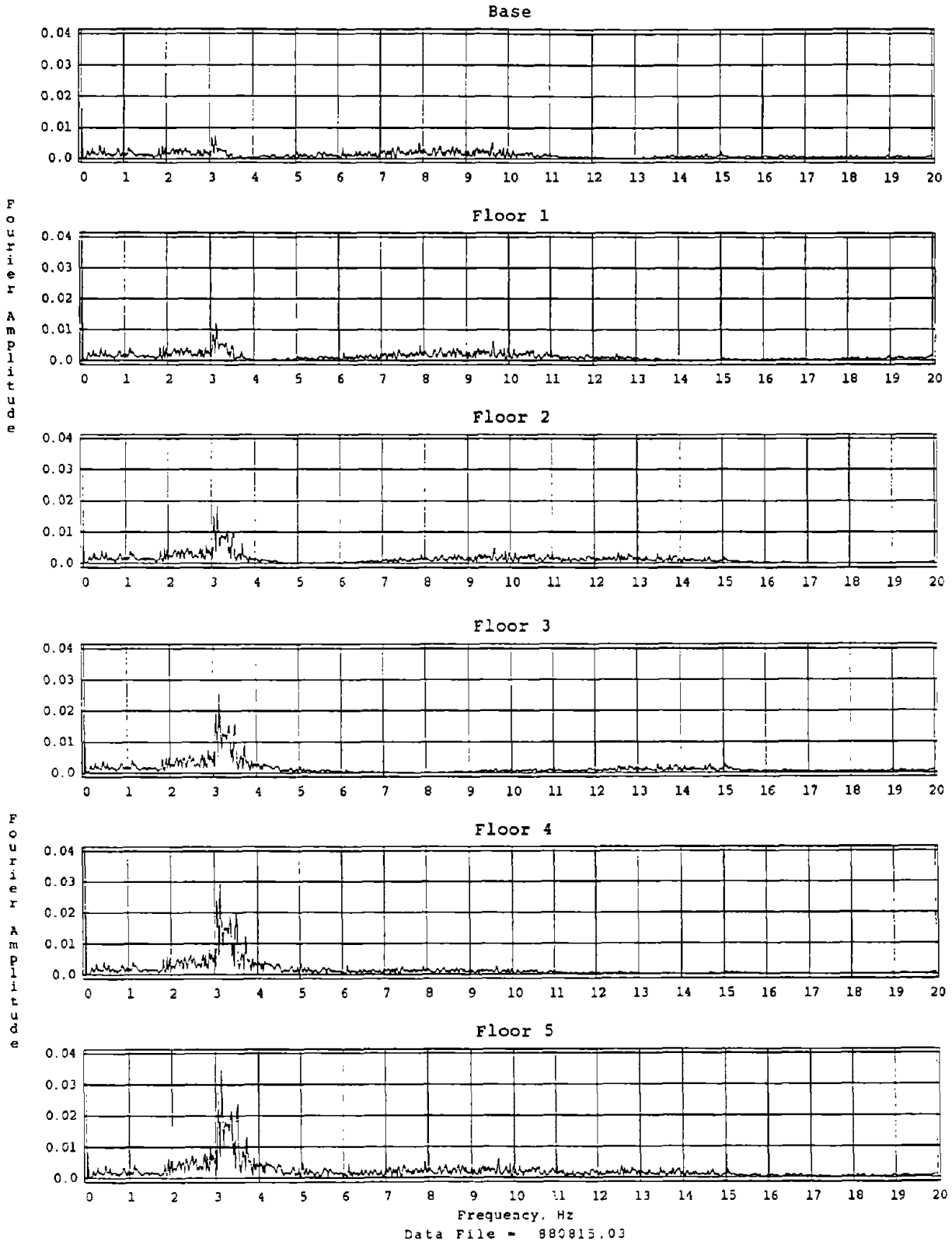

Figure 12 Fourier Spectra for Random Noise, span = 600

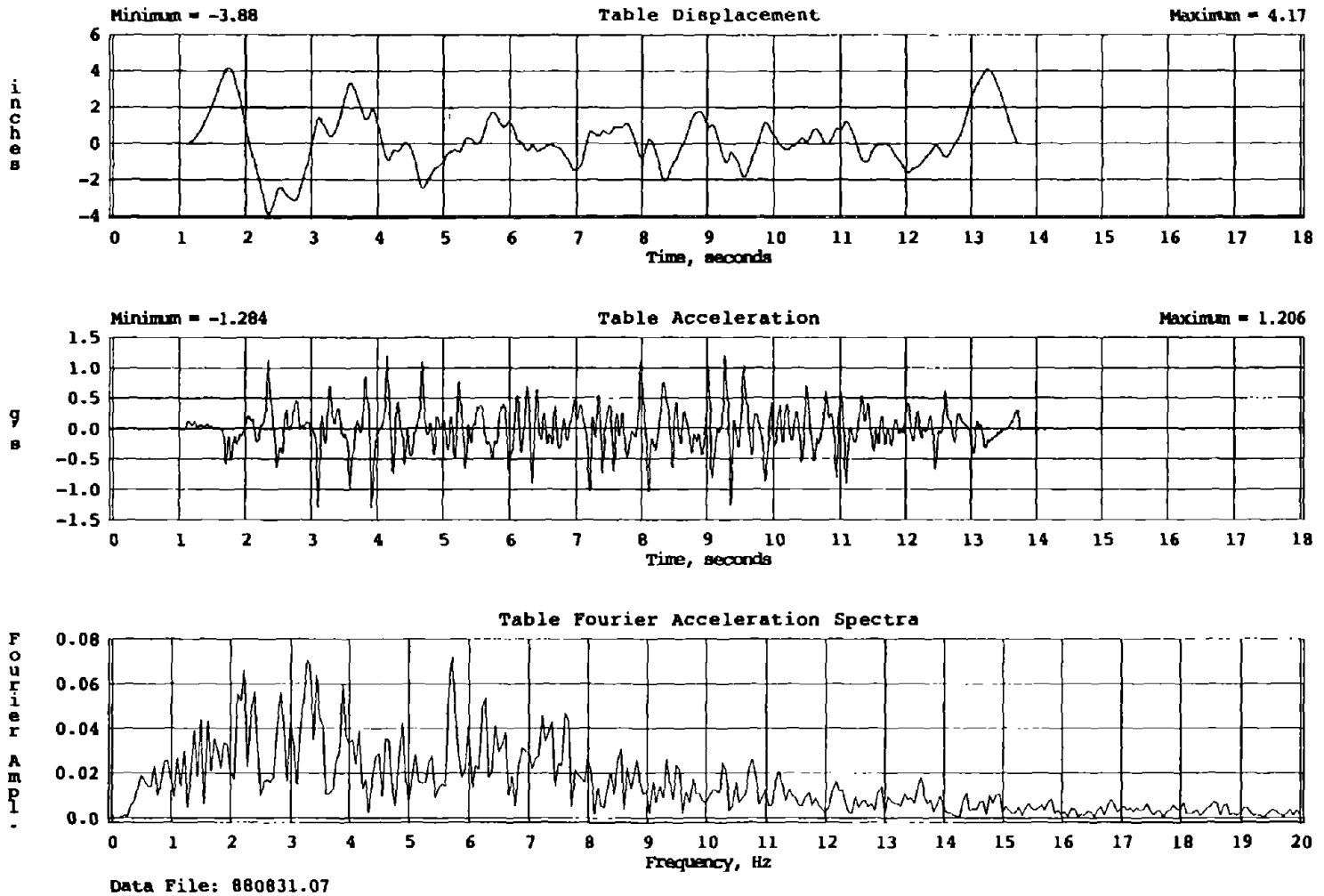

Figure 13 Displacement and Acceleration Time Histories and Fourier Acceleration Spectra for Chile, span = 800

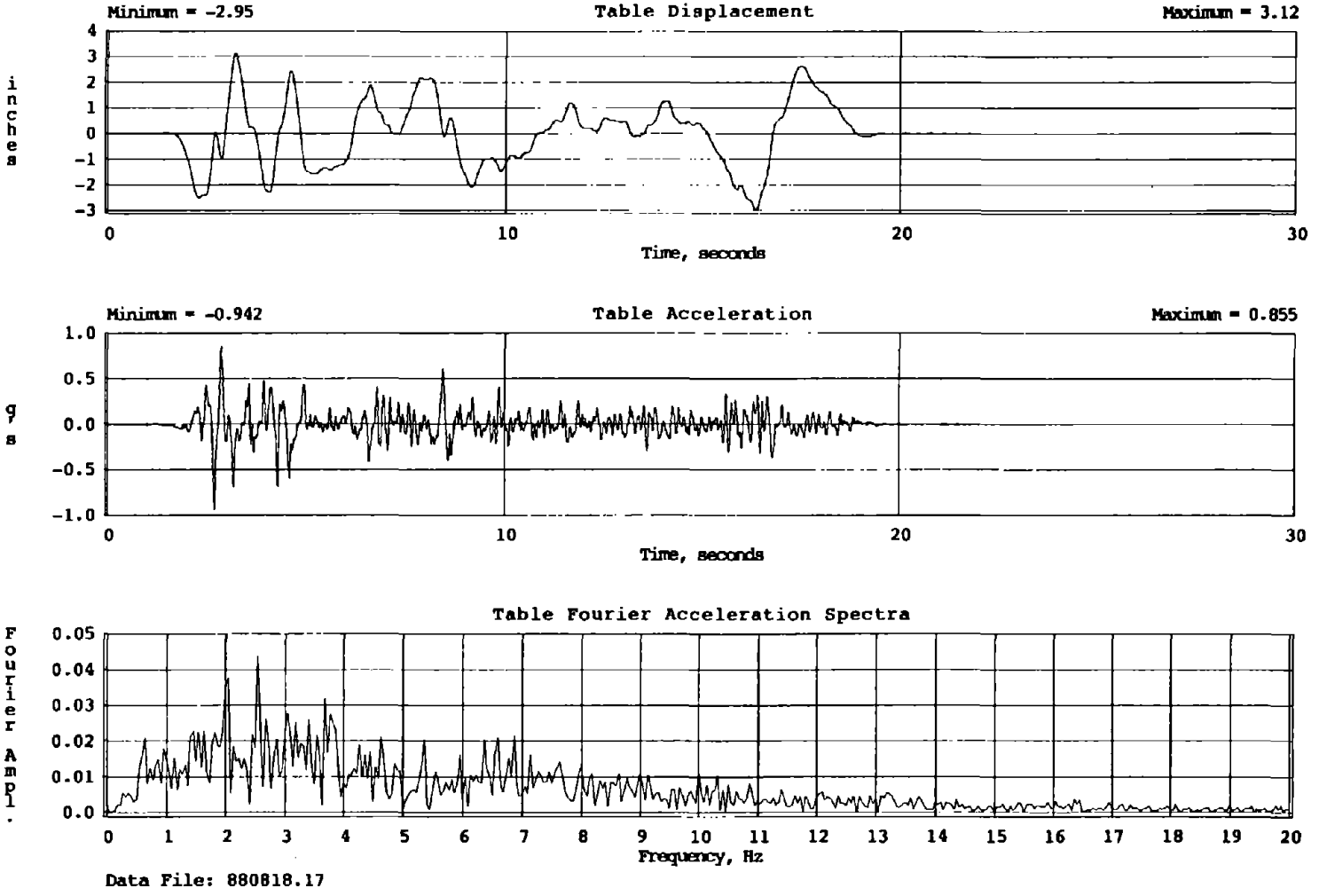

Figure 14 Displacement and Acceleration Time Histories and Fourier Acceleration Spectra for El Centro, span = 600

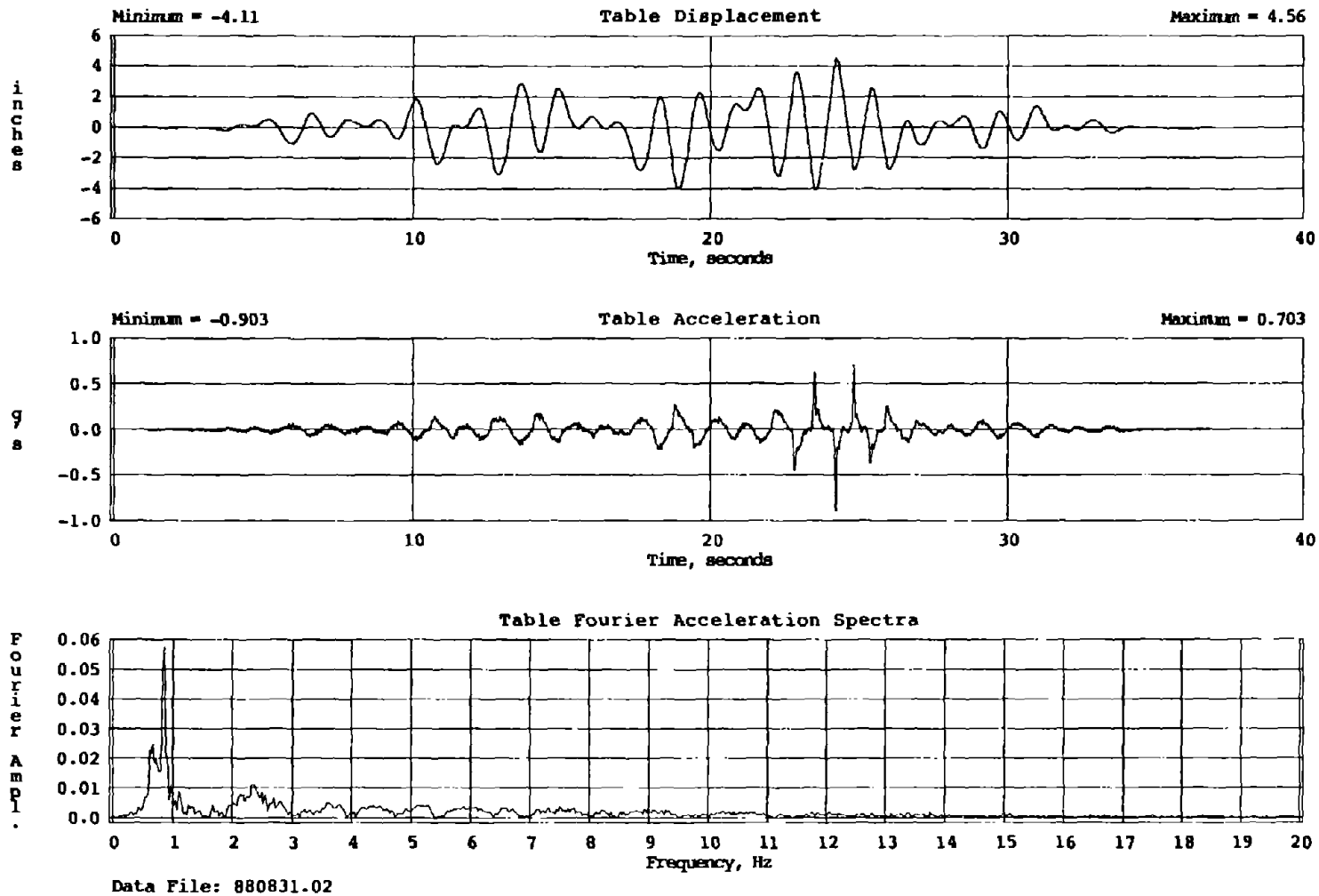

Figure 15 Displacement and Acceleration Time Histories and Fourier Acceleration Spectra for Mexico City, span = 900

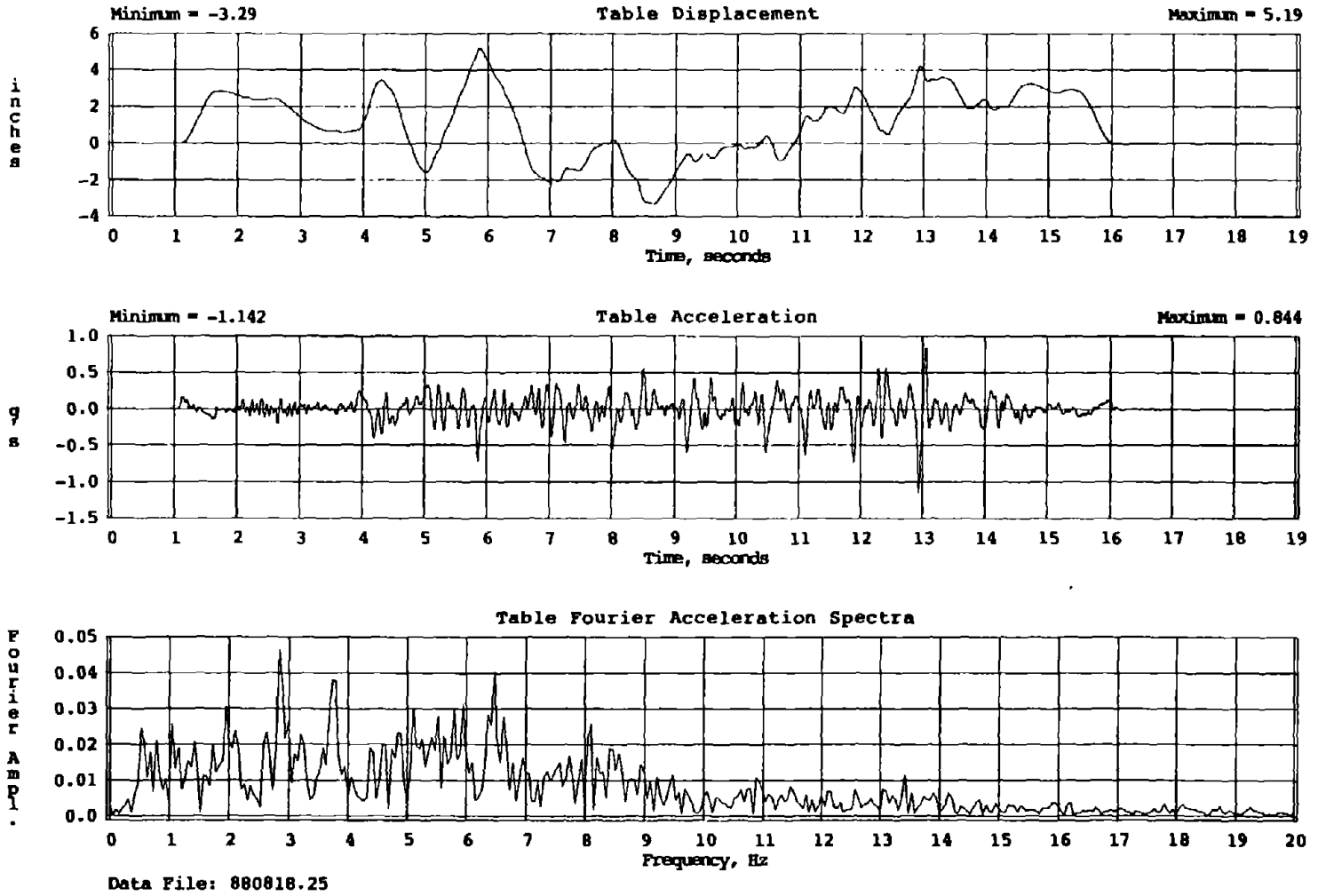

Figure 16 Displacement and Acceleration Time Histories and Fourier Acceleration Spectra for Olympia, span = 1000

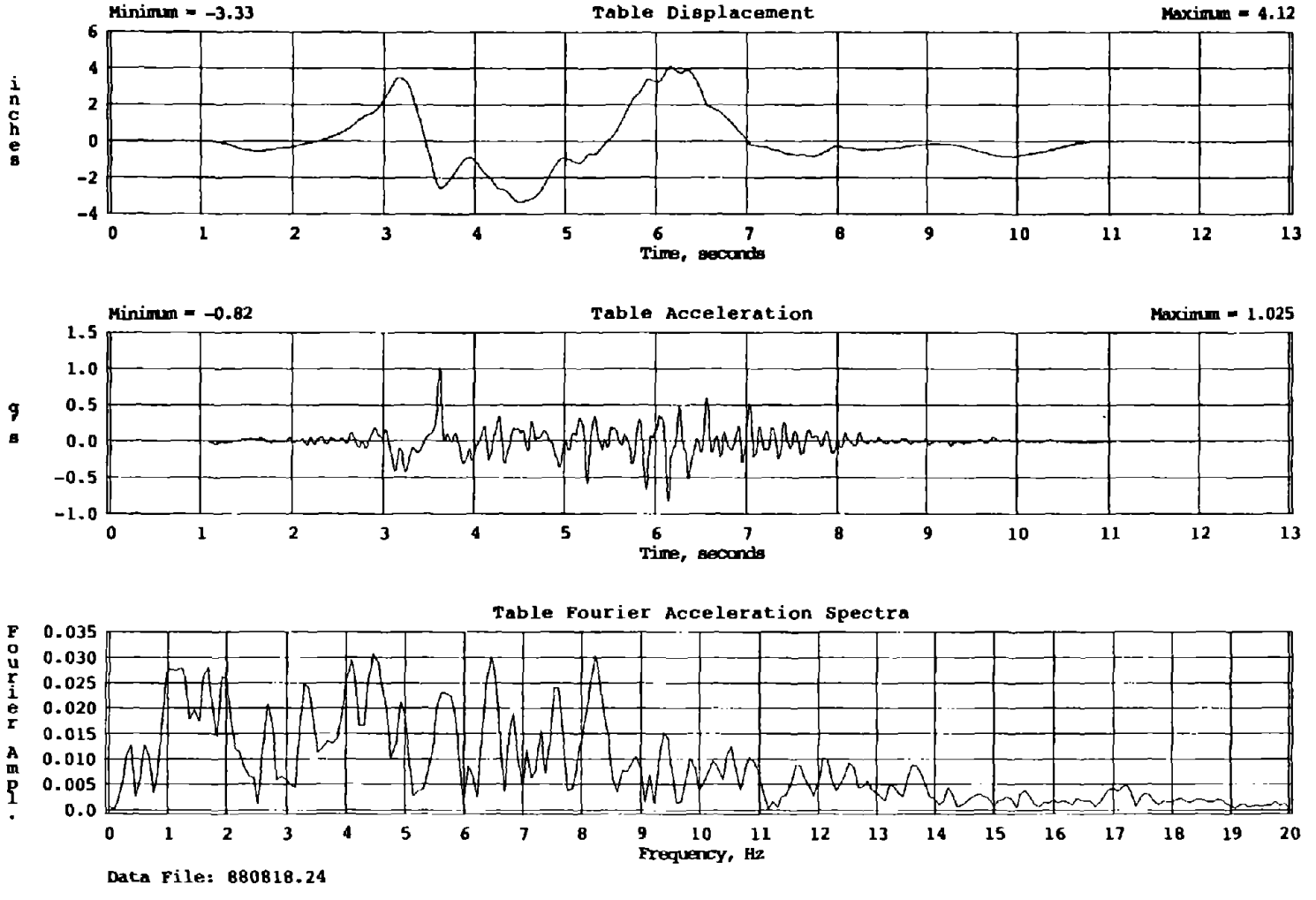

Figure 17 Displacement and Acceleration Time Histories and Fourier Acceleration Spectra for Pacoima Dam, span = 800

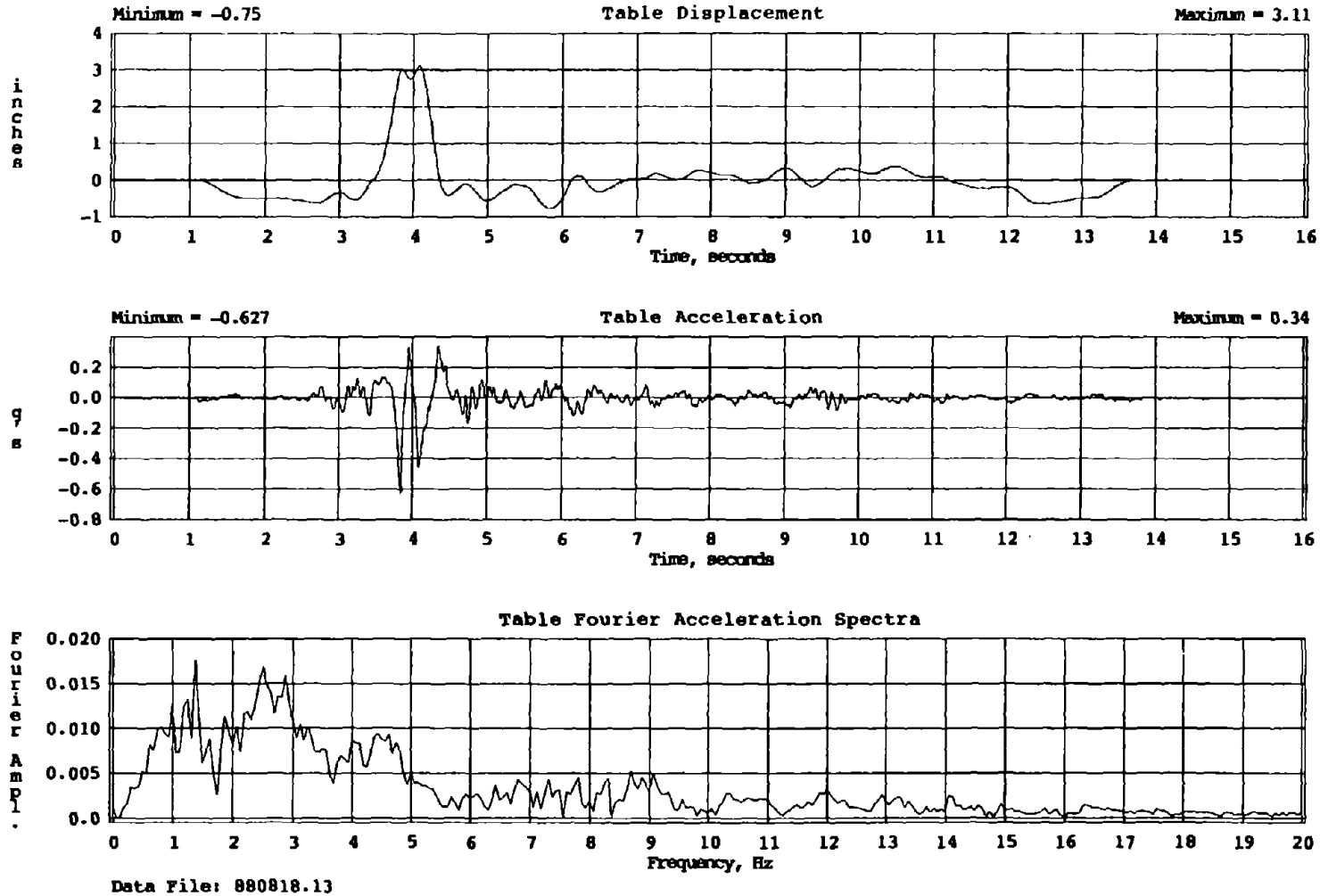

Figure 18 Displacement and Acceleration Time Histories and Fourier Acceleration Spectra for Parkfield, span = 600

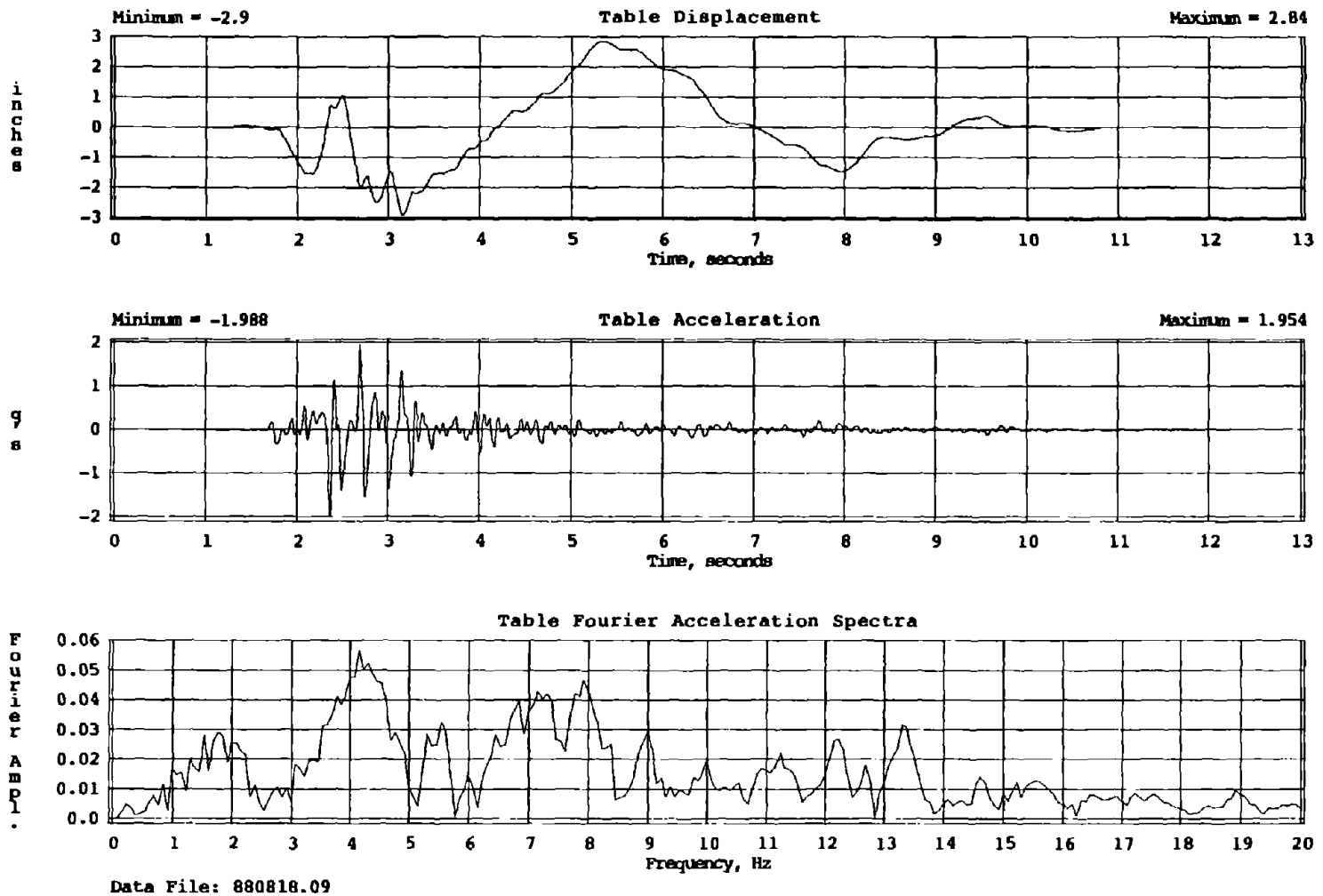

Figure 19 Displacement and Acceleration Time Histories and Fourier Acceleration Spectra for San Francisco, span = 600

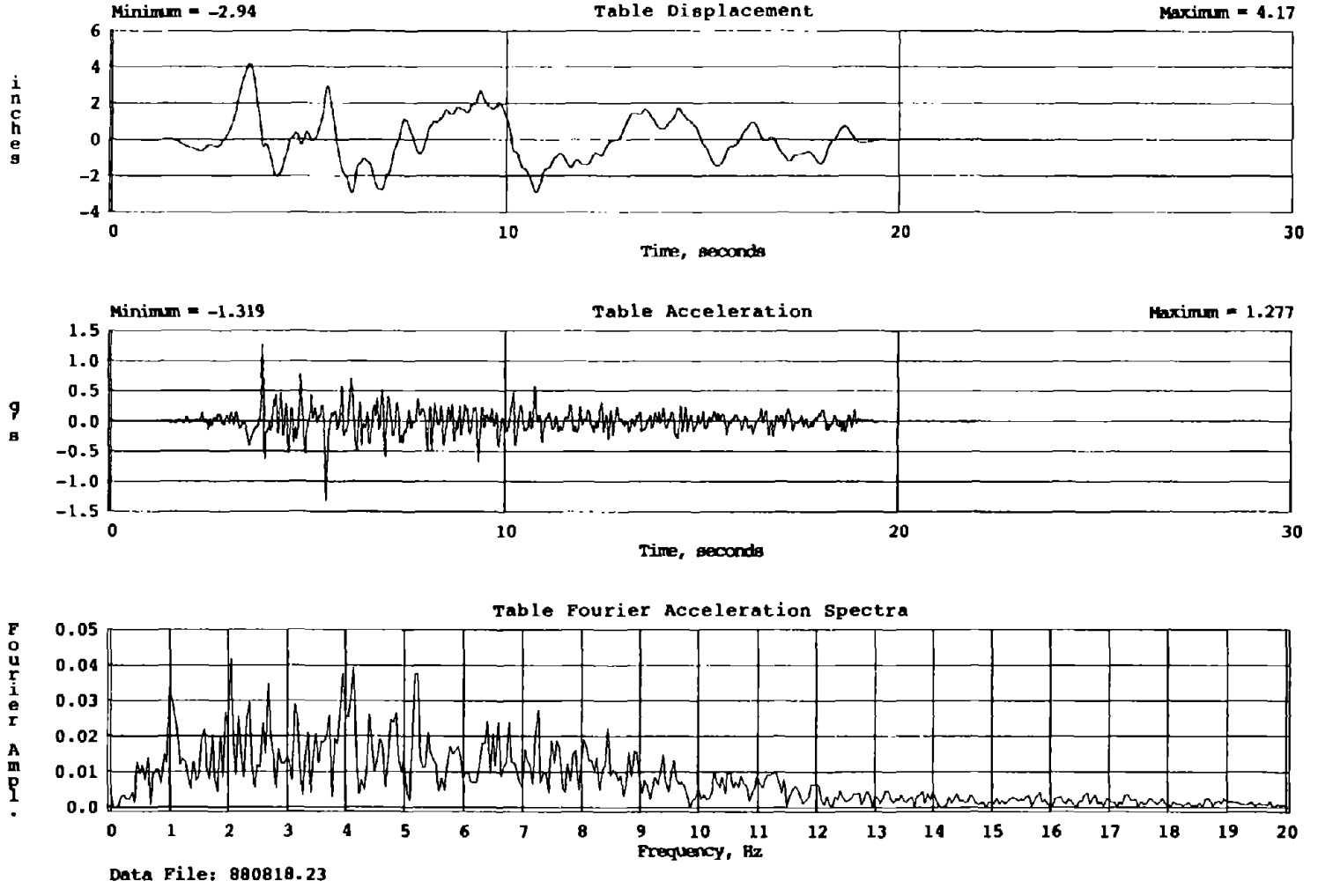

Figure 20 Displacement and Acceleration Time Histories and Fourier Acceleration Spectra for Taft, span = 800

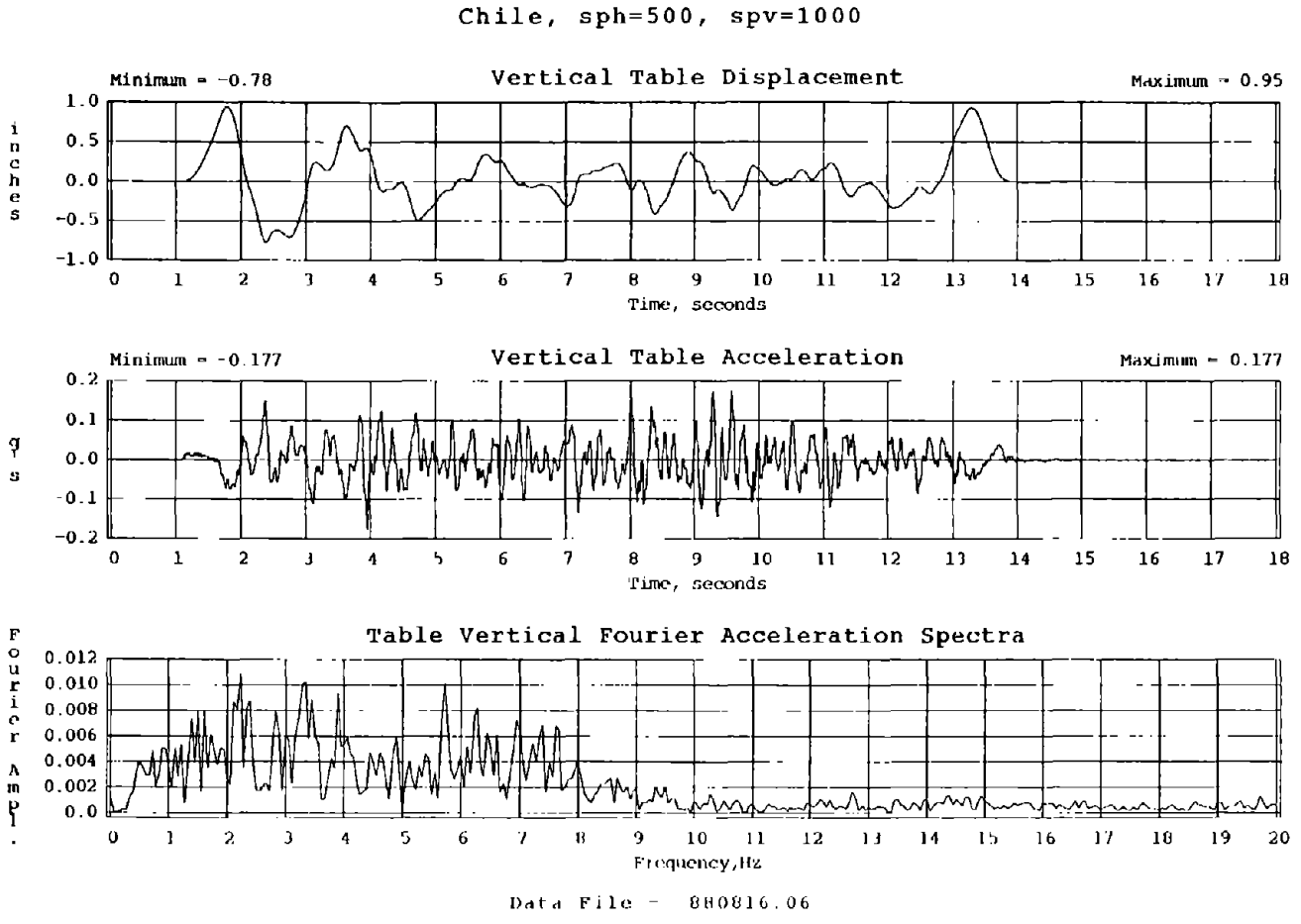

Figure 21 Vertical Displacement and Acceleration Time Histories and Fourier Acceleration Spectra for Chile, sph = 500, spv = 1000

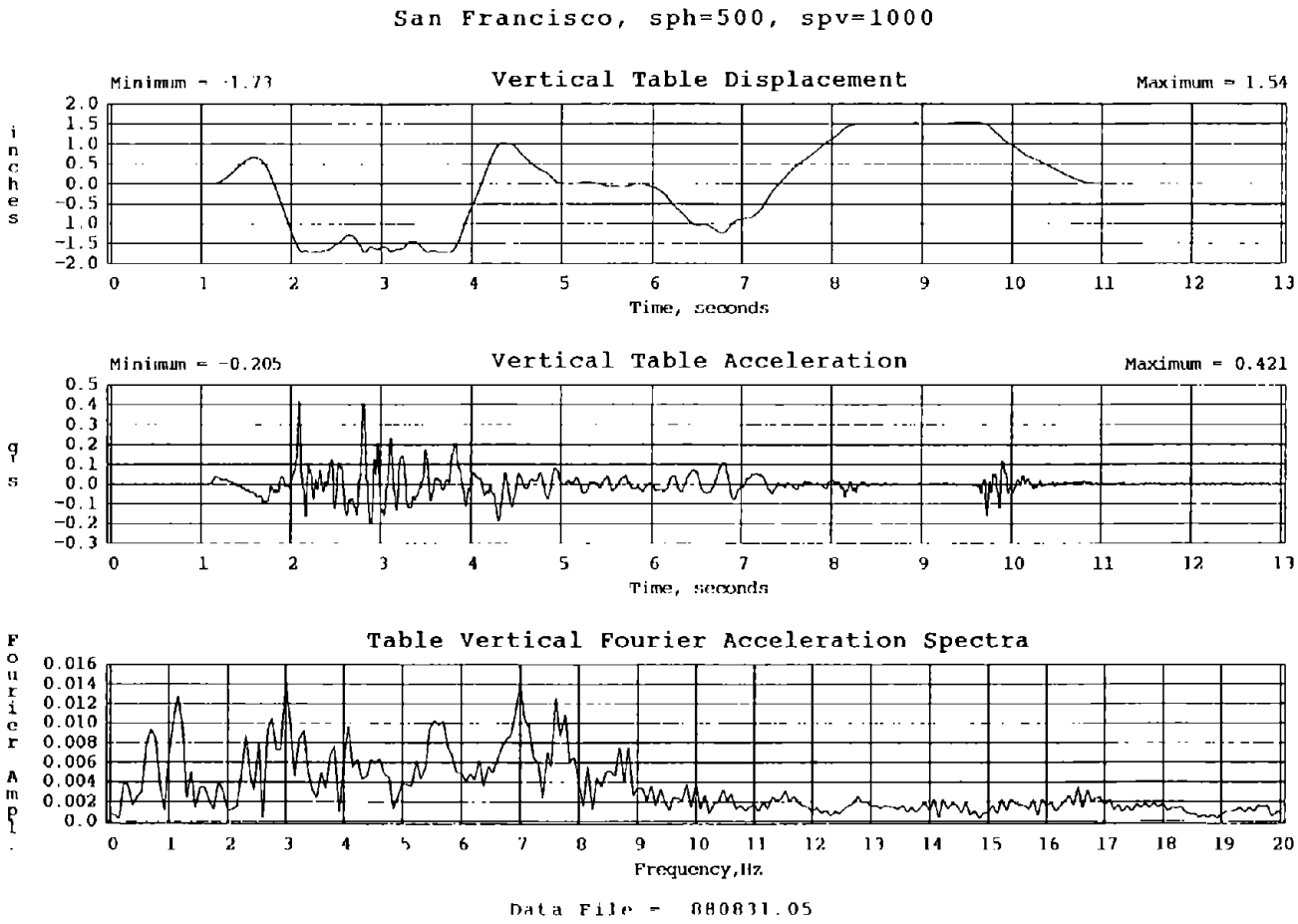

Figure 22 Vertical Displacement and Acceleration Time Histories and Fourier Acceleration Spectra for San Francisco, sph = 500, spv = 1000

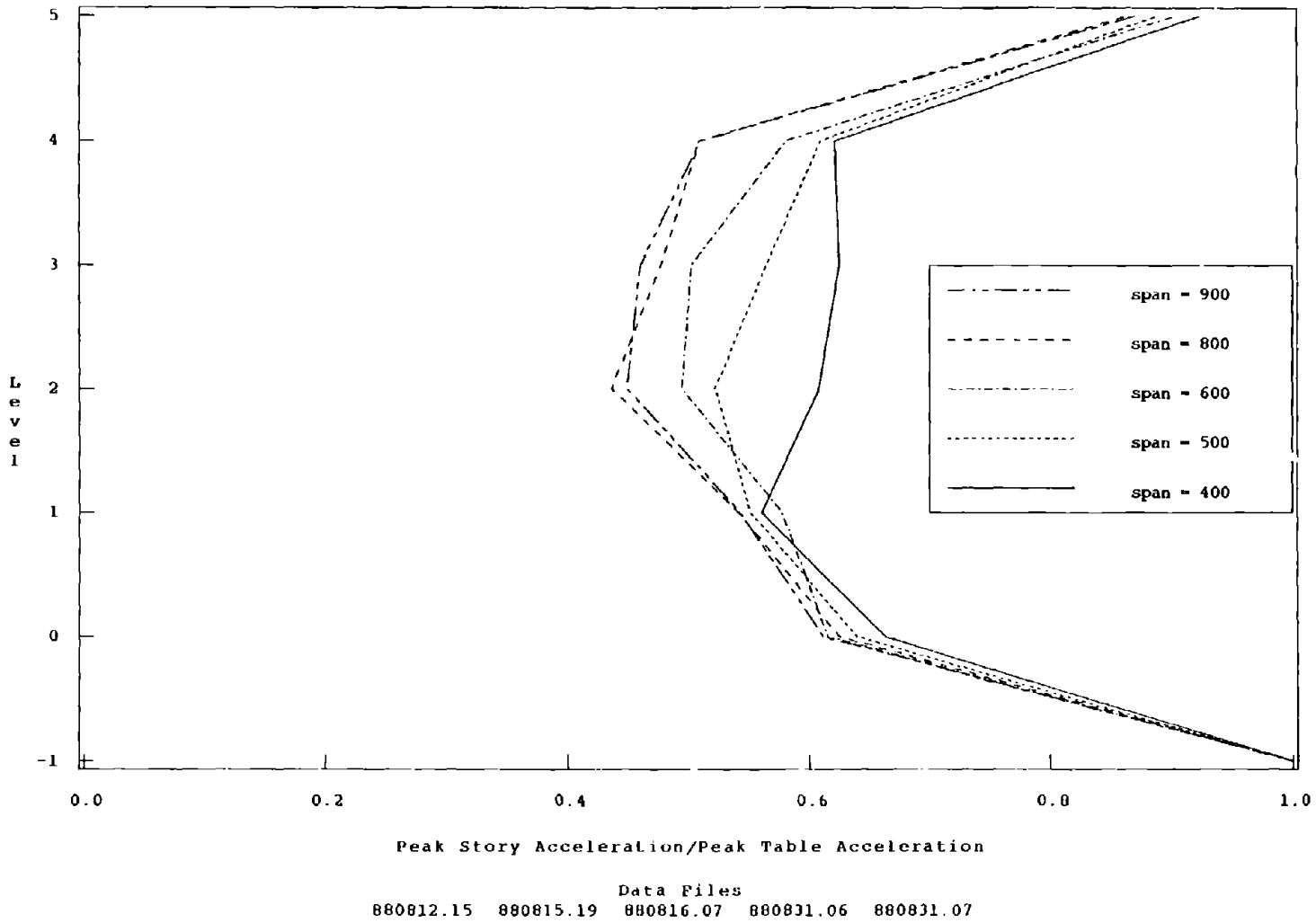

Figure 23 Normalized Accelerations Throughout Test Frame for Chile

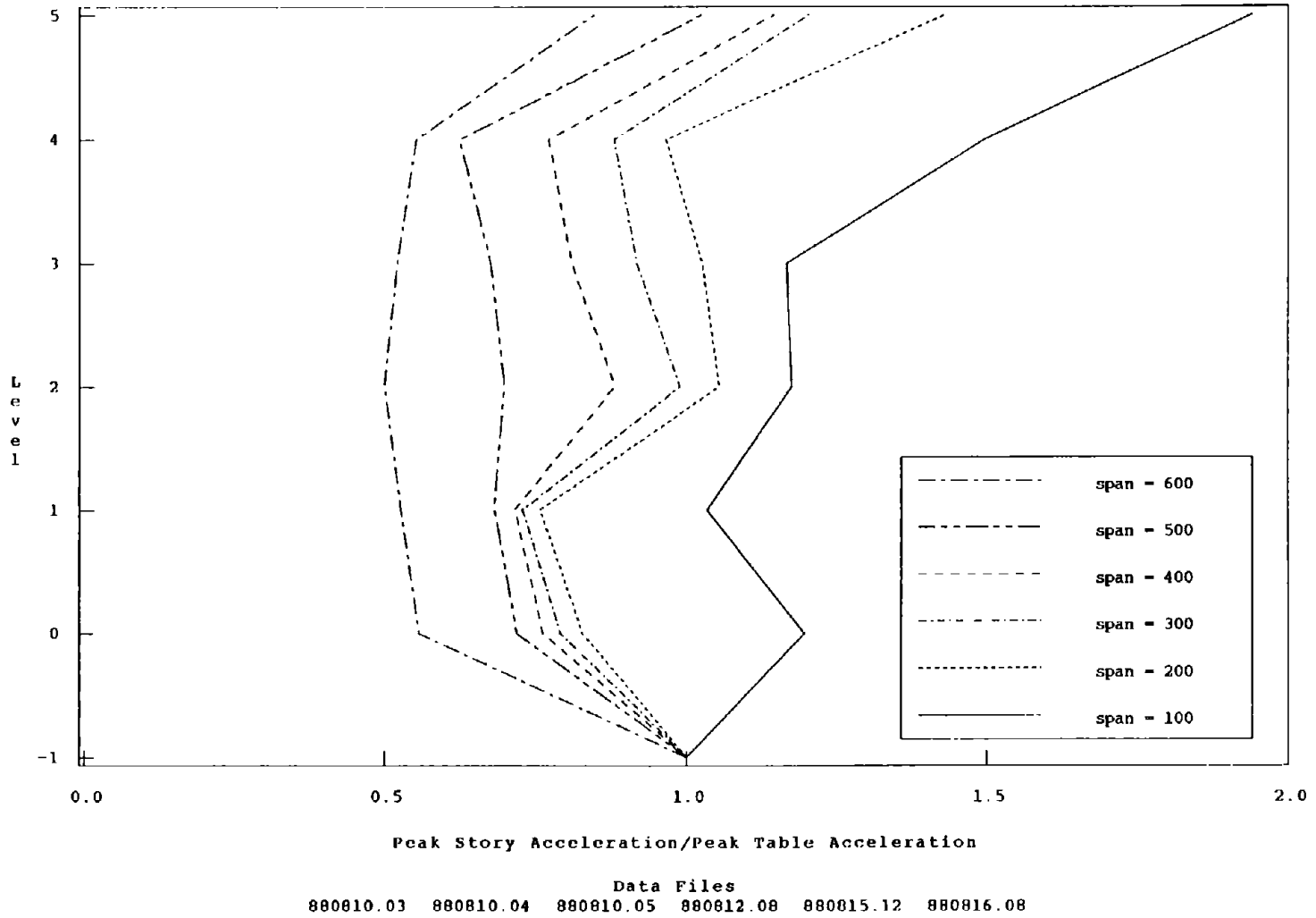

Figure 24 Normalized Accelerations Throughout Test Frame for El Centro.

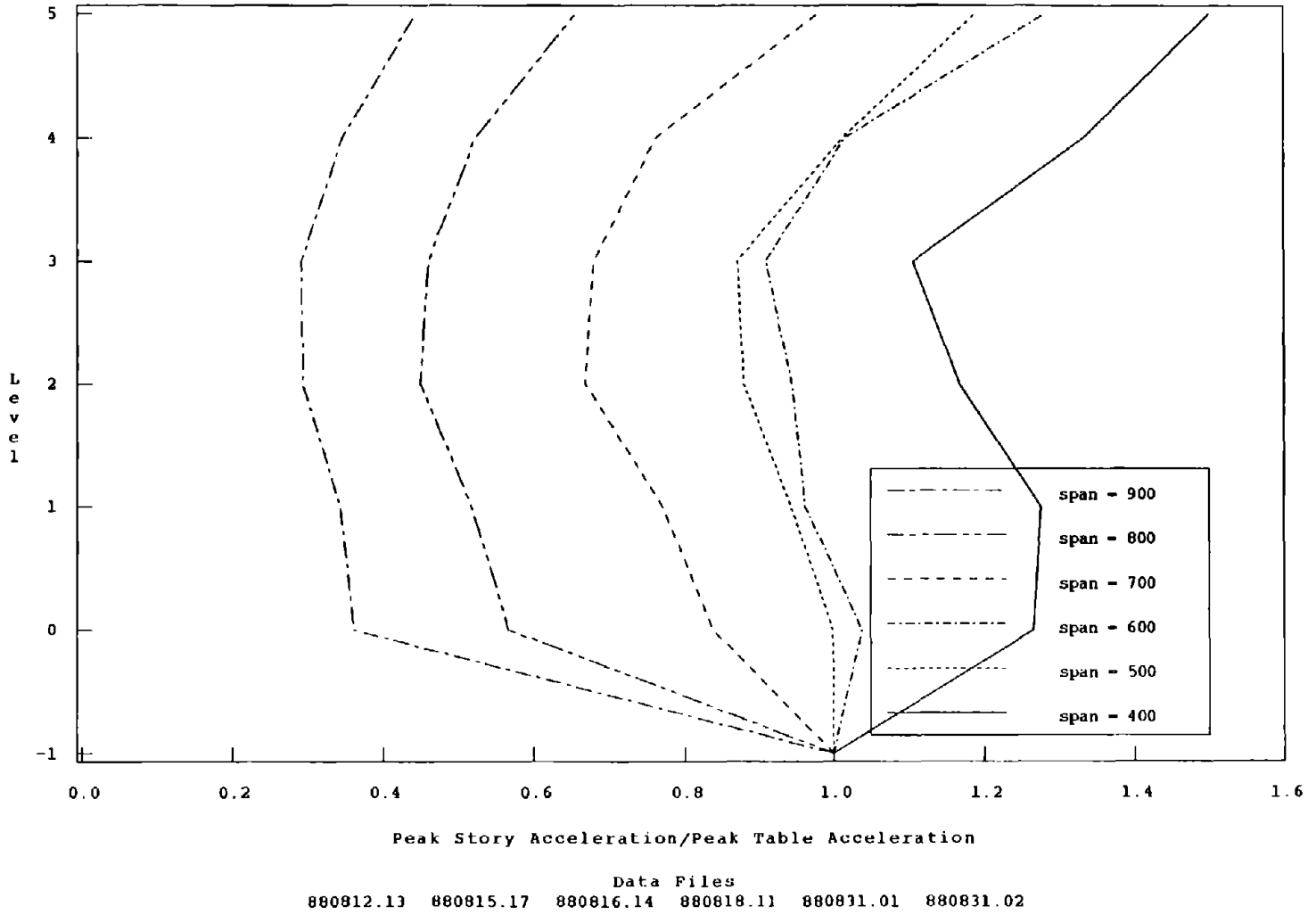

Figure 25 Normalized Accelerations Throughout Test Frame for Mexico City

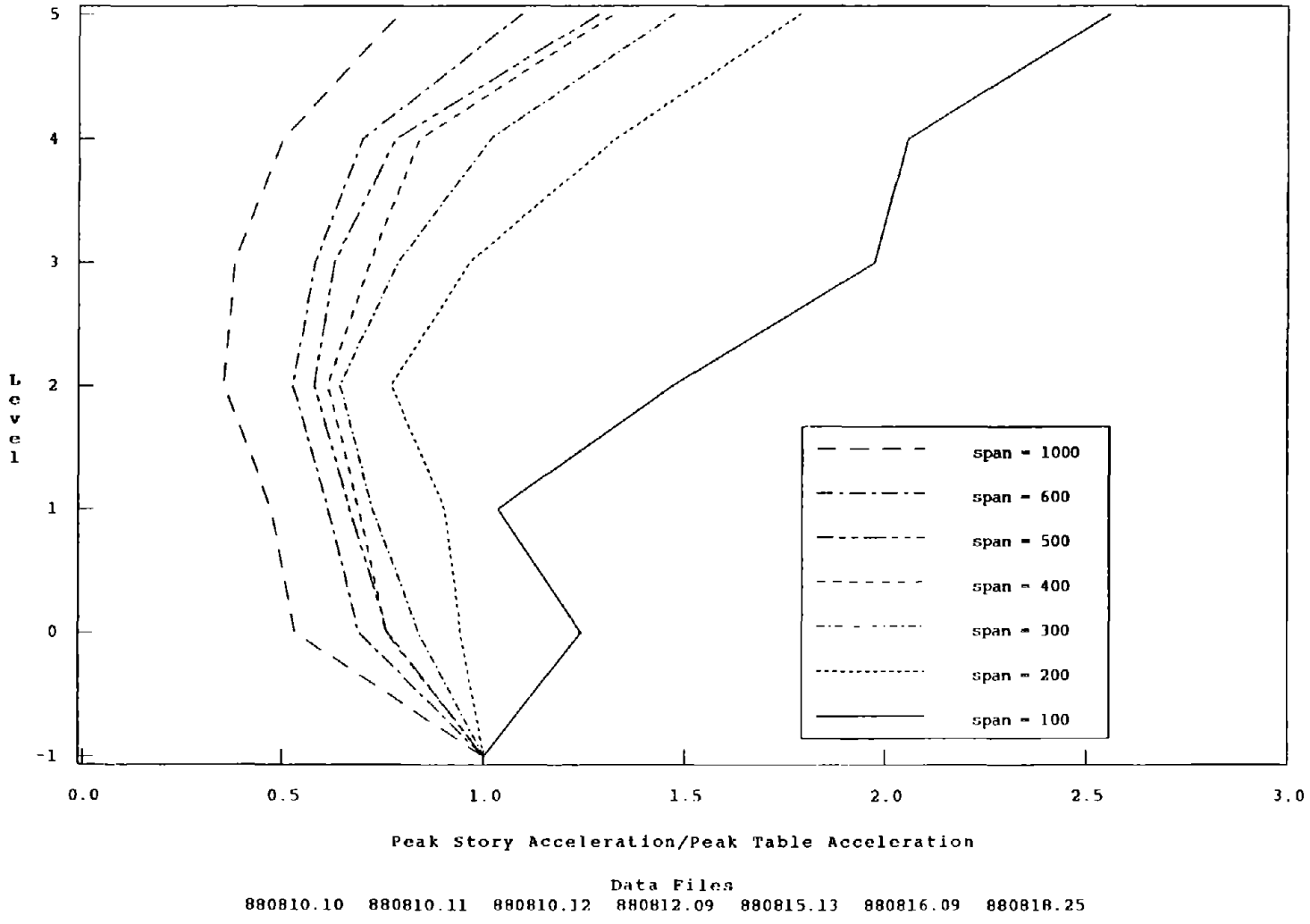

Figure 26 Normalized Accelerations Throughout Test Frame for Olympia

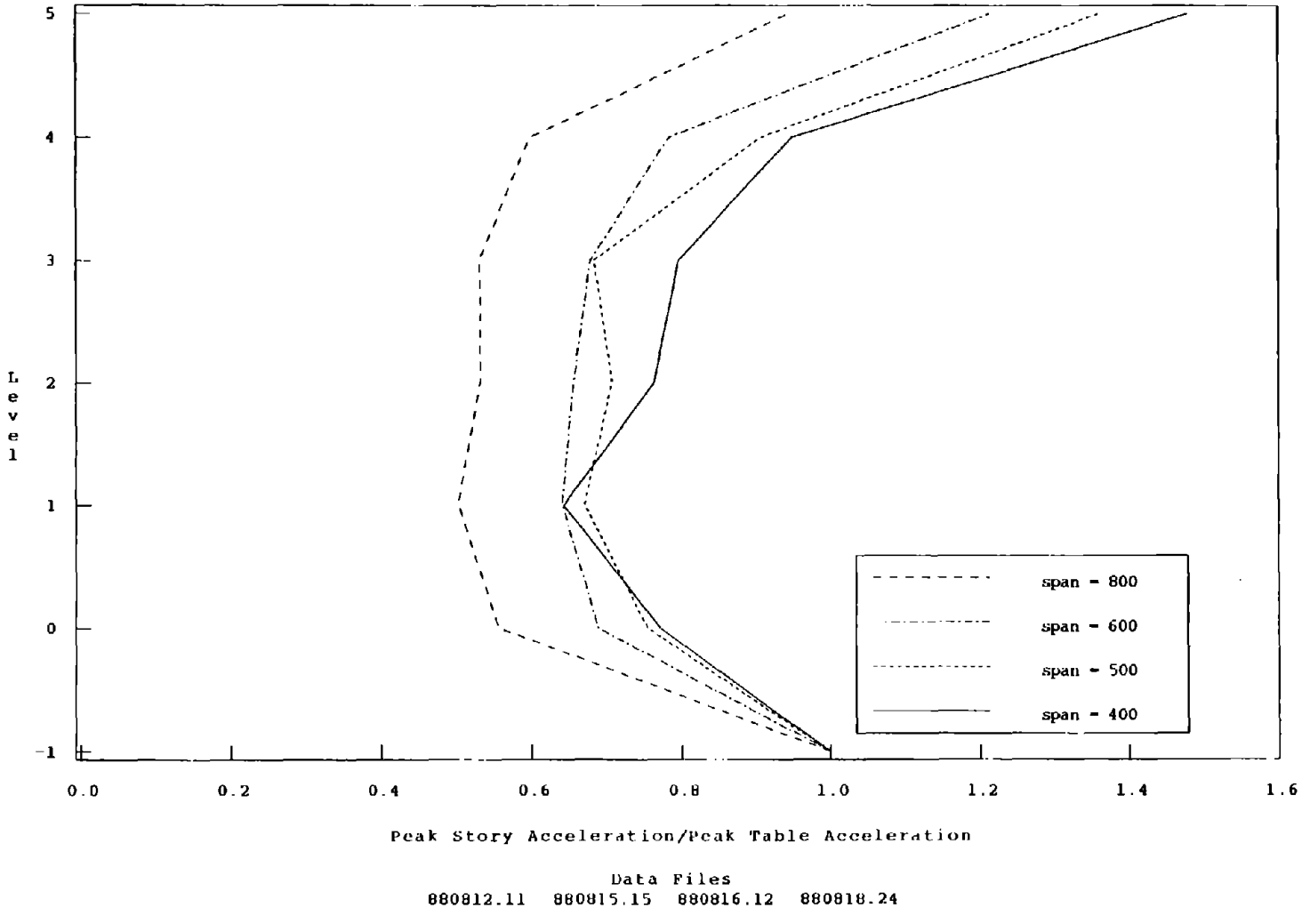

Figure 27 Normalized Accelerations Throughout Test Frame for Pacoima Dam

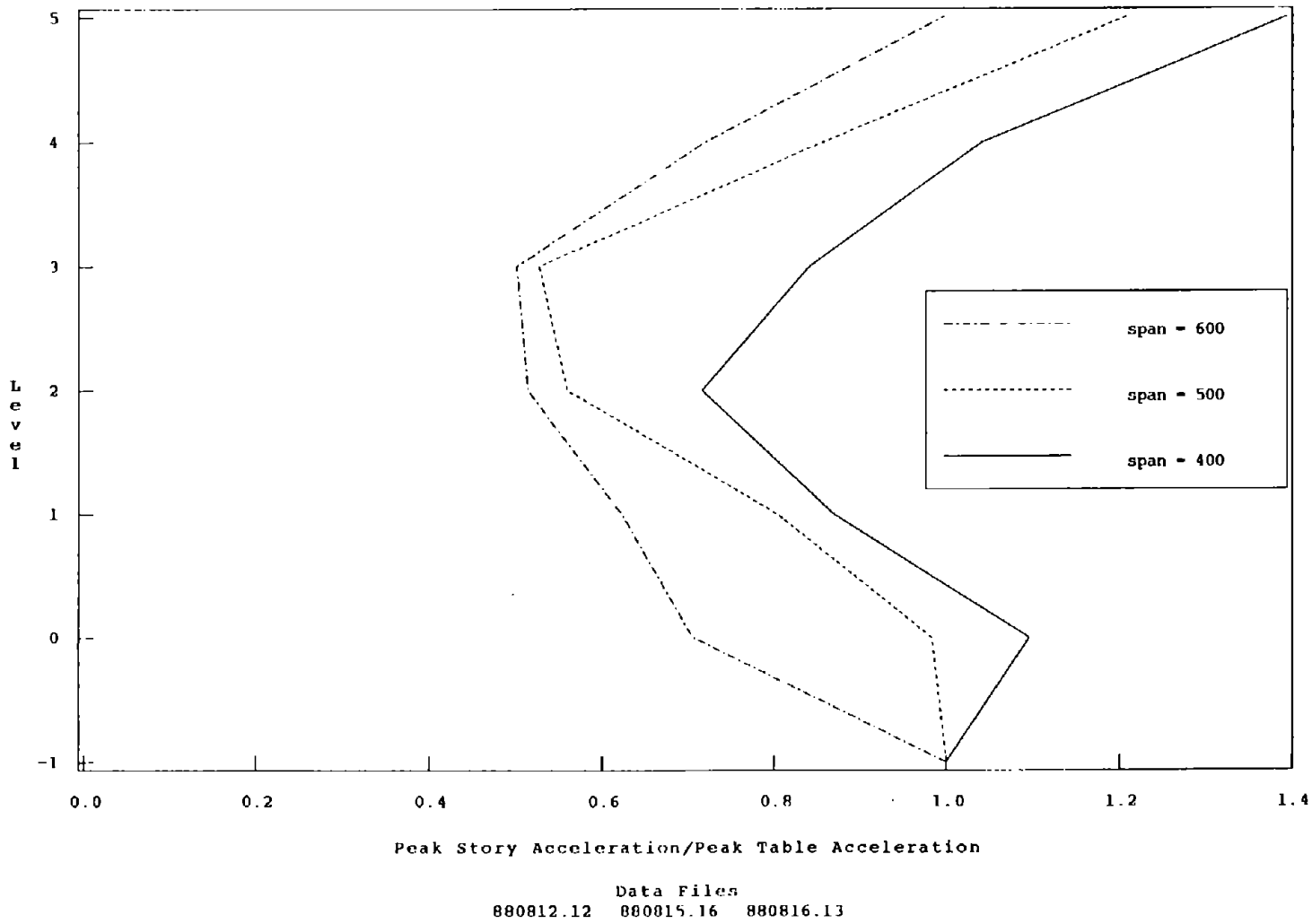

Figure 28 Normalized Accelerations Throughout Test Frame for Parkfield

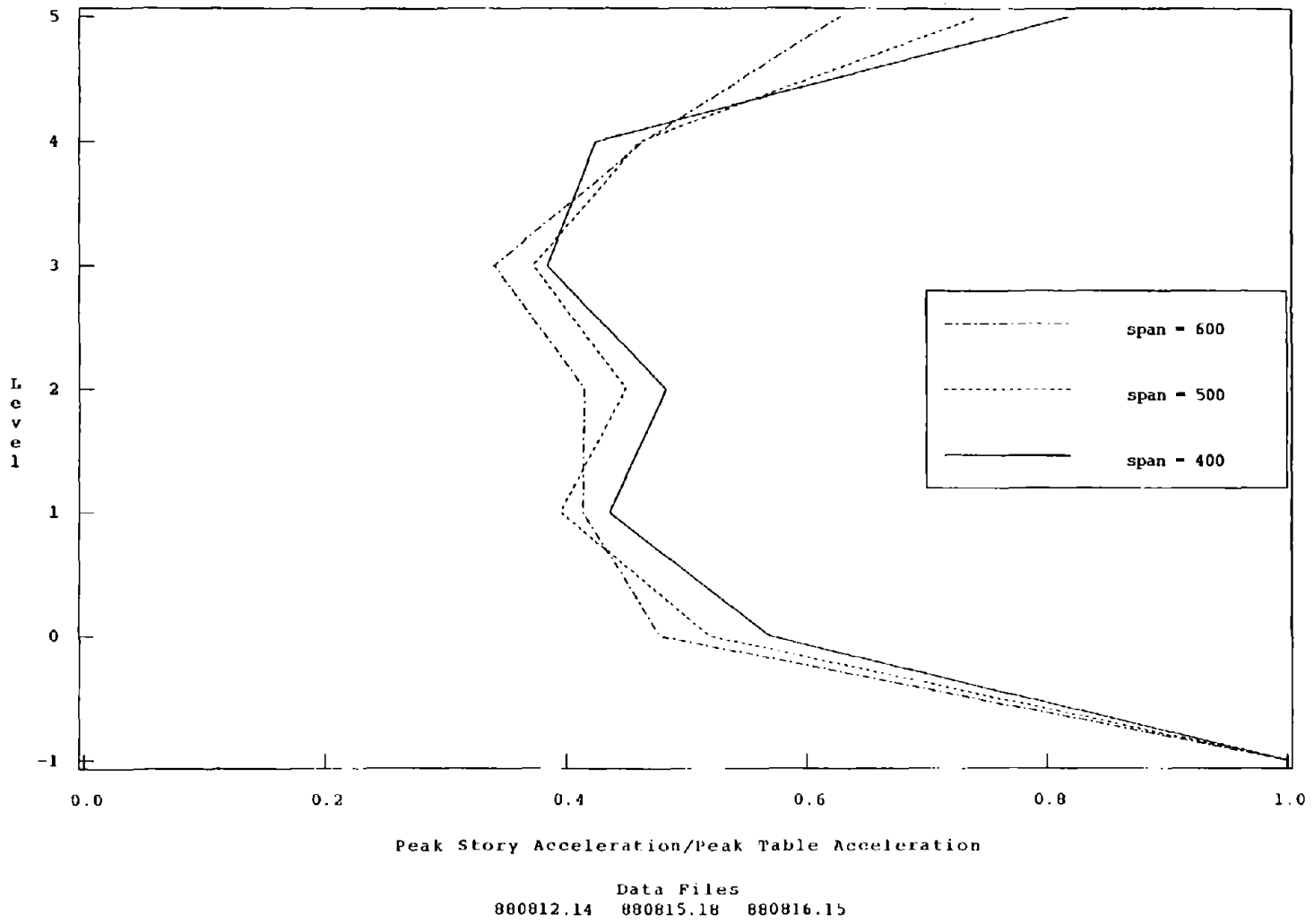

Figure 29 Normalized Accelerations Throughout Test Frame for San Francisco

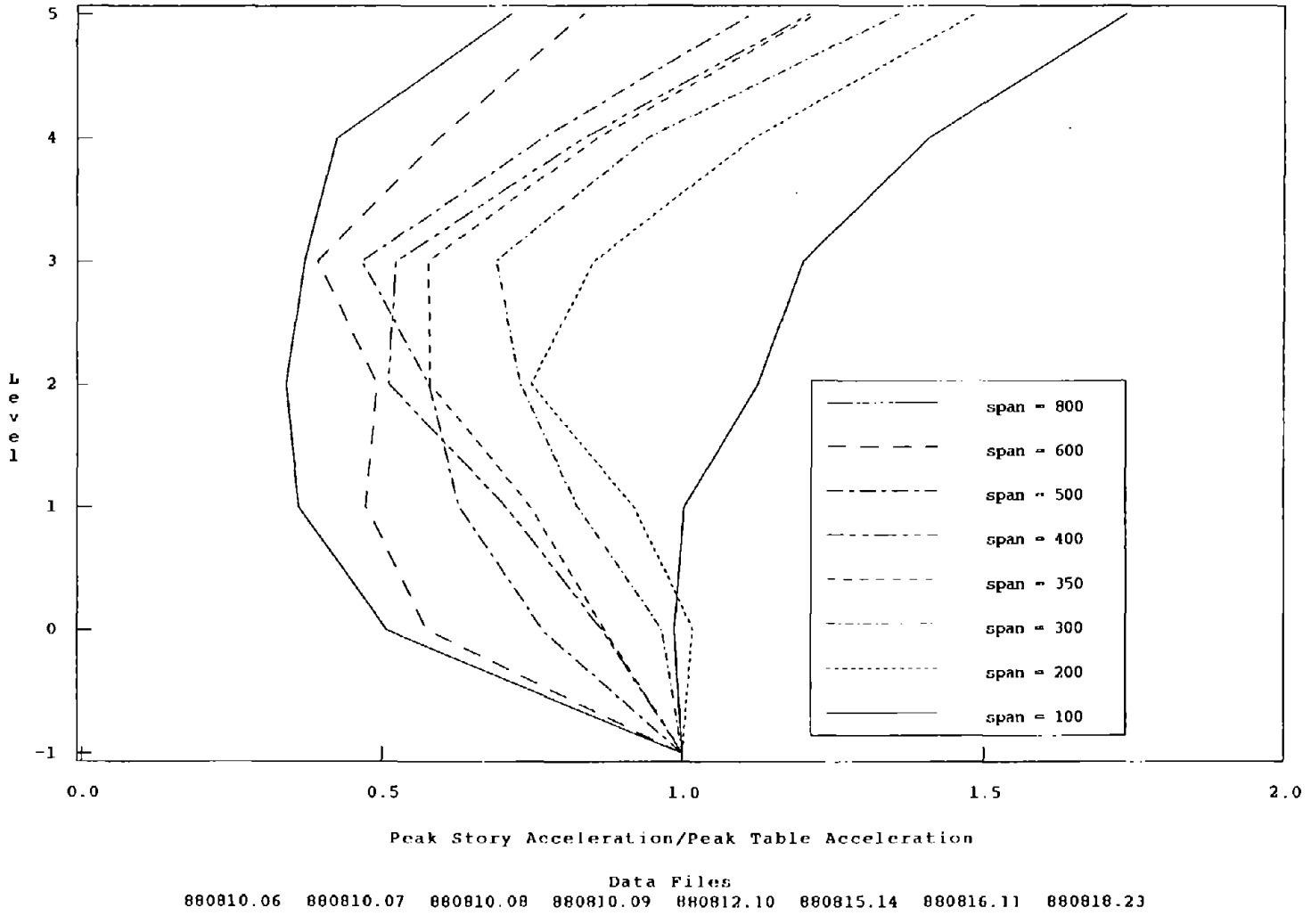

Figure 30 Normalized Accelerations Throughout Test Frame for Taft

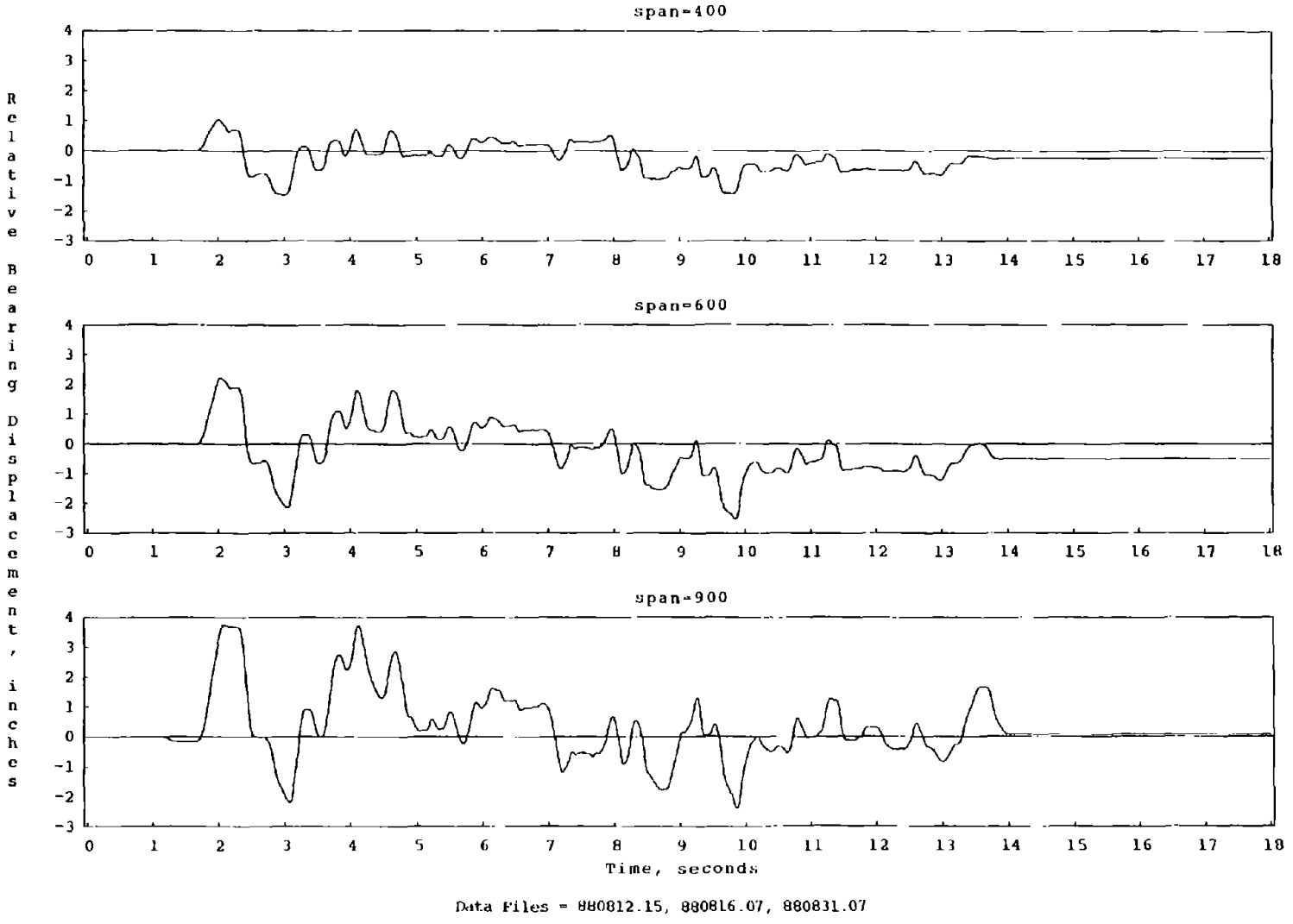

Figure 31 Relative Bearing Displacement Time Histories for Chile

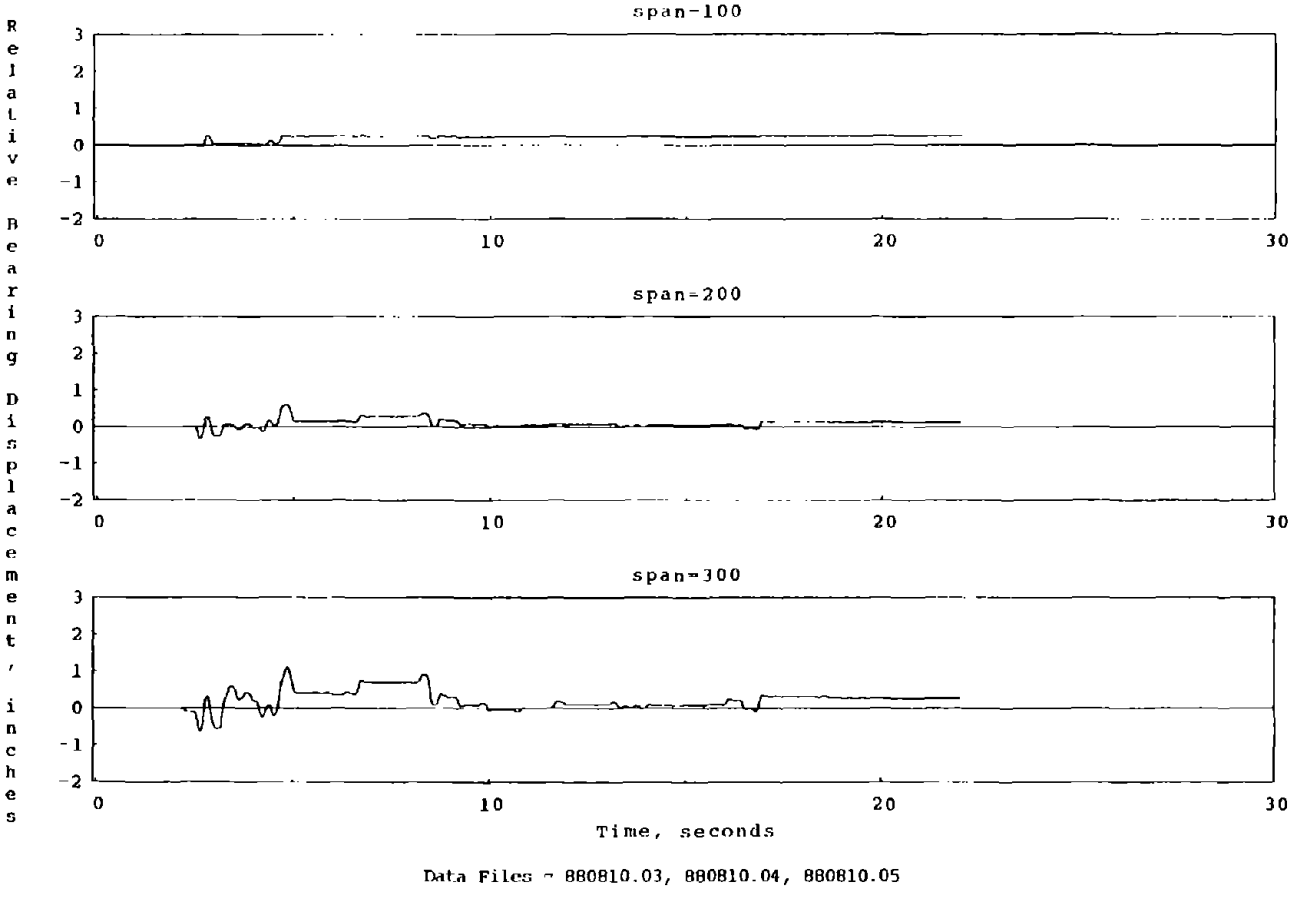

Figure 32 Relative Bearing Displacement Time Histories for El Centro

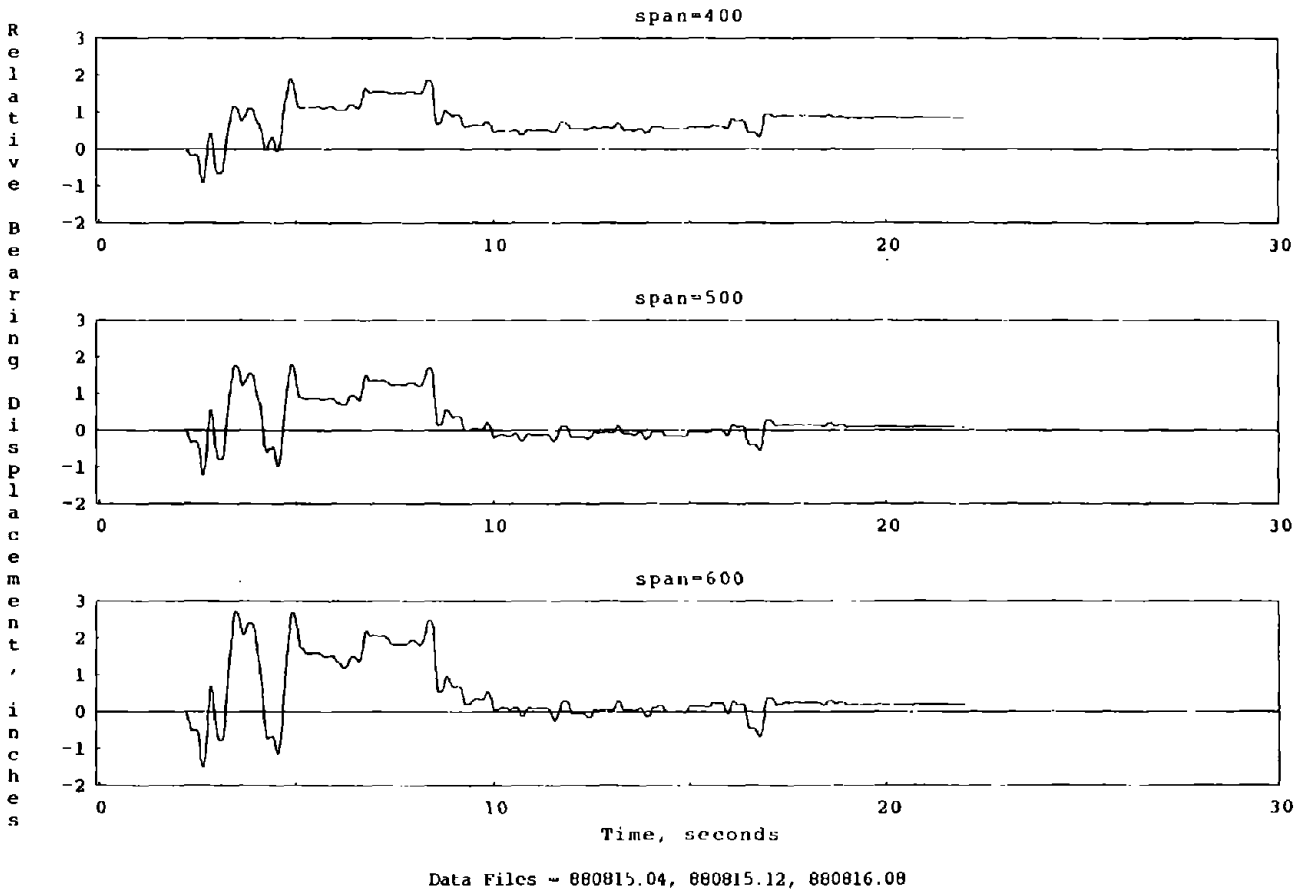

Figure 32 Relative Bearing Displacement Time Histories for El Centro (Continued)

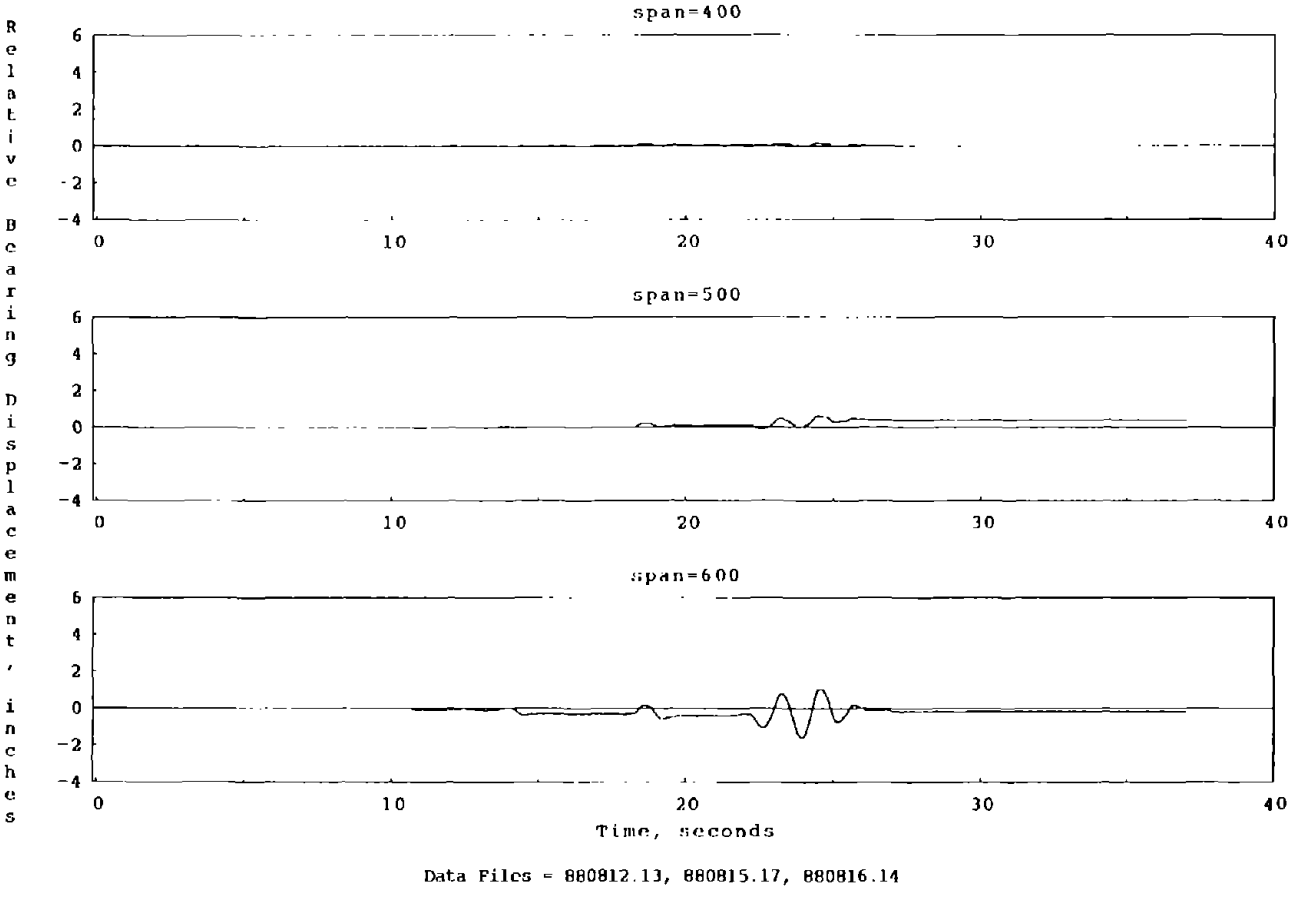

Figure 33 Relative Bearing Displacement Time Histories for Mexico City

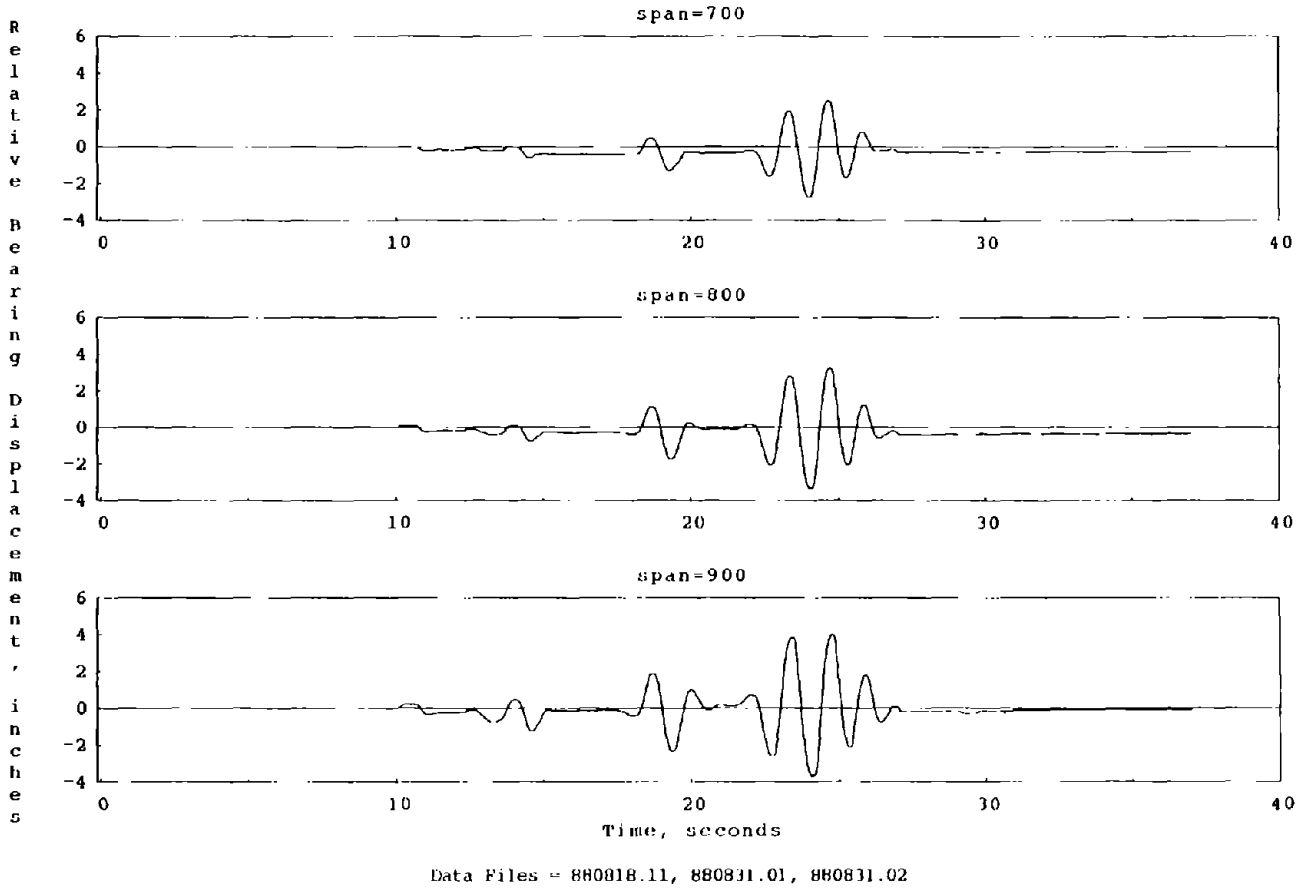

Figure 33 Relative Bearing Displacement Time Histories for Mexico City (Continued)

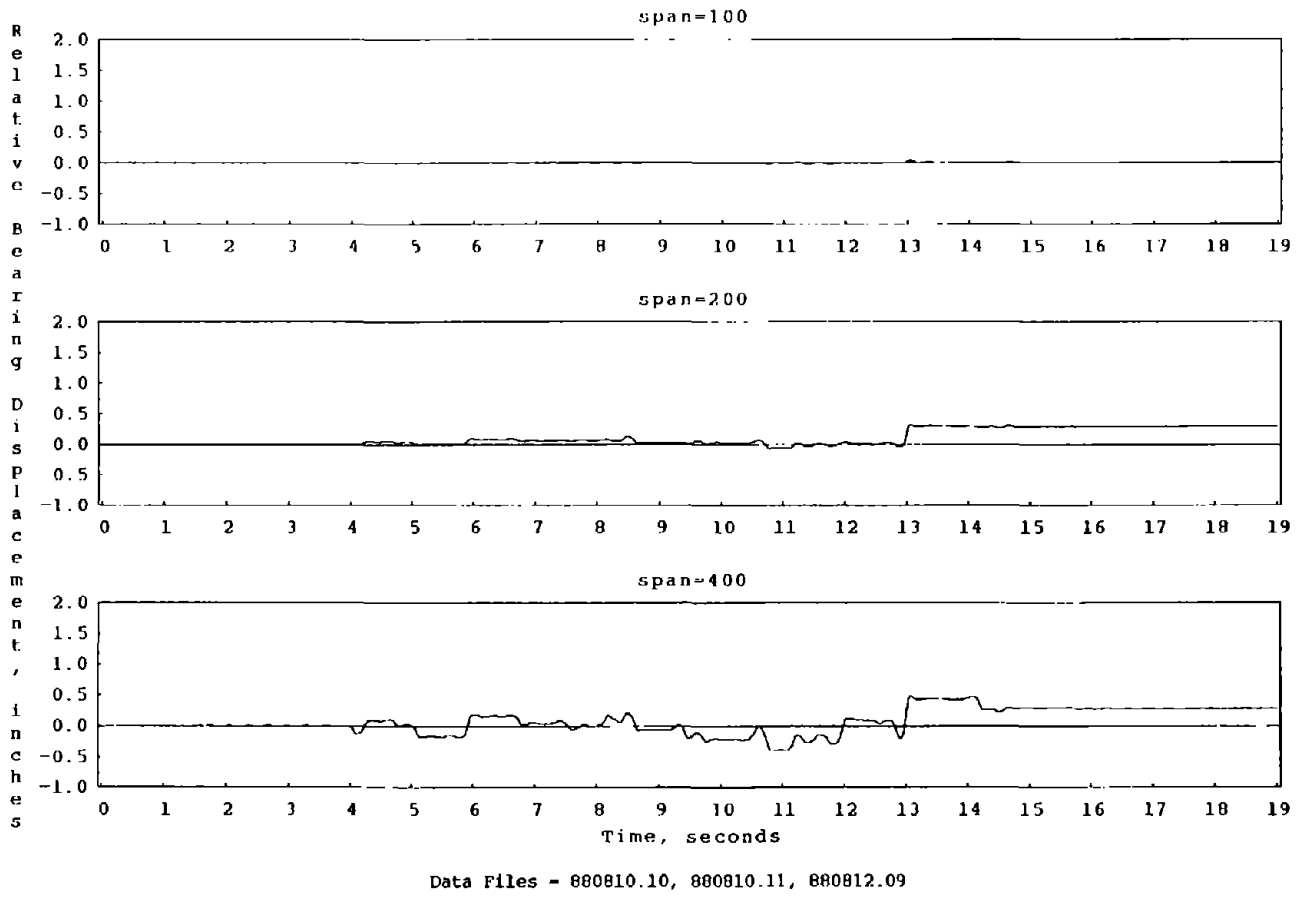

Figure 34 Relative Bearing Displacement Time Histories for Olympia

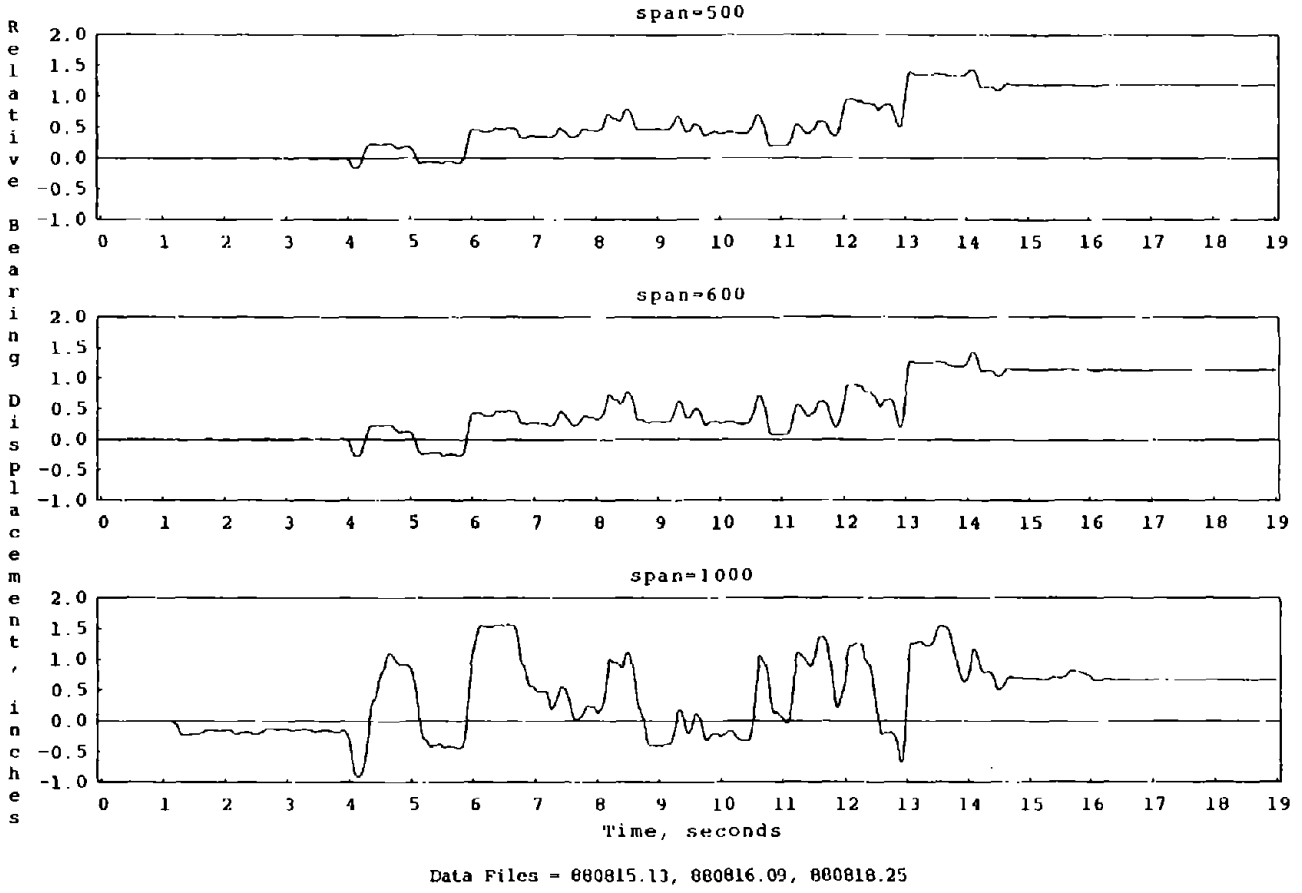

Figure 34 Relative Bearing Displacement Time Histories for Olympia (Continued)

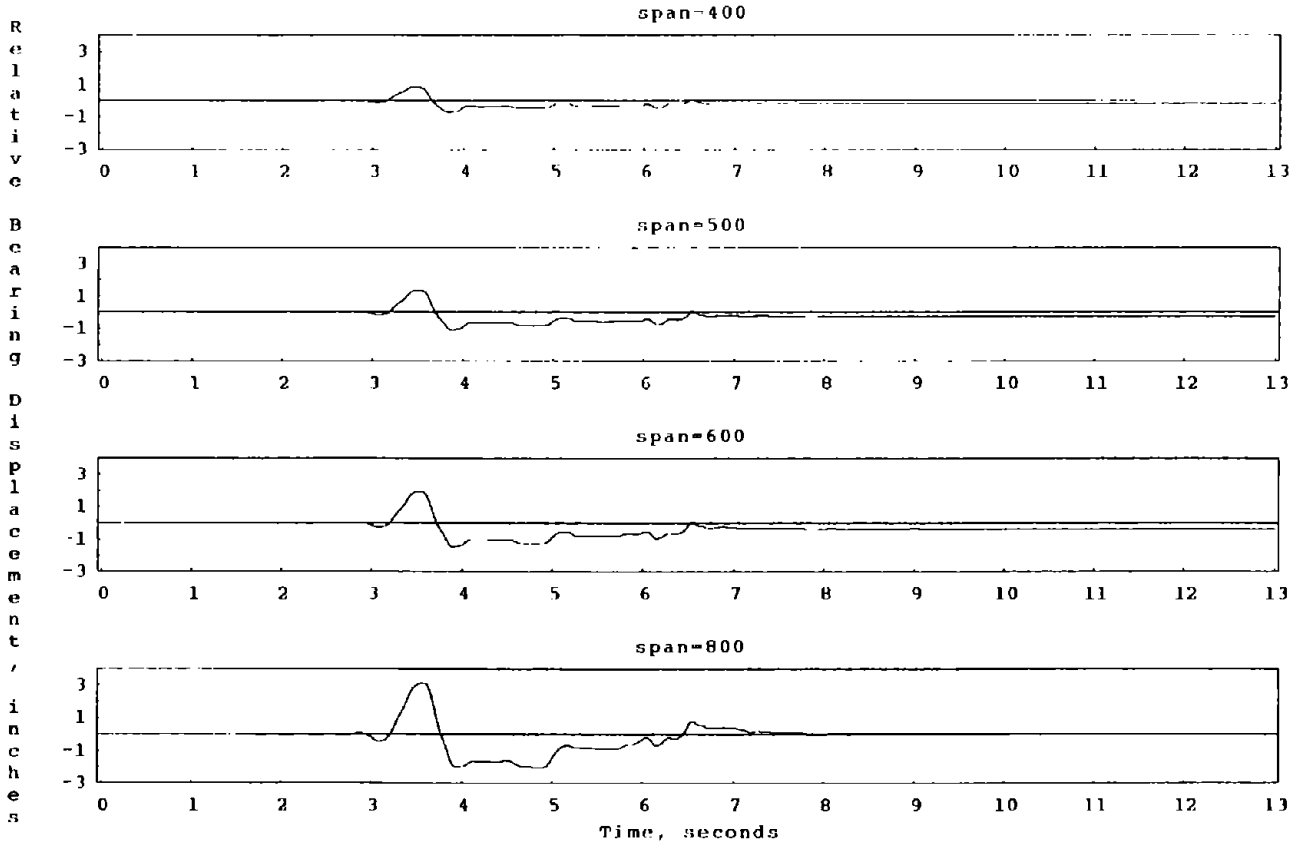

Figure 35 Relative Bearing Displacement Time Histories for Pacoima Dam

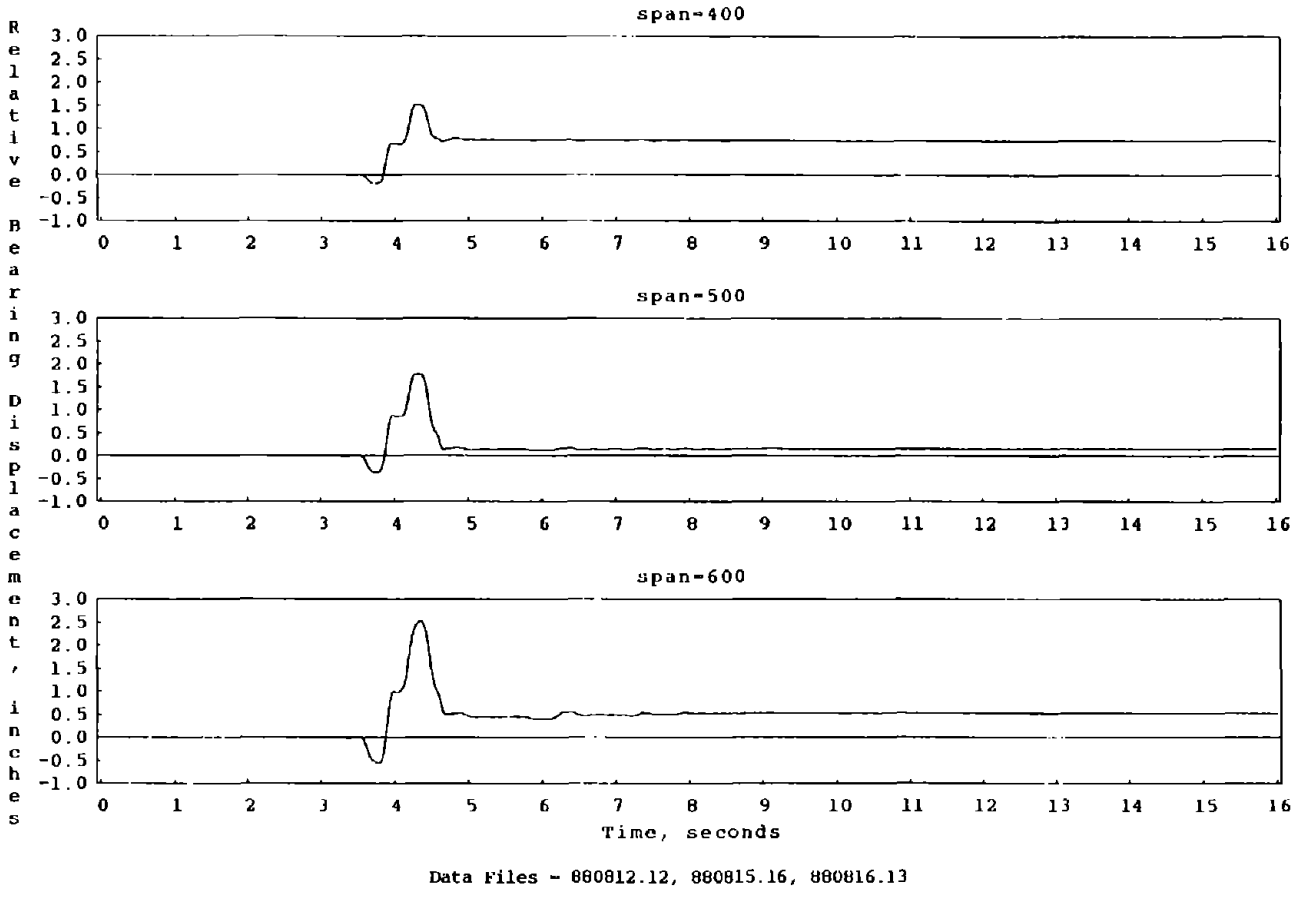

Figure 36 Relative Bearing Displacement Time Histories for Parkfield

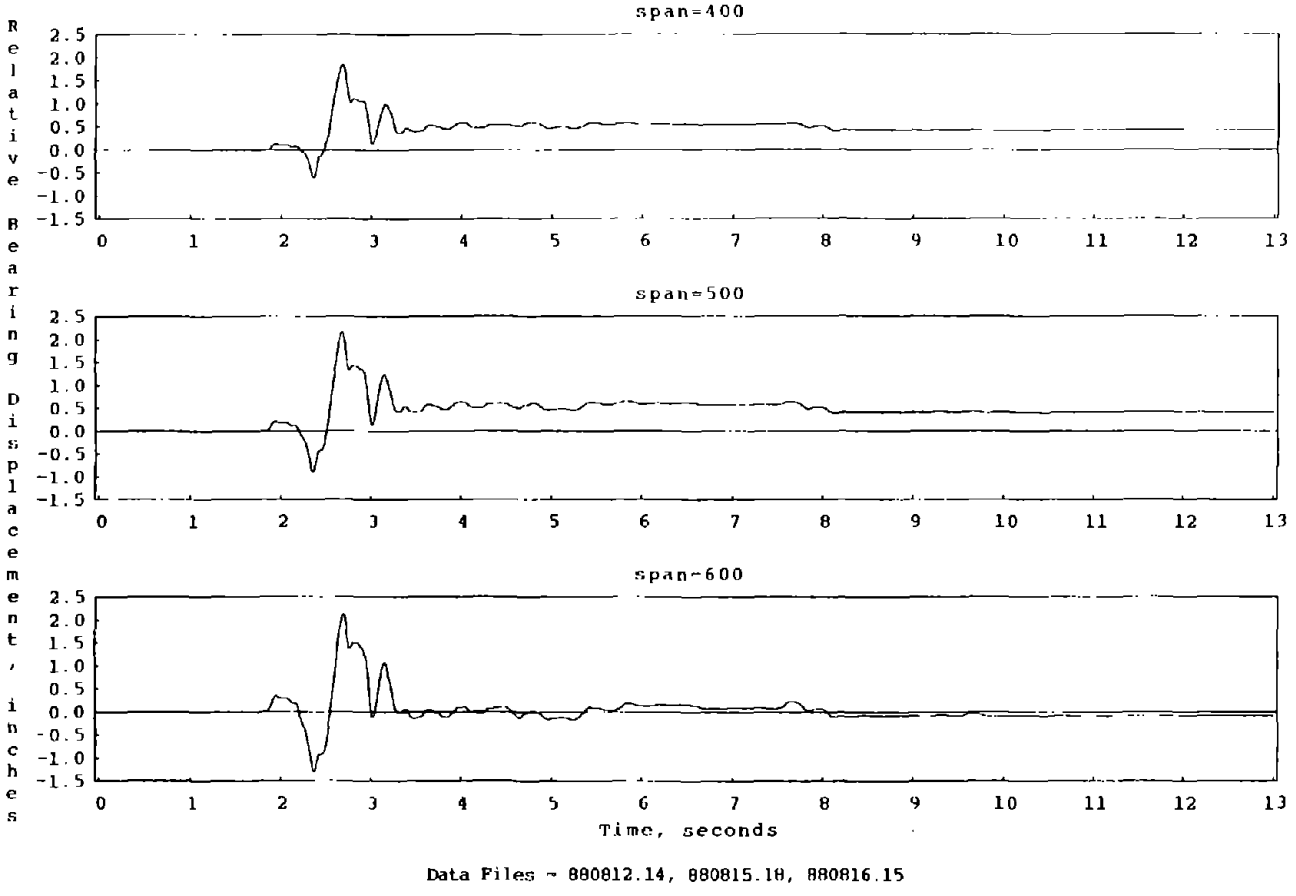

Figure 37 Relative Bearing Displacement Time Histories for San Francisco

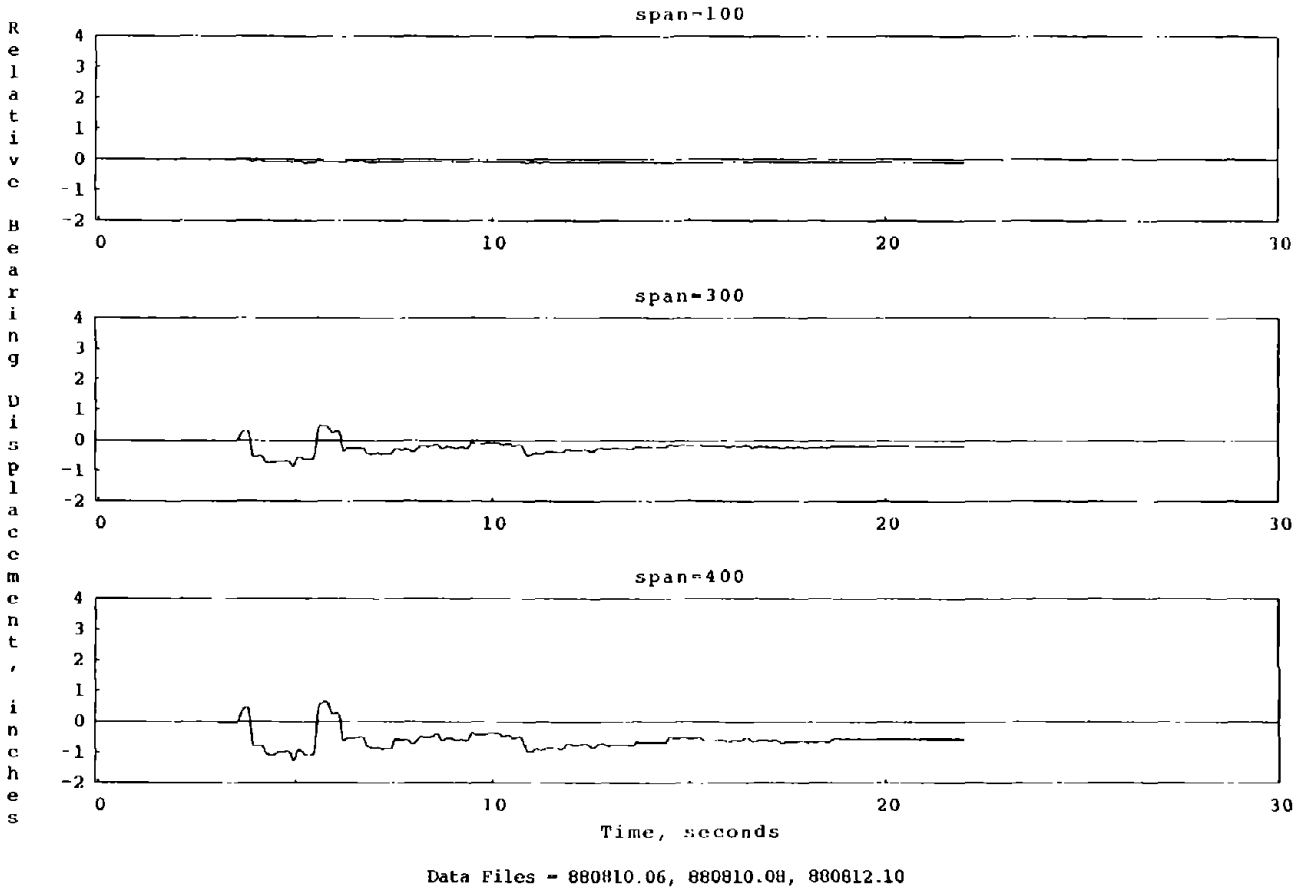

Figure 38 Relative Bearing Displacement Time Histories for Taft

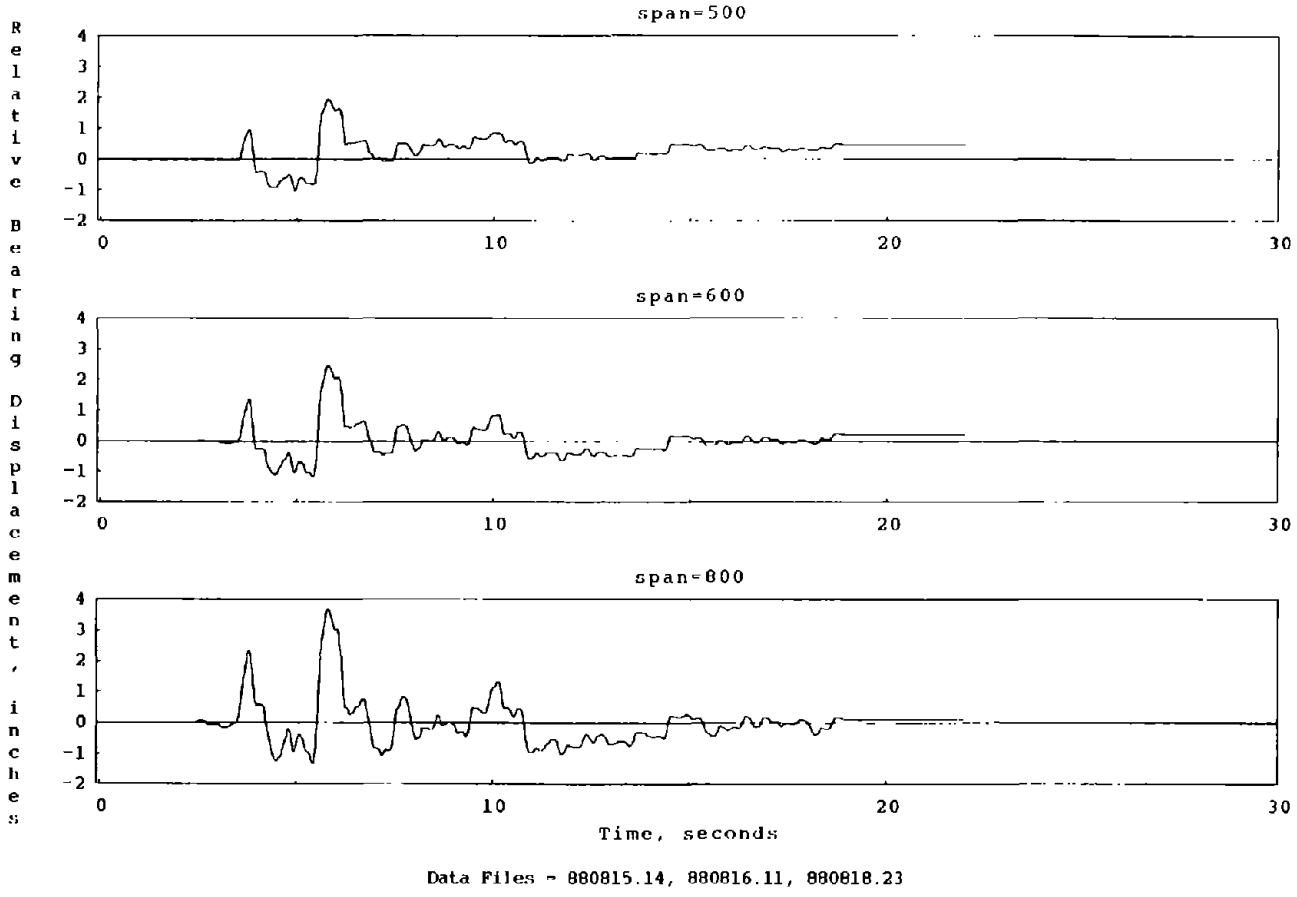

Figure 38 Relative Bearing Displacement Time Histories for Taft (Continued)

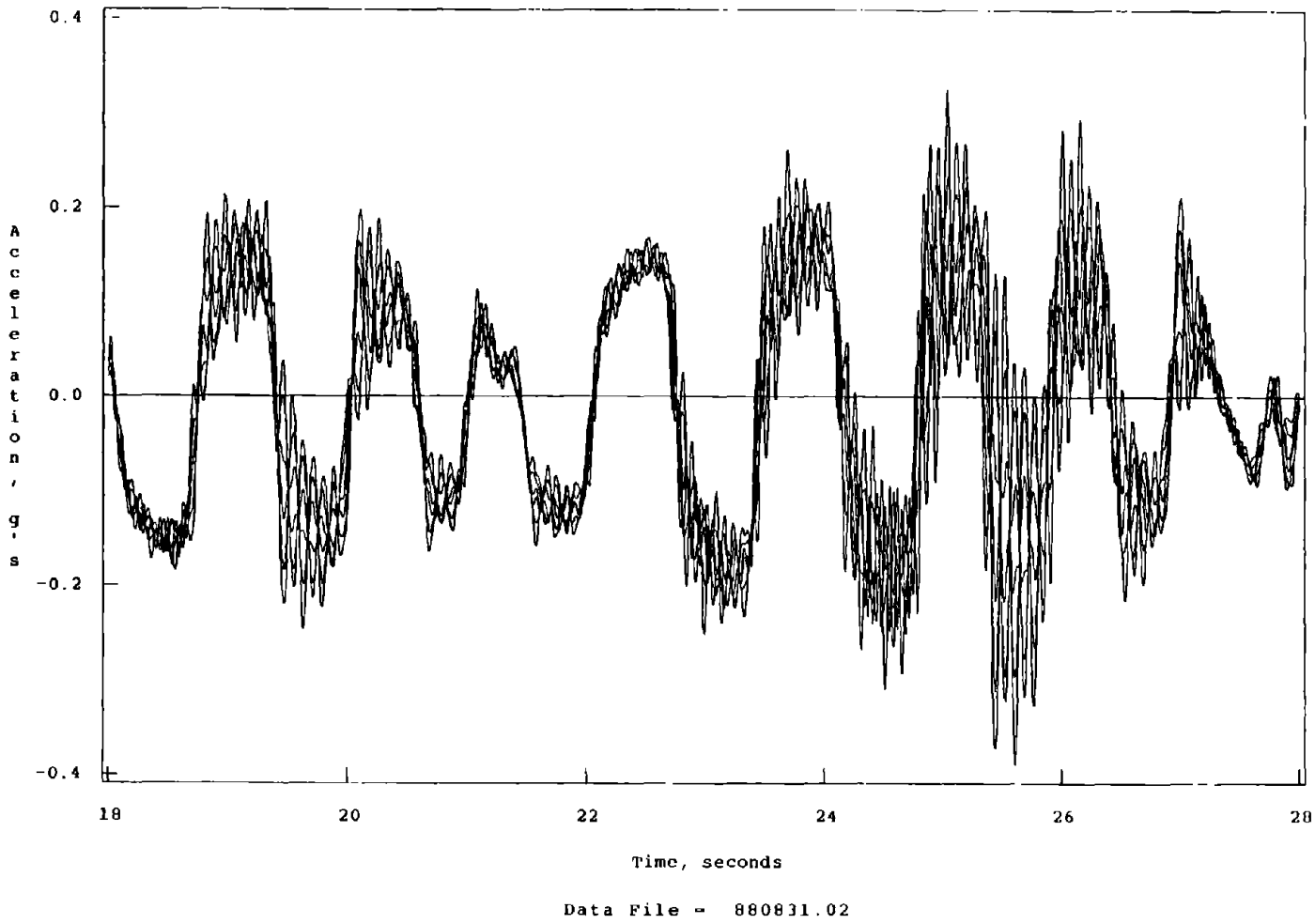

Figure 39 Superposed Frame Accelerations for Mexico City, span = 900

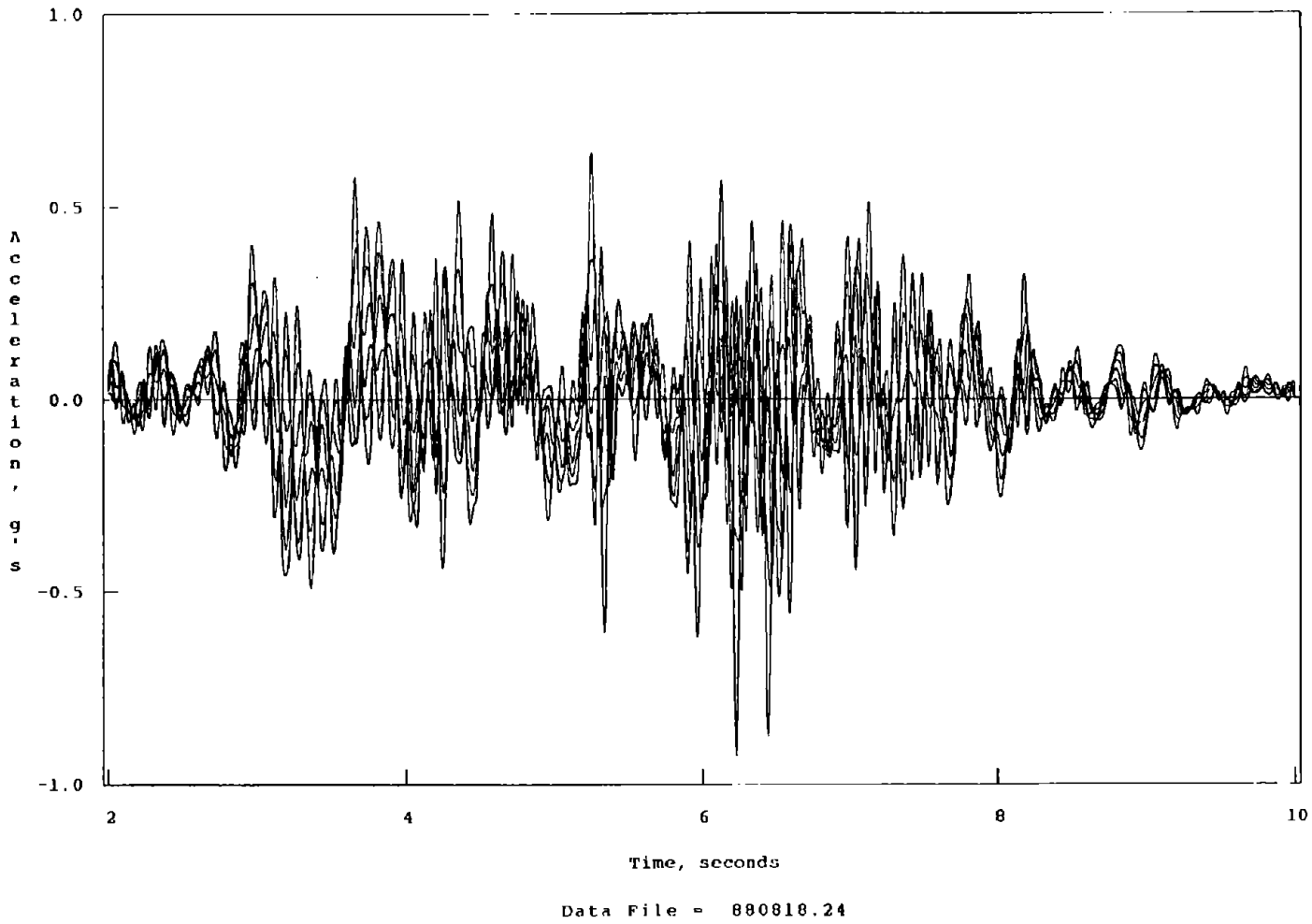

Figure 40 Superposed Frame Accelerations for Pacoima Dam, span = 800

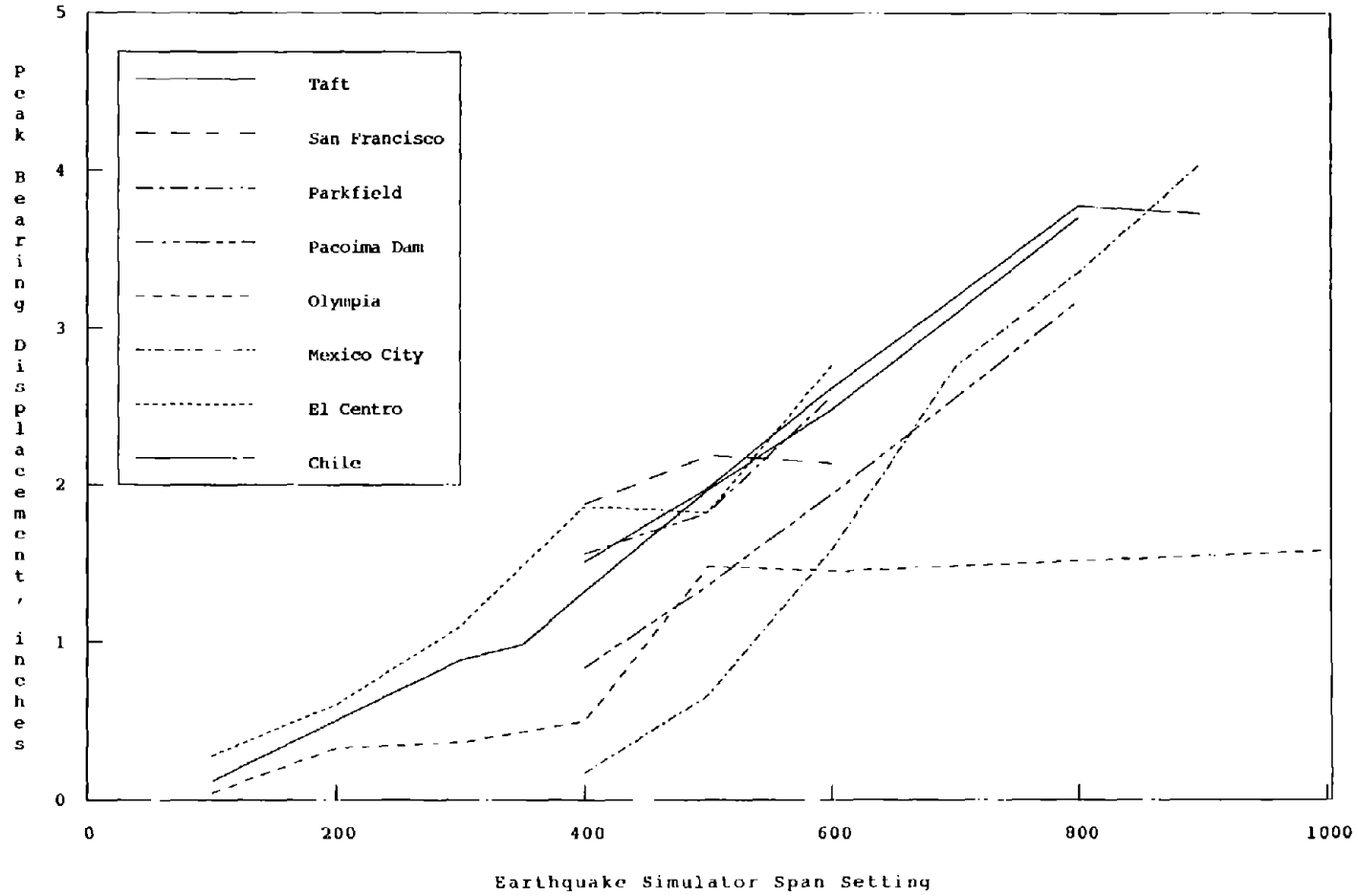

Figure 41 Plot of Maximum Bearing Displacement vs. Earthquake Simulator Span Setting

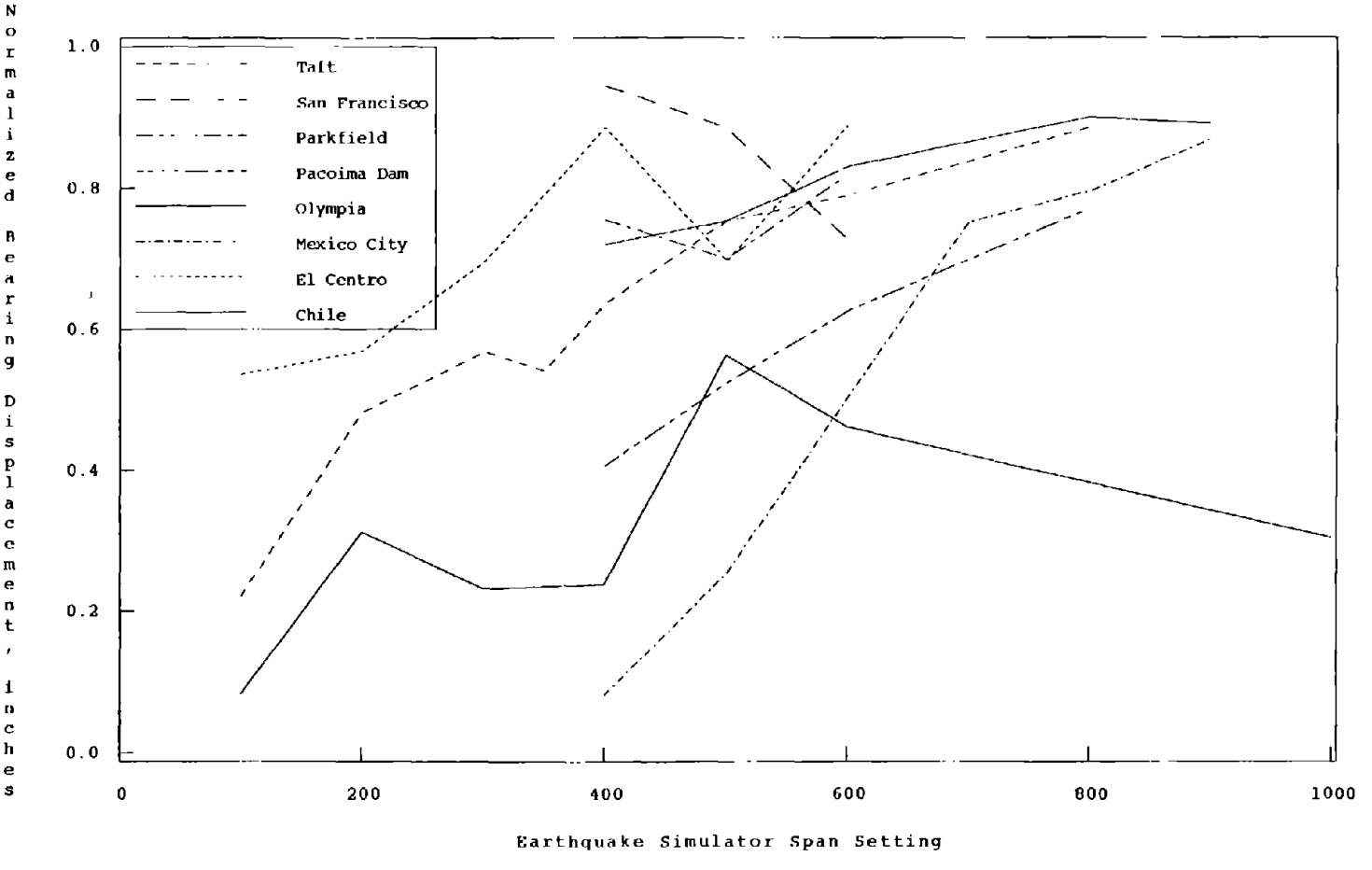

Figure 42 Plot of Normalized Maximum Bearing Displacement vs. Earthquake Simulator Span Setting

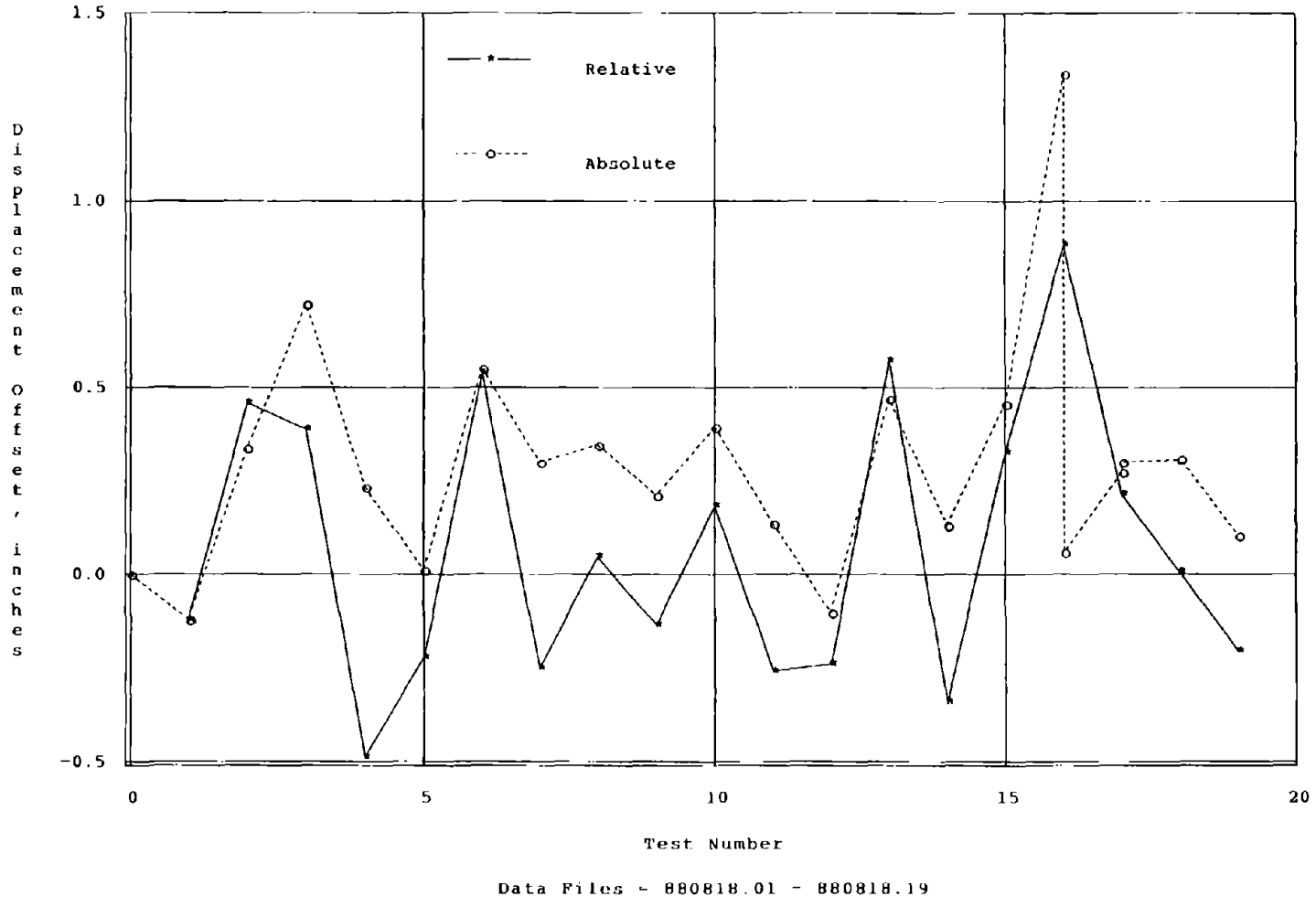

Figure 43 History of Relative and Absolute Offsets After Each Test

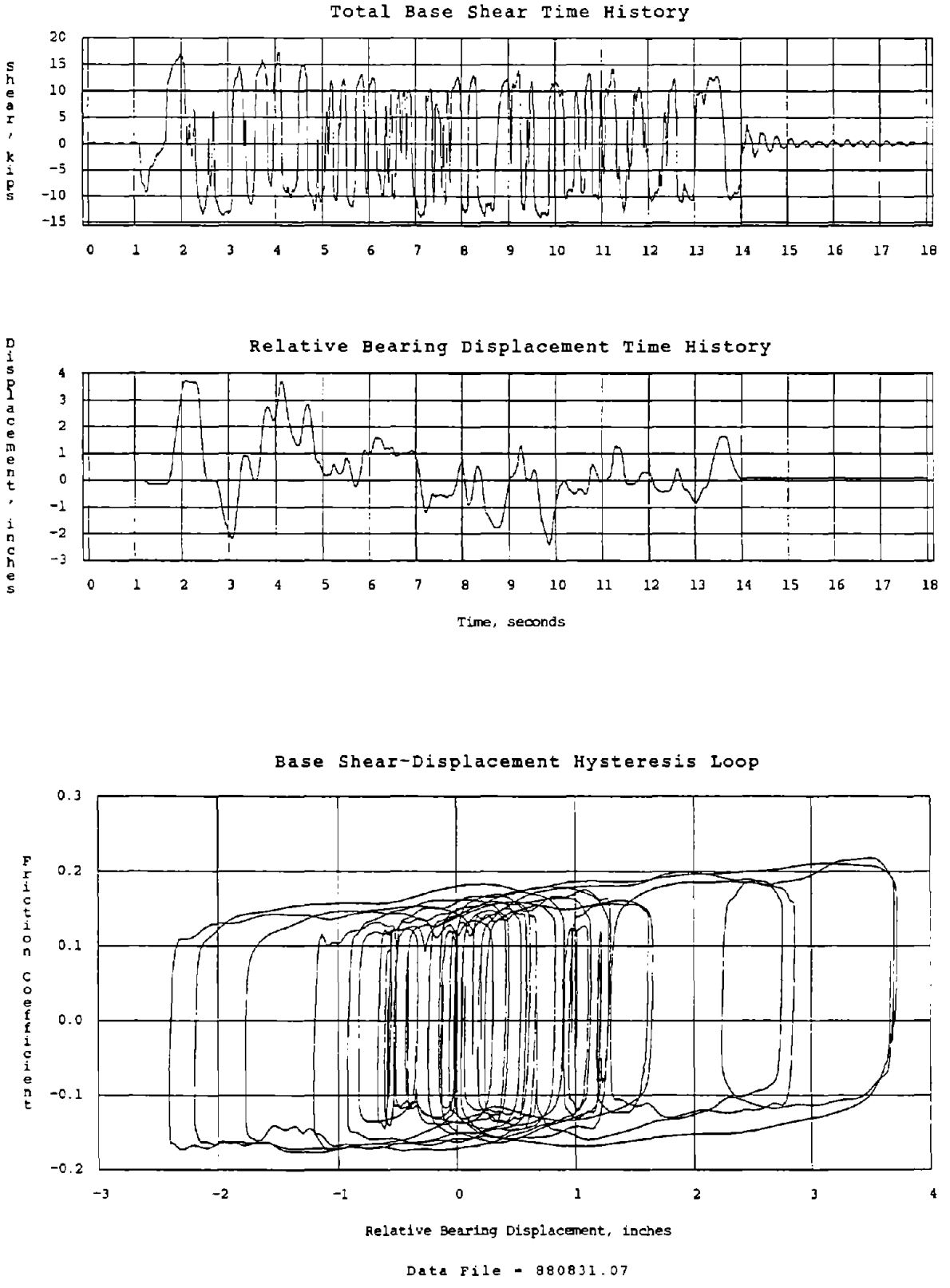

Figure 44 Hysteretic Behavior for Chile, span = 900

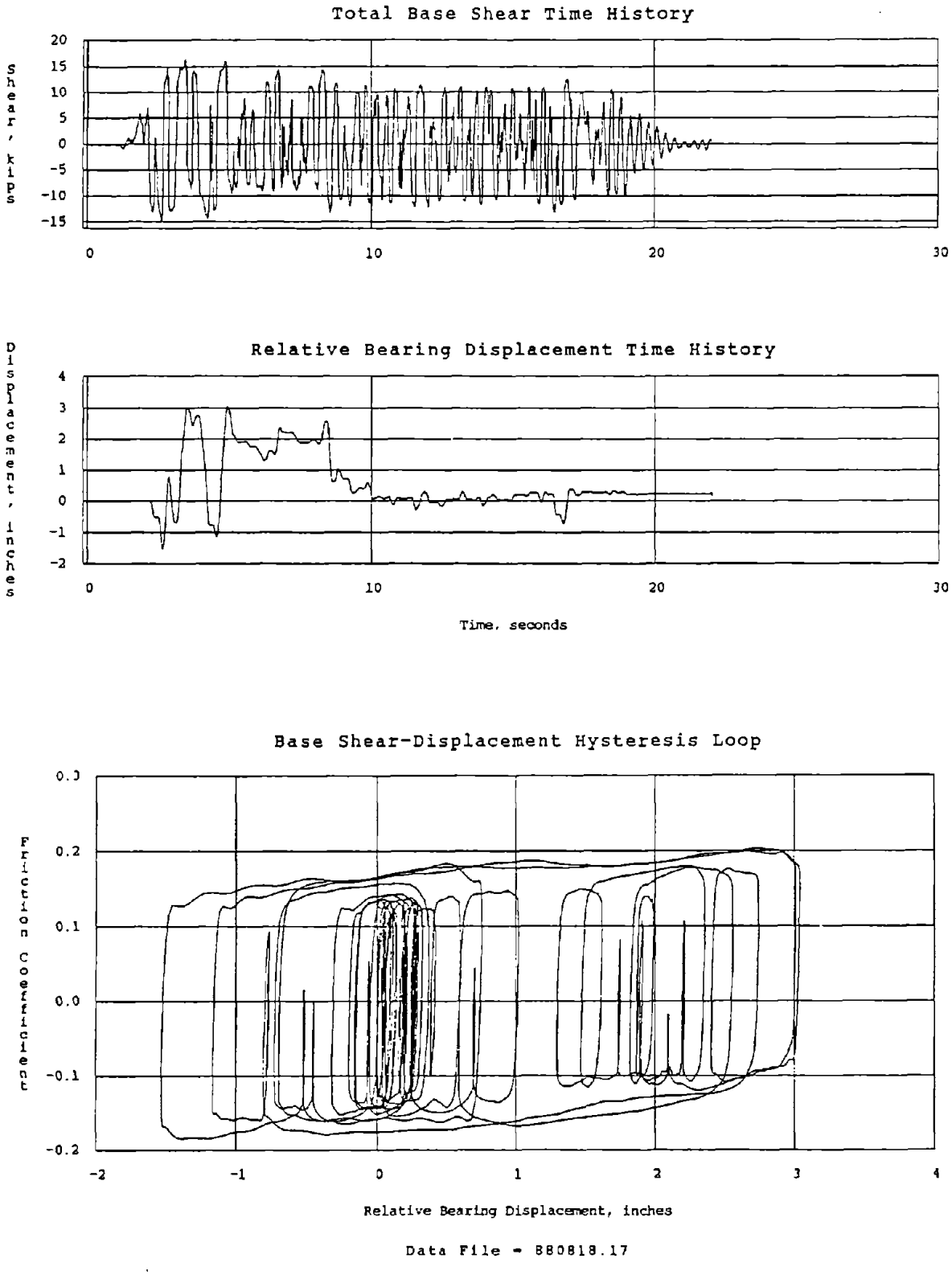

Figure 45 Hysteretic Behavior for El Centro, span = 600

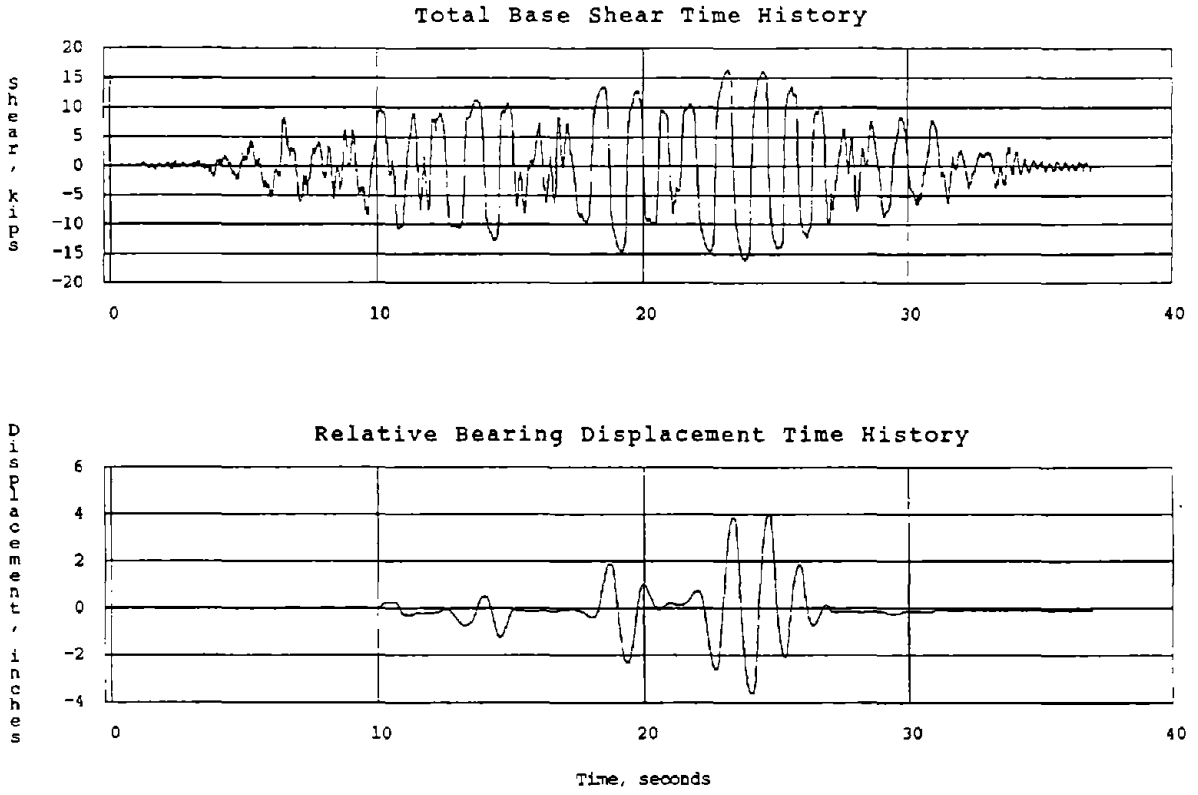

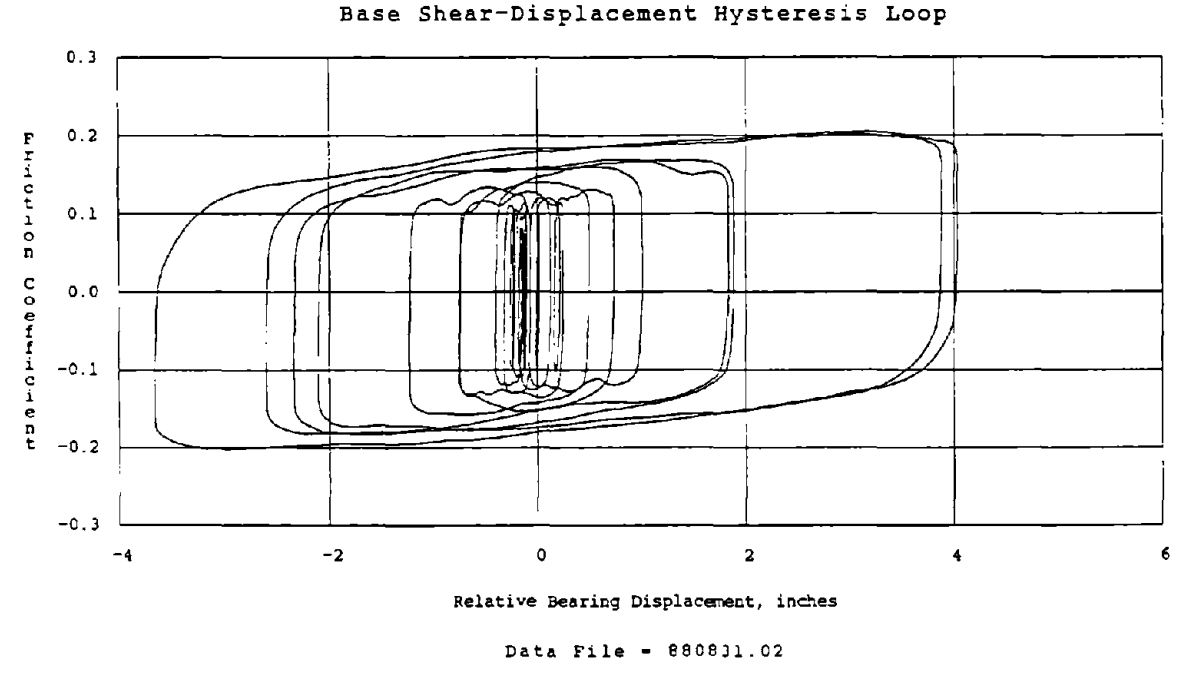

Figure 46 Hysteretic Behavior for Mexico City, span = 900

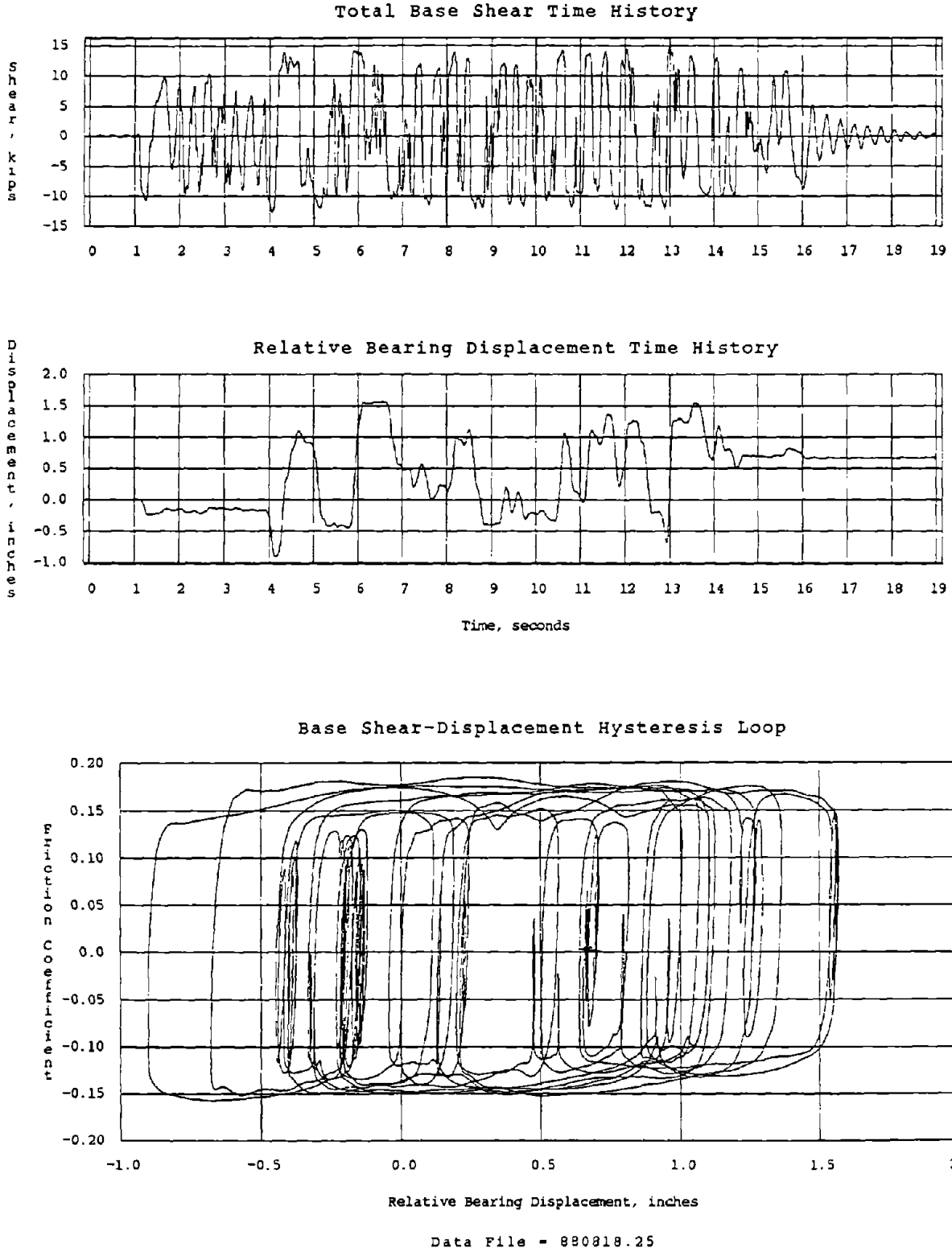

Figure 47 Hysteretic Behavior for Olympia, span = 1000

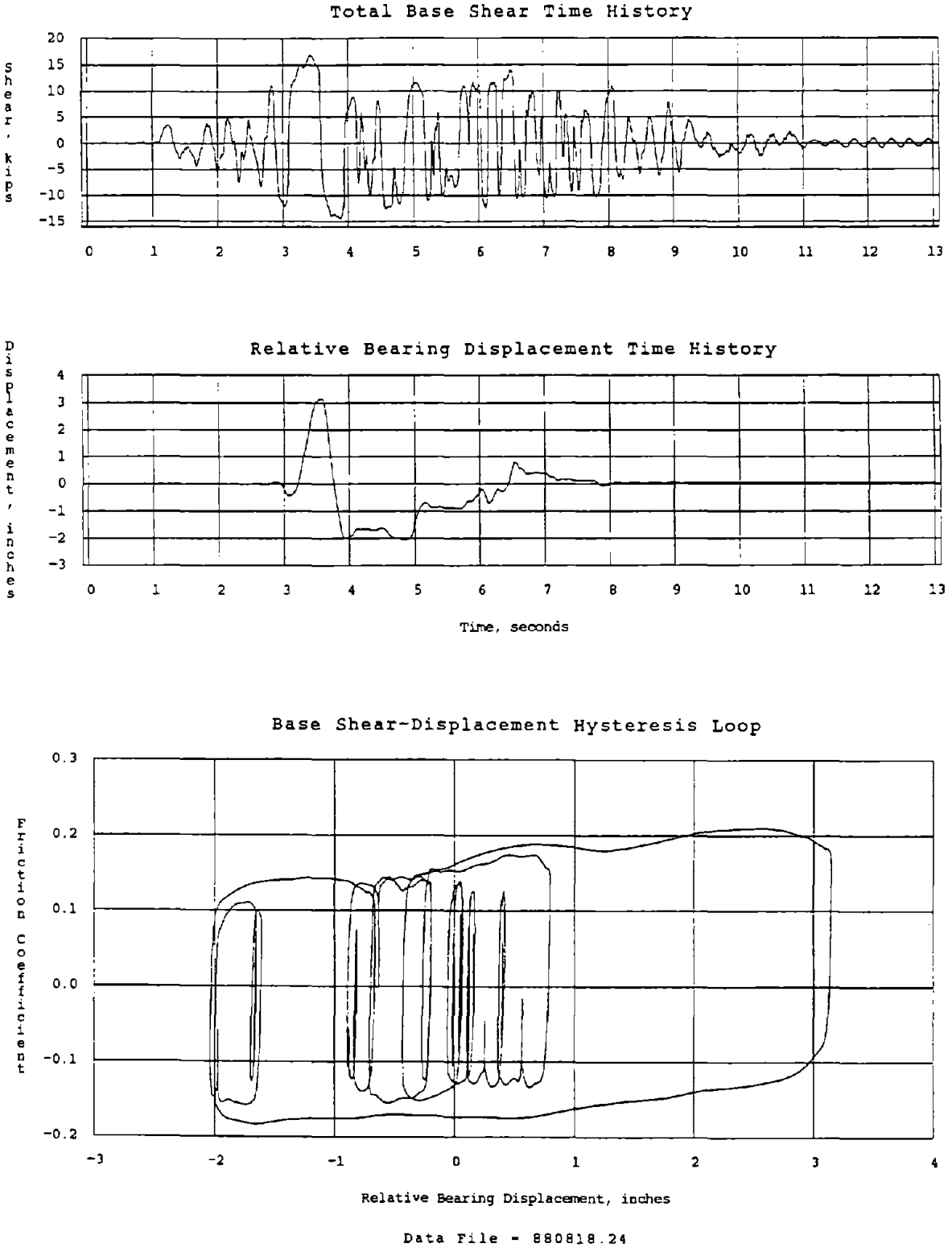

Figure 48 Hysteretic Behavior for Pacoima Dam, span = 800

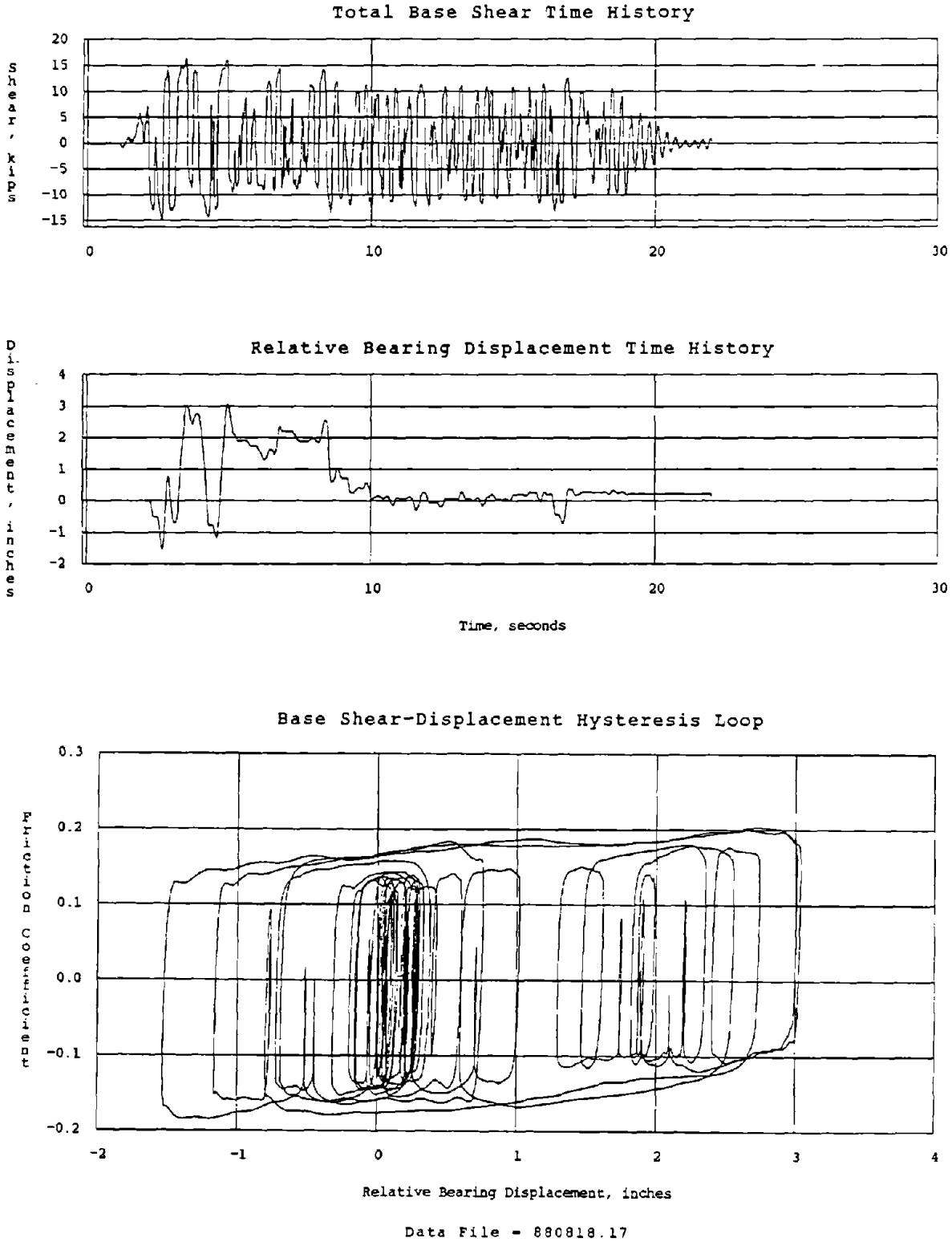

Figure 49 Hysteretic Behavior for Parkfield, span = 600

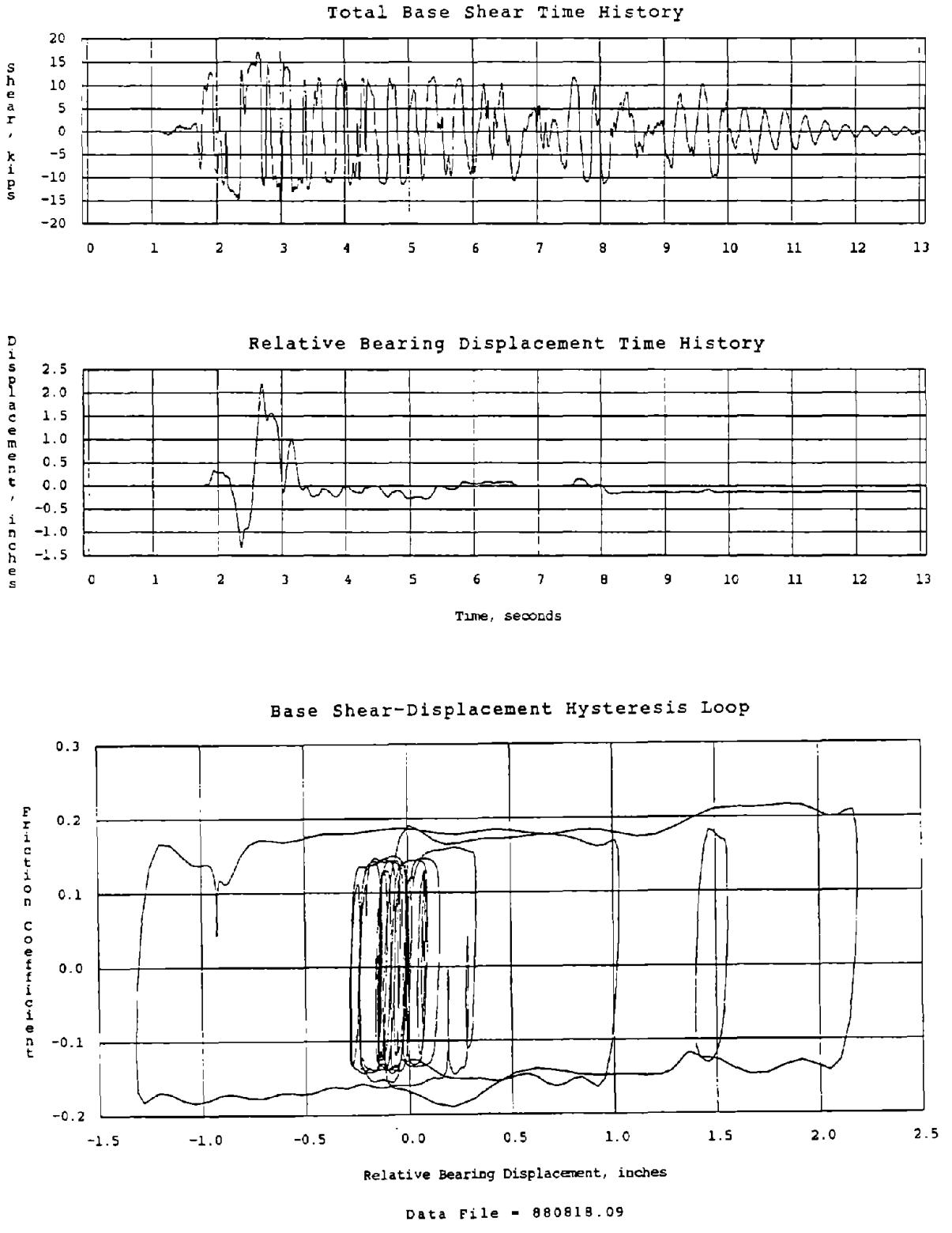

Figure 50 Hysteretic Behavior for San Francisco, span = 600

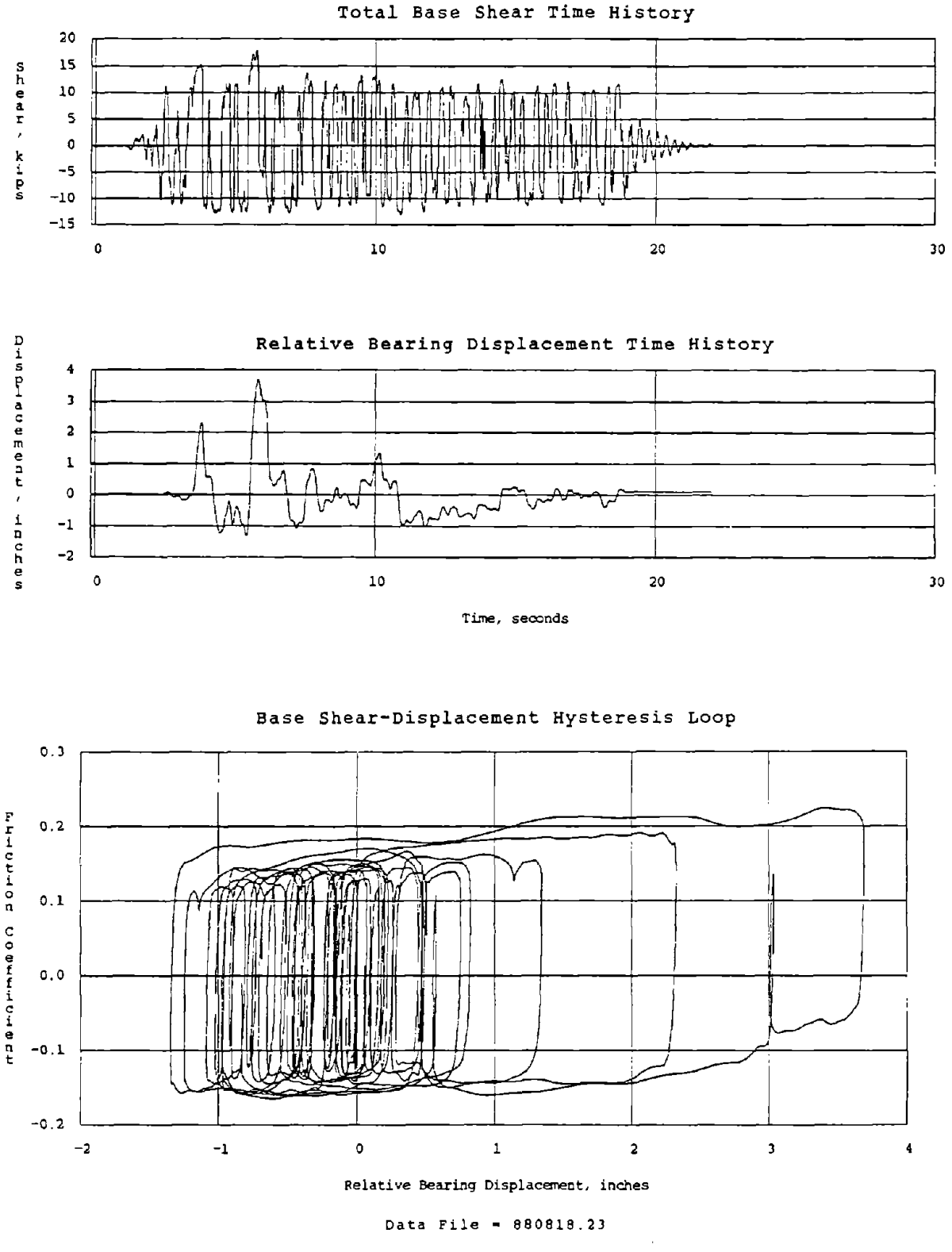

Figure 51 Hysteretic Behavior for Taft, span = 800

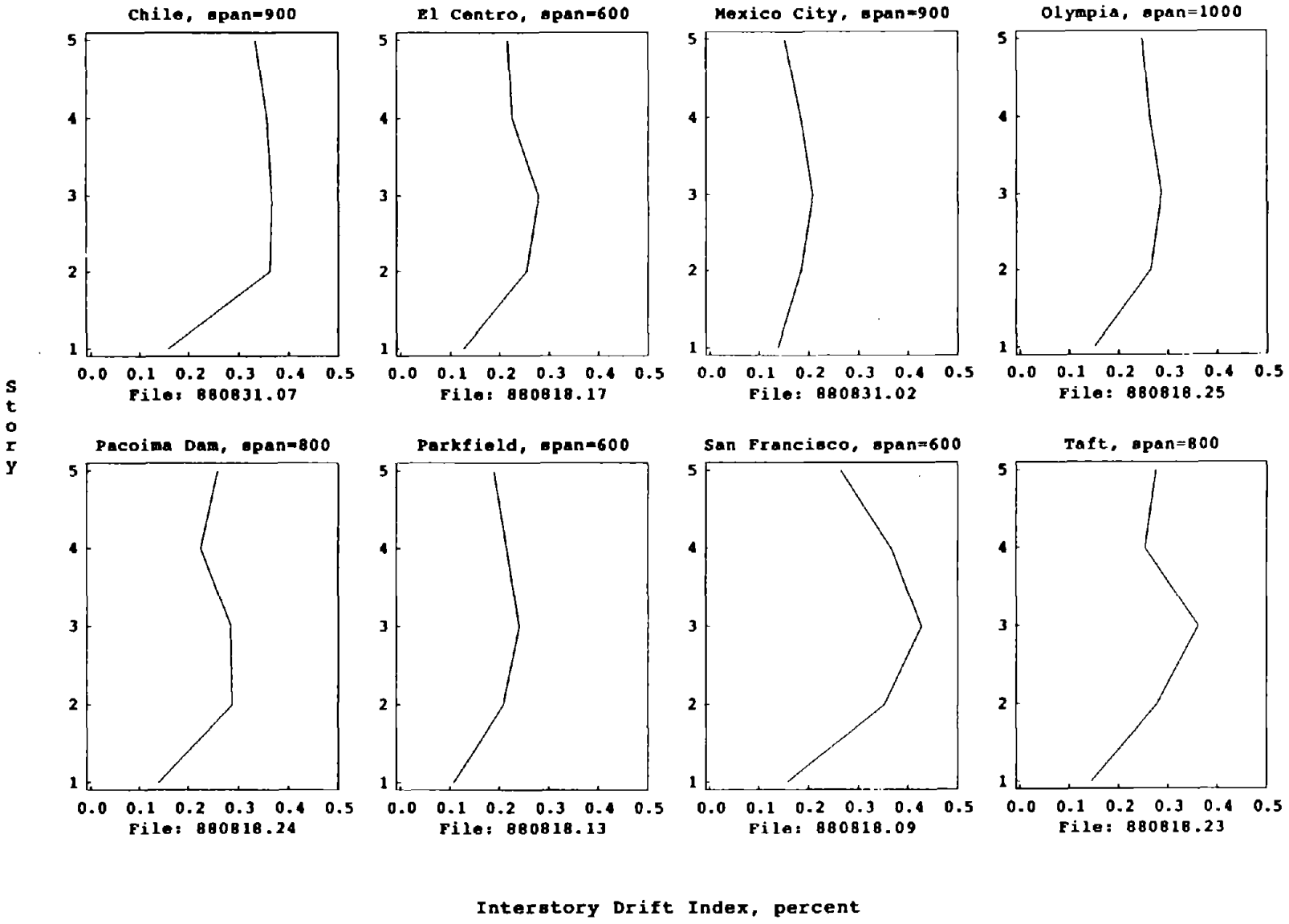

Figure 52 Interstory Drift Index Envelopes for the Maximum Span Test of each Earthquake Signal

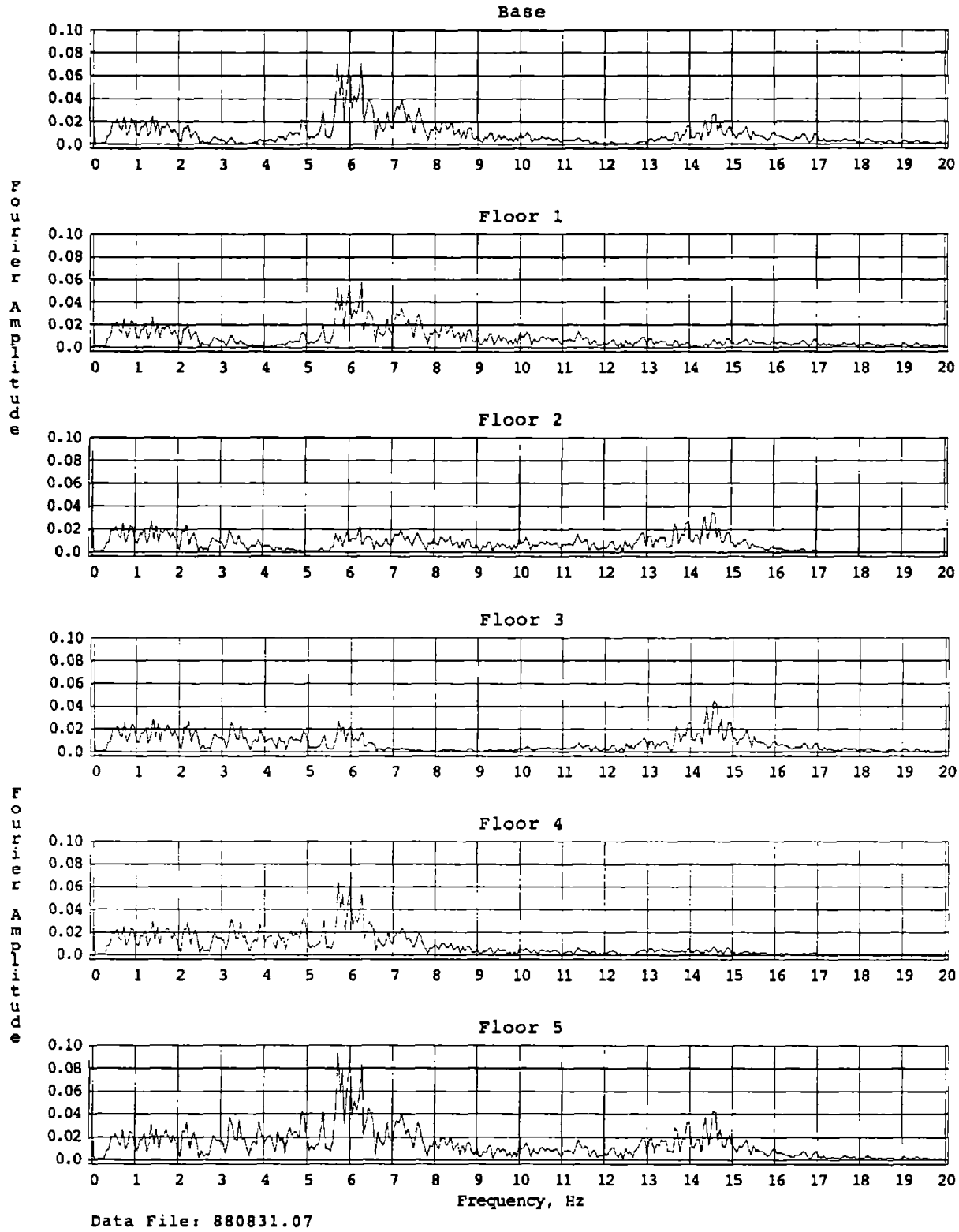

Figure 53 Fourier Spectra of Frame Accelerations for Chile, span = 900

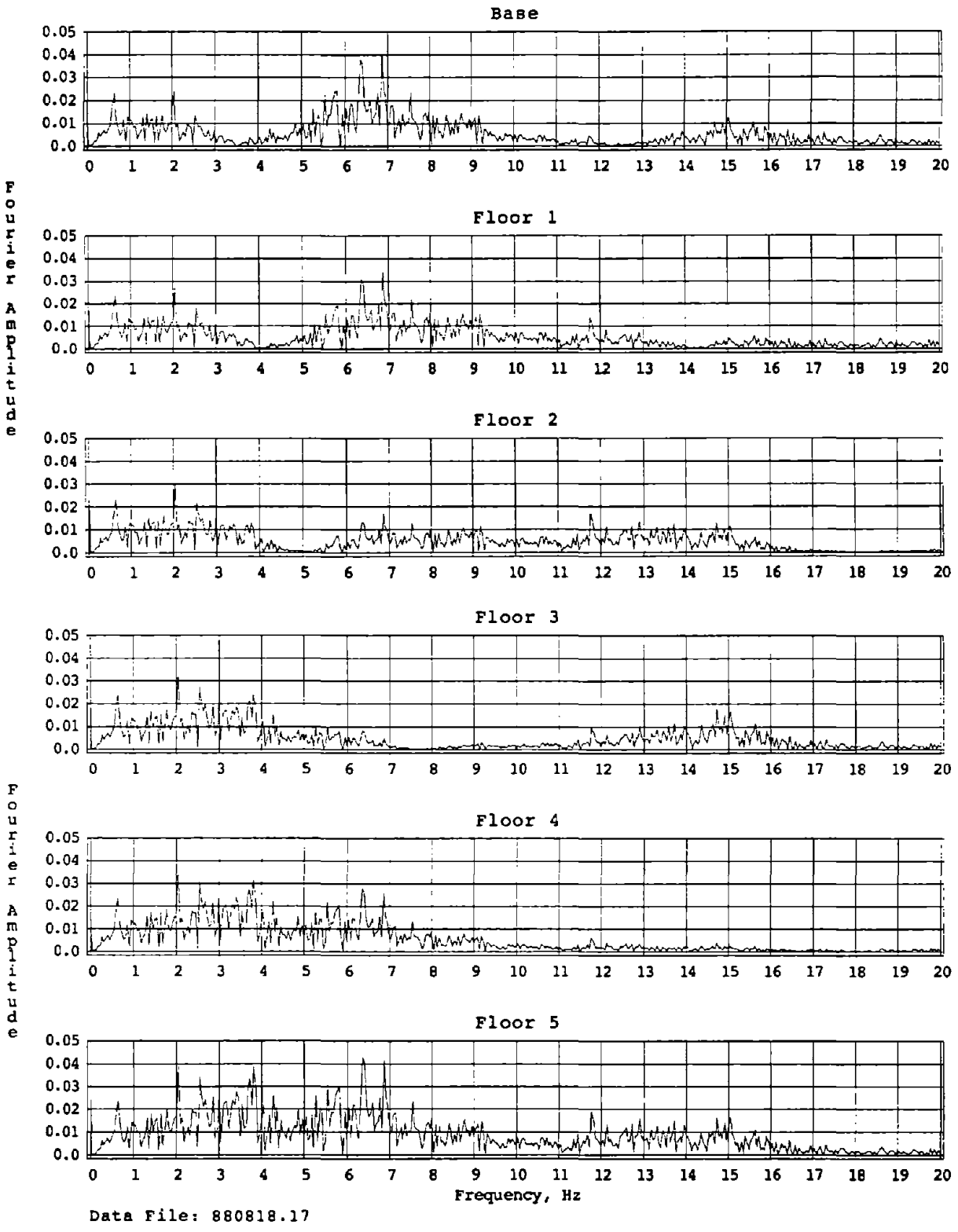

Figure 54 Fourier Spectra of Frame Accelerations for El Centro, span = 600

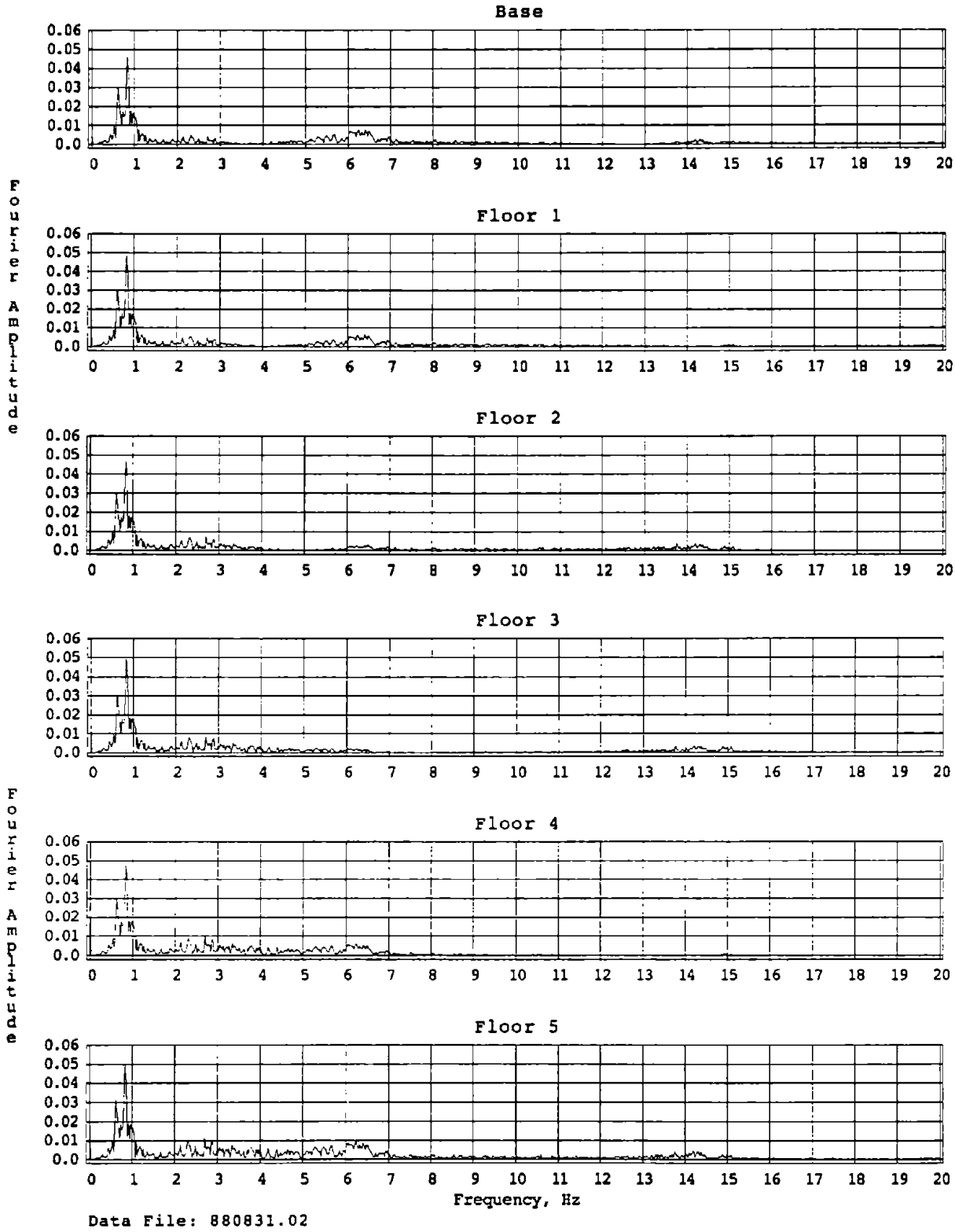

Figure 55 Fourier Spectra of Frame Accelerations for Mexico City, span = 900

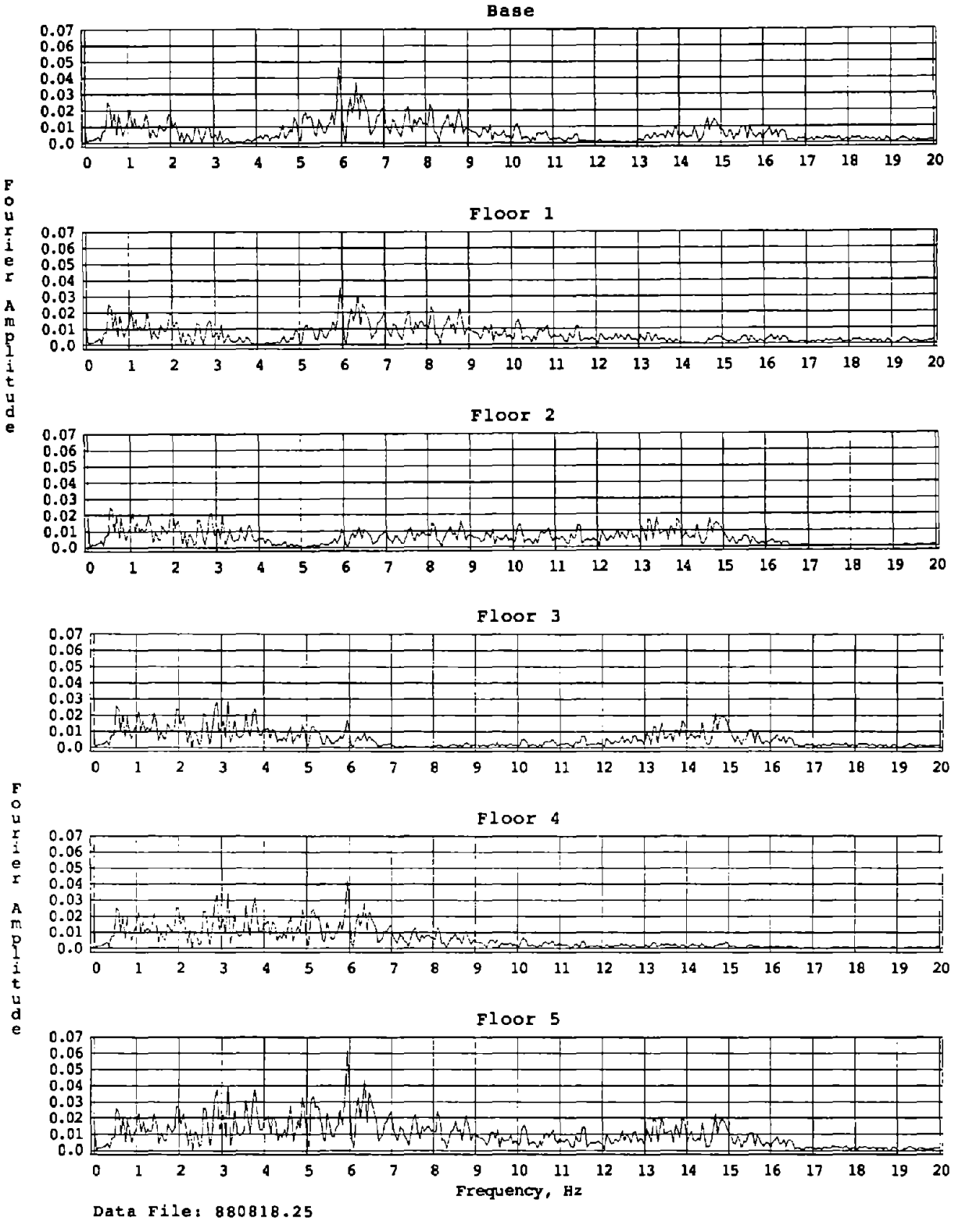

Figure 56 Fourier Spectra of Frame Accelerations for Olympia, span = 1000

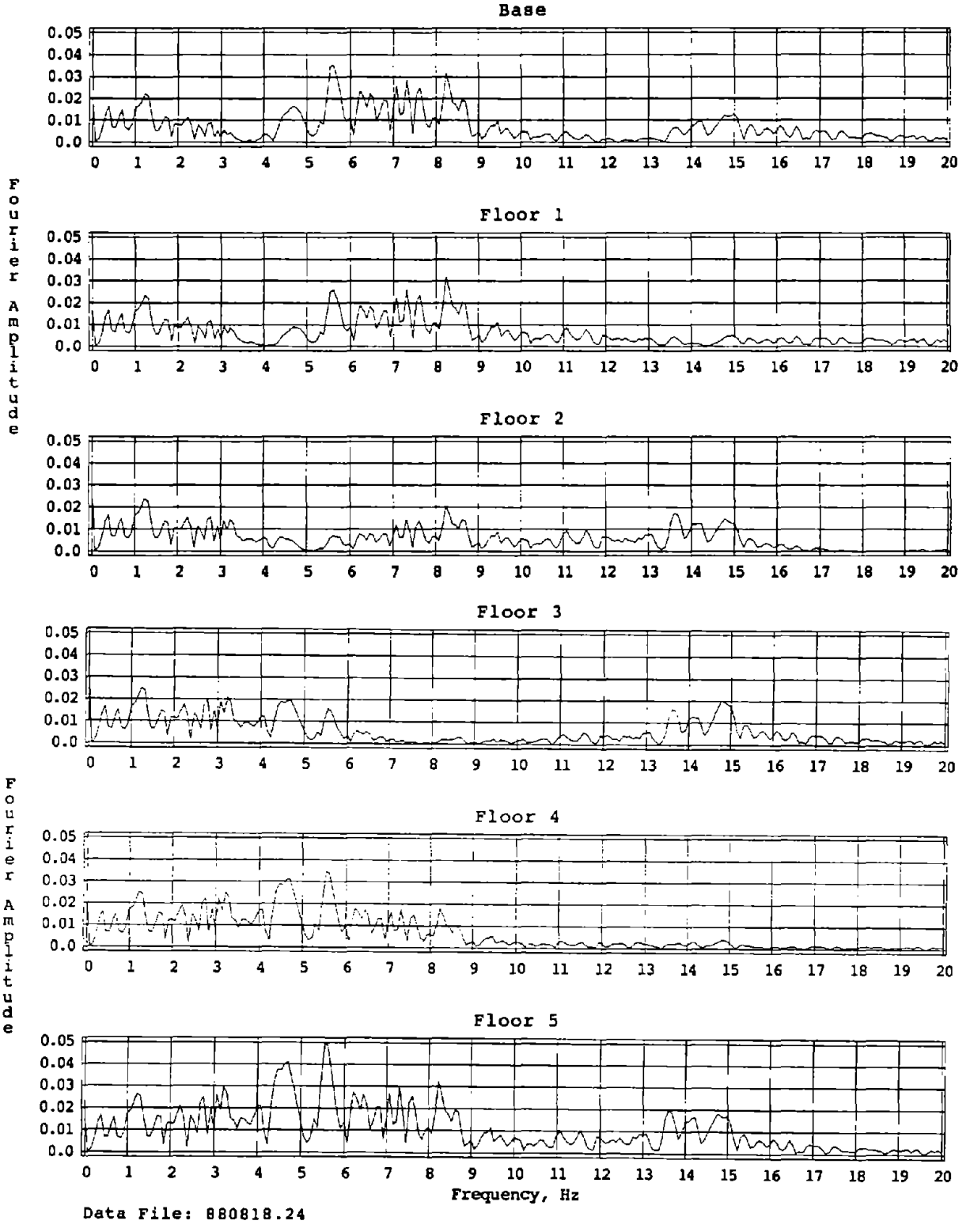

Figure 57 Fourier Spectra of Frame Accelerations for Pacoima Dam, span = 800

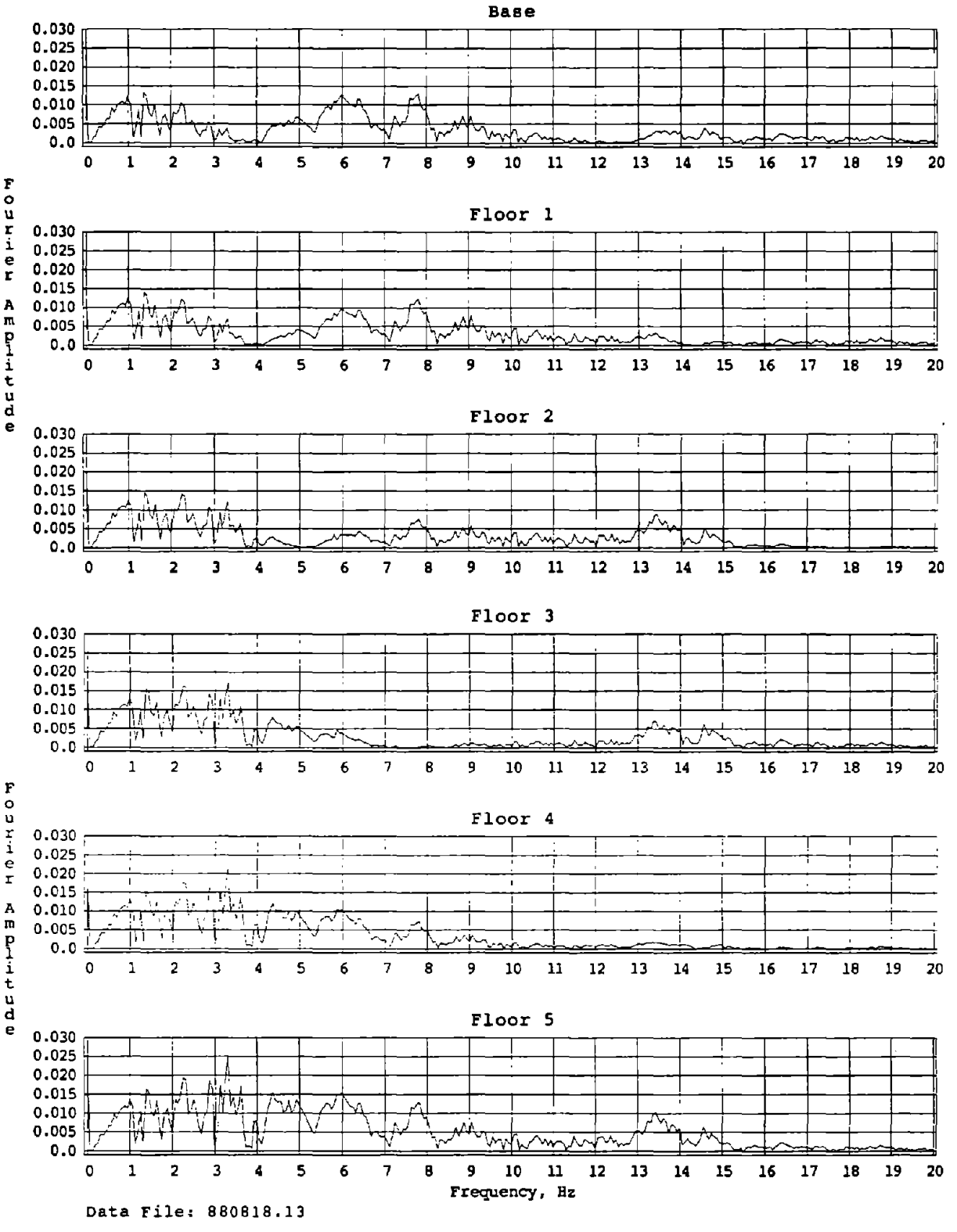

Figure 58 Fourier Spectra of Frame Accelerations for Parkfield, span = 600

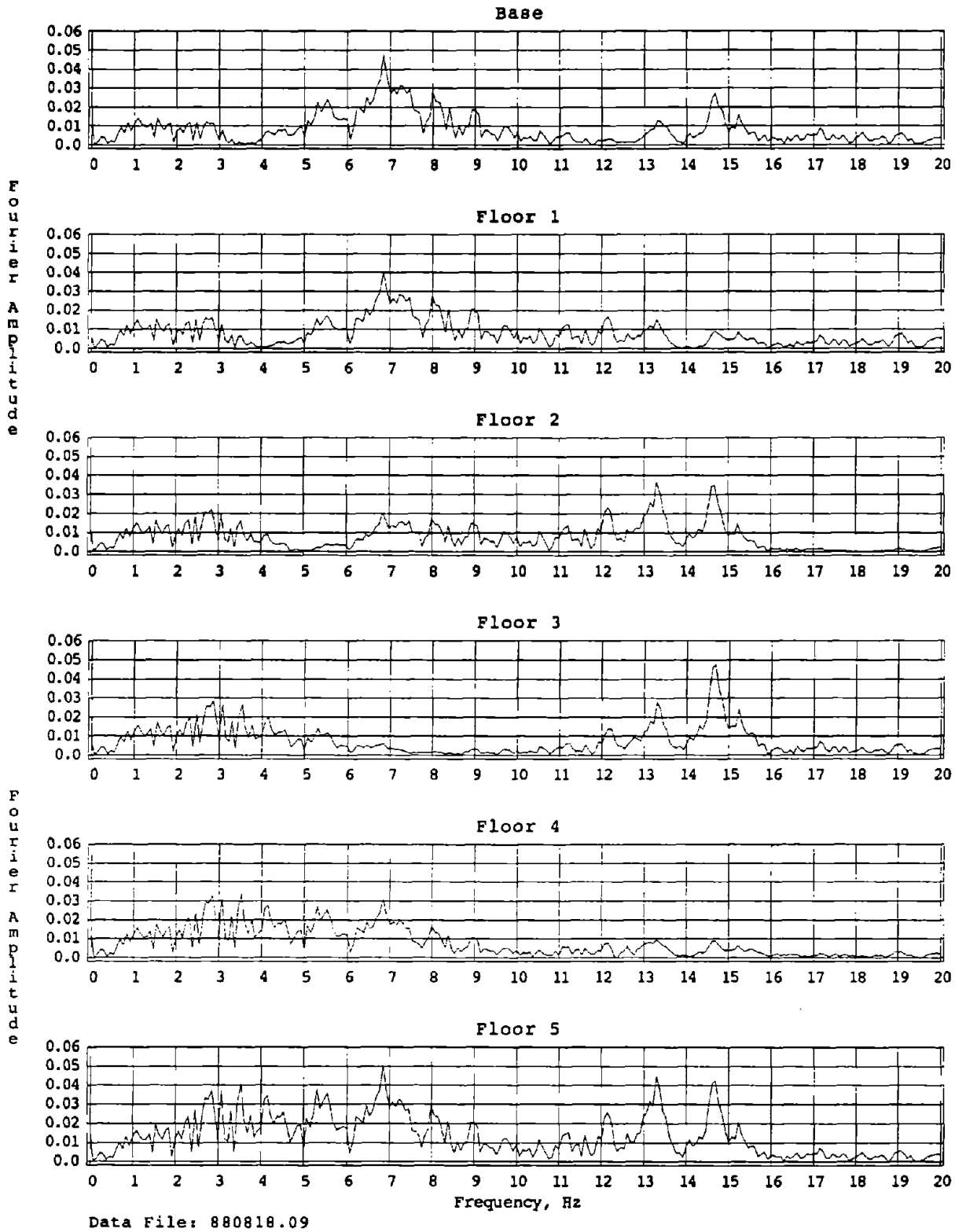

Figure 59 Fourier Spectra of Frame Accelerations for San Francisco, span = 600

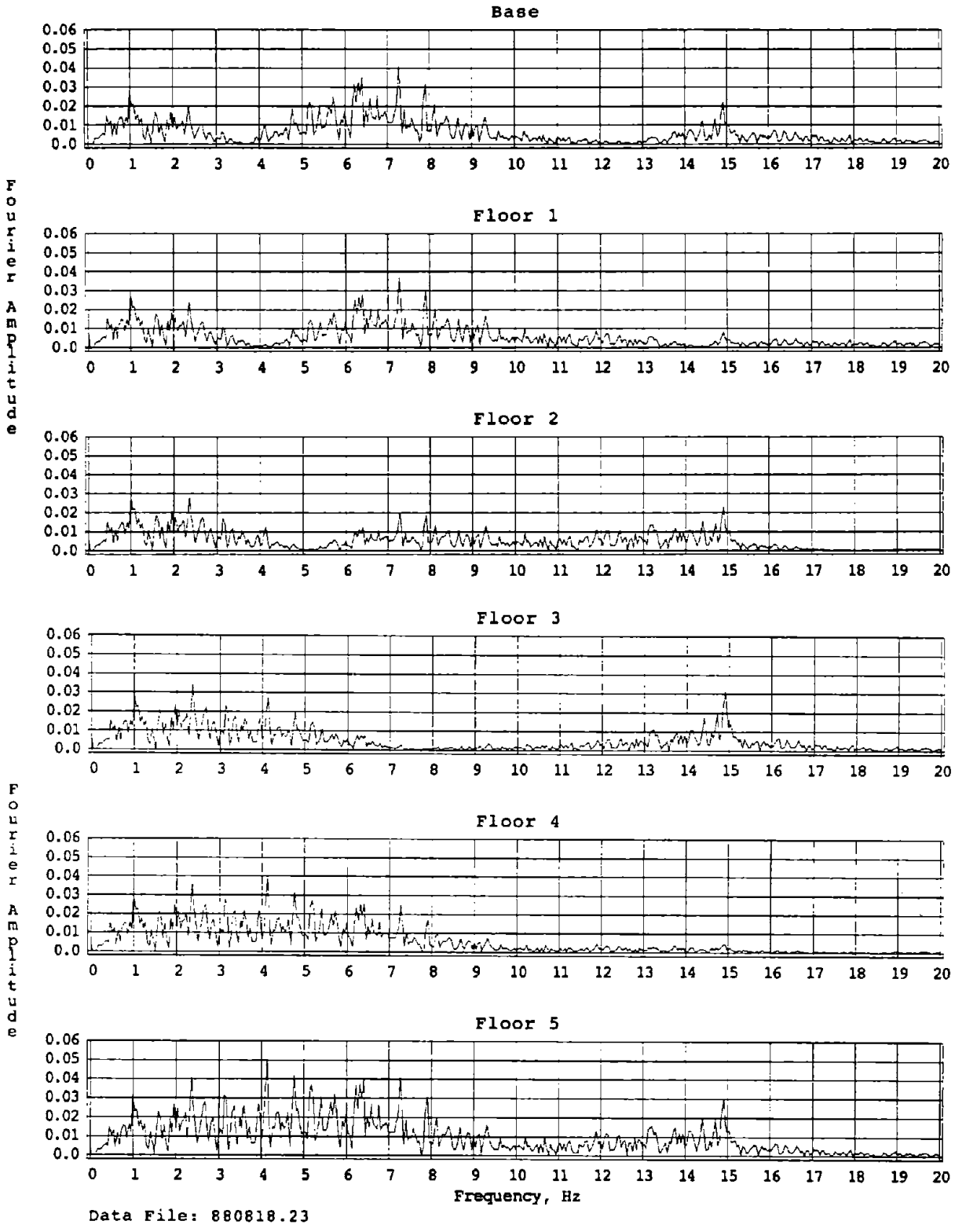

Figure 60 Fourier Spectra of Frame Accelerations for Taft, span = 800

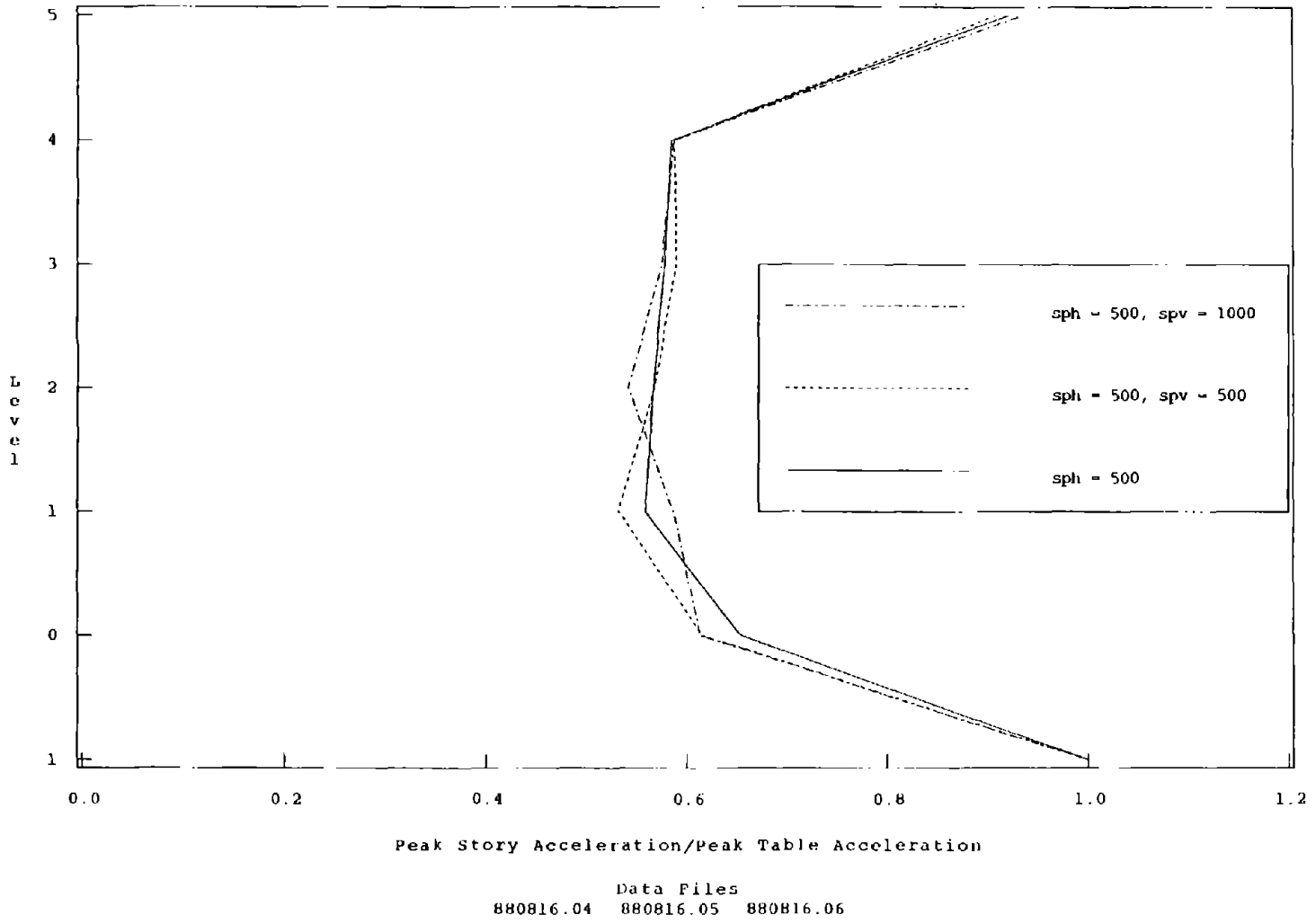

Figure 61 Normalized Accelerations Throughout Test Frame for Chile

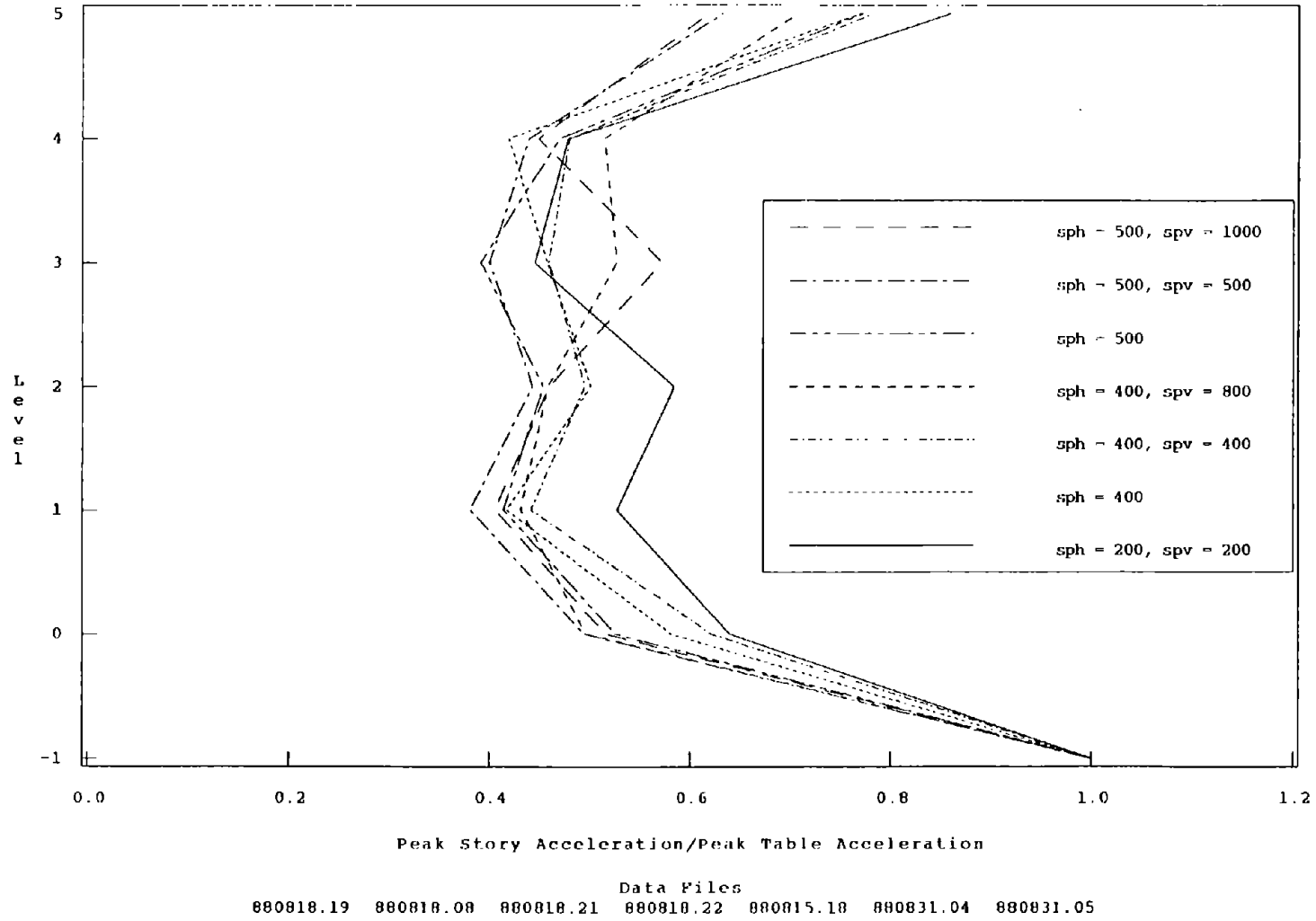

Figure 62 Normalized Accelerations Throughout Test Frame for San Francisco

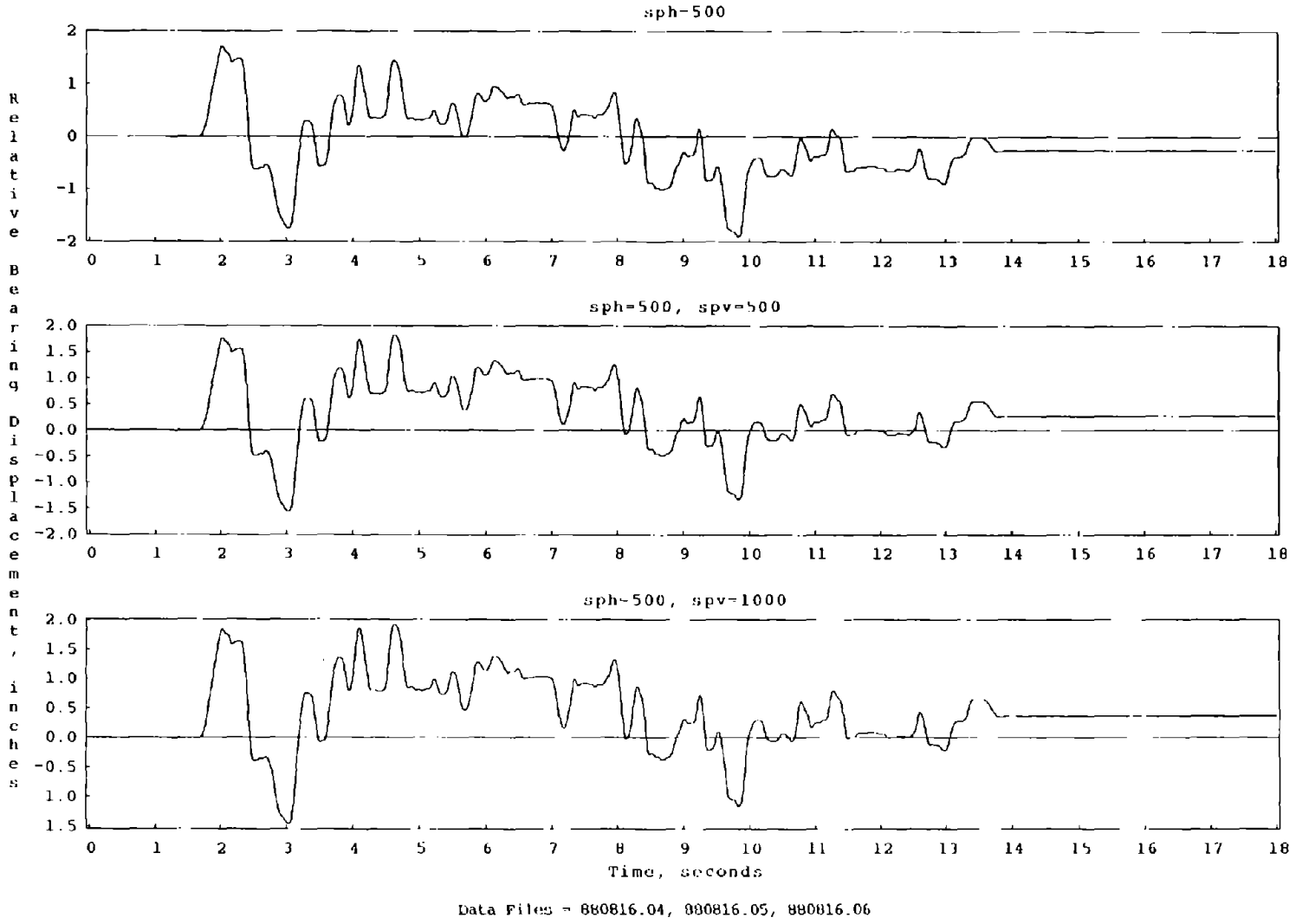

Figure 63 Relative Bearing Displacement Time Histories for Chile

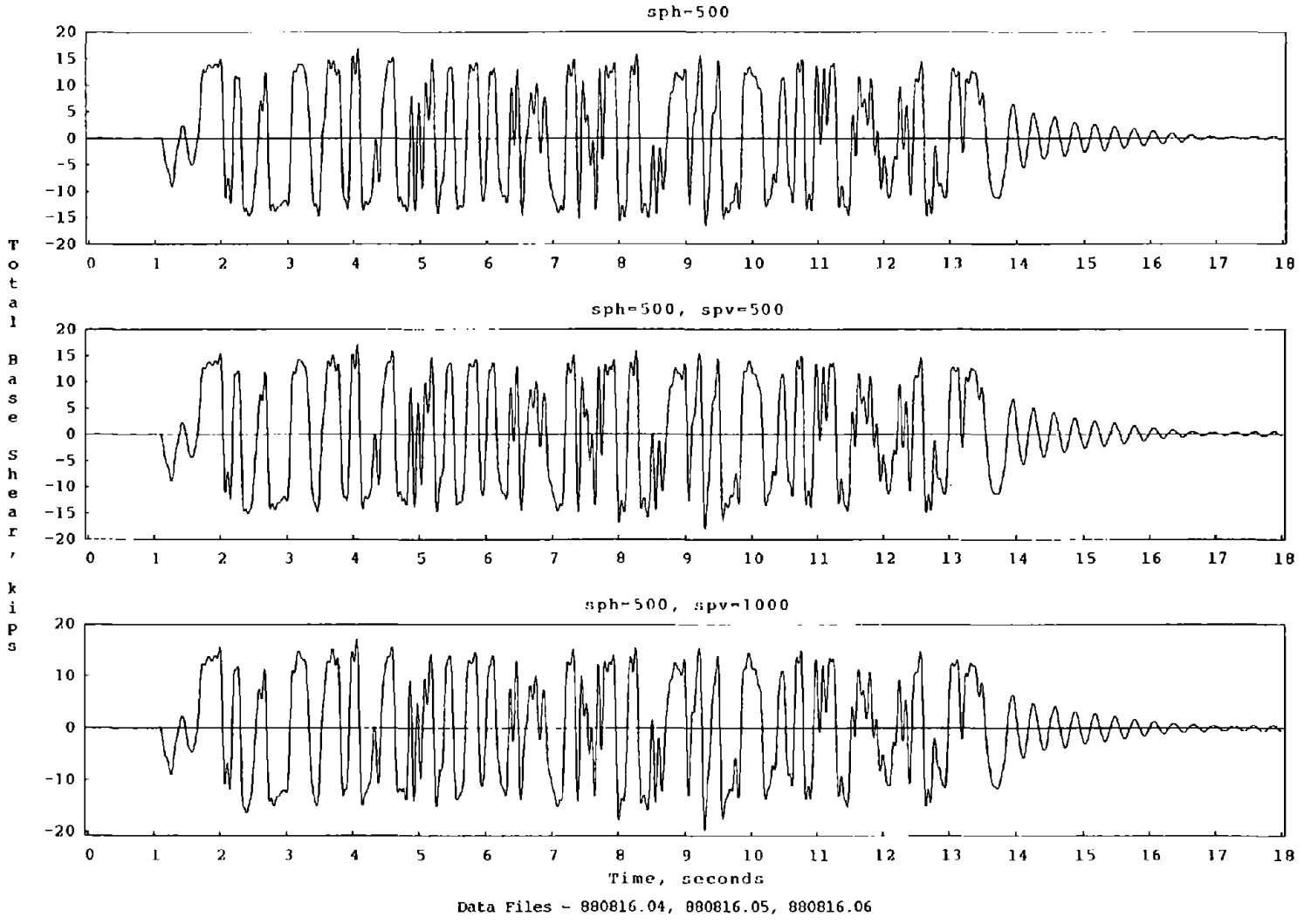

Figure 64 Total Base Shear Time Histories for Chile

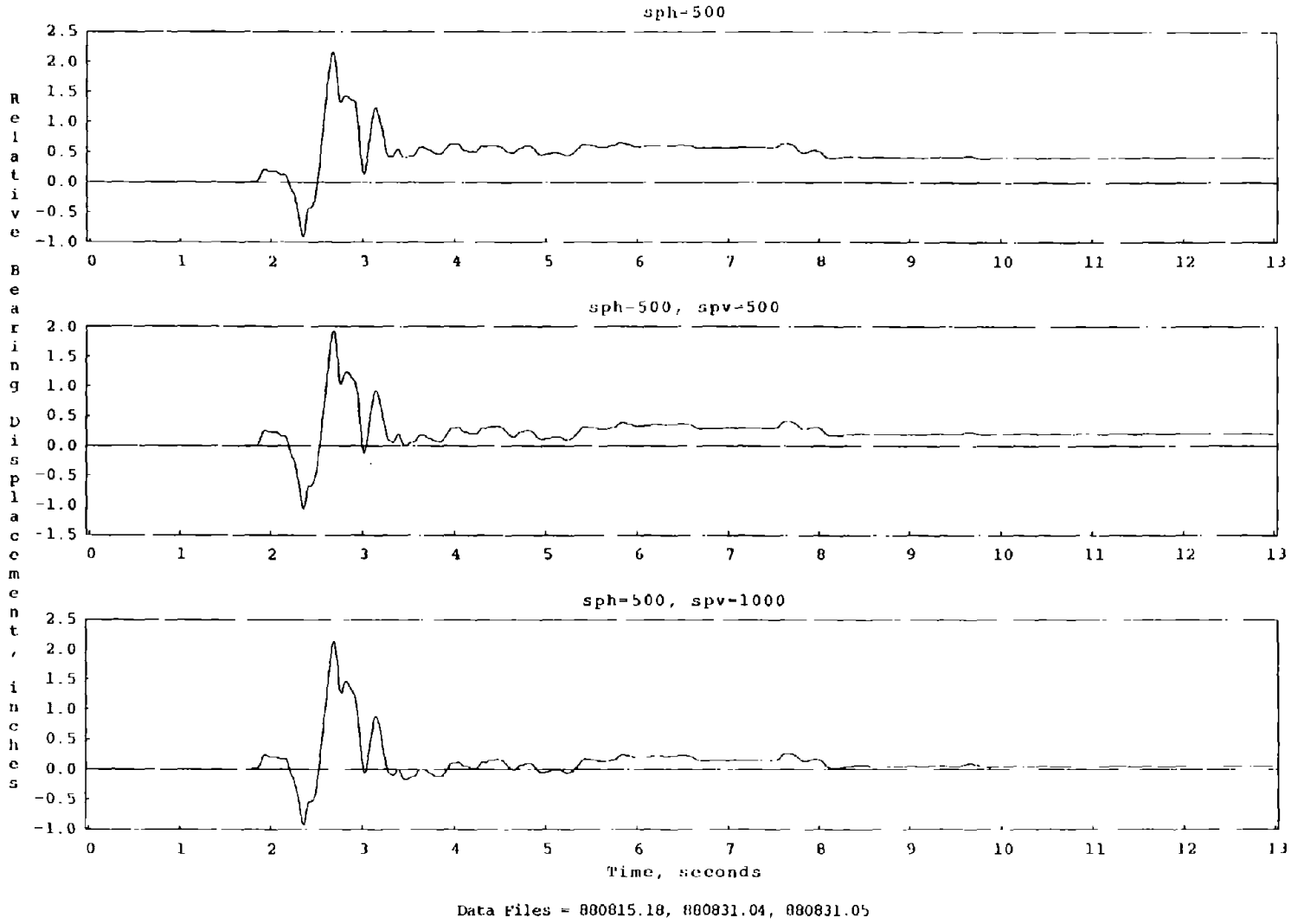

Figure 65 Relative Bearing Displacement Time Histories for San Francisco

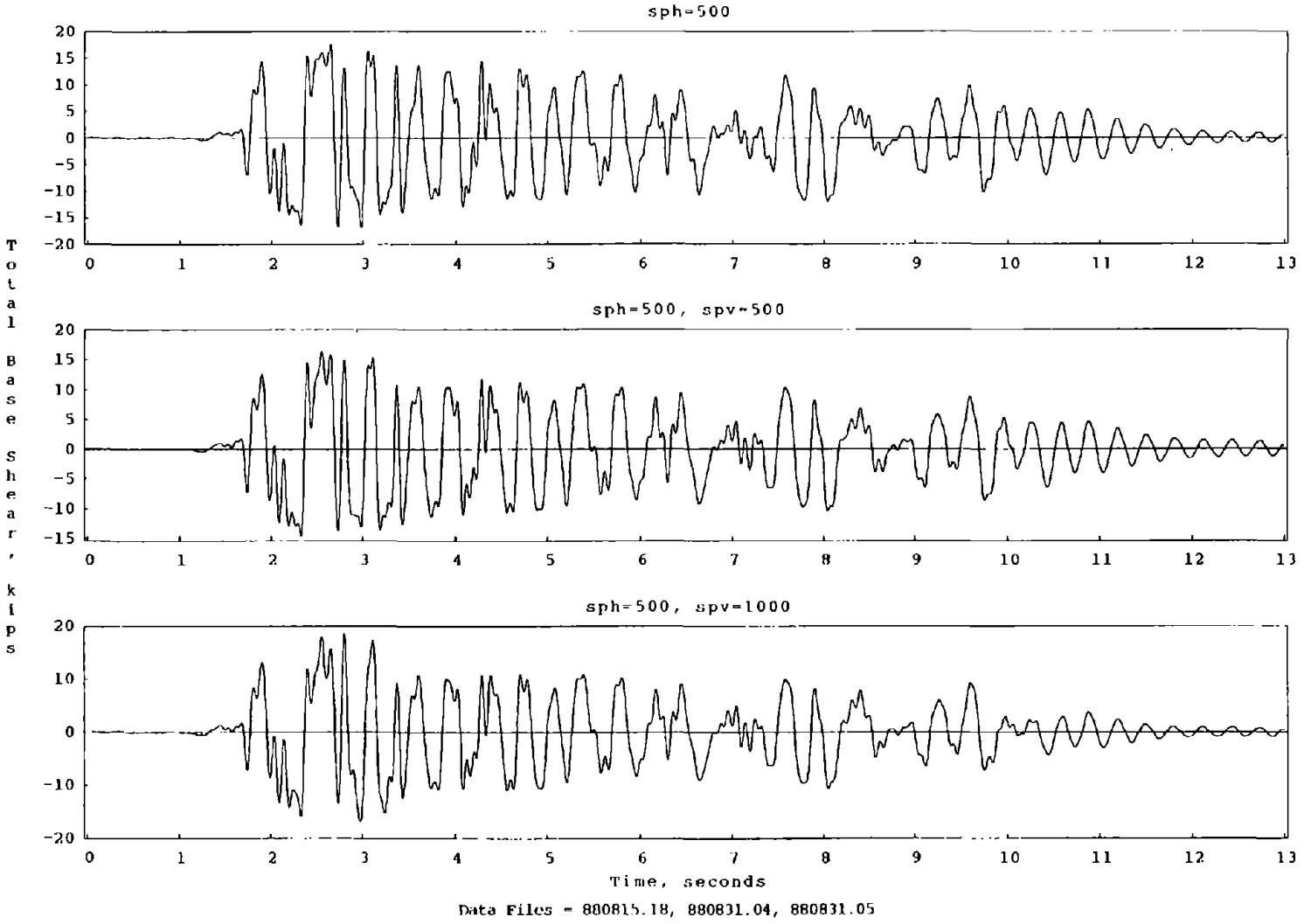

Figure 66 Total Base Shear Time Histories for San Francisco

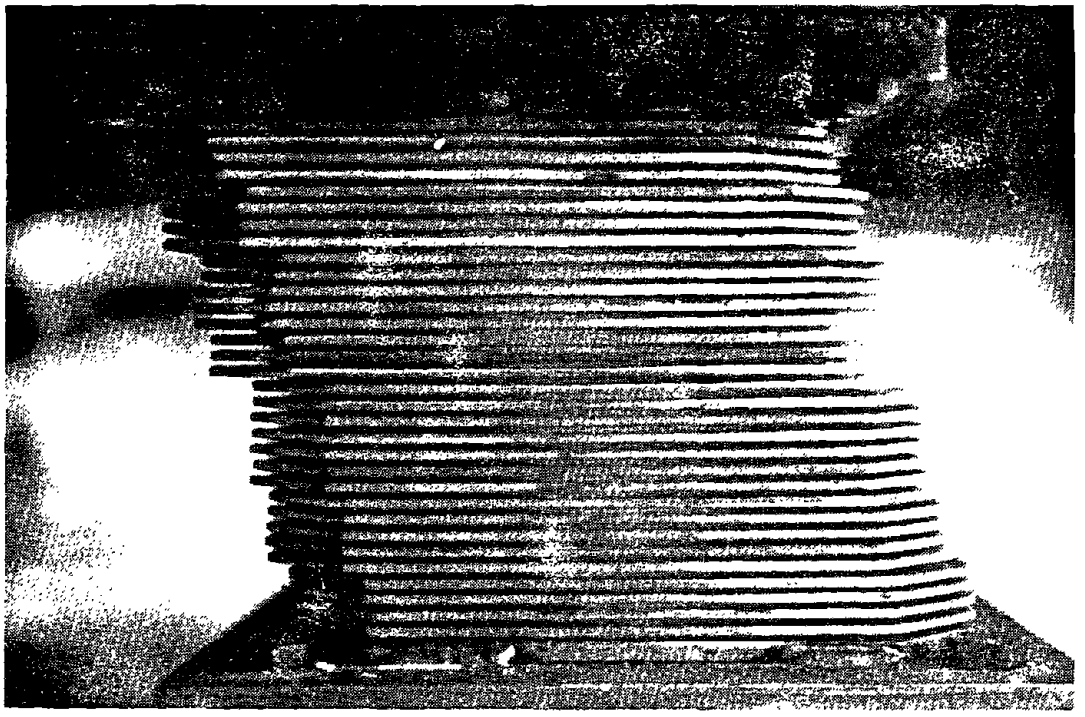

Figure 67 Sliding Deformations Concentrated on One Sliding Plane

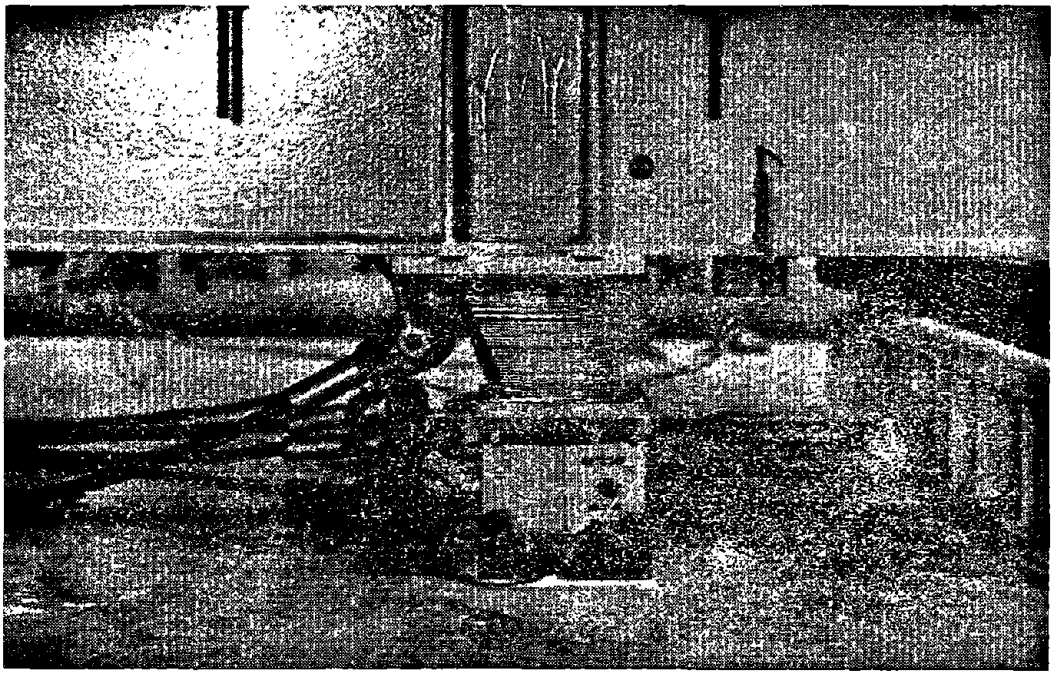

Figure 68 Sliding Deformations Distributed Evenly Across Bearing

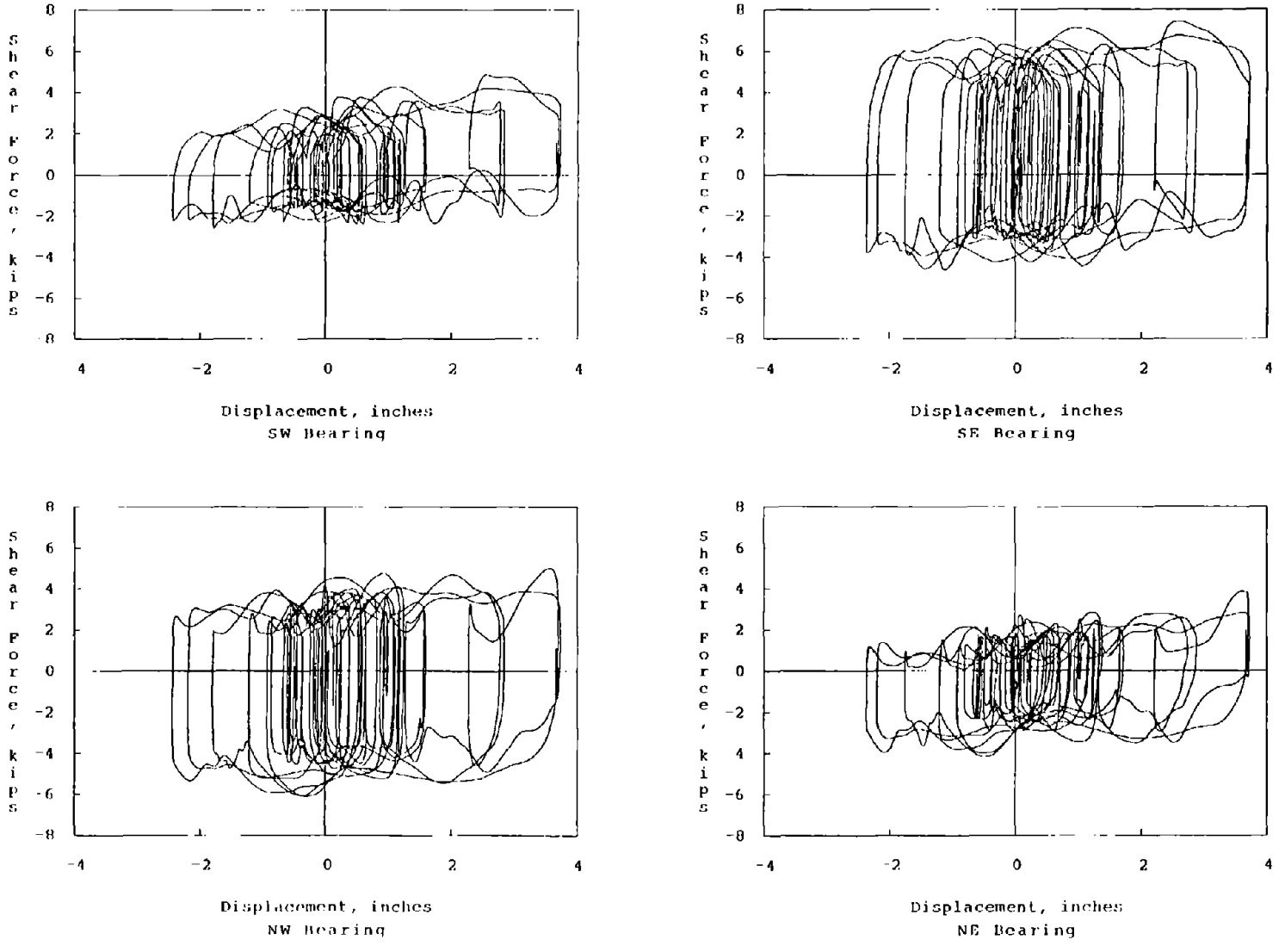

Figure 69 Hysteresis Loops of Individual Bearings for Chile, span = 900

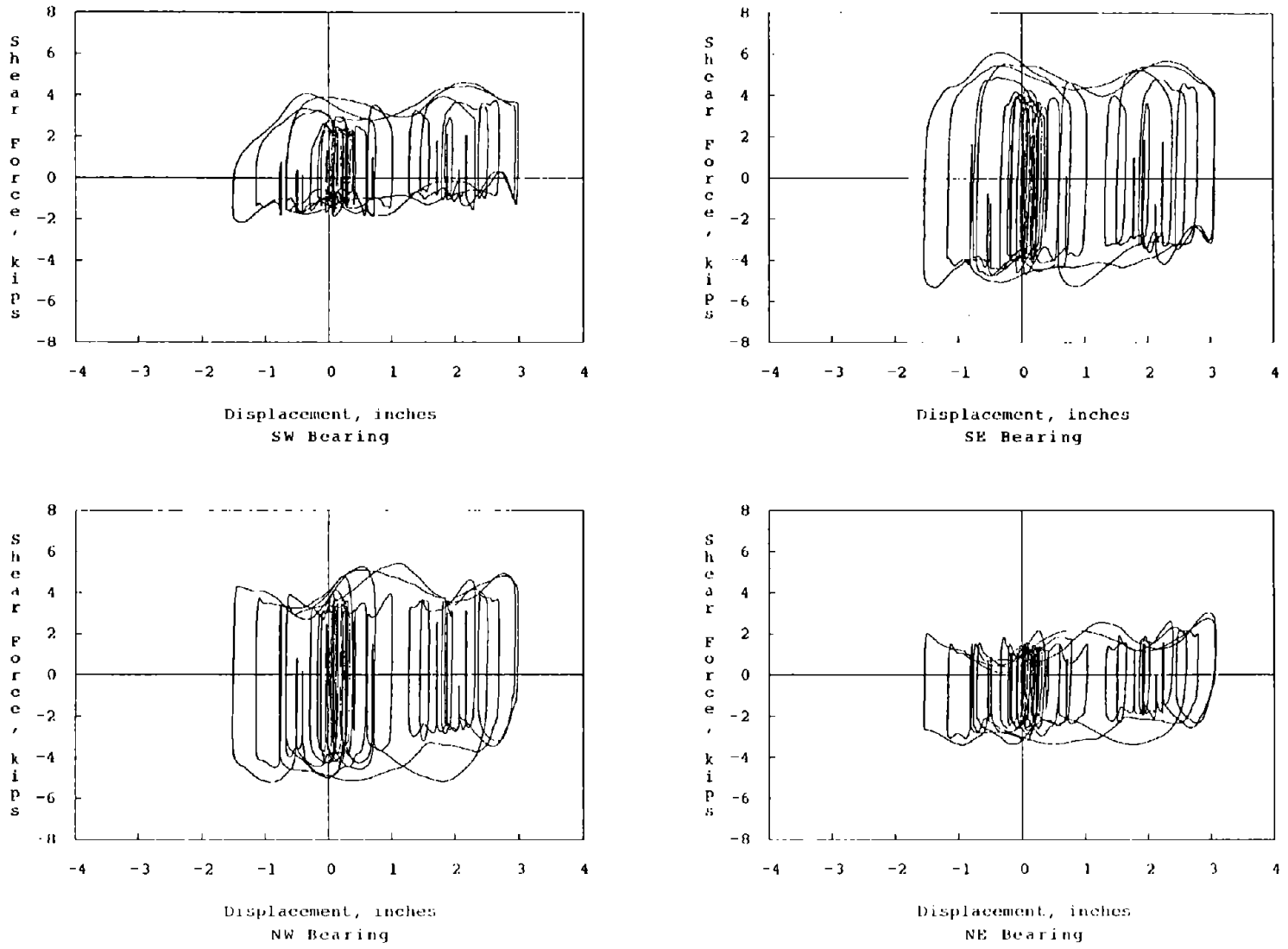

Figure 70 Hysteresis Loops of Individual Bearings for El Centro, span = 600

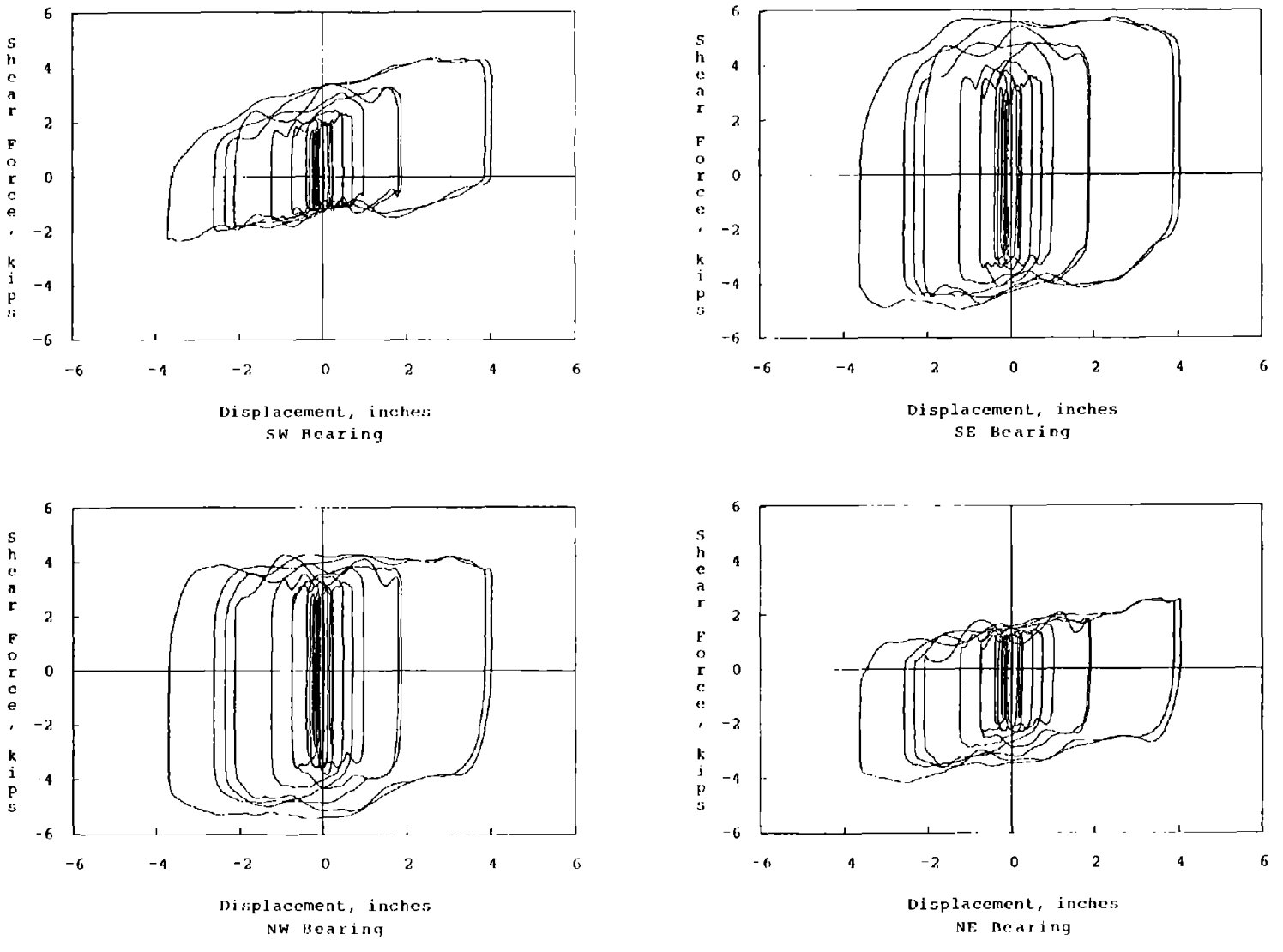

Figure 71 Hysteresis Loops of Individual Bearings for Mexico City, span = 900

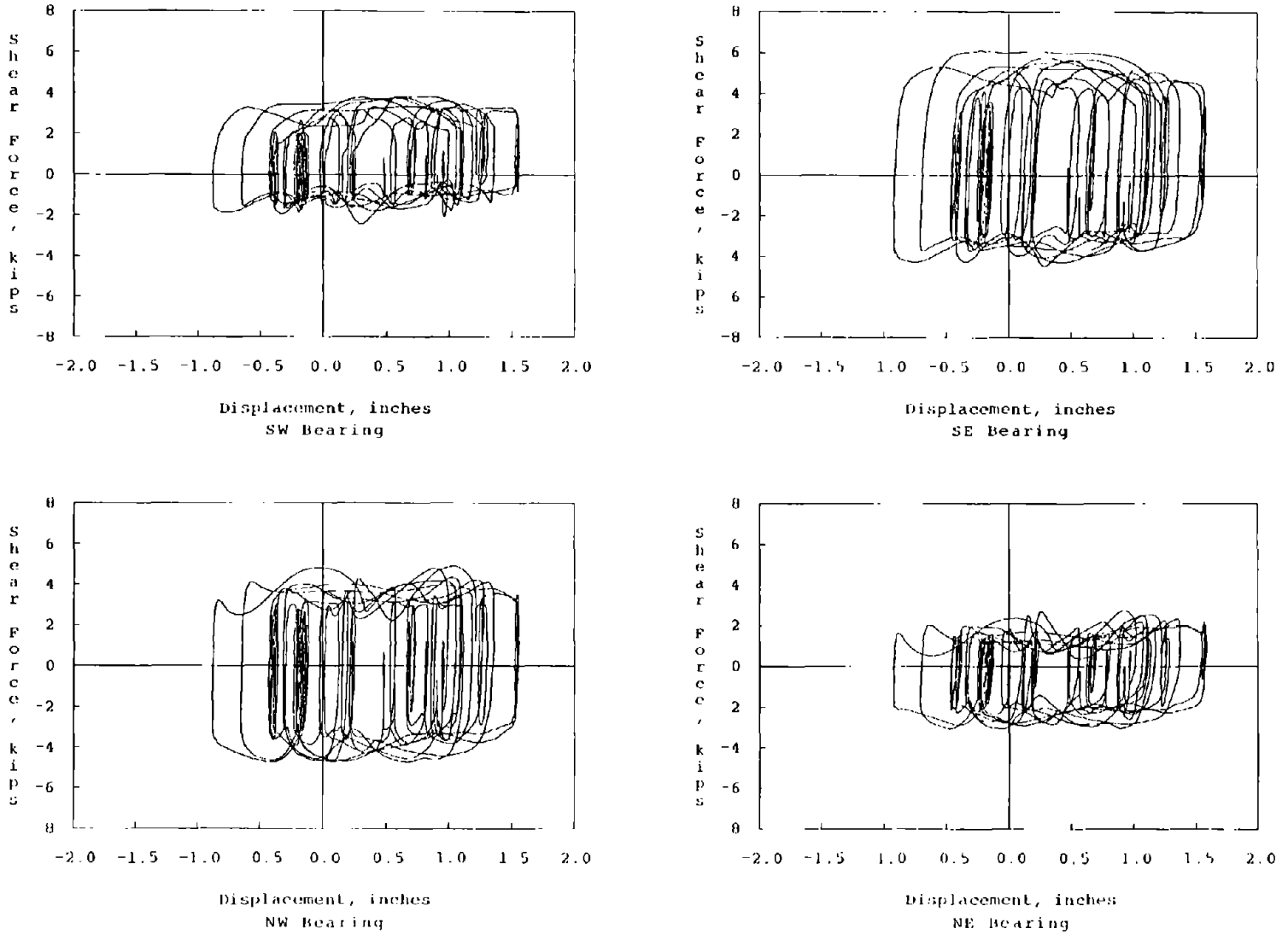

Figure 72 Hysteresis Loops of Individual Bearings for Olympia, span = 1000

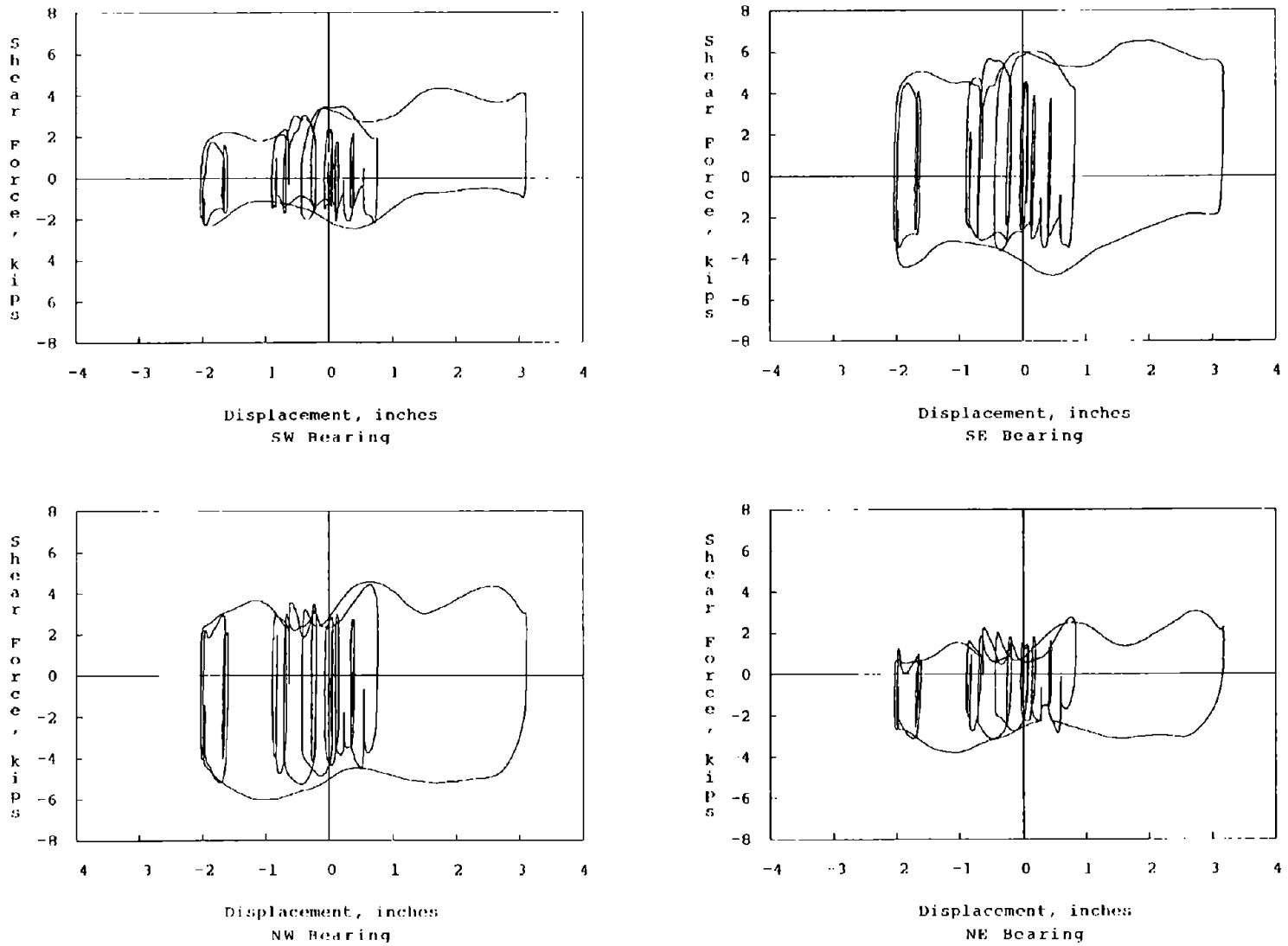

Figure 73 Hysteresis Loops of Individual Bearings for Pacoima Dam, span = 800

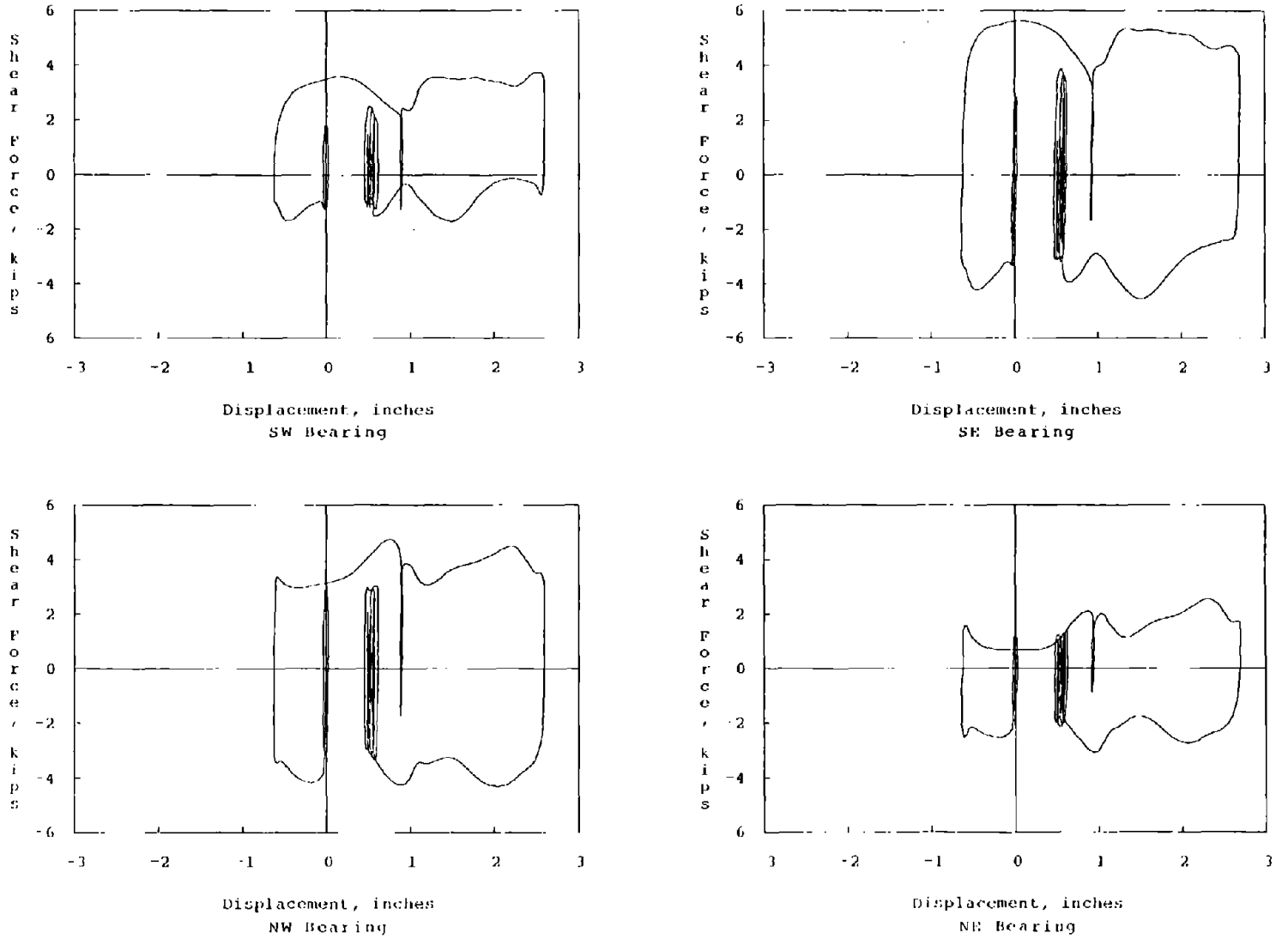

Figure 74 Hysteresis Loops of Individual Bearings for Parkfield, span = 600

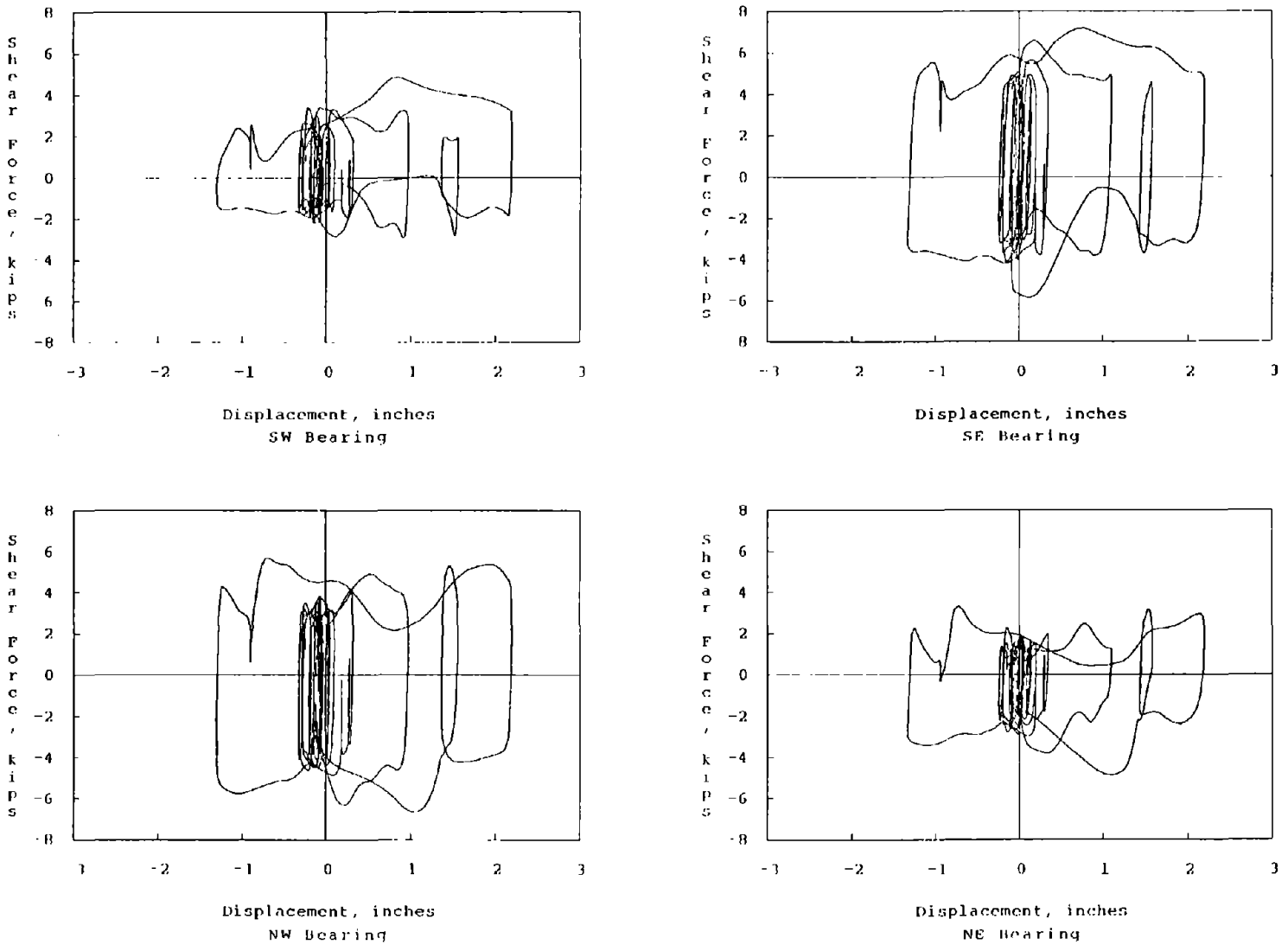

Figure 75 Hysteresis Loops of Individual Bearings for San Francisco, span = 600

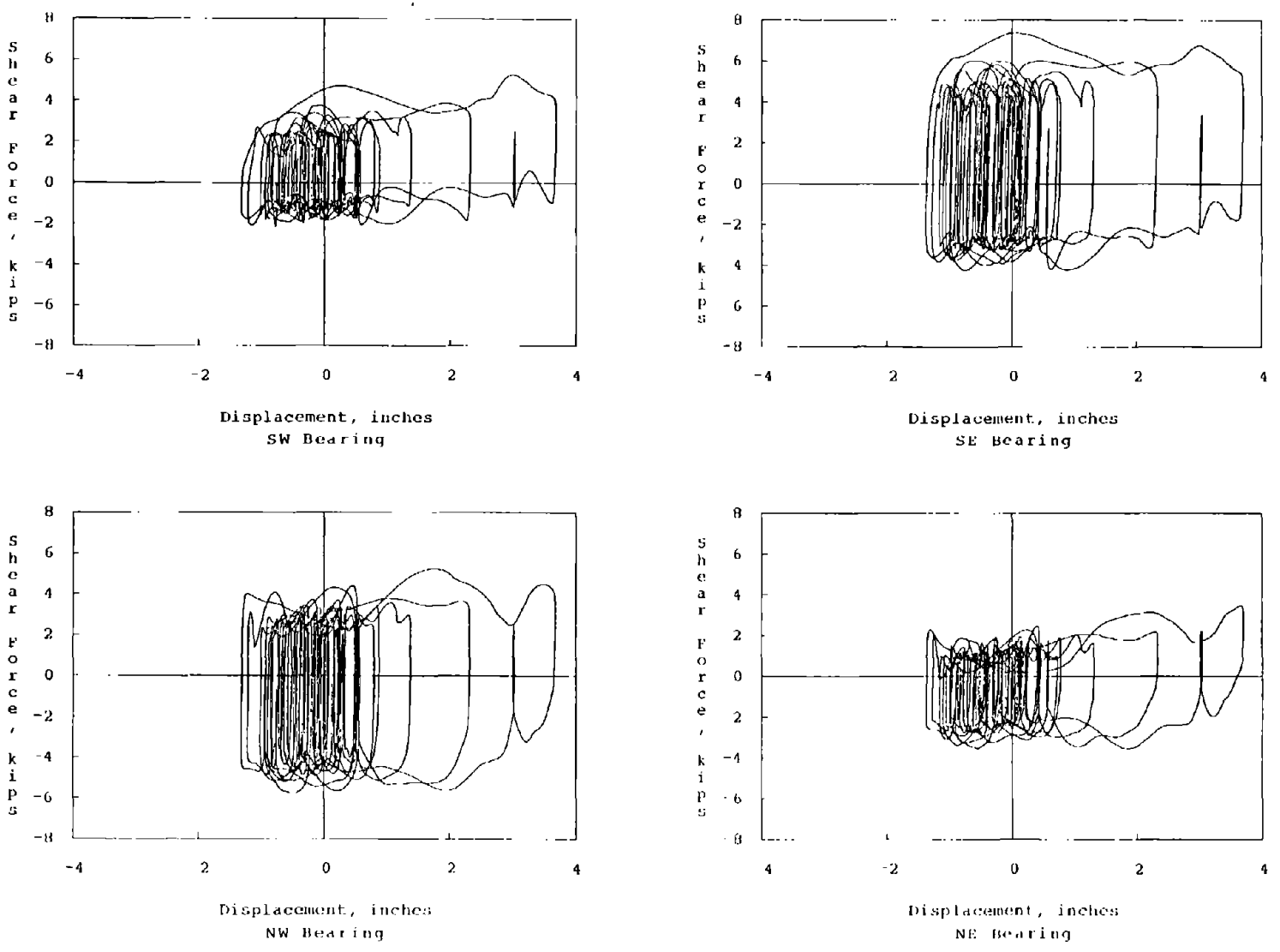

Figure 76 Hysteresis Loops of Individual Bearings for Taft, span = 800

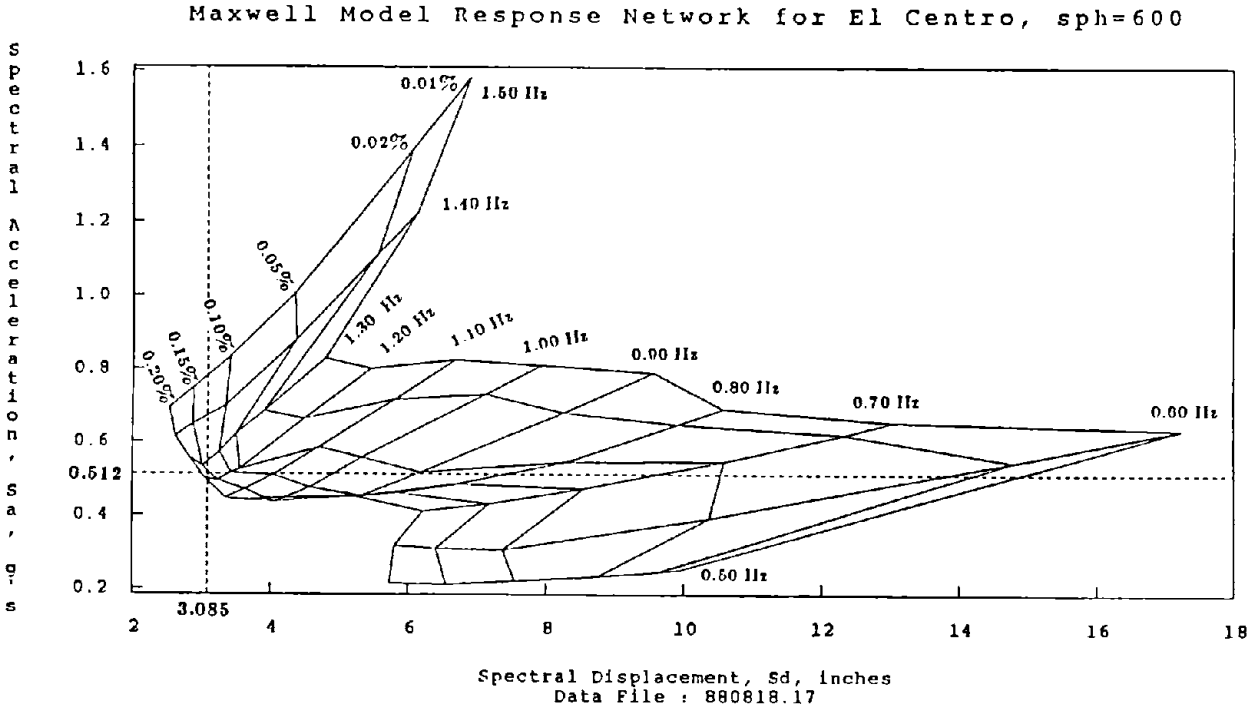

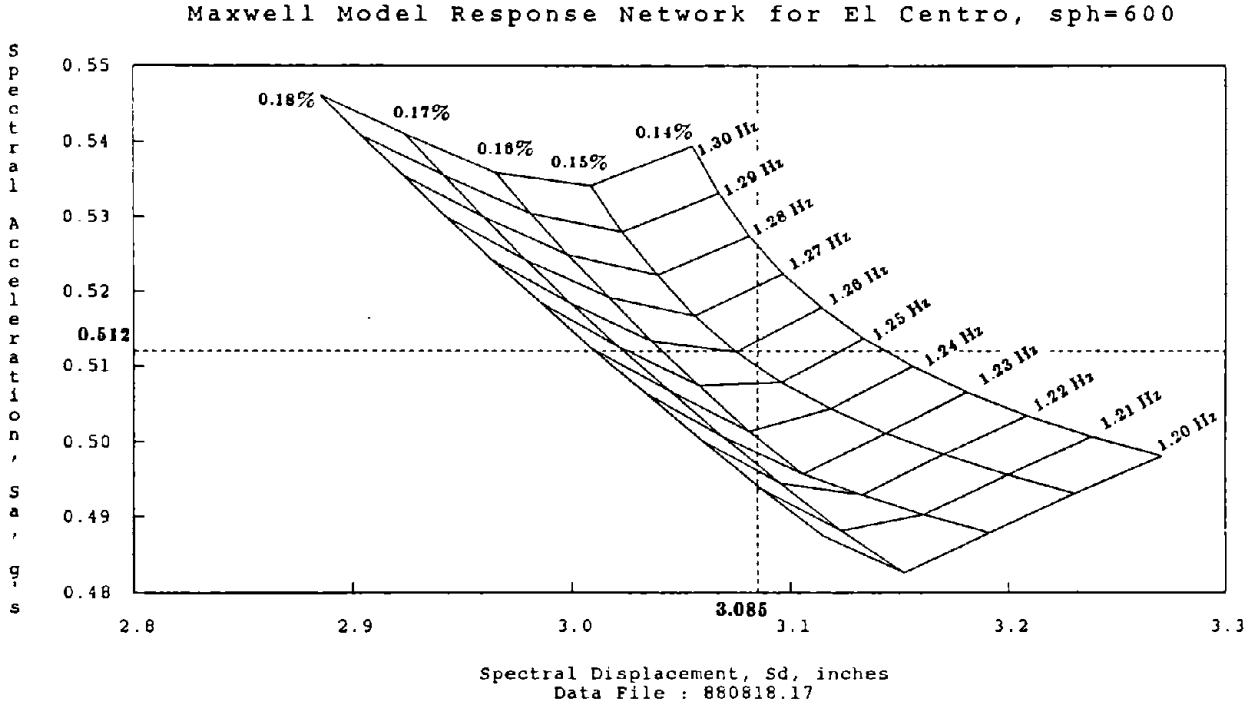

Figure 77 Response Network for El Centro, span = 600

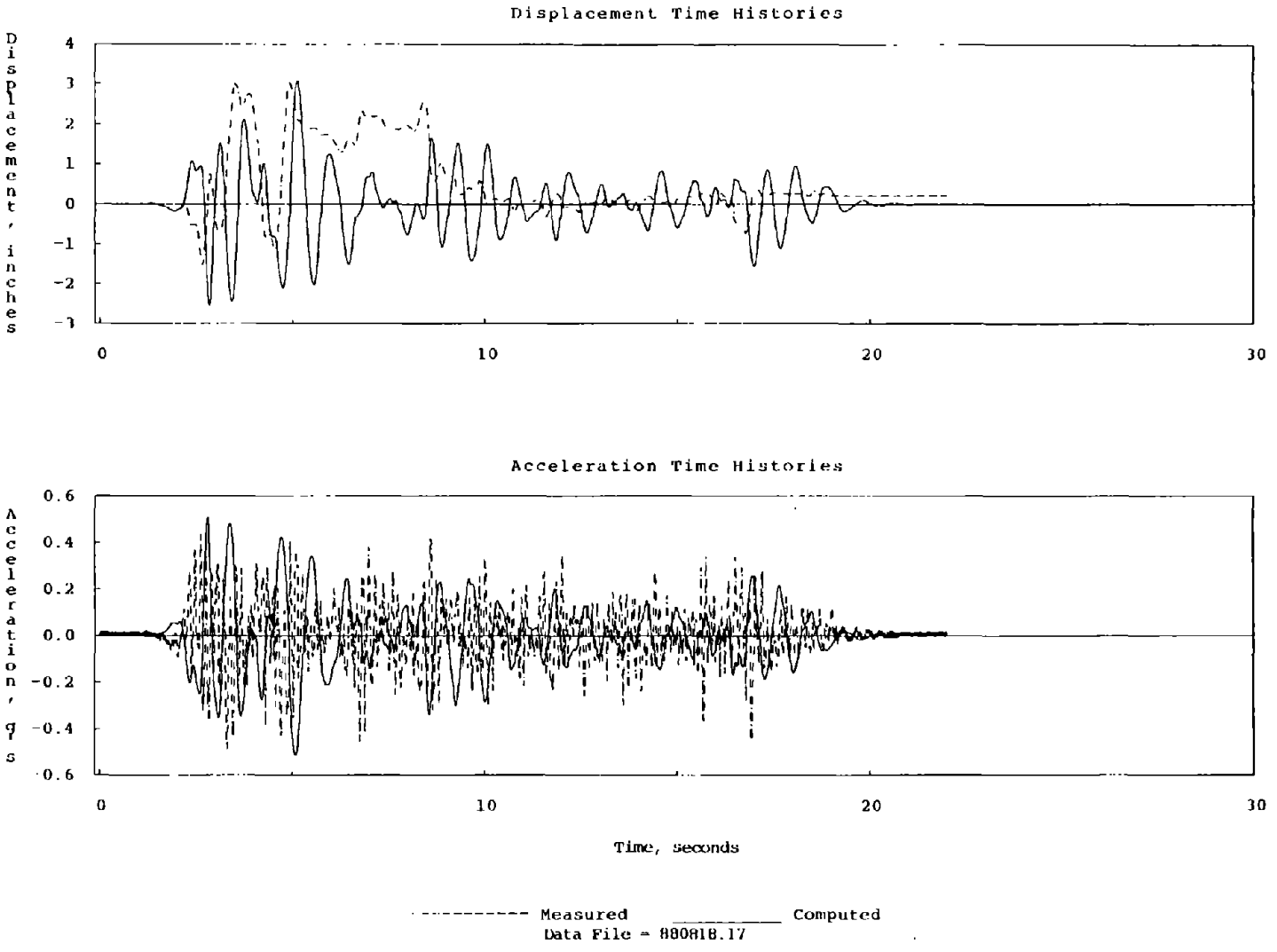

Figure 78 Comparison Between Calculated and Recorded Base Acceleration and Displacement Time Histories

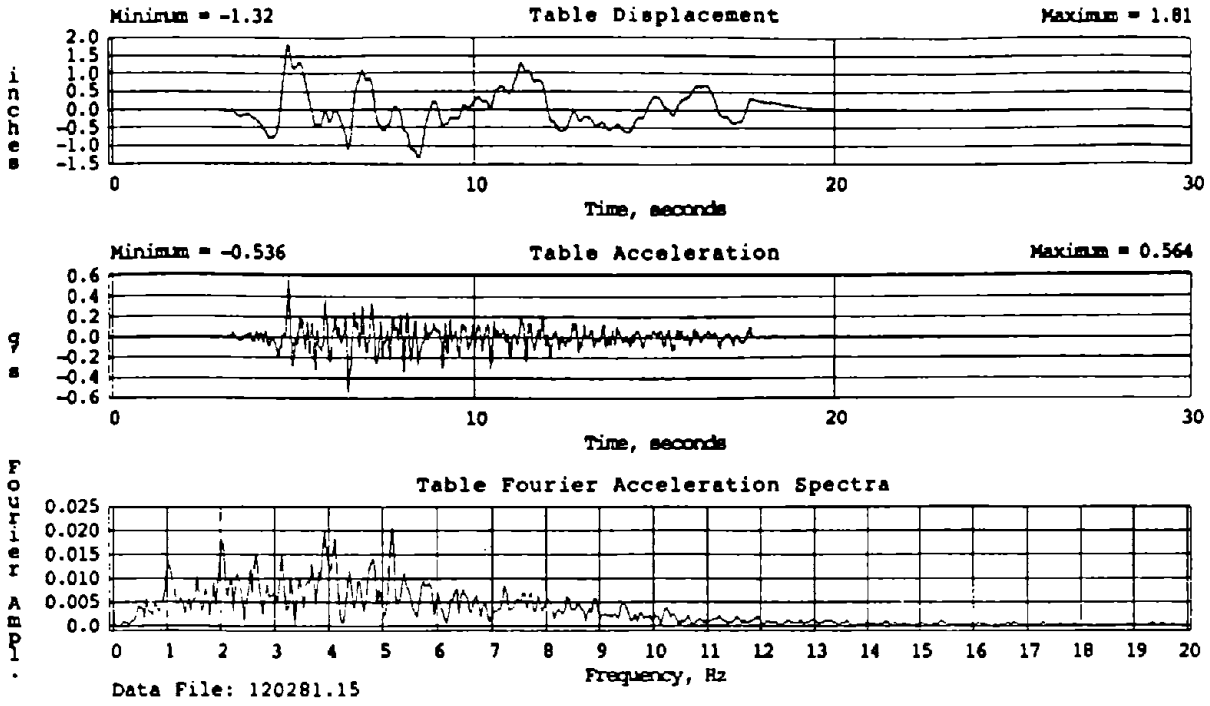

Figure 79 Displacement and Acceleration Time Histories and Fourier Acceleration Spectra of Taft Signal During Rubber Bearing Test Series, span = 350

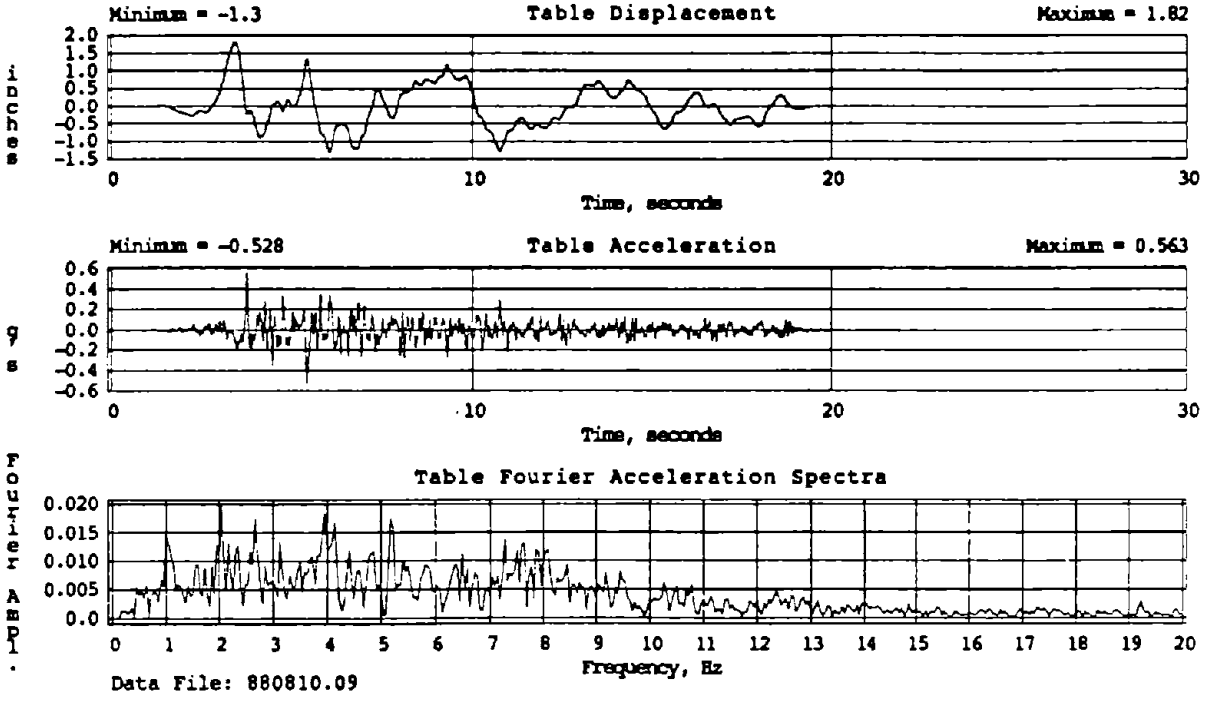

Figure 80 Displacement and Acceleration Time Histories and Fourier Acceleration Spectra of Taft Signal During R-FBI Test Series, span = 350

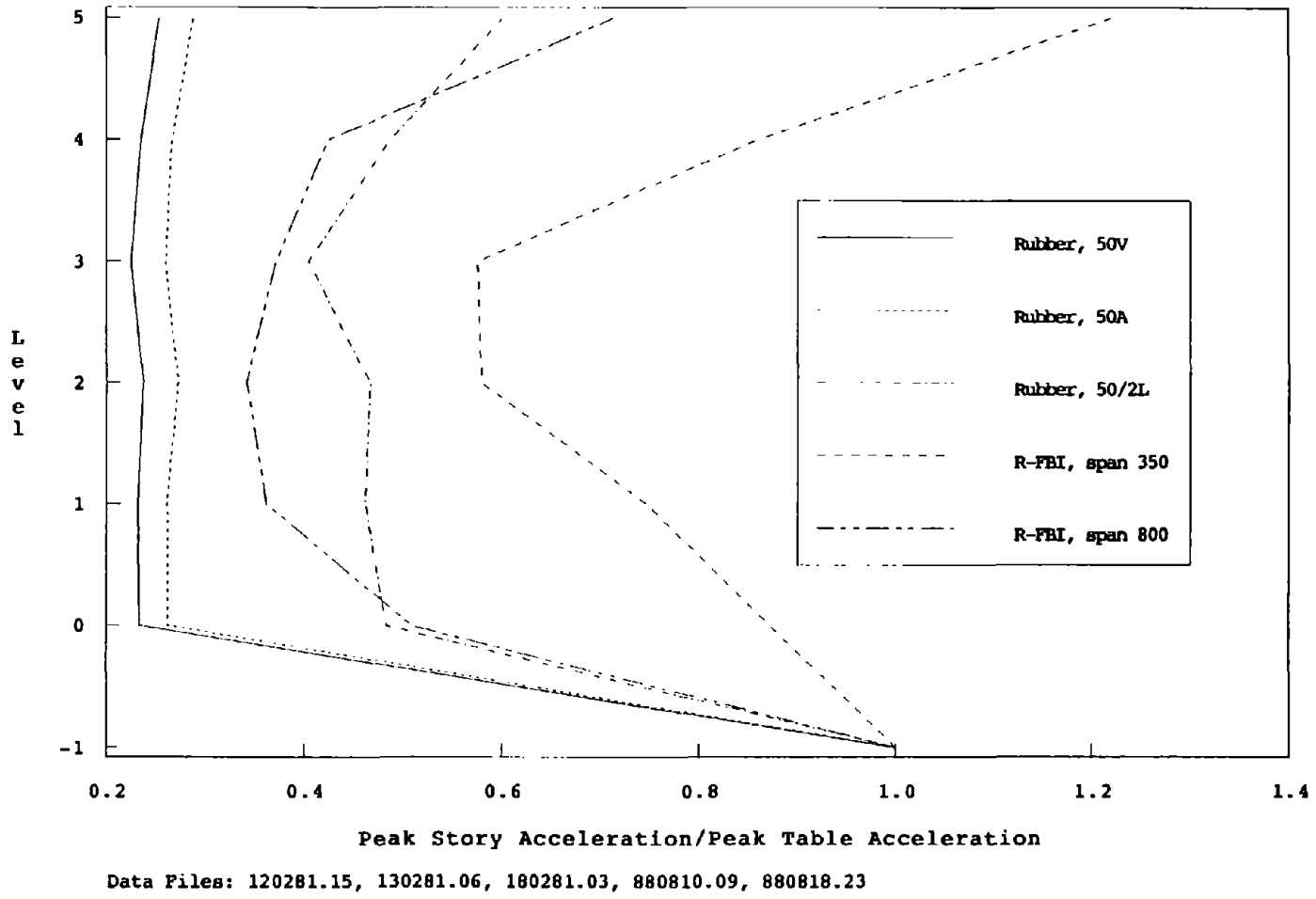

Figure 81 Normalized Accelerations Throughout Test Frame with Different Base Conditions for Taft, span = 350 and 800

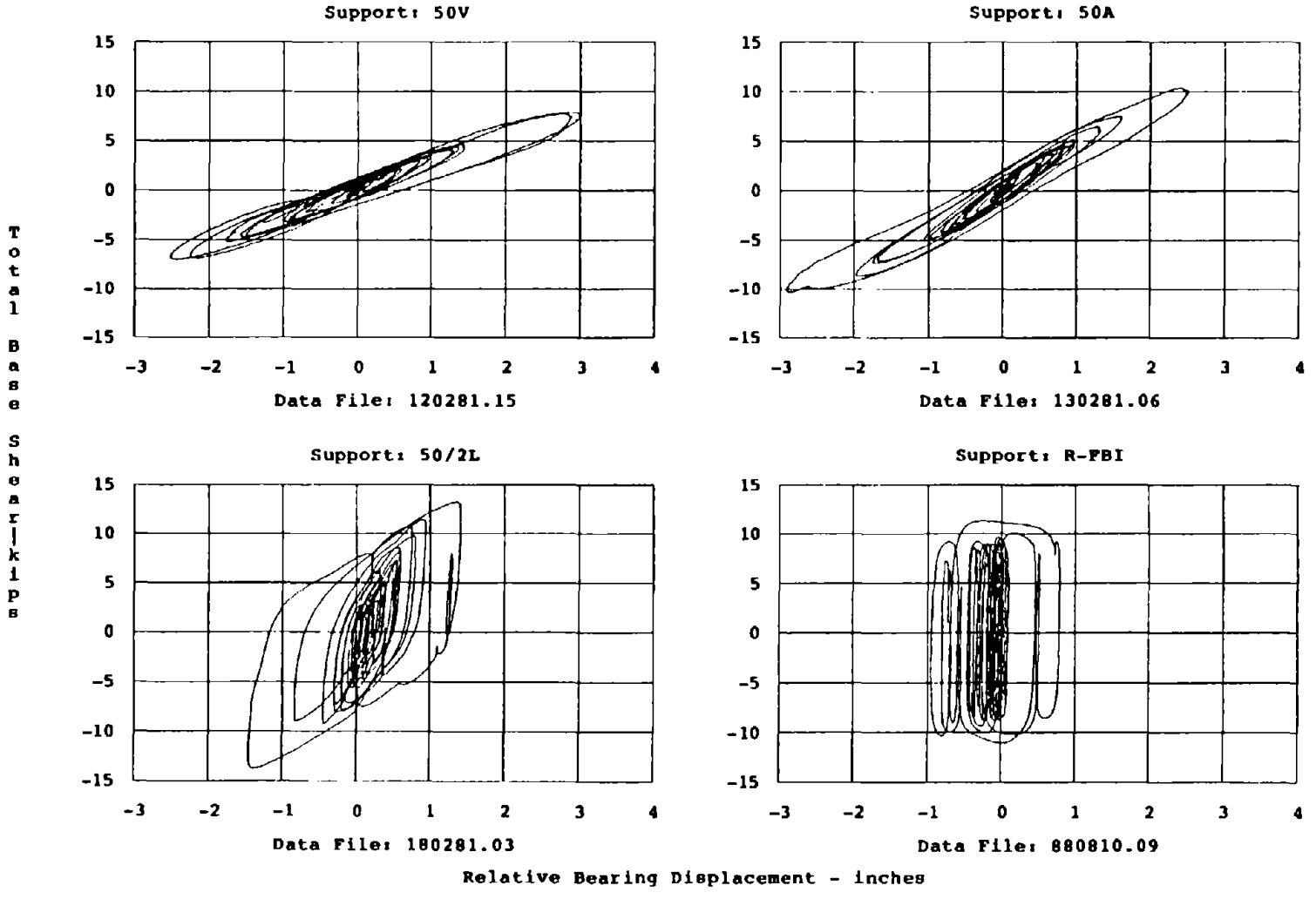

Figure 82 Hysteretic Behavior with Different Base Conditions for Taft, span = 350

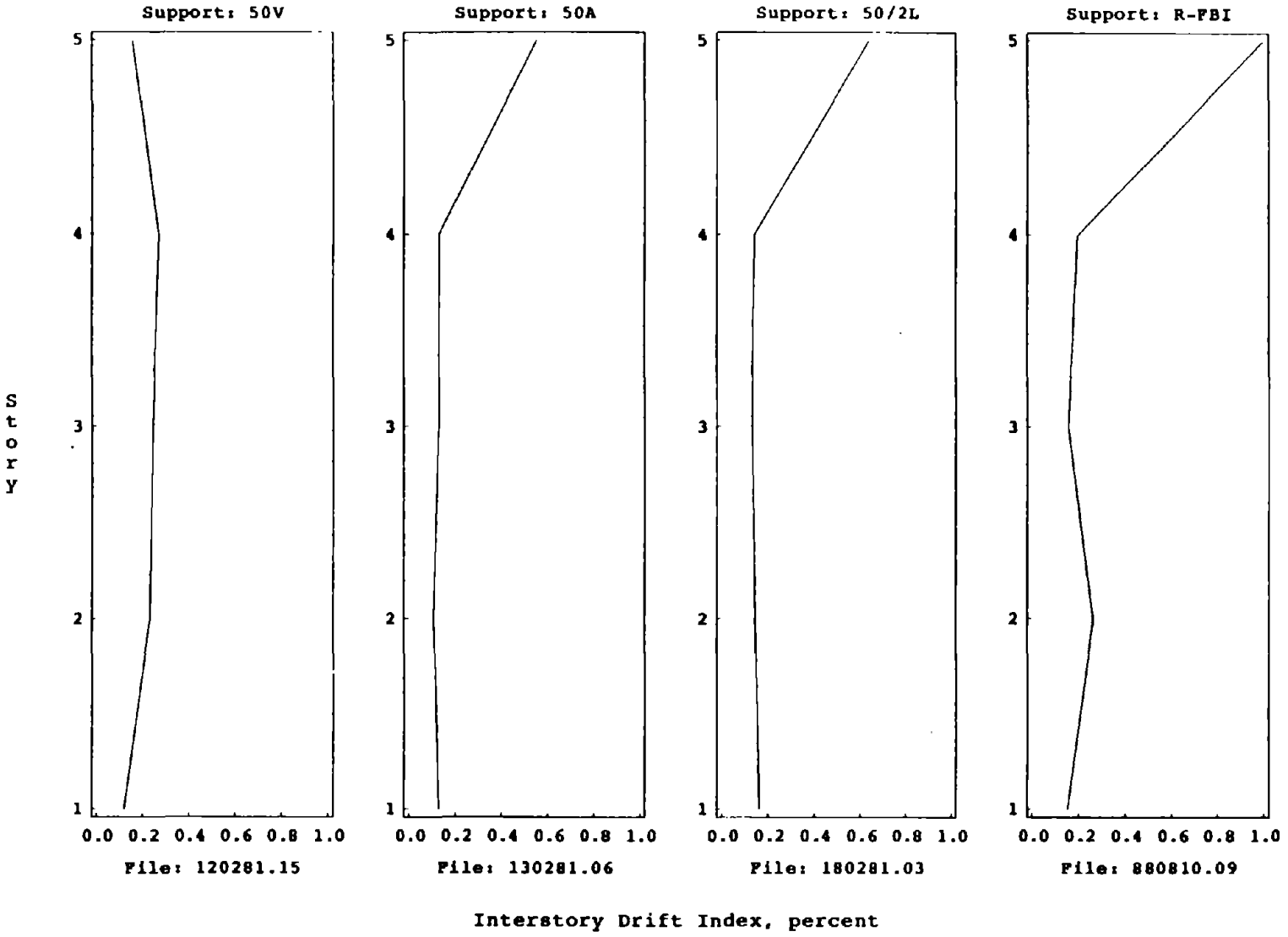

Figure 83 Interstory Drift Index Throughout Test Frame with Different Base Conditions for Taft, span = 350

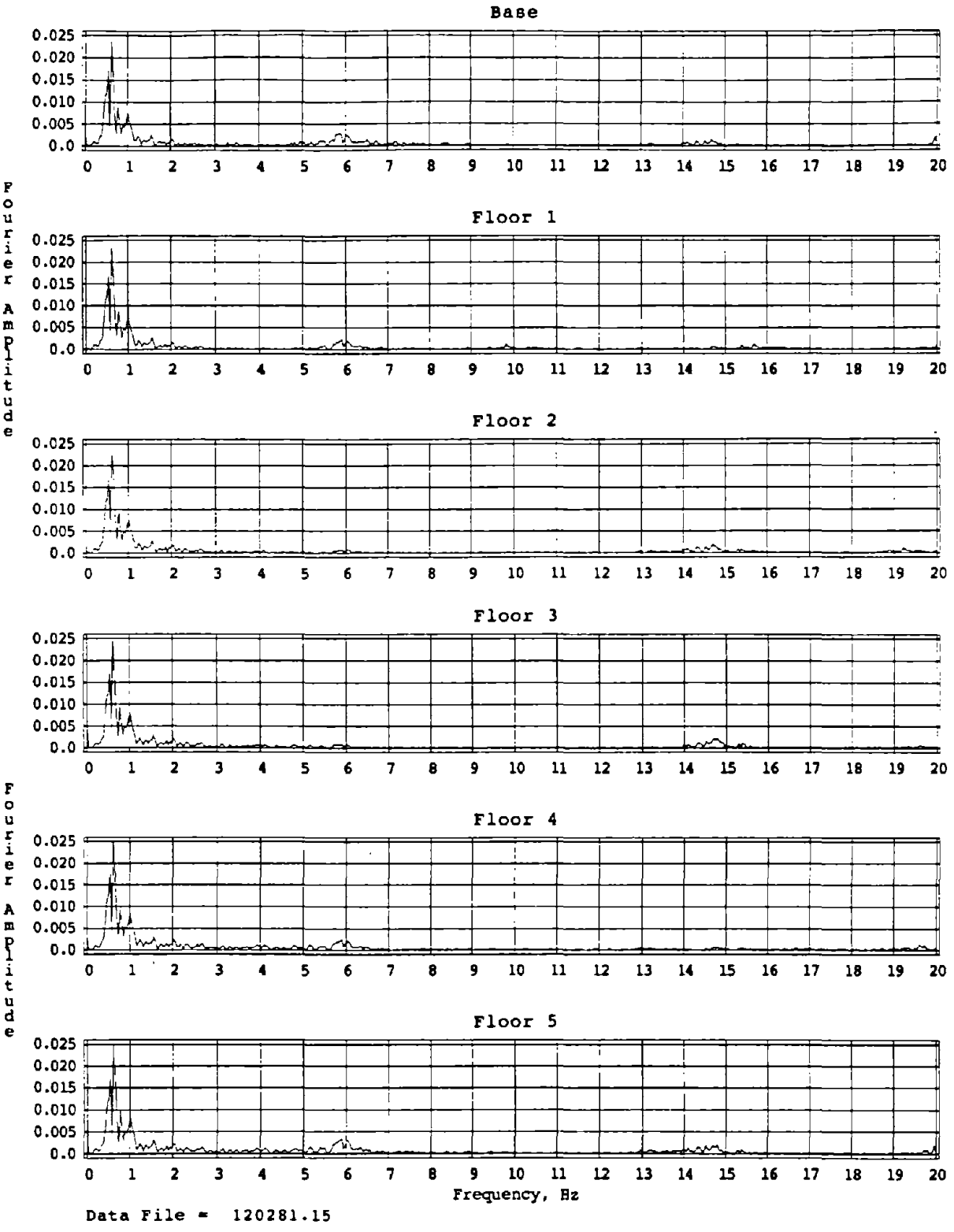

Figure 84 Fourier Spectra of Frame Accelerations Supported on Rubber Bearings with Veriprene Inserts, Taft span = 350

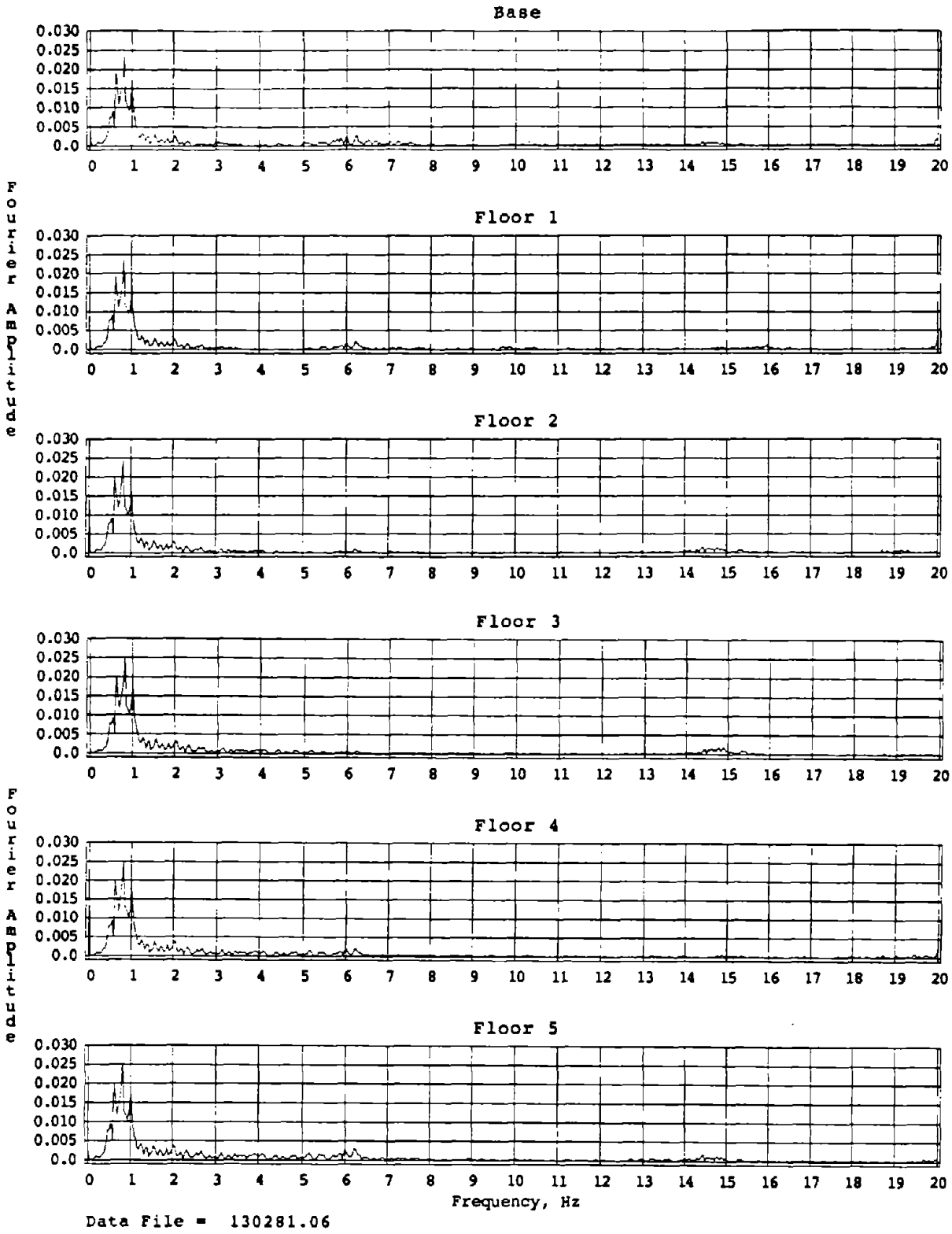

Figure 85 Fourier Spectra of Frame Accelerations Supported on Rubber Bearings with Adiprene Inserts, Taft span = 350

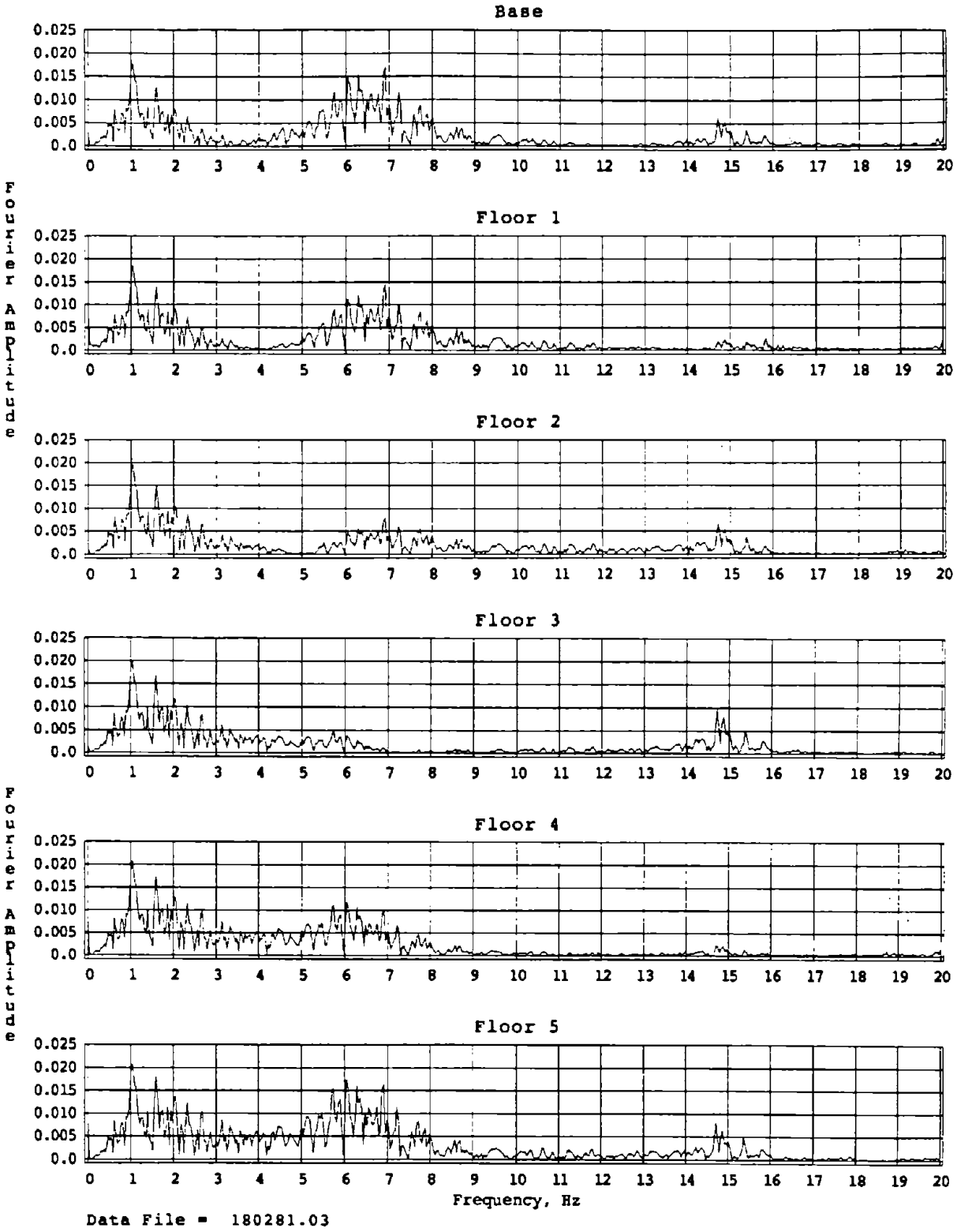

Figure 86 Fourier Spectra of Frame Accelerations Supported on Rubber Bearings with Lead Plugs, Taft span = 350

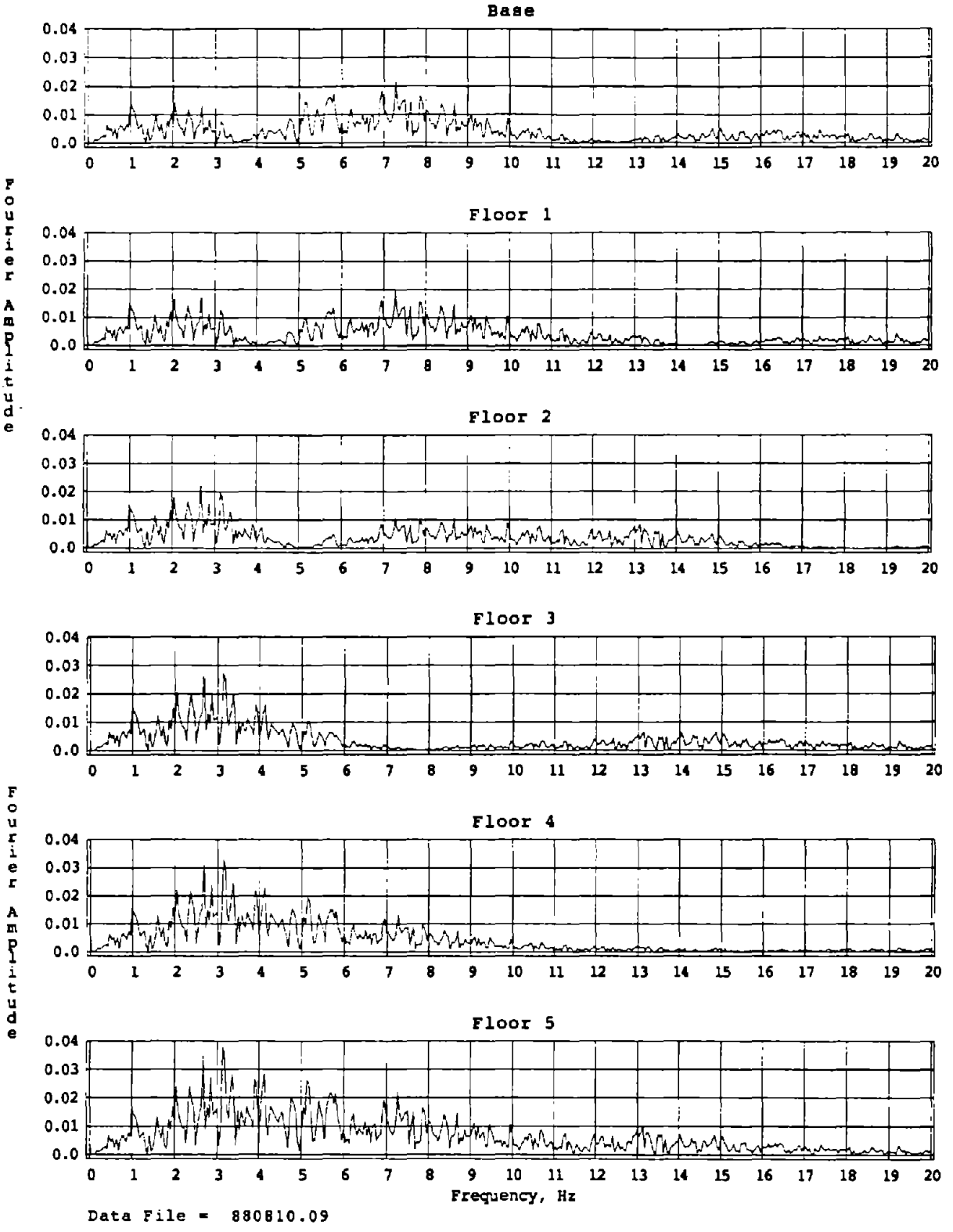

Figure 87 Fourier Spectra of Frame Accelerations Supported on R-FBI Bearings, Taft span = 350

APPENDIX

List of Instrumentation

Channel	Explanation	Units
1	Table h1 Displacement	inches
2	Table h2 Displacement	inches
3	Table Horizontal Acceleration	G's
4	Table Vertical Acceleration	G's
5	Table Pitch Acceleration	rad/sec^2
6	Table Roll Acceleration	rad/sec^2
7	not used	-
8	Table v1 Displacement	inches
9	Table v2 Displacement	inches
10	Table v3 Displacement	inches
11	Base Shear SW	kips
12	Base Moment SW	kip-in
13	Base Shear SE	kips
14	Base Moment SE	kip-in
15	Base Shear NW	kips
16	Base Moment NW	kip-in
17	Base Shear NE	kips
18	Base Moment NE	kip-in
19	Absolute Base Displacement W	inches
20	Absolute Base Displacement E	inches
21	Absolute Floor 1 Displacement W	inches
22	Absolute Floor 1 Displacement E	inches
23	Absolute Floor 2 Displacement W	inches
24	Absolute Floor 2 Displacement E	inches
25	Absolute Floor 3 Displacement W	inches
26	Absolute Floor 3 Displacement E	inches
27	Absolute Floor 4 Displacement W	inches
28	Absolute Floor 4 Displacement E	inches
29	Absolute Floor 5 Displacement W	inches
30	Absolute Floor 5 Displacement E	inches
31	Relative Bearing Displacement W	inches
32	Relative Bearing Displacement E	inches

33	Transverse Bearing Displacement N	inches
34	Transverse Bearing Displacement S	inches
35	Horizontal Base Acceleration W	G's
36	Horizontal Base Acceleration E	G's
37	Horizontal Floor 1 Acceleration W	G's
38	Horizontal Floor 1 Acceleration E	G's
39	Horizontal Floor 2 Acceleration W	G's
40	Horizontal Floor 2 Acceleration E	G's
41	Horizontal Floor 3 Acceleration W	G's
42	Horizontal Floor 3 Acceleration E	G's
43	Horizontal Floor 4 Acceleration W	G's
44	Horizontal Floor 4 Acceleration E	G's
45	Horizontal Floor 5 Acceleration W	G's
46	Horizontal Floor 5 Acceleration E	G's
47	Transverse Floor 5 Acceleration S	G's
48	Transverse Floor 5 Acceleration N	G's
49	Vertical Floor 5 Acceleration NW	G's
50	Vertical Floor 5 Acceleration NE	G's
51	Vertical Floor 5 Acceleration SW	G's
52	Vertical Floor 5 Acceleration SE	G's
53	Oscillator 1 Acceleration	G's
54	Oscillator 2 Acceleration	G's
55	Oscillator 3 Acceleration	G's

EARTHQUAKE ENGINEERING RESEARCH CENTER REPORT SERIES

EERC reports are available from the National Information Service for Earthquake Engineering(NISEE) and from the National Technical Information Service(NTIS). Numbers in parentheses are Accession Numbers assigned by the National Technical Information Service; these are followed by a price code. Contact NTIS, 5285 Port Royal Road, Springfield Virginia, 22161 for more information. Reports without Accession Numbers were not available from NTIS at the time of printing. For a current complete list of EERC reports (from EERC 67-1) and availability information, please contact University of California, EERC, NISEE, 1301 South 46th Street, Richmond, California 94804.

UCB/EERC-81/01 "Control of Seismic Response of Piping Systems and Other Structures by Base Isolation," by Kelly, J.M., January 1981, (PB81 200 735)A05.

UCB/EERC-81/02 "OPTNSR- An Interactive Software System for Optimal Design of Statically and Dynamically Loaded Structures with Nonlinear Response," by Bhatti, M.A., Ciampi, V. and Pister, K.S., January 1981, (PB81 218 851)A09.

UCB/EERC-81/03 "Analysis of Local Variations in Free Field Seismic Ground Motions," by Chen, J.-C., Lysmer, J. and Seed, H.B., January 1981, (AD-A099508)A13.

UCB/EERC-81/04 "Inelastic Structural Modeling of Braced Offshore Platforms for Seismic Loading," by Zayas, V.A., Shing, P.-S.B., Mahin, S.A. and Popov, E.P., January 1981, INEL4, (PB82 138 777)A07.

UCB/EERC-81/05 "Dynamic Response of Light Equipment in Structures," by Der Kiureghian, A., Sackman, J.L. and Nour-Omid, B., April 1981, (PB81 218 497)A04

UCB/EERC-81/06 "Preliminary Experimental Investigation of a Broad Base Liquid Storage Tank," by Bouwkamp, J.G., Kollegger, J.P. and Stephen, R.M., May 1981, (PB82 140 385)A03.

UCB/EERC-81/07 "The Seismic Resistant Design of Reinforced Concrete Coupled Structural Walls," by Aktan, A.E. and Bertero, V.V., June 1981, (PB82 113 358)A11

UCB/EERC-81/08 "Unassigned," by Unassigned, 1981.

UCB/EERC-81/09 "Experimental Behavior of a Spatial Piping System with Steel Energy Absorbers Subjected to a Simulated Differential Seismic Input," by Stiemer, S.F., Godden, W.G. and Kelly, J.M., July 1981, (PB82 201 898)A04.

UCB/EERC-81/10 "Evaluation of Seismic Design Provisions for Masonry in the United States," by Sveinsson, B.I., Mayes, R.L. and McNiven, H.D., August 1981, (PB82 166 075)A08.

UCB/EERC-81/11 "Two-Dimensional Hybrid Modelling of Soil-Structure Interaction," by Tzong, T.-J., Gupta, S. and Penzien, J., August 1981, (PB82 142 118)A04.

UCB/EERC-81/12 "Studies on Effects of Infills in Seismic Resistant R/C Construction," by Brokken, S. and Bertero, V.V., October 1981, (PB82 166 190)A09.

UCB/EERC-81/13 "Linear Models to Predict the Nonlinear Seismic Behavior of a One-Story Steel Frame," by Valdimarsson, H., Shah, A.H. and McNiven, H.D., September 1981, (PB82 138 793)A07.

UCB/EERC-81/14 "TLUSH: A Computer Program for the Three-Dimensional Dynamic Analysis of Earth Dams," by Kagawa, T., Mejia, L.H., Seed, H.B. and Lysmer, J., September 1981, (PB82 139 940)A06

UCB/EERC-81/15 "Three Dimensional Dynamic Response Analysis of Earth Dams," by Mejia, L.H. and Seed, H.B., September 1981, (PB82 137 274)A12.

UCB/EERC-81/16 "Experimental Study of Lead and Elastomeric Dampers for Base Isolation Systems," by Kelly, J.M. and Hodder, S.B., October 1981, (PB82 166 182)A05.

UCB/EERC-81/17 "The Influence of Base Isolation on the Seismic Response of Light Secondary Equipment," by Kelly, J.M., April 1981, (PB82 255 266)A04

UCB/EERC-81/18 "Studies on Evaluation of Shaking Table Response Analysis Procedures," by Blondet, J. M., November 1981, (PB82 197 278)A10.

UCB/EERC-81/19 "DELIGHT.STRUCT: A Computer-Aided Design Environment for Structural Engineering," by Balling, R.J., Pister, K.S. and Polak, E., December 1981, (PB82 218 496)A07.

UCB/EERC-81/20 "Optimal Design of Seismic-Resistant Planar Steel Frames," by Balling, R.J., Ciampi, V. and Pister, K.S., December 1981, (PB82 220 179)A07.

UCB/EERC-82/01 "Dynamic Behavior of Ground for Seismic Analysis of Lifeline Systems," by Sato, T. and Der Kiureghian, A., January 1982, (PB82 218 926)A05.

UCB/EERC-82/02 "Shaking Table Tests of a Tubular Steel Frame Model," by Ghanaat, Y. and Clough, R.W., January 1982, (PB82 220 161)A07.

UCB/EERC-82/03 "Behavior of a Piping System under Seismic Excitation: Experimental Investigations of a Spatial Piping System supported by Mechanical Shock Arrestors," by Schneider, S., Lee, H.-M. and Godden, W. G., May 1982, (PB83 172 544)A09.

UCB/EERC-82/04 "New Approaches for the Dynamic Analysis of Large Structural Systems," by Wilson, E.L., June 1982, (PB83 148 080)A05.

UCB/EERC-82/05 "Model Study of Effects of Damage on the Vibration Properties of Steel Offshore Platforms," by Shahrivar, F. and Bouwkamp, J.G., June 1982, (PB83 148 742)A10.

UCB/EERC-82/06 "States of the Art and Pratice in the Optimum Seismic Design and Analytical Response Prediction of R/C Frame Wall Structures," by Aktan, A.E. and Bertero, V.V., July 1982, (PB83 147 736)A05.

UCB/EERC-82/07 "Further Study of the Earthquake Response of a Broad Cylindrical Liquid-Storage Tank Model," by Manos, G.C. and Clough, R.W., July 1982, (PB83 147 744)A11.

UCB/EERC-82/08 "An Evaluation of the Design and Analytical Seismic Response of a Seven Story Reinforced Concrete Frame," by Charney, F.A. and Bertero, V.V., July 1982, (PB83 157 628)A09.

UCB/EERC-82/09 "Fluid-Structure Interactions: Added Mass Computations for Incompressible Fluid," by Kuo, J.S.-H., August 1982, (PB83 156 281)A07

UCB/EERC-82/10 "Joint-Opening Nonlinear Mechanism: Interface Smeared Crack Model," by Kuo, J.S.-H., August 1982, (PB83 149 195)A05.

UCB/EERC-82/11 "Dynamic Response Analysis of Techi Dam," by Clough, R.W., Stephen, R.M. and Kuo, J.S.-H., August 1982, (PB83 147 496)A06.

UCB/EERC-82/12 "Prediction of the Seismic Response of R/C Frame-Coupled Wall Structures," by Aktan, A.E., Bertero, V.V. and Piazzo, M., August 1982, (PB83 149 203)A09.

UCB/EERC-82/13 "Preliminary Report on the Smart 1 Strong Motion Array in Taiwan," by Bolt, B.A., Loh, C.H., Penzien, J. and Tsai, Y.B., August 1982, (PB83 159 400)A10.

UCB/EERC-82/14 "Seismic Behavior of an Eccentrically X-Braced Steel Structure," by Yang, M.S., September 1982, (PB83 260 778)A12.

UCB/EERC-82/15 "The Performance of Stairways in Earthquakes," by Roha, C., Axley, J.W. and Bertero, V.V., September 1982, (PB83 157 693)A07.

UCB/EERC-82/16 "The Behavior of Submerged Multiple Bodies in Earthquakes," by Liao, W.-G., September 1982, (PB83 158 709)A07.

UCB/EERC-82/17 "Effects of Concrete Types and Loading Conditions on Local Bond-Slip Relationships," by Cowell, A.D., Popov, E.P. and Bertero, V.V., September 1982, (PB83 153 577)A04.

UCB/EERC-82/18 "Mechanical Behavior of Shear Wall Vertical Boundary Members: An Experimental Investigation," by Wagner, M.T. and Bertero, V.V., October 1982, (PB83 159 764)A05.

UCB/EERC-82/19 "Experimental Studies of Multi-support Seismic Loading on Piping Systems," by Kelly, J.M. and Cowell, A.D., November 1982, (PB90 262 684)A07.

UCB/EERC-82/20 "Generalized Plastic Hinge Concepts for 3D Beam-Column Elements," by Chen, P. F.-S. and Powell, G.H., November 1982, (PB83 247 981)A13

UCB/EERC-82/21 "ANSR-II: General Computer Program for Nonlinear Structural Analysis," by Oughourlian, C.V. and Powell, G.H., November 1982, (PB83 251 330)A12.

UCB/EERC-82/22 "Solution Strategies for Statically Loaded Nonlinear Structures," by Simons, J.W. and Powell, G.H., November 1982, (PB83 197 970)A06.

UCB/EERC-82/23 "Analytical Model of Deformed Bar Anchorages under Generalized Excitations," by Ciampi, V., Eligehausen, R., Bertero, V.V. and Popov, E.P., November 1982, (PB83 169 532)A06.

UCB/EERC-82/24 "A Mathematical Model for the Response of Masonry Walls to Dynamic Excitations," by Sucuoglu, H., Mengi, Y. and McNiven, H.D., November 1982, (PB83 169 011)A07.

UCB/EERC-82/25 "Earthquake Response Considerations of Broad Liquid Storage Tanks," by Cambra, F.J., November 1982, (PB83 251 215)A09

UCB/EERC-82/26 "Computational Models for Cyclic Plasticity, Rate Dependence and Creep," by Mosaddad, B. and Powell, G.H., November 1982, (PB83 245 829)A08.

UCB/EERC-82/27 "Inelastic Analysis of Piping and Tubular Structures," by Mahasuverachai, M. and Powell, G.H., November 1982, (PB83 249 987)A07.

UCB/EERC-83/01 "The Economic Feasibility of Seismic Rehabilitation of Buildings by Base Isolation," by Kelly, J.M., January 1983 (PB83 197 988)A05.

UCB/EERC-83/02 "Seismic Moment Connections for Moment-Resisting Steel Frames," by Popov, E.P., January 1983, (PB83 195 412)A04.

UCB/EERC-83/03 "Design of Links and Beam-to-Column Connections for Eccentrically Braced Steel Frames," by Popov, E.P. and Malley, J.O., January 1983, (PB83 194 811)A04.

UCB/EERC-83/04 "Numerical Techniques for the Evaluation of Soil-Structure Interaction Effects in the Time Domain," by Bayo, E. and Wilson, E.L., February 1983, (PB83 245 605)A09.

UCB/EERC-83/05 "A Transducer for Measuring the Internal Forces in the Columns of a Frame-Wall Reinforced Concrete Structure," by Sause, R. and Bertero, V.V., May 1983, (PB84 119 494)A06.

UCB/EERC-83/06 "Dynamic Interactions Between Floating Ice and Offshore Structures," by Croteau, P., May 1983, (PB84 119 486)A16.

UCB/EERC-83/07 "Dynamic Analysis of Multiply Tuned and Arbitrarily Supported Secondary Systems," by Igusa, T. and Der Kiureghian, A., July 1983, (PB84 118 272)A11.

UCB/EERC-83/08 "A Laboratory Study of Submerged Multi-body Systems in Earthquakes," by Ansari, G.R., June 1983, (PB83 261 842)A17.

UCB/EERC-83/09 "Effects of Transient Foundation Uplift on Earthquake Response of Structures," by Yim, C.-S. and Chopra, A.K., June 1983, (PB83 261 396)A07.

UCB/EERC-83/10 "Optimal Design of Friction-Braced Frames under Seismic Loading," by Austin, M.A. and Pister, K.S., June 1983, (PB84 119 288)A06.

UCB/EERC-83/11 "Shaking Table Study of Single-Story Masonry Houses: Dynamic Performance under Three Component Seismic Input and Recommendations," by Manos, G.C., Clough, R.W. and Mayes, R.L., July 1983, (UCB/EERC-83/11)A08.

UCB/EERC-83/12 "Experimental Error Propagation in Pseudodynamic Testing," by Shiing, P.B. and Mahin, S.A., June 1983, (PB84 119 270)A09.

UCB/EERC-83/13 "Experimental and Analytical Predictions of the Mechanical Characteristics of a 1/5-scale Model of a 7-story R/C Frame-Wall Building Structure," by Aktan, A.E., Bertero, V.V., Chowdhury, A.A. and Nagashima, T., June 1983, (PB84 119 213)A07.

UCB/EERC-83/14 "Shaking Table Tests of Large-Panel Precast Concrete Building System Assemblages," by Oliva, M.G. and Clough, R.W., June 1983, (PB86 110 210/AS)A11.

UCB/EERC-83/15 "Seismic Behavior of Active Beam Links in Eccentrically Braced Frames," by Hjelmstad, K.D. and Popov, E.P., July 1983, (PB84 119 676)A09.

UCB/EERC-83/16 "System Identification of Structures with Joint Rotation," by Dimsdale, J.S., July 1983, (PB84 192 210)A06.

UCB/EERC-83/17 "Construction of Inelastic Response Spectra for Single-Degree-of-Freedom Systems," by Mahin, S. and Lin, J., June 1983, (PB84 208 834)A05.

UCB/EERC-83/18 "Interactive Computer Analysis Methods for Predicting the Inelastic Cyclic Behaviour of Structural Sections," by Kaba, S. and Mahin, S., July 1983, (PB84 192 012)A06.

UCB/EERC-83/19 "Effects of Bond Deterioration on Hysteretic Behavior of Reinforced Concrete Joints," by Filippou, F.C., Popov, E.P. and Bertero, V.V., August 1983, (PB84 192 020)A10.

UCB/EERC-83/20 "Correlation of Analytical and Experimental Responses of Large-Panel Precast Building Systems," by Oliva, M.G., Clough, R.W., Velkov, M. and Gavrilovic, P., May 1988, (PB90 262 692)A06.

UCB/EERC-83/21 "Mechanical Characteristics of Materials Used in a 1/5 Scale Model of a 7-Story Reinforced Concrete Test Structure," by Bertero, V.V., Aktan, A.E., Harris, H.G. and Chowdhury, A.A., October 1983, (PB84 193 697)A05.

UCB/EERC-83/22 "Hybrid Modelling of Soil-Structure Interaction in Layered Media," by Tzong, T.-J. and Penzien, J., October 1983, (PB84 192 178)A08.

UCB/EERC-83/23 "Local Bond Stress-Slip Relationships of Deformed Bars under Generalized Excitations," by Eligehausen, R., Popov, E.P. and Bertero, V.V., October 1983, (PB84 192 848)A09.

UCB/EERC-83/24 "Design Considerations for Shear Links in Eccentrically Braced Frames," by Malley, J.O. and Popov, E.P., November 1983, (PB84 192 186)A07.

UCB/EERC-84/01 "Pseudodynamic Test Method for Seismic Performance Evaluation: Theory and Implementation," by Shing, P.-S.B. and Mahin, S.A., January 1984, (PB84 190 644)A08.

UCB/EERC-84/02 "Dynamic Response Behavior of Kiang Hong Dian Dam," by Clough, R.W., Chang, K.-T., Chen, H.-Q. and Stephen, R.M., April 1984, (PB84 209 402)A08.

UCB/EERC-84/03 "Refined Modelling of Reinforced Concrete Columns for Seismic Analysis," by Kaba, S.A. and Mahin, S.A., April 1984, (PB84 234 384)A06.

UCB/EERC-84/04 "A New Floor Response Spectrum Method for Seismic Analysis of Multiply Supported Secondary Systems," by Asfura, A. and Der Kiureghian, A., June 1984, (PB84 239 417)A06.

UCB/EERC-84/05 "Earthquake Simulation Tests and Associated Studies of a 1/5th-scale Model of a 7-Story R/C Frame-Wall Test Structure," by Bertero, V.V., Aktan, A.E., Charney, F.A. and Sause, R., June 1984, (PB84 239 409)A09.

UCB/EERC-84/06 "Unassigned," by Unassigned, 1984.

UCB/EERC-84/07 "Behavior of Interior and Exterior Flat-Plate Connections subjected to Inelastic Load Reversals," by Zee, H.L. and Moehle, J.P., August 1984, (PB86 117 629/AS)A07.

UCB/EERC-84/08 "Experimental Study of the Seismic Behavior of a Two-Story Flat-Plate Structure," by Moehle, J.P. and Diebold, J.W., August 1984, (PB86 122 553/AS)A12.

UCB/EERC-84/09 "Phenomenological Modeling of Steel Braces under Cyclic Loading," by Ikeda, K., Mahin, S.A. and Dermitzakis, S.N., May 1984, (PB86 132 198/AS)A08.

UCB/EERC-84/10 "Earthquake Analysis and Response of Concrete Gravity Dams," by Fenves, G. and Chopra, A.K., August 1984, (PB85 193 902/AS)A11.

UCB/EERC-84/11 "EAGD-84: A Computer Program for Earthquake Analysis of Concrete Gravity Dams," by Fenves, G. and Chopra, A.K., August 1984, (PB85 193 613/AS)A05.

UCB/EERC-84/12 "A Refined Physical Theory Model for Predicting the Seismic Behavior of Braced Steel Frames," by Ikeda, K. and Mahin, S.A., July 1984, (PB85 191 450/AS)A09.

UCB/EERC-84/13 "Earthquake Engineering Research at Berkeley - 1984," by EERC, August 1984, (PB85 197 341/AS)A10.

UCB/EERC-84/14 "Moduli and Damping Factors for Dynamic Analyses of Cohesionless Soils," by Seed, H.B., Wong, R.T., Idriss, I.M. and Tokimatsu, K., September 1984, (PB85 191 468/AS)A04.

UCB/EERC-84/15 "The Influence of SPT Procedures in Soil Liquefaction Resistance Evaluations," by Seed, H.B., Tokimatsu, K., Harder, L.F. and Chung, R.M., October 1984, (PB85 191 732/AS)A04.

UCB/EERC-84/16 "Simplified Procedures for the Evaluation of Settlements in Sands Due to Earthquake Shaking," by Tokimatsu, K. and Seed, H.B., October 1984, (PB85 197 887/AS)A03.

UCB/EERC-84/17 "Evaluation of Energy Absorption Characteristics of Highway Bridges Under Seismic Conditions - Volume I (PB90 262 627)A16 and Volume II (Appendices) (PB90 262 635)A13," by Imbsen, R.A. and Penzien, J., September 1986.

UCB/EERC-84/18 "Structure-Foundation Interactions under Dynamic Loads," by Liu, W.D. and Penzien, J., November 1984, (PB87 124 889/AS)A11.

UCB/EERC-84/19 "Seismic Modelling of Deep Foundations," by Chen, C.-H. and Penzien, J., November 1984, (PB87 124 798/AS)A07.

UCB/EERC-84/20 "Dynamic Response Behavior of Quan Shui Dam," by Clough, R.W., Chang, K.-T., Chen, H.-Q., Stephen, R.M., Ghanaat, Y. and Qi, J.-H., November 1984, (PB86 115177/AS)A07.

UCB/EERC-85/01 "Simplified Methods of Analysis for Earthquake Resistant Design of Buildings," by Cruz, E.F. and Chopra, A.K., February 1985, (PB86 112299/AS)A12.

UCB/EERC-85/02 "Estimation of Seismic Wave Coherency and Rupture Velocity using the SMART 1 Strong-Motion Array Recordings," by Abrahamson, N.A., March 1985, (PB86 214 343)A07.

UCB/EERC-85/03 "Dynamic Properties of a Thirty Story Condominium Tower Building," by Stephen, R.M., Wilson, E.L. and Stander, N., April 1985, (PB86 118965/AS)A06.

UCB/EERC-85/04 "Development of Substructuring Techniques for On-Line Computer Controlled Seismic Performance Testing," by Dermitzakis, S. and Mahin, S., February 1985, (PB86 132941/AS)A08.

UCB/EERC-85/05 "A Simple Model for Reinforcing Bar Anchorages under Cyclic Excitations," by Filippou, F.C., March 1985, (PB86 112 919/AS)A05.

UCB/EERC-85/06 "Racking Behavior of Wood-framed Gypsum Panels under Dynamic Load," by Oliva, M.G., June 1985, (PB90 262 643)A04.

UCB/EERC-85/07 "Earthquake Analysis and Response of Concrete Arch Dams," by Fok, K.-L. and Chopra, A.K., June 1985, (PB86 139672/AS)A10.

UCB/EERC-85/08 "Effect of Inelastic Behavior on the Analysis and Design of Earthquake Resistant Structures," by Lin, J.P. and Mahin, S.A., June 1985, (PB86 135340/AS)A08.

UCB/EERC-85/09 "Earthquake Simulator Testing of a Base-Isolated Bridge Deck," by Kelly, J.M., Buckle, I.G. and Tsai, H.-C., January 1986, (PB87 124 152/AS)A06.

UCB/EERC-85/10 "Simplified Analysis for Earthquake Resistant Design of Concrete Gravity Dams," by Fenves, G. and Chopra, A.K., June 1986, (PB87 124 160/AS)A08.

UCB/EERC-85/11 "Dynamic Interaction Effects in Arch Dams," by Clough, R.W., Chang, K.-T., Chen, H.-Q. and Ghanaat, Y., October 1985, (PB86 135027/AS)A05.

UCB/EERC-85/12 "Dynamic Response of Long Valley Dam in the Mammoth Lake Earthquake Series of May 25-27, 1980," by Lai, S. and Seed, H.B., November 1985, (PB86 142304/AS)A05.

UCB/EERC-85/13 "A Methodology for Computer-Aided Design of Earthquake-Resistant Steel Structures," by Austin, M.A., Pister, K.S. and Mahin, S.A., December 1985, (PB86 159480/AS)A10.

UCB/EERC-85/14 "Response of Tension-Leg Platforms to Vertical Seismic Excitations," by Liou, G.-S., Penzien, J. and Yeung, R.W., December 1985, (PB87 124 871/AS)A08.

UCB/EERC-85/15 "Cyclic Loading Tests of Masonry Single Piers: Volume 4 - Additional Tests with Height to Width Ratio of 1," by Sveinsson, B., McNiven, H.D. and Sucuoglu, H., December 1985.

UCB/EERC-85/16 "An Experimental Program for Studying the Dynamic Response of a Steel Frame with a Variety of Infill Partitions," by Yanev, B. and McNiven, H.D., December 1985, (PB90 262 676)A05.

UCB/EERC-86/01 "A Study of Seismically Resistant Eccentrically Braced Steel Frame Systems," by Kasai, K. and Popov, E.P., January 1986, (PB87 124 178/AS)A14.

UCB/EERC-86/02 "Design Problems in Soil Liquefaction," by Seed, H.B., February 1986, (PB87 124 186/AS)A03.

UCB/EERC-86/03 "Implications of Recent Earthquakes and Research on Earthquake-Resistant Design and Construction of Buildings," by Bertero, V.V., March 1986, (PB87 124 194/AS)A05.

UCB/EERC-86/04 "The Use of Load Dependent Vectors for Dynamic and Earthquake Analyses," by Leger, P., Wilson, E.L. and Clough, R.W., March 1986, (PB87 124 202/AS)A12.

UCB/EERC-86/05 "Two Beam-To-Column Web Connections," by Tsai, K.-C. and Popov, E.P., April 1986, (PB87 124 301/AS)A04.

UCB/EERC-86/06 "Determination of Penetration Resistance for Coarse-Grained Soils using the Becker Hammer Drill," by Harder, L.F. and Seed, H.B., May 1986, (PB87 124 210/AS)A07.

UCB/EERC-86/07 "A Mathematical Model for Predicting the Nonlinear Response of Unreinforced Masonry Walls to In-Plane Earthquake Excitations," by Mengi, Y. and McNiven, H.D., May 1986, (PB87 124 780/AS)A06.

UCB/EERC-86/08 "The 19 September 1985 Mexico Earthquake: Building Behavior," by Bertero, V.V., July 1986.

UCB/EERC-86/09 "EACD-3D: A Computer Program for Three-Dimensional Earthquake Analysis of Concrete Dams," by Fok, K.-L., Hall, J.F. and Chopra, A.K., July 1986, (PB87 124 228/AS)A08.

UCB/EERC-86/10 "Earthquake Simulation Tests and Associated Studies of a 0.3-Scale Model of a Six-Story Concentrically Braced Steel Structure," by Uang, C.-M. and Bertero, V.V., December 1986, (PB87 163 564/AS)A17.

UCB/EERC-86/11 "Mechanical Characteristics of Base Isolation Bearings for a Bridge Deck Model Test," by Kelly, J.M., Buckle, I.G. and Koh, C.-G., November 1987, (PB90 262 668)A04.

UCB/EERC-86/12 "Effects of Axial Load on Elastomeric Isolation Bearings," by Koh, C.-G. and Kelly, J.M., November 1987.

UCB/EERC-87/01 "The FPS Earthquake Resisting System: Experimental Report," by Zayas, V.A., Low, S.S. and Mahin, S.A., June 1987.

UCB/EERC-87/02 "Earthquake Simulator Tests and Associated Studies of a 0.3-Scale Model of a Six-Story Eccentrically Braced Steel Structure," by Whittaker, A., Uang, C.-M. and Bertero, V.V., July 1987.

UCB/EERC-87/03 "A Displacement Control and Uplift Restraint Device for Base-Isolated Structures," by Kelly, J.M., Griffith, M.C. and Aiken, I.D., April 1987.

UCB/EERC-87/04 "Earthquake Simulator Testing of a Combined Sliding Bearing and Rubber Bearing Isolation System," by Kelly, J.M. and Chalhoub, M.S., 1987.

UCB/EERC-87/05 "Three-Dimensional Inelastic Analysis of Reinforced Concrete Frame-Wall Structures," by Moazzami, S. and Bertero, V.V., May 1987.

UCB/EERC-87/06 "Experiments on Eccentrically Braced Frames with Composite Floors," by Ricles, J. and Popov, E., June 1987.

UCB/EERC-87/07 "Dynamic Analysis of Seismically Resistant Eccentrically Braced Frames," by Ricles, J. and Popov, E., June 1987.

UCB/EERC-87/08 "Undrained Cyclic Triaxial Testing of Gravels-The Effect of Membrane Compliance," by Evans, M.D. and Seed, H.B., July 1987.

UCB/EERC-87/09 "Hybrid Solution Techniques for Generalized Pseudo-Dynamic Testing," by Thewalt, C. and Mahin, S.A., July 1987.

UCB/EERC-87/10 "Ultimate Behavior of Butt Welded Splices in Heavy Rolled Steel Sections," by Bruneau, M., Mahin, S.A. and Popov, E.P., September 1987.

UCB/EERC-87/11 "Residual Strength of Sand from Dam Failures in the Chilean Earthquake of March 3, 1985," by De Alba, P., Seed, H.B., Retamal, E. and Seed, R.B., September 1987.

UCB/EERC-87/12 "Inelastic Seismic Response of Structures with Mass or Stiffness Eccentricities in Plan," by Bruneau, M. and Mahin, S.A., September 1987, (PB90 262 650)A14.

UCB/EERC-87/13 "CSTRUCT: An Interactive Computer Environment for the Design and Analysis of Earthquake Resistant Steel Structures," by Austin, M.A., Mahin, S.A. and Pister, K.S., September 1987.

UCB/EERC-87/14 "Experimental Study of Reinforced Concrete Columns Subjected to Multi-Axial Loading," by Low, S.S. and Moehle, J.P., September 1987.

UCB/EERC-87/15 "Relationships between Soil Conditions and Earthquake Ground Motions in Mexico City in the Earthquake of Sept. 19, 1985," by Seed, H.B., Romo, M.P., Sun, J., Jaime, A. and Lysmer, J., October 1987.

UCB/EERC-87/16 "Experimental Study of Seismic Response of R. C. Setback Buildings," by Shahrooz, B.M. and Moehle, J.P., October 1987.

UCB/EERC-87/17 "The Effect of Slabs on the Flexural Behavior of Beams," by Pantazopoulou, S.J. and Moehle, J.P., October 1987, (PB90 262 700)A07.

UCB/EERC-87/18 "Design Procedure for R-FBI Bearings," by Mostaghel, N. and Kelly, J.M., November 1987, (PB90 262 718)A04.

UCB/EERC-87/19 "Analytical Models for Predicting the Lateral Response of R C Shear Walls: Evaluation of their Reliability," by Vulcano, A. and Bertero, V.V., November 1987.

UCB/EERC-87/20 "Earthquake Response of Torsionally-Coupled Buildings," by Hejal, R. and Chopra, A.K., December 1987.

UCB/EERC-87/21 "Dynamic Reservoir Interaction with Monticello Dam," by Clough, R.W., Ghanaat, Y. and Qiu, X-F., December 1987.

UCB/EERC-87/22 "Strength Evaluation of Coarse-Grained Soils," by Siddiqi, F.H., Seed, R.B., Chan, C.K., Seed, H B. and Pyke, R.M., December 1987.

UCB/EERC-88/01 "Seismic Behavior of Concentrically Braced Steel Frames," by Khatib, I., Mahin, S.A. and Pister, K.S., January 1988.

UCB/EERC-88/02 "Experimental Evaluation of Seismic Isolation of Medium-Rise Structures Subject to Uplift," by Griffith, M.C., Kelly, J.M., Coveney, V.A. and Koh, C.G., January 1988.

UCB/EERC-88/03 "Cyclic Behavior of Steel Double Angle Connections," by Astaneh-Asl, A. and Nader, M.N., January 1988.

UCB/EERC-88/04 "Re-evaluation of the Slide in the Lower San Fernando Dam in the Earthquake of Feb. 9, 1971," by Seed, H.B., Seed, R.B., Harder, L.F. and Jong, H.-L., April 1988.

UCB/EERC-88/05 "Experimental Evaluation of Seismic Isolation of a Nine-Story Braced Steel Frame Subject to Uplift," by Griffith, M.C., Kelly, J.M. and Aiken, I.D., May 1988.

UCB/EERC-88/06 "DRAIN-2DX User Guide.," by Allahabadi, R. and Powell, G.H., March 1988.

UCB/EERC-88/07 "Theoretical and Experimental Studies of Cylindrical Water Tanks in Base-Isolated Structures," by Chalhoub, M.S. and Kelly, J.M., April 1988.

UCB/EERC-88/08 "Analysis of Near-Source Waves: Separation of Wave Types using Strong Motion Array Recordings," by Darragh, R.B., June 1988.

UCB/EERC-88/09 "Alternatives to Standard Mode Superposition for Analysis of Non-Classically Damped Systems," by Kusainov, A.A. and Clough, R.W., June 1988.

UCB/EERC-88/10 "The Landslide at the Port of Nice on October 16, 1979," by Seed, H.B., Seed, R.B., Schlosser, F., Blondeau, F. and Juran, I., June 1988

UCB/EERC-88/11 "Liquefaction Potential of Sand Deposits Under Low Levels of Excitation," by Carter, D.P. and Seed, H.B., August 1988.

UCB/EERC-88/12 "Nonlinear Analysis of Reinforced Concrete Frames Under Cyclic Load Reversals," by Filippou, F.C. and Issa, A., September 1988.

UCB/EERC-88/13 "Implications of Recorded Earthquake Ground Motions on Seismic Design of Building Structures," by Uang, C.-M. and Bertero, V.V., November 1988.

UCB/EERC-88/14 "An Experimental Study of the Behavior of Dual Steel Systems," by Whittaker, A.S., Uang, C.-M. and Bertero, V.V., September 1988.

UCB/EERC-88/15 "Dynamic Moduli and Damping Ratios for Cohesive Soils," by Sun, J.I., Golesorkhi, R. and Seed, H.B., August 1988.

UCB/EERC-88/16 "Reinforced Concrete Flat Plates Under Lateral Load: An Experimental Study Including Biaxial Effects," by Pan, A. and Moehle, J., October 1988.

UCB/EERC-88/17 "Earthquake Engineering Research at Berkeley - 1988," by EERC, November 1988.

UCB/EERC-88/18 "Use of Energy as a Design Criterion in Earthquake-Resistant Design," by Uang, C.-M. and Bertero, V.V., November 1988.

UCB/EERC-88/19 "Steel Beam-Column Joints in Seismic Moment Resisting Frames," by Tsai, K.-C. and Popov, E.P., November 1988.

UCB/EERC-88/20 "Base Isolation in Japan, 1988," by Kelly, J.M., December 1988.

UCB/EERC-89/01 "Behavior of Long Links in Eccentrically Braced Frames," by Engelhardt, M.D. and Popov, E.P., January 1989.

UCB/EERC-89/02 "Earthquake Simulator Testing of Steel Plate Added Damping and Stiffness Elements," by Whittaker, A., Bertero, V.V., Alonso, J. and Thompson, C., January 1989.

UCB/EERC-89/03 "Implications of Site Effects in the Mexico City Earthquake of Sept. 19, 1985 for Earthquake-Resistant Design Criteria in the San Francisco Bay Area of California," by Seed, H.B. and Sun, J.I., March 1989.

UCB/EERC-89/04 "Earthquake Analysis and Response of Intake-Outlet Towers," by Goyal, A. and Chopra, A.K., July 1989.

UCB/EERC-89/05 "The 1985 Chile Earthquake: An Evaluation of Structural Requirements for Bearing Wall Buildings," by Wallace, J.W. and Moehle, J.P., July 1989.

UCB/EERC-89/06 "Effects of Spatial Variation of Ground Motions on Large Multiply-Supported Structures," by Hao, H., July 1989.

UCB/EERC-89/07 "EADAP - Enhanced Arch Dam Analysis Program: Users's Manual," by Ghanaat, Y. and Clough, R.W., August 1989.

UCB/EERC-89/08 "Seismic Performance of Steel Moment Frames Plastically Designed by Least Squares Stress Fields," by Ohi, K. and Mahin, S.A., August 1989.

UCB/EERC-89/09 "Feasibility and Performance Studies on Improving the Earthquake Resistance of New and Existing Buildings Using the Friction Pendulum System," by Zayas, V., Low, S., Mahin, S.A. and Bozzo, L., July 1989.

UCB/EERC-89/10 "Measurement and Elimination of Membrane Compliance Effects in Undrained Triaxial Testing," by Nicholson, P.G., Seed, R.B. and Anwar, H., September 1989.

UCB/EERC-89/11 "Static Tilt Behavior of Unanchored Cylindrical Tanks," by Lau, D.T. and Clough, R.W., September 1989.

UCB/EERC-89/12 "ADAP-88: A Computer Program for Nonlinear Earthquake Analysis of Concrete Arch Dams," by Fenves, G.L., Mojtahedi, S and Reimer, R.B., September 1989.

UCB/EERC-89/13 "Mechanics of Low Shape Factor Elastomeric Seismic Isolation Bearings," by Aiken, I.D., Kelly, J.M. and Tajirian, F.F., November 1989.

UCB/EERC-89/14 "Preliminary Report on the Seismological and Engineering Aspects of the October 17, 1989 Santa Cruz (Loma Prieta) Earthquake," by EERC, October 1989.

UCB/EERC-89/15 "Experimental Studies of a Single Story Steel Structure Tested with Fixed, Semi-Rigid and Flexible Connections," by Nader, M.N. and Astaneh-Asl, A., August 1989.

UCB/EERC-89/16 "Collapse of the Cypress Street Viaduct as a Result of the Loma Prieta Earthquake," by Nims, D.K., Miranda, E., Aiken, I.D., Whittaker, A.S. and Bertero, V.V., November 1989.

UCB/EERC-90/01 "Mechanics of High-Shape Factor Elastomeric Seismic Isolation Bearings," by Kelly, J.M., Aiken, I.D. and Tajirian, F.F., March 1990.

UCB/EERC-90/02 "Javid's Paradox: The Influence of Preform on the Modes of Vibrating Beams," by Kelly, J.M., Sackman, J.L. and Javid, A., May 1990.

UCB/EERC-90/03 "Earthquake Simulator Testing and Analytical Studies of Two Energy-Absorbing Systems for Multistory Structures," by Aiken, I.D. and Kelly, J.M., October 1990.

UCB/EERC-90/04 "Damage to the San Francisco-Oakland Bay Bridge During the October 17, 1989 Earthquake," by Astaneh, A., June 1990.

UCB/EERC-90/05 "Preliminary Report on the Principal Geotechnical Aspects of the October 17, 1989 Loma Prieta Earthquake," by Seed, R.B., Dickenson, S.E., Riemer, M.F., Bray, J.D., Sitar, N., Mitchell, J.K., Idriss, I.M., Kayen, R.E., Kropp, A., Harder, L.F., Jr. and Power, M.S., April 1990.

UCB/EERC-90/06 "Models of Critical Regions in Reinforced Concrete Frames Under Seismic Excitations," by Zulfiqar, N. and Filippou, F., May 1990.

UCB/EERC-90/07 "A Unified Earthquake-Resistant Design Method for Steel Frames Using ARMA Models," by Takewaki, I., Conte, J.P., Mahin, S.A. and Pister, K.S., June 1990.

UCB/EERC-90/08 "Soil Conditions and Earthquake Hazard Mitigation in the Marina District of San Francisco," by Mitchell, J.K., Masood, T., Kayen, R.E. and Seed, R.B., May 1990.

UCB/EERC-90/09 "Influence of the Earthquake Ground Motion Process and Structural Properties on Response Characteristics of Simple Structures," by Conte, J.P., Pister, K.S. and Mahin, S.A., July 1990.

UCB/EERC-90/10 "Experimental Testing of the Resilient-Friction Base Isolation System," by Clark, P.W. and Kelly, J.M., July 1990.